



HAL
open science

The creation of novel humanized mouse models for the assessment of innovative immunotherapies and vaccine evaluation

Yang Zeng

► **To cite this version:**

Yang Zeng. The creation of novel humanized mouse models for the assessment of innovative immunotherapies and vaccine evaluation. Immunology. Université Paris Saclay (COMUE), 2018. English. NNT : 2018SACLS327 . tel-01900581

HAL Id: tel-01900581

<https://theses.hal.science/tel-01900581v1>

Submitted on 22 Oct 2018

HAL is a multi-disciplinary open access archive for the deposit and dissemination of scientific research documents, whether they are published or not. The documents may come from teaching and research institutions in France or abroad, or from public or private research centers.

L'archive ouverte pluridisciplinaire **HAL**, est destinée au dépôt et à la diffusion de documents scientifiques de niveau recherche, publiés ou non, émanant des établissements d'enseignement et de recherche français ou étrangers, des laboratoires publics ou privés.

The creation of novel humanized mouse models for the assessment of innovative immunotherapies and vaccine evaluation

Thèse de doctorat de l'Université Paris-Saclay
Préparée à l'Université Paris-Sud

École doctorale N°568: Signalisations et Réseaux
intégratifs en Biologie (Biosigne)

Spécialité de doctorat: Sciences de la vie et de la santé

Thèse présentée et soutenue à Villejuif,
Le 04 Octobre 2018, par

M^{me} Yang ZENG

Composition du Jury:

| | |
|---|--------------------|
| Mme Colette Kanellopoulos-LANGEVIN Professeur, Université Paris Diderot | Président |
| Mme Monica SALA Professeur, Institut Pasteur | Rapporteur |
| M. Yongzheng WU Professeur, Institut Pasteur | Rapporteur |
| M. David OJCIUS Professeur, University of the Pacific | Examineur |
| M. Eric TARTOUR Professeur, INSERM U970 | Examineur |
| M. Bernard CHARPENTIER Professeur, Université-Paris-Sud | Examineur |
| M. Yu Chun LONE Professeur, Université-Paris-Sud | Directeur de thèse |

**THESE DE DOCTORAT
DE
L'UNIVERSITE PARIS-SACLAY**

**PREPAREE A
L'UNIVERSITE PARIS SUD**

ÉCOLE DOCTORALE N°568
Signalisations et Réseaux intégratifs en Biologie (Biosigne)
Spécialité de doctorat: Sciences de la vie et de la santé

PAR
M^{me} Yang ZENG

**The creation of novel humanized mouse models for the assessment of
innovative immunotherapies and vaccine evaluation**

Thèse présentée et soutenue au Kremlin Bicêtre, le 04 Octobre 2018

Composition du Jury:

**Professeur Colette Kanellopoulos-LANGEVIN
Professeur Monica SALA
Professeur Yongzheng WU
Professeur David OJCIUS
Professeur Eric TARTOUR
Professeur Bernard CHARPENTIER
Professeur Yu Chun LONE**

**Président du jury
Rapporteur
Rapporteur
Examineur
Examineur
Examineur
Directeur de thèse**

Acknowledgements

I would like to express all my deepest and sincerest gratitude to all the persons who cared, supported and helped me during my Ph.D studies.

My deepest and foremost gratitude goes first to my supervisor Dr. Yuchun Lone, for his kindness guidance during the design of our project, his encouragement and patience during the implementation of experiments, as well as the writing and revising of this thesis. His scientific enthusiasm and patience are the immense power supported me. Yuchun Lone and his wife Xianghui Liu treat me like their own child to make me feel at home in Paris. I could not complete my Ph.D study without their help. I would like to express my sincerest appreciate to Dr. Yuchun Lone and Xianghui Liu.

I would like to express my heartfelt gratitude to Dr. Yusen Zhou, my supervisor in China, the director of laboratory of Molecular pathogen biology, Beijing Institute of Microbiology and Epidemiology. Thanks for his constructive advices and powerful encourage in this project, and his generous help and support in my life and scientific career prospect.

My sincere gratitude is reserved for all the members of the jury. I am thankful to Professor Colette Kanellopoulos-LANGEVIN for kindly accepting to chair this thesis committee. I would like to thank the reviewers of this thesis: Professor Monica SALA and Professor Yongzheng WU for taking time to carefully review this thesis. I am grateful to Professor David OJCIUS, Professor Eric TARTOUR and Professor Bernard CHARPENTIER for accepting to evaluate my work and participating as examiners.

I would like to express my heartfelt gratitude to Dr. Bing LIU, Dr. Yu LAN and my my lovely colleagues in 307 Hospital, for their understanding, support and generous help.

A special thanks to China Scholarship Council for their financial support during my Ph.D studies in Paris.

I warmly thanks to all the members and colleagues of INSERM U1197, Professor Antoine DURRBACH, Professor Georges UZAN, Professor Aime VAZQUEZ, Xinyue WANG, Bingrun LIU, Akayla GABA, Vincent LECOZ, Severine LECOURT, Lola

LECRU, Mélanie BRUNEL and Julien GIRON-MICHEL. Thanks for your help in the immunology, bioinformatics, statistics, techniques and data analysis, I learned a lot from weekly conference. I appreciated all your support of my daily life in Paris. They also help me to communicate and cope with “Titre de séjour” and “CAF”. I also appreciate them for teaching me to speak and learn French, we enjoy delicious food every week. Thanks to Professor Marie-Thérèse RUBIO at Hôpital Saint Antoine, for her help in the collection of samples. I am pleased to thank Dr. Zhitao RU for many great ideas, suggestions and help.

I also would like to sincerely thank Dr. Shihui SUN, Dr. Guangyu ZHAO, Dr. Zhihua KOU, Dr. Junfeng LI, and all the members of Molecular pathogen biology laboratory, Beijing Institute of Microbiology and Epidemiology. Xiaojun ZHOU, Xiaopeng DAI, Hongjie QIU, Tongtong GAO, Yuting JIANG, Dan LI, Nianping SONG, et al. Thanks for your kindness help in this project and my daily life. The memory was so beautiful and unforgettable, and sincere friendship was the most precious asset that I have harvested.

I also would like to express my gratitude to my lovely friends and roommates in Paris, Xiaoyan ZHU, Shiwei WANG, Zongbei DAI, Yifei ZHU, Diya SU, Jing LI, Xiaotong CHEN, Yi LIANG and so on. Thanks for you accompany, encouragement, we enjoyed delicious food, we enjoyed wonderful journey, we shared each other's happiness and sorrow. I hope we could have a bright future, miss each other everywhere in the world, our friendship last forever. That was the most unforgettable memory in my life.

I would like to express my deepest appreciation to my beloved husband Dr. Cheng LIU, for his loving, understanding and encouragement. Thank you for taking care of our parents during these years. Thank you for your unconditional support of our decision, even the hazards, standing together regardless of situation. I love you forever.

Last but definitely the most important, I would like to give my most sincere gratitude to my parents. They are my strong backing and my dynamic source of learning, and they gave me unconditional love. There is an inexhaustible power on the road of my life. Thanks for the support and encouragement of my parents-in-law. I am grateful to have such a warm family. I hope my parents and my parents-in-law will always be healthy and happy. This is my greatest wish!

TABLE OF CONTENTS

| | |
|--|-----------|
| ABSTRACT | 5 |
| RESUME | 6 |
| LIST OF ABBREVIATIONS | 7 |
| PREFACE | 10 |
| INTRODUCTION | 17 |
| 1. Immunity | 18 |
| 1.1 The innate immunity | 18 |
| 1.2 The adaptive immunity | 19 |
| 2. Major histocompatibility complex (MHC) | 21 |
| 2.1 Discovery and identification of MHC molecules | 22 |
| 2.2 The classification of MHC molecules | 22 |
| 2.3 Human HLA and murine H-2 molecules | 25 |
| 2.4 The function of MHC molecules | 26 |
| 2.4.1 To present antigens | 26 |
| 2.4.2 Participation in the differentiation and development of T cells | 31 |
| 2.4.3 Involvement in the genetic regulation of immune responses | 32 |
| 2.4.4 Regulate the innate immune responses | 33 |
| 2.4.5 Other functions of MHC in immune responses | 33 |
| 2.5 HLA genes are highly polymorphic | 35 |
| 2.6 Distribution of HLA alleles worldwide | 36 |
| 2.7 The association between HLA and human diseases | 37 |
| 3. Animal models in scientific research | 40 |
| 3.1 Human MHC transgenic mouse models | 41 |
| 4. Immuno-deficient mouse models | 42 |
| 4.1 SCID (C.B-17 SCID) mice | 44 |
| 4.2 Rag1^{-/-} and Rag2^{-/-} mice | 46 |
| 4.3 NOD/SCID (NOD/LtSz-scid) mice | 46 |
| 4.4 Hu-BLT-SCID (human bone marrow-liver-thymus SCID) | 46 |
| 4.5 N/S-S/GM/3 mice and N/S-β2m^{-/-}-S/GM/3 mice | 47 |

| | |
|--|------------|
| 4.6 NOG/NSG mice | 47 |
| 4.7 NSGS (NOD/LtSz-scid IL-2RG-SGM3)..... | 48 |
| 4.8 MITRG and MISTRG | 49 |
| 4.9 NSGW mice..... | 49 |
| 5. HSC transplantation (HSCT) | 49 |
| 5.1 The identification of human HSC phenotypes..... | 50 |
| 5.2 In vitro amplification of human HSC..... | 52 |
| 5.3 The other factors effect human HSC transplantation | 52 |
| 6. Vaccines | 53 |
| 6.1 Human oncogenic viruses, associated diseases and vaccines | 54 |
| 6.2 Epitopes-based vaccines..... | 55 |
| 6.3 Personalized vaccines for cancer immunotherapy | 56 |
| RESULTS | 58 |
| Part 1. Creation of an immuno-deficient HLA-transgenic mouse (HUMAMICE) and functional validation of human immunity after transfer of HLA-matched human cells | 59 |
| Abstract..... | 61 |
| Introduction | 62 |
| Methods..... | 64 |
| Results | 69 |
| Discussion..... | 80 |
| Conclusions | 83 |
| Part 2. Generation of human MHC (HLA-A11/DR1) transgenic mice vaccine evaluation | 86 |
| Abstract..... | 88 |
| Introduction | 89 |
| Materials and methods | 91 |
| Results | 100 |
| Discussion..... | 113 |
| Conclusions | 115 |

| | |
|---|------------|
| Part 3. A novel helper-dependent adenovirus-based cell culture model for Hepatitis C virus replication and production..... | 117 |
| Part 4. Upregulation of MicroRNA-146a by hepatitis B virus x protein contributes to hepatitis development by downregulating complement factor H | 129 |
| Part 5. Multi-organ damage in human dipeptidyl peptidase 4 transgenic mice infected with Middle East Respiratory Syndrome-Coronavirus..... | 143 |
| Part 6. Differences in the pathogenicity and inflammatory responses induced by avian influenza A/H7N9 Virus infection in BALB/c and C57BL/6 mouse models | 159 |
| Part 7. Manuscript “Identification of novel HLA-A11-restricted T-cell epitopes in the Ebola virus nucleoprotein..... | 170 |
| GENERAL DISCUSSION | 203 |
| CHAPTER 1 | 204 |
| Creation of an immuno-deficient HLA-transgenic mouse (HUMAMICE) and functional validation of human immunity after transfer of HLA-matched human cells | 204 |
| 1. The development history of immuno-deficient mouse models | 204 |
| 1.1 The initial establishment of immuno-deficient mouse models | 204 |
| 1.2 The optimization of immuno-deficient mouse models..... | 205 |
| 1.3 The comparison between hu-SRC-SCID and hu-PBL-SCID mice | 206 |
| 2. The construction strategy of HUMAMICE | 207 |
| 2.1 The role of Rag2, Perforin and IL-2γ in immune system..... | 207 |
| 2.2 The establishment of HUMAMICE | 208 |
| 2.3 The immuno-deficiency characteristics of HUMAMICE | 210 |
| 3. The xenogeneic hPBMCs transplantation in HUMAMICE..... | 210 |
| 3.1 The reconstitution characteristics in HUMAMICE after hPBMC engraftment | 211 |
| 3.2 The following HBsAg immunization of HUMAMICE | 212 |
| 4. The humanized optimization of immune-deficient mouse models | 212 |
| CHAPTER II..... | 214 |

| | |
|---|------------|
| Generation of human MHC (HLA-A11/DR1) transgenic mice vaccine evaluation | 214 |
| | |
| 1. Current situation of humanized mouse models | 214 |
| 1.1 The defects of current mouse models | 215 |
| 1.2 The association between HLA and the occurrence of diseases | 218 |
| 1.3 Dominant MHC alleles are different between continents | 219 |
| 2. The development state of HLA transgenic mouse models | 220 |
| 2.1 The strategy optimization of HLA transgenic mouse models | 220 |
| 2.2 The construction strategy of HLA-A11/DR1 transgenic mice | 221 |
| 3. The generation of homozygous HLA-A11/DR1 transgenic mice | 222 |
| 4. The application of HLA-A11/DR1 transgenic mice to the evaluation of vaccines | 223 |
| 4.1 The verification of HLA-A11/DR1 mice with reported epitopes | 223 |
| 4.2 The evaluation of HLA-A11/DR1 mice in candidate vaccines and commercial vaccines | 224 |
| 4.3 The identification of novel HLA-A11 restricted epitopes of EBOV and MERS-CoV | 226 |
| CONCLUSIONS | 228 |
| PERSPECTIVES | 230 |
| 1. Further optimization and development of HUMAMICE | 230 |
| 2. The improvement of HLA transgenic mouse models | 231 |
| REFERENCES | 233 |

ABSTRACT

Animal models play critical roles in pre-clinical researches, while there are several limitations. The physiological and immunological states in murine and non-human primates are still distinct from those of human to a certain extent, especially the MHC restriction, which cannot eliminate the influence of species specificity in pre-clinical experiments. The aim of our work was to generate a higher level of “HLA humanized” transgenic mice which could mimic human immune responses with more accuracy and reliability; furthermore, to apply the novel models to the evaluation of human transplantation, the identification of new epitopes, and the evaluation of candidate vaccines and drugs.

In the first part, a novel immuno-deficient HLA transgenic mouse strain HLA-A2^{+/+}/DR1^{+/+}/H2-β_{2m}^{-/-}/IAβ^{-/-}/Rag2^{-/-}/IL-2rγ^{-/-}/Perf^{-/-} HUMAMICE were established, which expressed human HLA molecules instead of murine H-2 and present no murine lymphocytes. This immuno-deficient status was reversed by transferring the functional HLA-matched hPBMCs and thus producing mice with an immuno-competent status. Then, led to high lymphocyte engraftment without GvHD. Immunization of HBsAg vaccine resulted robust and reproducible production of specific antibodies. In conclusion, these results indicated that the hPBMCs-HUMAMICE model represents a promising model to dissect human immune responses towards human diseases.

In the second part, the Chinese/East Asian HLA dominant HLA-A11/DR1 (HLA-A11^{+/+}/DR1^{+/+}/H-2-β_{2m}^{-/-}/IAβ^{-/-}) transgenic mouse strain was established. This novel mouse strain possesses HLA-A11-restricted characteristics and capacity to respond to antigens. Immunization of mice with a recombinant HBV vaccine or a recombinant HIV-1 protein resulted in the generation of IFN-γ-producing cytotoxic T lymphocytes and specific antibodies. Furthermore, we identified two HLA-A11 restricted epitopes of EBOV GP protein and four of MERS-CoV S protein. Above all, HLA-A11/DR1 mice could facilitate the identification of Chinese dominant HLA-restricted CTL and Th epitopes and provide a new promising technical tool to understand immunological mechanisms and new vaccines.

Taken together, we created two novel and promising humanized mouse models carrying human HLA restriction which could be applied as pathogen infection models, in tumor studies, transplantation mechanism, and the evaluation of vaccines and drugs.

Keyword: HUMAMICE, immuno-deficient mice, immune reconstitution, MHC, HLA-A11/DR1 transgenic mice, vaccine evaluation

RESUME

Les modèles animaux jouent un rôle crucial dans les recherches précliniques, mais il existe plusieurs limites. Les états physiologiques et immunologiques chez les murins et les primates non humains sont radicalement différents de ceux de l'homme, en particulier la restriction au CMH, qui ne peut éliminer l'influence de la spécificité de l'espèce dans les expériences précliniques. Le but du travail était de générer un niveau plus élevé de souris transgéniques «HLA humanisées» qui pourraient imiter les réponses immunitaires humaines avec plus de précision et de fiabilité; à viser d'appliquer pour l'évaluation préclinique de la transplantation humaine, à l'identification de nouveaux épitopes et à l'évaluation des vaccins et des médicaments candidats.

Dans la première partie, nous rapportons d'une nouvelles souris transgéniques HLA immunodéficiente «HUMAMICE». Des souris HLA-A2^{+/+}/DR1^{+/+}/H-2-β2m^{-/-}/IAβ^{-/-}/Rag2^{-/-}/IL-2γ^{-/-}/Perf^{-/-} ont été établies, lesquelles exprimaient des molécules HLA humaines au lieu de H-2 murines et ne présent pas de lymphocytes murins. Ce statut immunodéficient a été inversé en transférant les cellules hPBMC HLA appariées fonctionnelles pour produisant des souris ayant un statut immuno-compétent avec un système immunitaire humain fonctionnel. L'immunisation du vaccin HBsAg a permis d'obtenir une production robuste et reproductible d'anticorps spécifiques.

En conclusion, ces résultats indiquent que le modèle hPBMC-HUMAMICE représente un modèle prometteur pour disséquer les réponses immunitaires humaines aux maladies humaines.

Dans la seconde partie de cette étude, les souris HLA-A11^{+/+}/DR1^{+/+}/H-2-β2m^{-/-}/IAβ^{-/-} ont été établies. Cette nouvelle souche de souris possède une caractéristique restreinte par HLA-A11 et une capacité normale à répondre aux antigènes. L'immunisation de souris avec un vaccin recombinant HBsAg contre le VHB ou une protéine recombinante du VIH-1 a entraîné la génération de lymphocytes T cytotoxiques producteurs d'IFN-γ et d'anticorps spécifiques. En outre, nous avons identifié deux épitopes restreints par HLA-A11 de la protéine GP EBOV et quatre de la protéine MERS-CoV S. En fin, ce modèle de souris HLA-A11/DR1 pourra faciliter l'identification des épitopes de lymphocytes cytotoxiques et auxiliaires restreints par le HLA-A11 dominant en Chine. Le modèle constitue un nouvel outil technique prometteur pour comprendre les mécanismes immunologiques et les nouveaux vaccins pour les populations d'Asie de l'Est.

Durant cette thèse, nous avons créé deux modèles de souris humanisées novateurs et prometteurs portant une restriction HLA humaine qui pourraient servir de modèles d'infection pathogène et étudier les tumeurs, les mécanismes de transplantation et l'évaluation des vaccins et des médicaments.

Mots clés: HUMAMICE, Souris immunodéficientes, reconstitution immunitaire, CMH, HLA-A11/DR1 souris transgénique

LIST OF ABBREVIATIONS

A: absorbance

Aa: amino acid

Ab: antibody

Amp: ampicillin

APC: antigen presenting cell

β_2m : β_2 -microglobulin

bp: base pair

BAS: bovine serum albumin

CD3: CD3 molecule

CD4: CD4 molecule

CD8: CD8 molecule

CTL: cytotoxic T lymphocyte

DEPC: diethylpyrocarbonate

DNA: deoxyribonucleic acid

DC: dendritic cell

DMEM: dulbecco's minimum essential medium

dNTP: deoxy-ribonucleotide triphosphate

EBOV: Ebola virus

ELISA: enzyme-linked immuno sorbent assay

ELISPOT: enzyme-linked immunospot assay

FACS: Fluorescence-Activated Cell Sorting

FBS: fetal bovine serum

FCM: flow cytofluorometry

FITC: fluorescein isothiocyanate

g: gram

gDNA: genome DNA

GvHD: graft-versus-host disease

h: hour (s)

H-2: histocompatibility-2

HBsAg: hepatitis B surface antigen

HBV: hepatitis B virus

HIV: human immune-deficiency virus

HLA: human leucocyte antigen
HRP: horseradish peroxidase
IgG: immunoglobulin G
IFN- γ : interferon-gamma
IL-2 γ : interleukin 2 receptor gamma
Kb: kilobase
LB: Luria-Bertani broth
MERS: Middle East Respiratory syndrome
MHC: major histocompatibility complex
min: minute(s)
mg: milligram
mL: milliliter
mM: millimole per liter
NC: negative control
NK: natural killer cell
nM: nanomole/L
NOD: non-obese diabetic
NSG: NOD/SCID gamma
OD: optical density
PBMC: peripheral blood mononuclear cell
PBS: phosphste-buffered saline
PBST: phosphate buffer solution tween-20
PCR: polymerase chain reaction
Perf: perforin
Rag2: recombination activating gene 2
Real-Time PCR: real-time quantitative polymerase chain PCR
rpm: rounds per minute
SCID: severe combined immune-deficiency
SDS: sodium dodecyl sulfate
sec: second (s)
T CD4⁺: CD4⁺ T lymphocyte
T CD8⁺: CD8⁺ T lymphocyte
TAE: tris/acetate/EDTA buffer
Taq: thermusaquaticus DNA polymerase

TCR: T cell receptor

TE: tris/EDTA buffer

Tris: Tris (hydroxymethyl) aminomethane

Tris-HCl: tris/hydrochloric acid buffer

U: unit

µg: micro gramme

µL: micro litre

µm: micron

µM: micromole per liter

WT: wild type

PREFACE

This work is a part of a large project led by Dr. Yuchun Lone at INSERM UMR 1197 and University Paris-Sud (University Paris-Saclay) “The creation of HUMAMICE: development of humanized mice for the assessment of innovative biotherapies, immunotherapies and stem-cell therapies”. This project is developed in close collaboration with Professor Yusen Zhou, the director of laboratory of molecular pathogen biology, the State Key Laboratory of Pathogen and Biosecurity, Beijing Institute of Microbiology and Epidemiology. The French and Chinese teams are collaborated on the development and optimization of humanized mouse models, and applying the new mouse models to the evaluation and development of vaccines and immuno-transplantation.

Human HLA molecules replaced murine H-2 molecules in human MHC class-I or II transgenic mice which could eliminate the competitive inhibition of endogenous H-2 molecules in immune responses, resulted in a more accurate and efficient mouse model with expression of human HLA molecules. In the first part of our study, we constructed an immuno-deficient MHC transgenic mouse model (HLA-A2^{+/+}/DR1^{+/+}/H-2-β₂m^{-/-}/IAβ^{-/-}/Rag2^{-/-}/IL-2γ^{-/-}/Perf^{-/-}) (HLA-A2 with the highest frequency among HLA class-I alleles, accounts for 30-50% of global human population) and an hPBMC-transplantation mouse model. This, provides a technical support for the study of pathogen infection, tumors, transplantation mechanisms, the evaluation of vaccines and drugs prototypes. In the second part, we generated a new homozygous HLA-A11/DR1 transgenic mouse strain (HLA-A11^{+/+}/DR1^{+/+}/H-2-β₂m^{-/-}/IAβ^{-/-}) which carried Chinese dominant HLA class I (HLA-A11) and II (HLA-DR1) alleles (HLA-A11 accounts for about 20-30% of total population in Asia), and applied to the evaluation of vaccines, which could identify HLA restricted CTL epitopes of pathogens, and to design and optimize the novel epitopes-based vaccines. Meanwhile, from the third to the sixth part, we elaborated an HDAd-based strategy for HCV replication and production in vitro, we studied the upregulation of MicroRNA-146a by HBV X protein and its contribution to hepatitis development by downregulating complement factor H, we analyzed the pathogenesis of MERS-CoV infection in DPP4 transgenic mouse model, and we studied the differences in the pathogenicity and inflammatory responses induced by Avian Influenza A/H7N9 virus infection in BALB/c and C57BL/6 mouse models.

1. Manuscript “Creation of an immunodeficient HLA-transgenic mouse (HUMAMICE) and functional validation of human immunity after transfer of HLA-matched human cells” (Yang Zeng, Bingrun Liu, Marie-Thèrese Rubio, Xinyue Wang, David M. Ojcius, Ruoping Tang, Antoine Durrbach, Zhitao Ru, Yusen Zhou, Yu-Chun Lone*. PLoS One. 2017 Apr 11;12(4):e0173754)

Research on human immunology has been hindered by the lack of optimal small animal models, given that the protective immune responses of human and non-human species show some differences. However, due to the ethical constraints and the high cost of clinical trials, it is urgent to improve the current pre-clinical animal models that can mimic faithfully human physiology, particularly the human immune system (HIS). HIS mice had been generated recently by engrafting human hematopoietic stem cells (hHSCs) or human peripheral mononuclear cells (hPBMCs) into highly immunodeficient mice such as NSG, NOG or NRG mice. However, a major experimental drawback for studies using these models is the rapid onset of Graft-versus-Host Disease (GvHD). In the present study, we overcome this limitation by generating new immunodeficient mice named "HUMAMICE" (HLA-A2^{+/+}/DR1^{+/+}/H-2-β₂m^{-/-}/IAβ^{-/-}/Rag2^{-/-}/IL-2rγ^{-/-}/Perf^{-/-} mice), which expressed human HLA molecules instead of mouse MHC molecules (H-2), and whose immuno-deficient status was reversed by transferring functional HLA-matched PBMCs thus producing mice with an immuno-competent status with a functional human immune system. We showed that in the HLA-matched context of this novel mouse model, the hPBMC-transfer led to high lymphocytes engraftment rates without GvHD over two months. Furthermore, to evaluate the utility of the hPBMC-HUMAMICE, we immunized them with commercial vaccine of Hepatitis B virus (HBsAg, Hepvac@) which resulted in robust and reproducible production of high levels of HBsAg specific antibodies, implying that both transferred T and B lymphocytes were functional in HUMAMICE. These responses are comparable to those observed in human clinical trials with this identical vaccine. In conclusion, these findings indicated that the HLA matched-hPBMC-HUMAMICE represents a promising model for dissecting human immune responses towards various human diseases, including infectious diseases, cancers and tumors, and to facilitate the development of novel vaccines and cellular therapies.

2. Manuscript “Generation of human MHC (HLA-A11/DR1) transgenic mice for vaccine evaluation” (Yang Zeng, Tongtong Gao, Guangyu Zhao, Yuting Jiang, Yi Yang, Hong Yu, Zhihua Kou, Yuchun Lone, Shihui Sun* & Yusen Zhou*. *Hum Vaccin Immunother.* 2016 Mar 3;12(3):829-36)

The rapid occurrence of emerging infectious diseases demonstrates an urgent need for a new preclinical experimental model that reliably replicates human immune responses. Here, a new homozygous humanized human leukocyte antigen (HLA)-A11/DR1 transgenic mouse (HLA-A11^{+/+}/DR1^{+/+}/H-2-β₂m⁻/IAβ⁻) was generated by crossing HLA-A11 transgenic mice with HLA-A2^{+/+}/DR1^{+/+}/H-2-β₂m⁻/IAβ⁻ mice. The HLA-A11-restricted immune response of this mouse model was then examined. HLA-A11 transgenic mice expressing a chimeric major histocompatibility complex (MHC) molecule comprising the α1, α2, and β₂m domains of human HLA-A11 and the α3 transmembrane and cytoplasmic domains of murine H-2D^b were generated. The correct integration of HLA-A11 and HLA-DR1 into the genome of the HLA-A11/DR1 transgenic mice (which lacked the expression of endogenous H-2-I/II molecules) was then confirmed. Immunizing mice with a recombinant HBV vaccine or a recombinant HIV-1 protein resulted in the generation of IFN-γ-producing cytotoxic T lymphocyte (CTL) and antigen-specific antibodies. The HLA-A11-restricted CTL response was directed at HLA immunodominant epitopes. These mice represent a versatile animal model for studying the immunogenicity of HLA CTL epitopes in the absence of a murine MHC-restricted response. The established animal model will also be useful for evaluating and optimizing T cell-based vaccines and for studying differences in antigen processing between mice and humans.

3. Manuscript “A novel helper-dependent adenovirus-based cell culture model for Hepatitis C virus replication and production” (Xiaojun Zhou[#], Yang Zeng[#], Junfeng Li, Yan Guo, Yuanhui Fu, Jinsheng He, Shihui Sun* and Yusen Zhou*. *Virol J.* 2013 Aug 30;10:273)

By using the Hepatitis C virus (HCV) genotype 2a JFH-1 or its chimeric strains, an HCV infection system had been previously developed through several methods— such

as in vitro-transcribed JFH1-RNA transfection or stable transfection of the JFH1 cDNA into human hepatoma Huh-7 cell line or its derivatives. However, other reliable methods for delivery of the HCV genome into cells are still worth trying. The helper-dependent adenovirus (HDAAd) is devoid of all viral coding sequences and has a package capacity of 37 kb, which is suitably large for the delivery of the HCV genome. Here we report a new method for delivery of the HCV genome into Huh-7 and HepG2 cells by using the HDAAd vector. Our results demonstrated that the infection of Huh-7 cells with the HDAAdJFH1 virus led to efficient HCV replication and virion production. We found that the HCV viral RNA levels could reach 10^7 copies per milliliter in the culture medium. HDAAdJFH1-infected Huh-7 cells could be cultured for 8 passages with the culture medium remaining infectious for naïve Huh-7 cells throughout this period. This infection system proved effective for evaluating the anti-HCV effects of IFN- α in Huh-7 cells. Co-infection of HepG2 cells with the HDAAdJFH1 and HDAAdmiR-122 virus also resulted in HCV expression and replication. This is the first report of an HDAAd-based strategy for HCV replication and production in vitro.

4. Manuscript “Upregulation of MicroRNA-146a by hepatitis B virus x protein contributes to hepatitis development by downregulating complement factor H” (Junfeng Li, Xiaopeng Dai, Wei Zhang, Shihui Sun, **Yang Zeng**, Guangyu Zhao, Zhihua Kou, Yan Guo, Hong Yu, Lanying Du, Shibo Jiang, Yusen Zhou. **MBio**. 2015 **Mar 24;6(2)**)

Hepatic injuries in hepatitis B virus (HBV) patients are caused by immune responses of the host. In our previous study, microRNA-146a (miR-146a), an innate immunity-related miRNA, and complement factor H (CFH), an important negative regulator of the alternative pathway of complement activation, were differentially expressed in HBV-expressing and HBV free hepatocytes. Here, the roles of these factors in HBV-related liver inflammation were analyzed in detail. The expression levels of miR-146a and CFH in HBV-expressing hepatocytes were assessed via analyses of hepatocyte cell lines, transgenic mice, adenovirus-infected mice, and HBV-positive human liver samples. The expression level of miR-146a was upregulated in HBV expressing Huh-7 hepatocytes, HBV-expressing mice, and patients with HBV infection. Further results demonstrated that the HBV X protein (HBx) was responsible for its effects on miR-

146a expression through NF- κ B-mediated enhancement of miR-146a promoter activity. HBV/HBx also downregulated the expression of *CFH* mRNA in hepatocyte cell lines and the livers of humans and transgenic mice. Furthermore, overexpression and inhibition of miR-146a in Huh-7 cells downregulated and upregulated *CFH* mRNA levels, respectively. Luciferase reporter assays demonstrated that miR-146a downregulated *CFH* mRNA expression in hepatocytes via 3-untranslated-region (UTR) pairing. The overall effect of this process *in vivo* is to promote liver inflammation. These results demonstrate that the HBx-miR-146a-CFH-complement activation regulation pathway might play an important role in the immunopathogenesis of chronic HBV infection. These findings have important implications for understanding the immunopathogenesis of chronic hepatitis B and developing effective therapeutic interventions. HBV remains an important pathogen and can cause severe liver diseases, including hepatitis, liver cirrhosis, and hepatocellular carcinoma. Although HBV was found in 1966, the molecular mechanisms of pathogenesis are still poorly understood. In the present study, we found that the HBx promoted the expression of miR-146a, an innate immunity-related miRNA, through the NF- κ B signal pathway and that increasingly expressed miR-146a downregulated its target CFH, an important negative regulator of the complement alternative pathway, leading to the promotion of liver inflammation. We demonstrated that the HBx-miR-146a-CFH-complement activation regulation pathway is potentially an important mechanism of immunopathogenesis caused by chronic HBV infection. Our data provide a novel molecular mechanism of HBV pathogenesis and thus help to understand the correlations between the complement system, an important part of innate immunity, and HBV-associated disease. These findings will also be important to identify potential therapeutic targets for HBV infection.

5. Manuscript “Multi-organ damage in human dipeptidyl peptidase 4 transgenic mice infected with Middle East Respiratory Syndrome-Coronavirus” (Guangyu Zhao[#], Yuting Jiang[#], Hongjie Qiu, Tongtong Gao, **Yang Zeng**, Yan Guo, Hong Yu, Junfeng Li, Zhihua Kou, Lanying Du, Wenjie Tan, Shibo Jiang, Shihui Sun*, Yusen Zhou*. **PLoS One. 2015 Dec 23;10(12):e0145561**)

The Middle East Respiratory Syndrome Coronavirus (MERS-CoV) causes severe acute respiratory failure and considerable extrapulmonary organ dysfunction with substantial high mortality. For the limited number of autopsy reports, small animal models are urgently needed to study the mechanisms of MERS-CoV infection and pathogenesis of the disease and to evaluate the efficacy of therapeutics against MERS-CoV infection. In this study, we developed a transgenic mouse model globally expressing codon-optimized human dipeptidyl peptidase 4 (hDPP4), the receptor for MERS-CoV. After intranasal inoculation with MERS-CoV, the mice rapidly developed severe pneumonia and multi-organ damage, with viral replication being detected in the lungs on day 5 and in the lungs, kidneys and brains on day 9 post-infection. In addition, the mice exhibited systemic inflammation with mild to severe pneumonia accompanied by the injury of liver, kidney and spleen with neutrophil and macrophage infiltration. Importantly, the mice exhibited symptoms of paralysis with high viral burden and viral positive neurons on day 9. Taken together, this study characterizes the tropism of MERS-CoV upon infection. Importantly, this hDPP4-expressing transgenic mouse model will be applicable for studying the pathogenesis of MERS-CoV infection and investigating the efficacy of vaccines and antiviral agents designed to combat MERS-CoV infection.

6. Manuscript “Differences in the pathogenicity and inflammatory responses induced by avian influenza A/H7N9 virus infection in BALB/c and C57BL/6 mouse models” (Guangyu Zhao[#], Chenfeng Liu[#], Zhihua Kou[#], Tongtong Gao, Ting Pan, Xiaohong Wu, Hong Yu, Yan Guo, **Yang Zeng**, Lanying Du, Shibo Jiang, Shihui Sun*, Yusen Zhou*. **PLoS One. 2014 Mar 27;9(3):e92987**)

Avian influenza A/H7N9 virus infection causes pneumonia in humans with a high case fatality rate. However, virus-induced modulation of immune responses is being recognized increasingly as a factor in the pathogenesis of this disease. In this study, we compared the pathogenicity of A/H7N9 infection in BALB/c and C57BL/6 mouse models and investigated the putative involvement of proinflammatory cytokines in lung injury and viral clearance. In both mouse strains, A/Anhui/1/2013 (H7N9) infection with 10^6 TCID₅₀ resulted in viral replication in lung, severe body weight loss and acute lung injury. During the early infection stage, infected C57BL/6 mice exhibited more severe lung injury, slower recovery from lung damage, less effective viral clearance,

higher levels of IL-6, MCP-1, and IL-1 β , and lower levels of TNF- α and IFN- γ than infected BALB/c mice. These results suggest that TNF- α and IFN- γ may help suppress viral gene expression and increase viral clearance, and that IL-6 and MCP-1 may contribute to lung injury in A/H7N9-infected individuals. In addition, lung damage and the distribution of virus antigen in tissues were similar in young and middle-aged mice. These results suggest that the more serious lung injury in middle-aged or older H7N9 cases is not mainly caused by differences in viral replication in the lung but probably by a dysregulated immune response induced by underlying comorbidities. These results indicate that the extent of dysregulation of the host immune response after H7N9 virus infection most probably determines the outcome of H7N9 virus infection.

7. Manuscript “Identification of novel HLA-A11-restricted T-cell epitopes in the Ebola virus nucleoprotein” (Dan Li, Pei Li, Nianping Song, Yuting Jiang, **Yang Zeng**, Guangyu Zhao, Yunzhi Fa, Huahu Ye, Yuchun Lone, Yusen Zhou, Shihui Sun, Lin Zeng. *Microbes Infect.* **2018 May 15. pii: S1286-4579(18)30097-2**)

The Ebola virus (EBOV) is a very contagious virus that is highly fatal in humans and animals. The largest epidemic was in West Africa in 2014, in which over 11,000 people died. However, to date, there are no licensed vaccines against it. Studies show that CD4⁺ and CD8⁺ T-cell responses, especially cytotoxic T-lymphocyte (CTL) responses, play key roles in protecting individuals from EBOV infection. Since HLA-restricted epitope vaccines are likely to be effective and safe immunization strategies for infectious diseases, the present study screened for CTL epitopes in the EBOV-nucleoprotein that are restricted by HLA-A11 (a common allele in Chinese people). Predictive computer analysis of the amino-acid sequence of EBOV-nucleoprotein identified ten putative HLA-A11-restricted epitopes. ELISPOT assay of immunized HLA-A11/DR1 transgenic mice showed that five (GR-9, VR-9, EK-9, PK-9, and RK-9) induced effective CTL responses. Additional epitope analyses will aid the design of epitope vaccines against EBOV.

INTRODUCTION

1. Immunity

Immunity is the capacity to protect the multicellular organisms to against injury (physical and chemical), irradiation, and to fight infection and disease. It is regulated to maintain tolerance to self-antigens to avoid the emergence of allergy and autoimmune diseases. Immunity involves both innate immunity and adaptive immunity [1] (Figure 1). The innate immunity acts as a barrier of a wide range of pathogens. The adapt immunity generate antigen-specific immunity against pathogens.

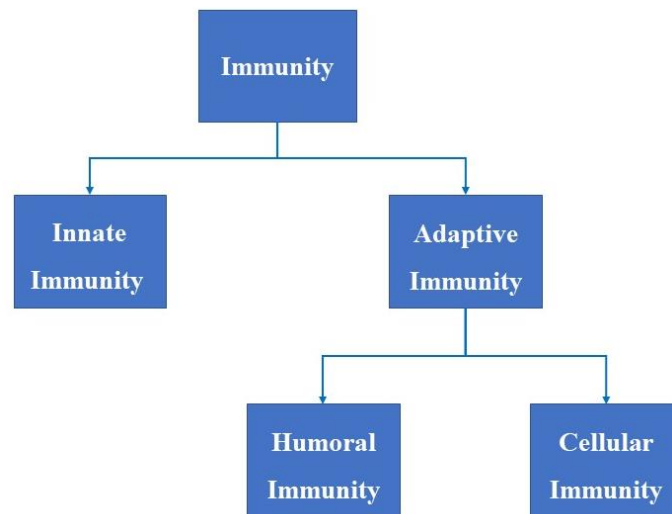


Figure 1. Immunity involves both innate immunity and adaptive immunity.

1.1 The innate immunity

The non-specific immunity is the barrier towards a wide range of pathogens carrying antigens. The innate immune system in mammals is composed of bone marrow derived cells which are programmed to recognize foreign substances and react against them after birth. Cells participated in innate immunity including monocytes, macrophages, dendritic cells (DC), granulocytes, NK cells, NKT cells, etc, which do not express specific antigen recognition receptors. The pathogen recognition receptors (PRR) of these cells identify the common molecular structures - pathogen associated molecular patterns (PAMP) of pathogens, infected cells, cancer cells and aging cells, such as the lipopolysaccharide (LPS) of gram-negative bacteria, the lipoteichoic acid (LTA) of gram-positive bacteria, the peptidoglycan (PGN) and the heat shock proteins

(HSP), etc. The activation of PRR produces non-specific anti-infection, anti-tumor or other immune protection, as well as participated in the initiation and regulation of adaptive immune responses.

1.2 The adaptive immunity

The specific immunity (adaptive immunity) generate antigen-specific immune responses towards pathogens. The adaptive immune response is acquired by individuals in contact with certain specific foreign antigens, and is also known as the acquired immunity. The response process is relatively slower with respect to innate immunity, but the efficiency of antigen elimination is higher, and the specificity is higher.

Depending on differences in immune cells and products that mediate and participate in adaptive immunity, adaptive immunity contains both **humoral immunity** and **cellular immunity**. T and B lymphocytes which with specific antigen recognition receptors (TCR or BCR) are the main implementer of adaptive immunity. After the recognition of foreign antigens such as pathogens, T and B lymphocytes undergone the activation, proliferation and differentiation, to produce effector cells and effector molecules (such as cytokines), and eventually to eliminate foreign antigens. Another property of adaptive immune system is self-recognition and self-tolerance, to avoid the emergence of autoimmune diseases.

The major functions of the adaptive immune system include:

- ◆ Recognition of specific “non-self” antigens in the presence of “self” antigens during the process of antigen presentation.
- ◆ Generation of immune responses that are tailored to maximally eliminate the specific pathogens or pathogen-infected cells.
- ◆ Development of immunological memory, in which pathogens are “remembered” through memory B cells and memory T cells. The time course of an immune response was summarized in Figure 2.

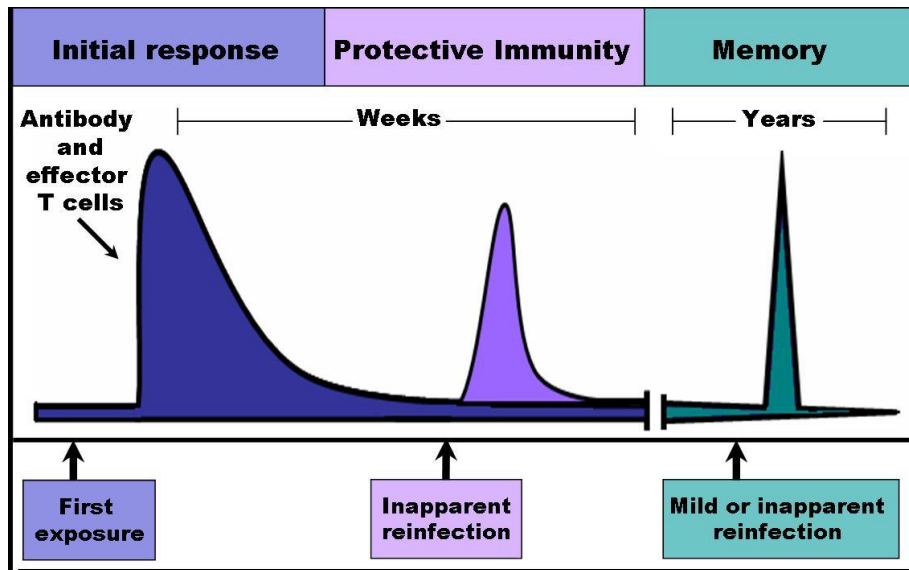


Figure 2. The time course of immune responses.

Depending on whether was acquired by contact with pathogens/diseases or through vaccination, the adaptive immunity could be divided into “**naturally-acquired immunity**” and “**artificially-acquired immunity**” (Table 1). Both naturally-acquired immunity and artificially-acquired immunity can be further sub-divided into long-term active immunity or short-term passive immunity, which depended on whether hosts could build up long-term active immunity by antigens stimulation or short-term passive immunity acquired through passive transfer of antibodies.

Table 1. Sources of the adaptive immunity

| | Naturally-acquired immunity | Artificially-acquired immunity |
|----------------|---|--|
| Active | Antigen enters the body via injury or infection | Antigens are introduced in vaccines |
| Passive | Antibodies pass from mother to fetus via placenta or infant via breast milk | Preformed antibodies in immune serum are introduced by injection |

The major characteristics of non-specific immunity and specific immunity was summarized in Table 2. Both specific and non-specific immunity of immune system create and keep a dynamic biological balanced environment where “health” can be regarded as a physical state, the self is immunologically spared, and foreign antigen is inflammatorily and immunologically eliminated. “Disease” will arise when foreign antigens cannot be eliminated or self-antigen is not spared.

Table 2. The major characteristics of innate immunity and adaptive immunity

| Terms | Innate immunity | Adaptive immunity |
|--|---|---|
| Antigens | Pathogen associated molecular patterns (PAMP) | Specific antigens of pathogens or non-self-antigens |
| Recognition receptors | Pathogen recognition receptors (PRR) (Genome-encoded) | T cell receptors (TCR) / B cell receptors (BCR) |
| Effect phase | Immediately ~ 96 h | >96 h |
| Immunological memory | No | Yes |
| Cells participated in responses | Monocytes/Macrophage/DC/ Neutrophil/NK/NKT/ $\gamma\delta$ T/B1 | $\alpha\beta$ T/ $\gamma\delta$ T/B1/B2 |
| Other components | Skin/Mucosal epithelium/ Complement/Cytokine/Interleukin | Antibodies/Cytokine/Interleukin |

2. Major histocompatibility complex (MHC)

Major histocompatibility complex (MHC) is a series of gene which encodes cell surface proteins essential for adaptive immune system to recognize and present foreign antigens in vertebrates, which also determined the histocompatibility between individuals. The main function of MHC is to present epitopes of endogenous and exogenous antigens, and then to display them on the cell surface to recognized by T lymphocytes. MHC molecules mediate the interactions of leukocytes and determine the compatibility between donors and recipients during clinical HSC transplantation.

MHC is one of the most polymorphic gene systems which is found in mammals. The products of MHC genes are involved in the initiation and regulation of immune responses, as well as the differentiation and development of T lymphocytes, have extremely important immunological role.

2.1 Discovery and identification of MHC molecules

Peter A. Gorer discovered and described MHC molecules and mouse H-2 molecules in 1936 [2]. MHC molecules were first identified in inbred murine strains. The first human HLA antigen was detected by Jean Dausset from the sera of three patients who received multiple transfusions in 1958. George Snell[3] identified a chromosome fragment in mice which was responsible for the acute rejection after skin grafting. This gene fragment contained H-2 complex, and thus constructed syngeneic mouse carrying allogenic antigens, which with the same genetic background, and at the same time the H-2 structure was different. Snell won the 1980 Nobel prize in medicine and physiology together with Baruj Benacerraf and Jean Dausset, because of elucidating that H-2 molecules genetically determined structures on the cell surface which regulated immunological reactions.

2.2 The classification of MHC molecules

MHC family is divided into three classes: MHC class-I, II and III. MHC Class-I molecules have $\alpha 1/\alpha 2/\alpha 3/\beta 2$ -microglobin domains and can be recognized by TCR of $CD8^+$ T cells (Figure 3A). The antigen binding cleft of MHC Class-I molecules is formed by $\alpha 1$ and $\alpha 2$ domain. MHC Class II molecules have $\alpha 1/\alpha 2/\beta 1/\beta 2$ domains and can be recognized by TCR of $CD4^+$ T cells. While, the antigen binding cleft of MHC Class-II molecules is formed by $\alpha 1$ and $\beta 1$ domain (Figure 3B). MHC Class-III molecules have different physiologic roles compare to MHC Class-I and II, which are encoded between them in the short arm of human chromosome 6. MHC Class-III molecules include several secreted proteins with immune functions: components (such as C2, C4, and B factor), cytokines (such as $TNF-\alpha$, LTA, and LTB) and heat shock proteins.

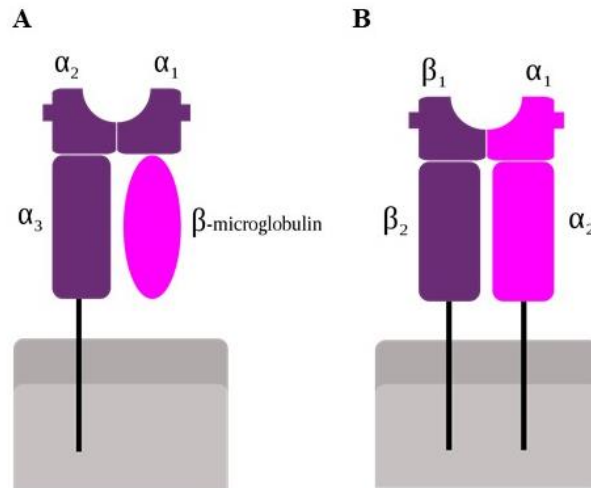


Figure 3. The structure of MHC class I (A) and class II (B) molecules. A. MHC Class-I molecules have $\alpha 1/\alpha 2/\alpha 3/\beta 2$ -microglobulin domains and can be recognized by TCRs of $CD8^+$ T cells. The antigen binding cleft of MHC Class-I molecules is formed by $\alpha 1$ and $\alpha 2$ domain. B. MHC Class-II molecules have $\alpha 1/\alpha 2/\beta 1/\beta 2$ domains and can be recognized by TCRs of $CD4^+$ T cells. While, the antigen binding cleft of MHC Class-II molecules is formed by $\alpha 1$ and $\beta 1$ domain.

As different T lymphocytes expressed different TCRs, different MHC molecules could present specific MHC-restricted epitopes of an antigen to given T lymphocytes with different affinity. The genomic landscape of MHC molecule is summarized in Figure 4.

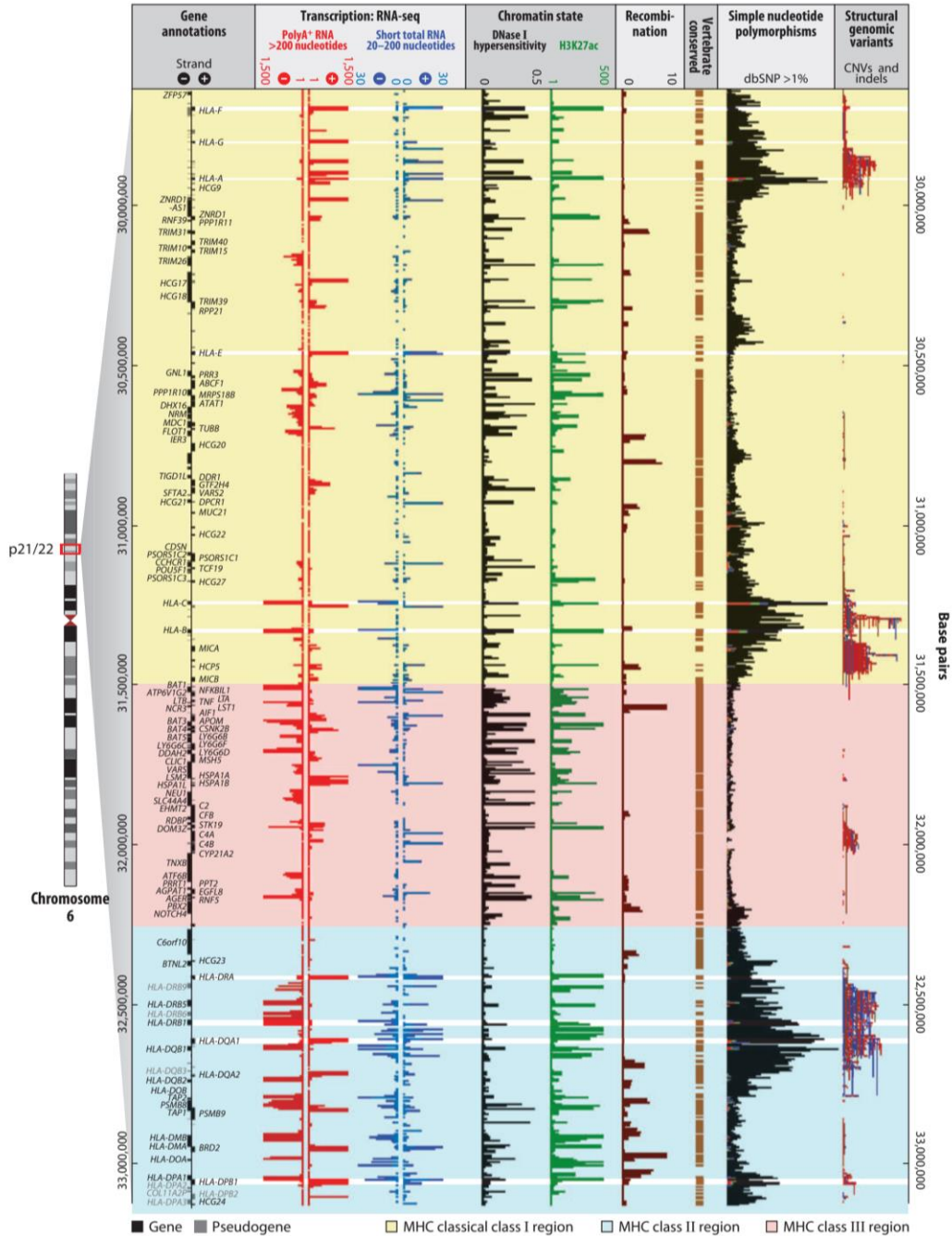


Figure 4. The genomic landscape of MHC molecules. The human MHC-HLA is one of the first large genomic regions which is fully sequenced. It contains about 260 genes in a ~4-Mb span on chromosomal region 6p21.3. Figure from *Knight JC et al, Annu Rev Genomics Hum Genet. 2013;14:301-23.*

2.3 Human HLA and murine H-2 molecules

Human MHC, named human lymphocyte antigen (HLA) is a gene complex responsible for histocompatibility. HLA complex represents the most complicated human gene clusters ever found. The alleles of HLA genes are highly polymorphic, which signifies that different HLA alleles could regulate and accommodate the adaptive immune system, and gave expression to the biological polymorphism in human beings.

HLA complex is located on human chromosome 6p21.31, and is approximately 3600 kb in length, consisted of 224 loci, of which 128 loci are functional genes. According to the function of its encoded products, HLA gene complex is divided into classic HLA gene (classic HLA class-I gene and classic HLA class-II gene) and immune function-related genes (the main function is to participate in antigen processing, innate immunity and immune regulation). HLA complex family contains of three classes: HLA class-I, class-II and class-III molecules. HLA class-I molecules present three loci: HLA-A, HLA-B and HLA-C, encoding the heavy chain (α chain) in HLA-A, HLA-B and HLA-C heterodimer respectively, and the light chain is β_2 -microglobin (β_2 -m) which coded gene is located on chromosome 15. While HLA class-II molecules include classic HLA class-II gene (HLA-DR/HLA-DP/HLA-DQ) and immune function-related gene (HLA-DM/HLA-DO). HLA class II genes code for α and β chains (designated A and B) of HLA-DR, HLA-DP and HLA-DQ.

Histocompatibility-2 (H-2) is the MHC complex of murine which equivalented to human HLA, which is located on murine chromosome 17. The structure and organization of MHC molecules is similar between species. Both species have three main class-I genes, which named H2-K, H2-D and H2-L in mice. Compared with human HLA class-I, murine MHC class-I gene H-2K has been translocated, which splits class-I region in human and mouse MHC class-I molecules. Murine β_2 m is encoded by a gene located on chromosome 2. The genetic structure schematic of human HLA and mice H-2 is shown in Figure 5.

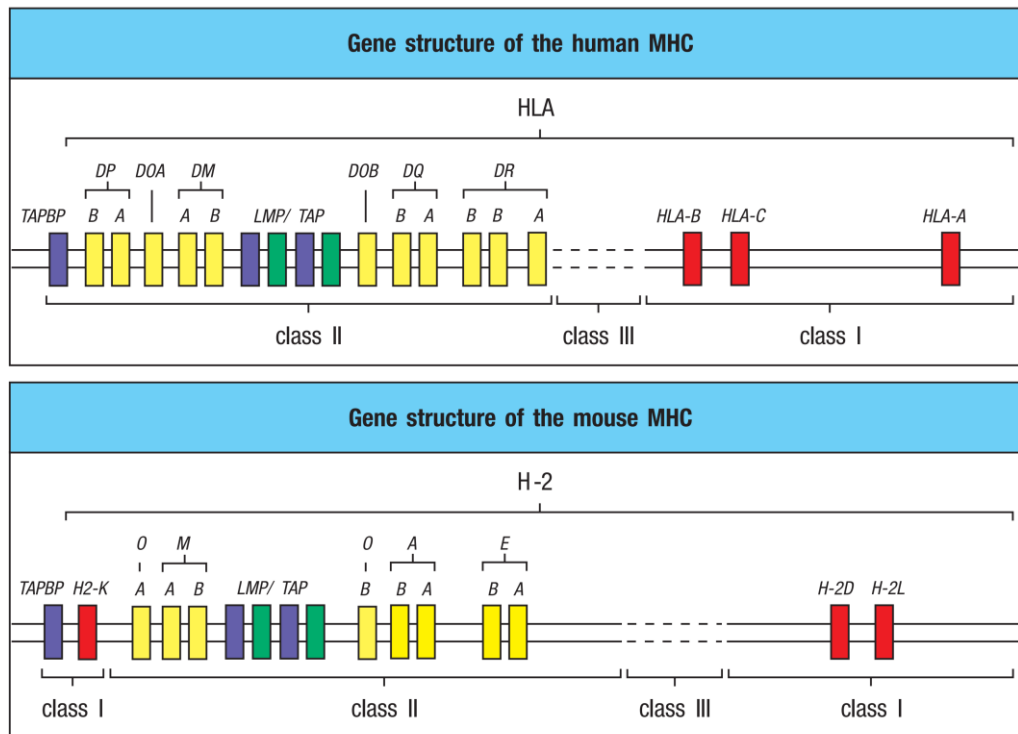


Figure 5. The genetic structure schematic of human HLA and mice H-2.

2.4 The function of MHC molecules

2.4.1 To present antigens

MHC is the mediator for intracellular or foreign peptides to present to TCRs of T lymphocytes. MHC allows immune system to bind, recognize and tolerate the self-antigens. MHC class I and II molecules bind to TCR of CD4 and CD8, respectively, and CD4/CD8 co-receptors on T lymphocytes. Then, the epitopes of antigens in the groove of MHC molecules will interact with the variable Ig-like domain of TCR to trigger the activation of T cells.

The function of MHC class-I molecules is presenting endogenous antigenic peptides to CD8⁺ T cells. For example, MHC class I molecules present the viral peptides on the surface of the infected cells, and then it will be destroyed CD8⁺ T lymphocytes (Cytotoxic T lymphocytes). The peptides presented by MHC class-I molecules are about 8-11 amino acids in length. The structure of MHC class I molecules determined by X-ray crystallography is shown in Figure 6.

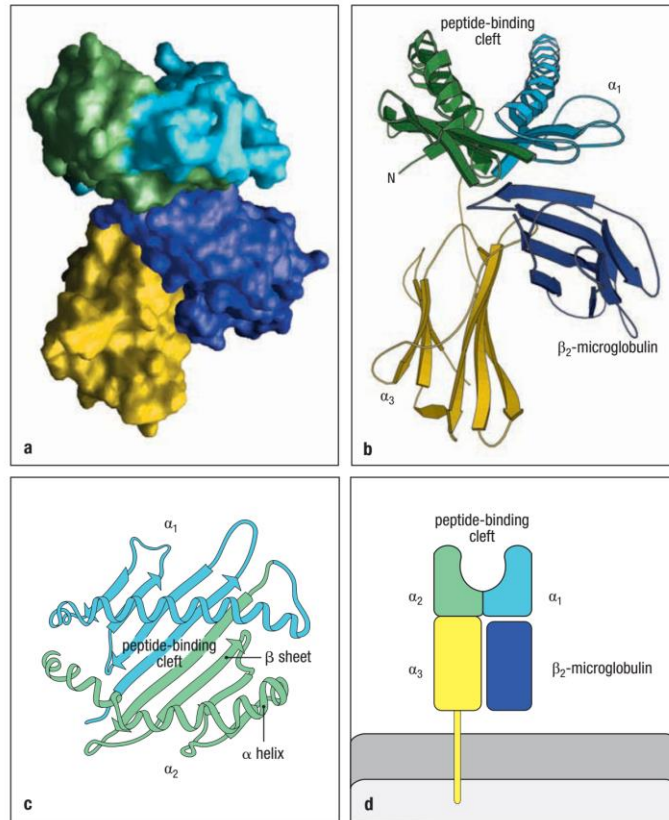


Figure 6. The structure of an MHC class I molecule determined by X-ray crystallography. Figure from text book *Janeway's Immunobiology 9th Edition, 2017* by Garland Science, Taylor & Francis Group, LLC (ISBN 978-0-8153-4505-3).

MHC class II molecules are composed of two transmembrane glycoprotein chains, α and β chain, each chain has two domains, as shown schematically in Figure 7D. Figure 7A shows a computer graphic representation of MHC class II molecule, in this case the human protein HLA-DR1, and Figure 7B shows the equivalent ribbon diagram. The $\alpha 2$ and $\beta 2$ domains, like $\alpha 3$ and $\beta 2$ -microglobulin domains of MHC class I molecules, have amino acid sequence and structural similarities to immunoglobulin C domains; in MHC class II molecules the two domains forming the peptide-binding cleft are contributed by different chains and are therefore not joined by a covalent bond (shown in Figure 7C and 7D). Another important difference is the peptide-binding groove of MHC class II molecules is open at both ends.

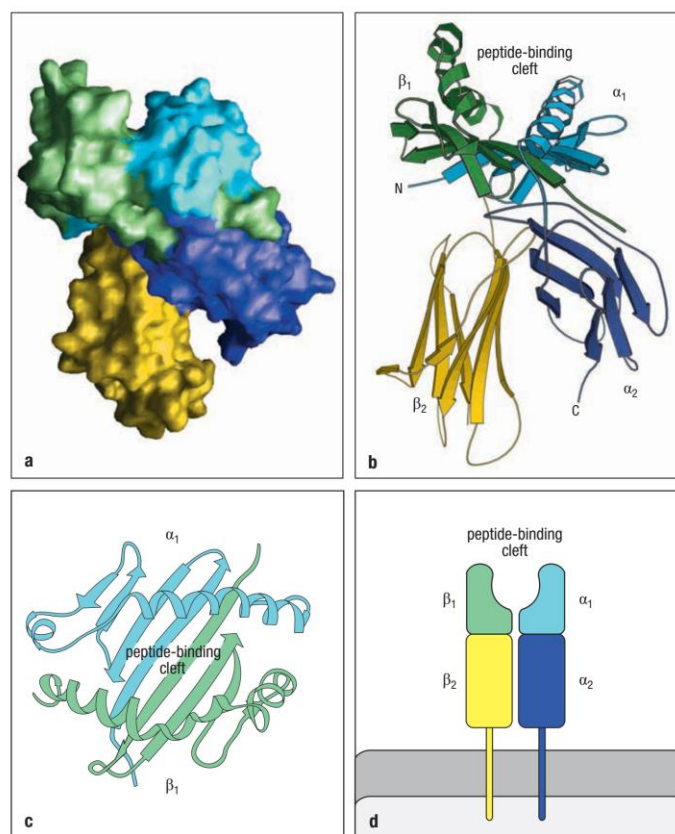


Figure 7. MHC class II molecules resemble MHC class I molecules in overall structure. Figure from text book *Janeway's Immunobiology 9th Edition, 2017* by Garland Science, Taylor & Francis Group, LLC (ISBN 978-0-8153-4505-3).

Foreign antigenic peptides from the outside of cells are presented by MHC class-II molecules to $CD4^+$ T cells (Helper T cells). These foreign peptides are about 10-30 amino acids in length, hence longer than the length of endogenous peptides. These foreign antigens activate $CD4^+$ T cells, which induce B cells to produce specific antibodies to foreign antigens. The characteristics of MHC class I and II molecules are summarized in Table 3.

Table 3. The characteristics of MHC class I and II molecules

| | MHC class I molecules | MHC class II molecules |
|--|---|--|
| Structure | $\alpha 1/\alpha 2/\alpha 3/\beta 2m$ | $\alpha 1/\alpha 2/\beta 1/\beta 2$ |
| Antigen binding cleft | $\alpha 1$ and $\alpha 2$ | $\alpha 1$ and $\beta 1$ |
| Binding location with T cells | $\alpha 3$ with CD8 molecule | $\beta 2$ with CD4 molecule |
| Classification | HLA-A, HLA-B, HLA-C | HLA-DR, HLA-DQ, HLA-DP |
| The characteristics of antigens | 8-11 amino acids | 10-30 amino acids |
| Tissue contribution | Present on most nucleated cells | Present only on antigen-presenting cells (APC) |
| Function | Binding endogenous antigens, presenting antigen to CD8 ⁺ T cells | Binding exogenous antigens, presenting antigen to CD4 ⁺ T cells |
| Antigen binding cleft | $\alpha 1$ and $\alpha 2$ | $\alpha 1$ and $\beta 1$ |

For antigens loading in HLA class-I molecules, these antigens must enter the DC cytoplasm to be processed by proteasome complex. Antigen fragments will be cut down by the proteasome into 8-11 amino acid which can be pumped through the transporter of antigen processing (TAP), thereby gaining access to the endoplasmic reticulum, where HLA class-I molecule loading with fragments of 8-11 aa take place, followed by transport to the cell surface.

For antigens loading in HLA class-II molecules, those antigens will enter the endosomal system, where cathepsins could digest the antigens, followed by loading of HLA class-II with fragments of 10-30 amino acids at low pH and following DC maturation, transport to the cell surface. Once DCs have fully matured, they interact with CD8⁺ and CD4⁺ T cells by stimulating TCRs with antigens presented by HLA class-I or II molecules, respectively, and costimulatory molecules such as CD28. Activated and primed CD8⁺ T cells can kill the tumor cells via ligation of TCRs with antigen presented by HLA class-I molecules (Figure 8 and Figure 9).

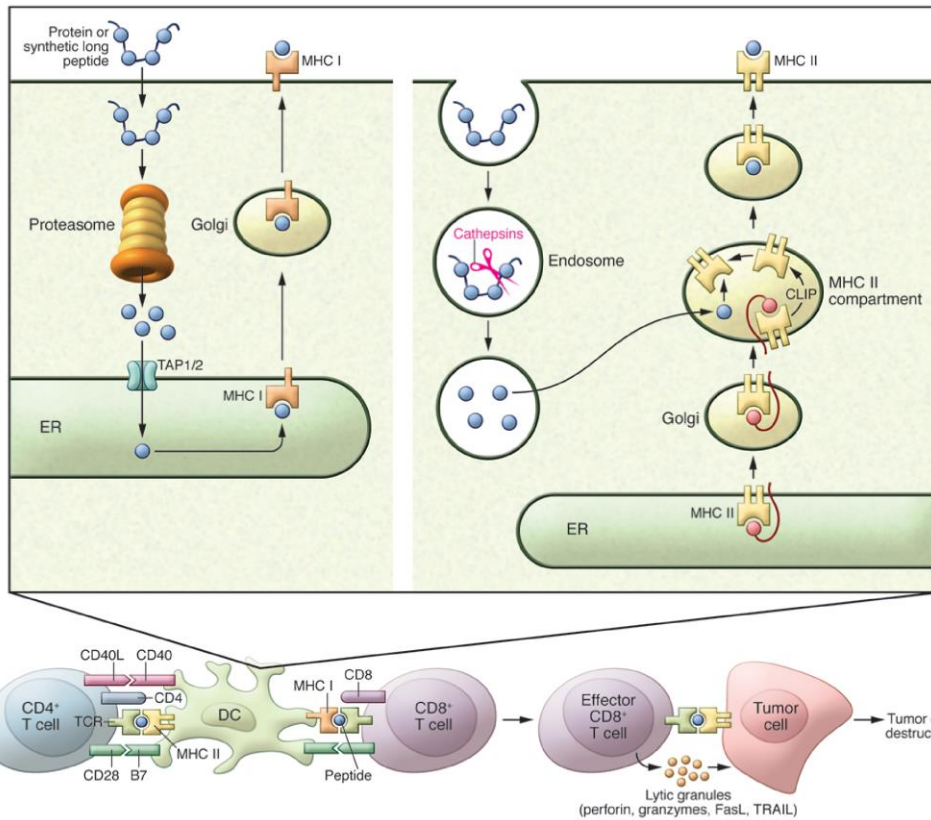


Figure 8. The processing of MHC class I and II molecules to recognize and present antigens. From *Cornelis J.M. Melief et al, Therapeutic cancer vaccines, J Clin Invest. 2015 Sep;125(9):3401-12.*

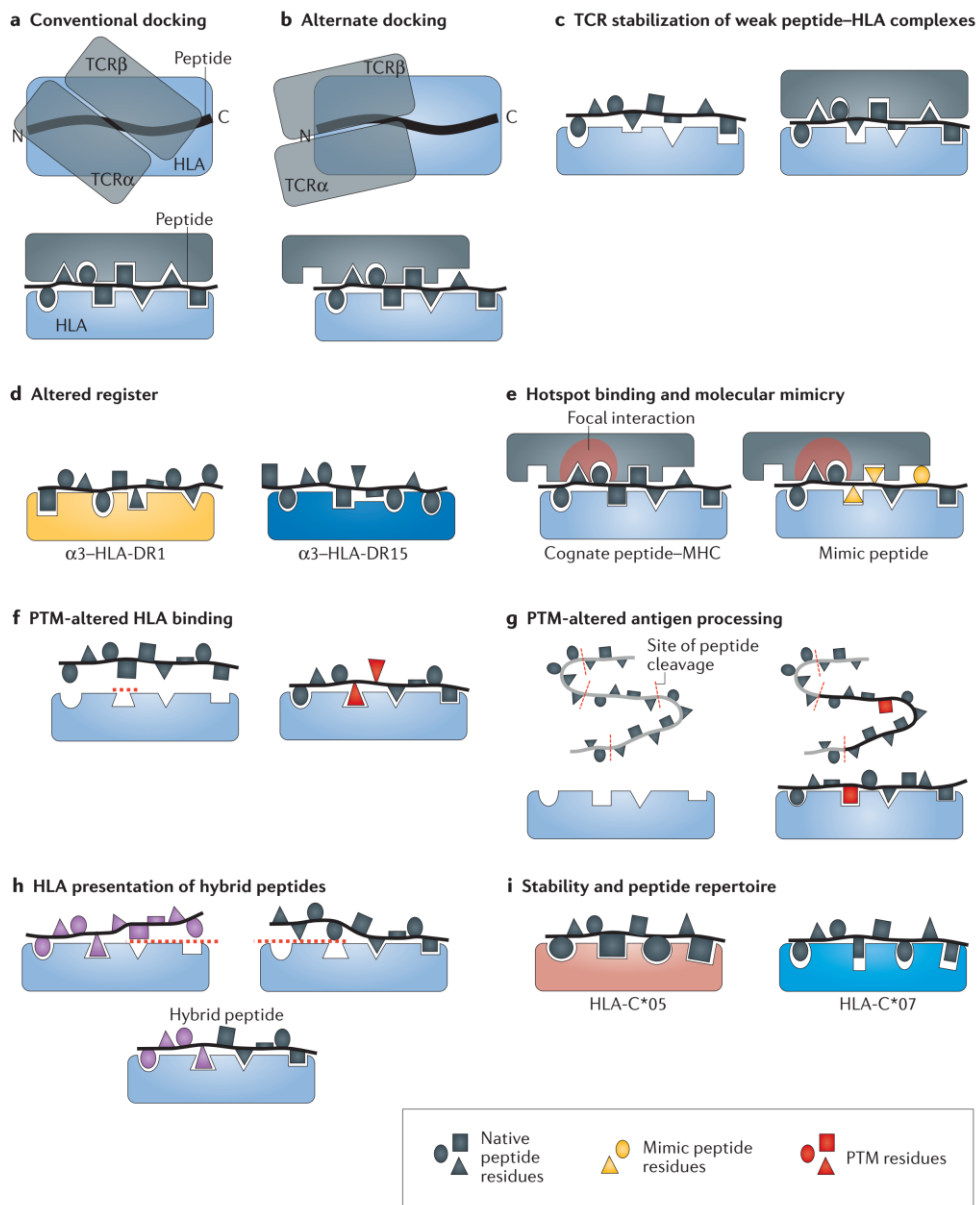


Figure 9. HLA-dependent molecular mechanisms of peptides and T cell receptors (TCR) binding. Reviewed by *Lars Fugger et al*, *HLA variation and disease, Nat Rev Immunol. 2018 May;18(5):325-339.* (PTM: post-translational modification)

2.4.2 Participation in the differentiation and development of T cells

T cell progenitors enter thymus from the circulation and then gradually differentiate and develop into mature T cells within thymic microenvironment (Figure 10). MHC class I and II molecules mediated the positive and negative selections of thymocytes, so that thymus progenitors could go through CD4⁺CD8⁻ double negative (DN, DN1-

DN4) stage to CD4⁺CD8⁺ double positive (DP) stage, and eventually differentiated into CD4⁺ and CD8⁺ single positive (SP) cells to obtain the restriction of MHC class I or II and the specificity to antigens, as well as the tolerance to autoantigen to avoid the emergence of autoimmune diseases.

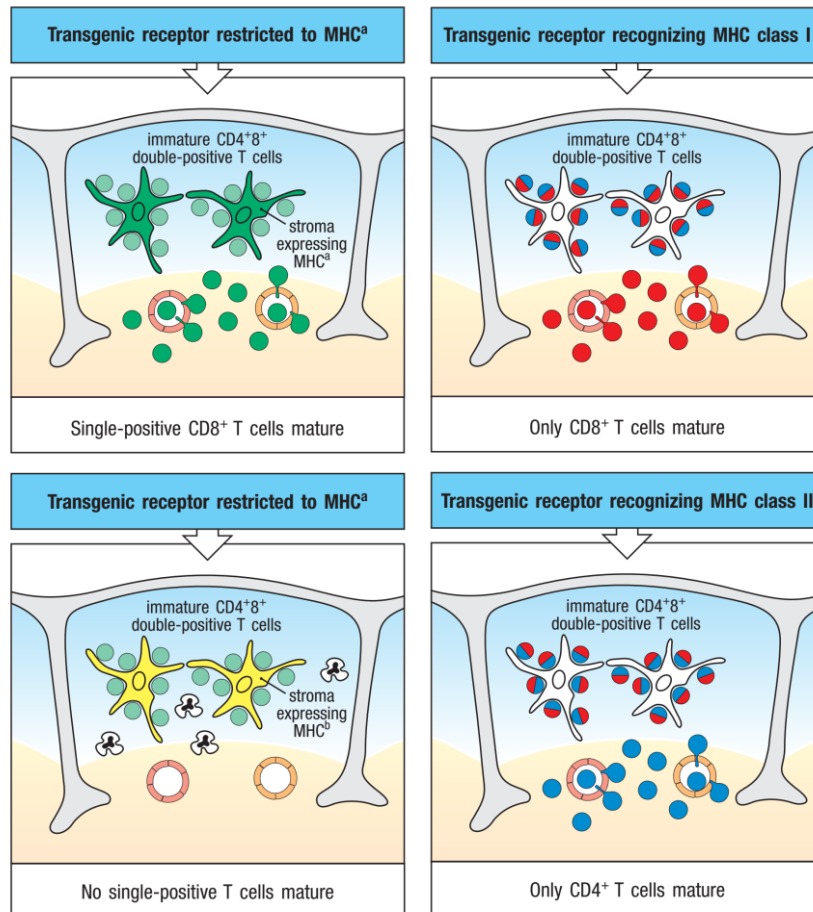


Figure 10. Positive selection is demonstrated by the development of T cells expressing rearranged T-cell receptor transgenes. The MHC molecules that induce positive selection determine co-receptor specificity. Figure from text book *Janeway's Immunobiology 9th Edition, 2017* by Garland Science, Taylor & Francis Group, LLC (ISBN 978-0-8153-4505-3).

2.4.3 Involvement in the genetic regulation of immune responses

MHC is also involved in the genetic regulation of immune responses as the high polymorphism of MHC molecules is at the origin of the difference in the ability of

different individuals in responding to the same antigen. The high polymorphism of MHC leads to the change of amino acid sequences and of protein structures of the encoded MHC molecules, which leads to the differences in the ability of different individuals to bind to the same antigens. This shows the genetic regulation of immune responses by MHC at the population level.

2.4.4 Regulate the innate immune responses

Besides of the functions discussed above, MHC molecules also regulate innate immune responses.

◆ MHC molecules participate in the complement reaction and inflammatory response.

The classical MHC class III gene is a gene complex encoding the complement component involved in the complement response and the regulation of immune diseases/disorders. Inflammation-related genes participate in the initiation and regulation of the inflammatory reaction and play vital roles in stress response.

◆ MHC molecules take part in the mediation of the activity of NK cells. MHC class I molecules expressed on the surface of own cells could bind to the inhibitory receptors expressed on the surface of NK cells. Thereby, it triggers the inhibitory signals and inhibits the activity of NK cells, so that normal/healthy cells will not be damaged by NK cells. Whereas the expression of MHC class I molecules on the surface of certain target cells (such as tumor cells, virus-infected cells) is reduced or absent, the inhibitory signal of NK cells is blocked, induced the activation of NK cells, targeting unhealthy cells which will be destroyed.

2.4.5 Other functions of MHC in immune responses

Besides presenting antigens and regulating immune responses, MHC complex also play critical roles in many other aspects, such as the histocompatibility between recipients and donors in transplantation. MHC class-I molecules are expressed on the surface of all nucleated cells. The expression of MHC class-I molecules in some malignant cells

is weakened or even absent, resulted in the low efficiency of activation of specific CD8⁺ T cells, and lead to the tumors escaping to immune surveillance eventually.

MHC molecules may protect against or fail to protect against cancers[4]. On the other hand, cells without expression of MHC class-II molecules in certain autoimmune diseases (Figure 11), can be induced to express MHC class-II molecules, such as the islet β cells in insulin-dependent diabetes mellitus and the enteric cells in celiac disease. The mechanism of aberrant expression and its immunopathological significance mentioned above are still unclear and need to be illuminated, which perhaps related to the over-activation of immune cells by MHC class-II molecules.

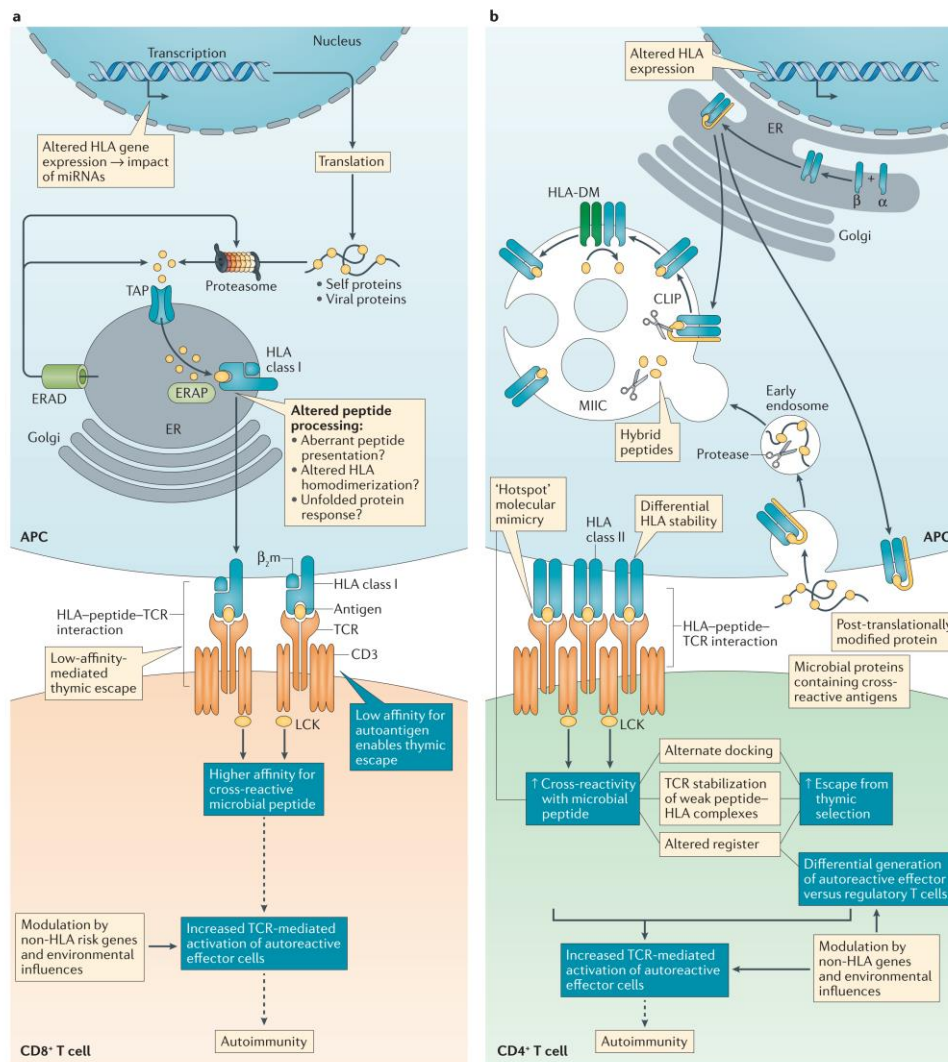


Figure 11. HLA-peptides-T cell receptors interactions could promote autoimmunity. Reviewed by *Lars Fugger et al, HLA variation and disease, Nat Rev Immunol. 2018 May;18(5):325-339.*

The MHC-peptide complex is a complex between MHC molecules and the autoantigens or alloantigen. After the recognition and binding, T cells will tolerate the autoantigens, while activate to alloantigen, which corresponds to the homeostasis and health state. The disease and imbalance state will occur when the principle above was disrupted. MHC molecules of different species have both similarities and differences in structure and functions[5]. These differences have led to many pre-clinical trials on experimental animals that have not been clinically validated. It also prompted the necessity and importance of the development of humanized MHC transgenic mouse models.

2.5 HLA genes are highly polymorphic

HLA complex is the most polymorphic gene system in human beings ever found (as shown in Figure 12 and Table 4). HLA system is a good community marker and has a high value for the study of human origin, migration, miscellaneous and the high incidence of several diseases in particular population[6]. There are more than thousands of alleles in HLA-A, HLA-B, HLA-C and HLA DR, far more than the numbers of alleles in HLA-DP and HLD-DQ.

Table 4. The alleles of HLA class I and II molecules

| Numbers of HLA Alleles | | | |
|-------------------------------|------|--------|------|
| HLA class-I molecules | 6376 | HLA-A | 2041 |
| | | HLA-B | 2668 |
| | | HLA-C | 1667 |
| HLA class-II molecules | 2050 | HLA-DR | 1213 |
| | | HLA-DP | 370 |
| | | HLA-DQ | 467 |

A kind of HLA allele found on a single chromosome is referred as an HLA haplotype. The expression of HLA alleles is codominant which means that the products of both

alleles at a locus expressed equally in one cell and could present the peptides of antigens to T lymphocytes simultaneously. The extensive polymorphism at each HLA allele and loci double the numbers of different HLA expressed in an individual, which increased the diversity in human population level.

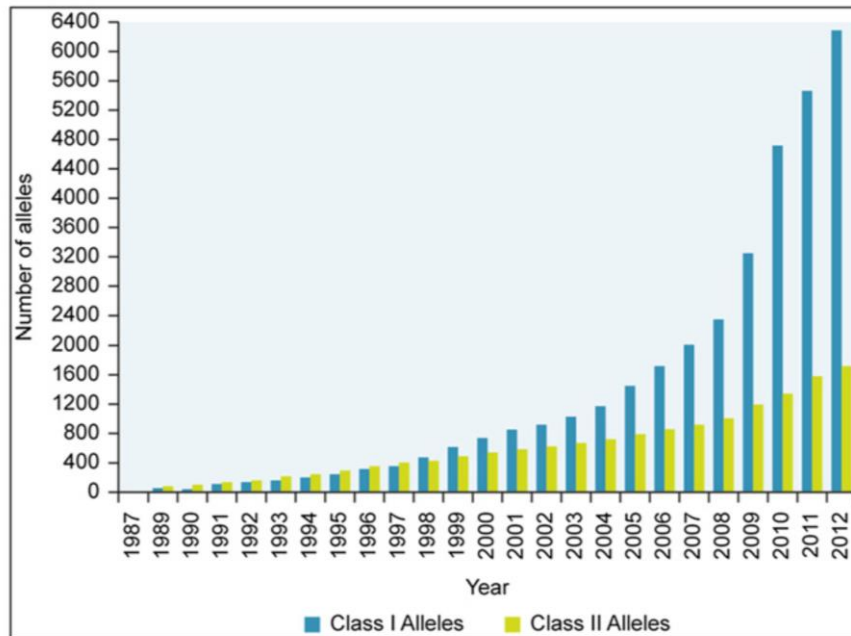


Figure 12. Defined HLA class I and class II alleles from 1968-2012. Graph taken from <http://www.ebi.ac.uk/imgt/hla/intro.html>, copyright SGE Marsh 07/2012, with permission.

2.6 Distribution of HLA alleles worldwide

The dominant HLA class I and II alleles are different from Europe, Asia and other continents (Figure 13). HLA-A02 with the highest frequency among HLA class-I alleles, accounts for 30-50% of global human population. While HLA-A11 accounts for about 20-30% of total population in Asia, only about 10% of Europe, America and Middle East, which have significant differences. Among HLA class II alleles, HLA-DR01 with the highest gene frequency in European and American populations, around 20-25%, while HLA-DR01 accounts for about 10-15% of Asia population. HLA-DR09 and HLA-DR15 with higher gene frequency distribution in Asia population, the phenotypic frequencies are 31.2% and 27.1%, respectively.

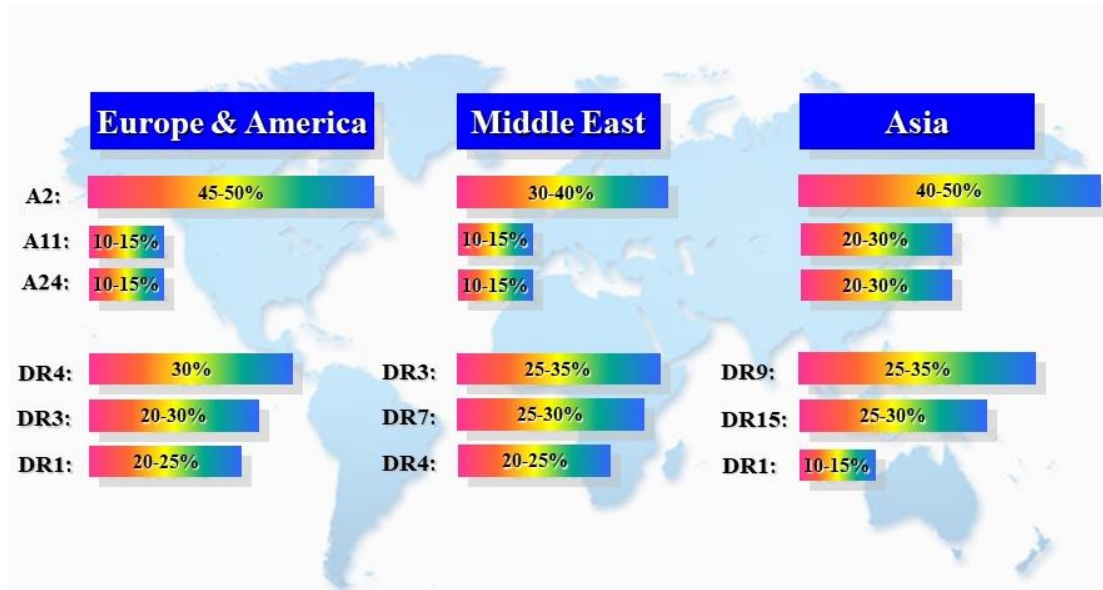


Figure 13. The dominant HLA alleles are different between continents.

2.7 The association between HLA and human diseases

More and more researches have revealed the association between HLA molecules and several human diseases (Figure 14). HLA molecules have proven to be important to physiology, protect immune response and inversely deleterious to autoimmune diseases. Some HLA alleles show associations with some autoimmune diseases, inflammatory and infectious diseases (as summarized in Figure 14 and Figure 15). Technological advances enabled the determination and mechanisms of the association between specific HLA molecule and diseases. Many HLA molecules are associated with the occurrence of autoimmune diseases. **HLA-B27** antigen was found in over 90% of Ankylosing Spondylitis (AS) patients, while proof-positive evidences had confirmed that the risk of incidence of AS and other associated inflammatory diseases in HLA-B27 carriers is increased [7]; Nevertheless, the mechanisms involved in the aberrant antigen presentation or T cell activation have not been clarified yet. Besides this, several HLA had relation with the occurrence of certain diseases, such as **HLA-DR4** and rheumatoid arthritis (RA)[8], **HLA-DQ8** and insulin-dependent diabetes mellitus (IDDM)[9], etc. Furthermore, susceptibility to some infectious diseases is also associated with HLA, such as tuberculosis, leprosy and HIV (Figure 16). The potential mechanisms of HLA associated impact on viral control is summarized in Figure 16.

| Table 1 Autoimmune disease–HLA associations for which molecular mechanisms of action have been identified | | | |
|---|--|---|---------------|
| HLA allomorph (effect on disease) | Autoimmune disease | Molecular mechanism of action | Refs |
| Alternate docking | | | |
| HLA-DR15 (risk) | Multiple sclerosis | <ul style="list-style-type: none"> • Alternate docking of a TCR may allow MBP peptide-specific T cells to escape thymic selection • In the periphery, such cells may be cross-reactive with microbial peptides | 15,16 |
| Low-affinity-mediated thymic escape | | | |
| HLA-A*02:01 (risk) | T1D | <ul style="list-style-type: none"> • Low affinity of a TCR for preproinsulin signal peptide–HLA may allow autoreactive T cells to escape thymic selection • This mechanism may depend on the thymic expression level of the autoantigen • In the periphery, these cells may bind microbial peptides with a high affinity | 17–19 |
| TCR stabilization of weak peptide–HLA complexes | | | |
| HLA-DR4 (risk) | Multiple sclerosis | <ul style="list-style-type: none"> • Weak MBP peptide–HLA-DR4 interaction is stabilized by binding of a patient-derived TCR • Low autoantigen density in the thymus may enable escape of autoreactive T cells from negative selection • Higher autoantigen density in the periphery could trigger an autoreactive response | 20–22 |
| Altered register | | | |
| HLA-DQ2 and HLA-DQ8 (risk) | T1D | <ul style="list-style-type: none"> • Insulin B-chain peptide binds HLA-DQ2 and HLA-DQ8 with a low-affinity peptide register • Low affinity may allow autoreactive T cells to escape thymic selection • In the periphery, autoreactive T cells may be cross-reactive with microbial peptides via molecular mimicry | 23,24 |
| HLA-DR15 (risk) HLA-DR1 (dominant protection) | Goodpasture disease | <ul style="list-style-type: none"> • HLA-DR15 and HLA-DR1 both bind an α3-chain of type IV collagen peptide (α3_{135–145}) but with a different binding register • When HLA-DR1 is present, this promotes the generation of autoantigen-specific regulatory T cells as opposed to effectors | 25 |
| 'Hotspot' molecular mimicry | | | |
| HLA-DR15 (risk) | Multiple sclerosis | <ul style="list-style-type: none"> • The probability of aberrant, off-target TCR reactivity induced by pathogen-derived peptides is increased for autoreactive TCRs with a highly focused footprint that predominantly binds only a small area of peptide • Patient TCRs have been identified that cross-react with HLA-DR15-restricted MBP and <i>Escherichia coli</i> or EBV-derived peptides | 16, 26–28, 32 |
| Post-translational modification | | | |
| HLA-DQ2.5 and HLA-DQ8 (risk) | Coeliac disease | <ul style="list-style-type: none"> • HLA-DQ2.5 and HLA-DQ8 present deamidated gliadins with a high kinetic stability, leading to sustained antigen presentation that may promote a pathogenic T cell response | 38–41 |
| HLA-DR4 (risk) | Rheumatoid arthritis | <ul style="list-style-type: none"> • Citrullination of autoantigens (for example, vimentin) facilitates binding to HLA-DR4 • Citrullination can also modify peptide cleavage, enabling retention of autoantigens | 34,35 |
| HLA-DR4 (risk) | T1D | <ul style="list-style-type: none"> • Vicinal disulfide bond creation in an insulin A-chain peptide presented by HLA-DR4 is needed for recognition by a patient-derived autoreactive TCR | 37 |
| Hybrid peptides | | | |
| HLA-DQ8 (risk) | T1D | <ul style="list-style-type: none"> • Hybrid proinsulin peptides present in pancreatic β-cells may drive a breakdown in immune tolerance | 51 |
| Regulation of HLA expression | | | |
| MHC risk variants in distal intergenic XL9 regulatory element | Systemic lupus erythematosus | <ul style="list-style-type: none"> • Risk variants alter the binding of the IRF4 and CTCF factors that regulate the transcription of <i>HLA-DRB1</i>, <i>HLA-DQA1</i> and <i>HLA-DQB1</i>, resulting in a 2.5-fold increase in the levels of the HLA-DR and HLA-DQ proteins implicated in lupus | 52 |
| Highly expressed HLA-C allotypes (risk) | Crohn's disease | <ul style="list-style-type: none"> • HLA-C allotypes with a high expression correlate with Crohn's disease risk • This expression is partly regulated by the microRNA miR-148a, which is itself subject to regulation by genetic variation | 53 |
| HLA stability | | | |
| HLA-DQ2 and HLA-DQ8 (risk) HLA-DQ6 (protection) | T1D, coeliac disease T1D, autoimmune polyglandular syndrome, IgA deficiency | <ul style="list-style-type: none"> • HLA-DQ2 and HLA-DQ8 instability could confer risk by allowing escape of autoreactive T cells from thymic negative selection but also by the formation of weak peptide–HLA complexes in the periphery with a range of autoantigens • By a converse mechanism, the stability of HLA-DQ6 may confer protection against autoimmune disease; despite such a mechanism, HLA-DQ6 confers risk of narcolepsy | 71–76 |

CTCF, transcriptional regulator CTCF; EBV, Epstein–Barr virus; IgA, immunoglobulin A; IRF4, interferon regulatory factor 4; MBP, myelin basic protein; T1D, type 1 diabetes; TCR, T cell receptor.

Figure 15. The associations between HLA and autoimmune diseases. Reviewed by Fugger L et al, *HLA variation and disease. Nat Rev Immunol. 2018 May;18(5):325-339.*

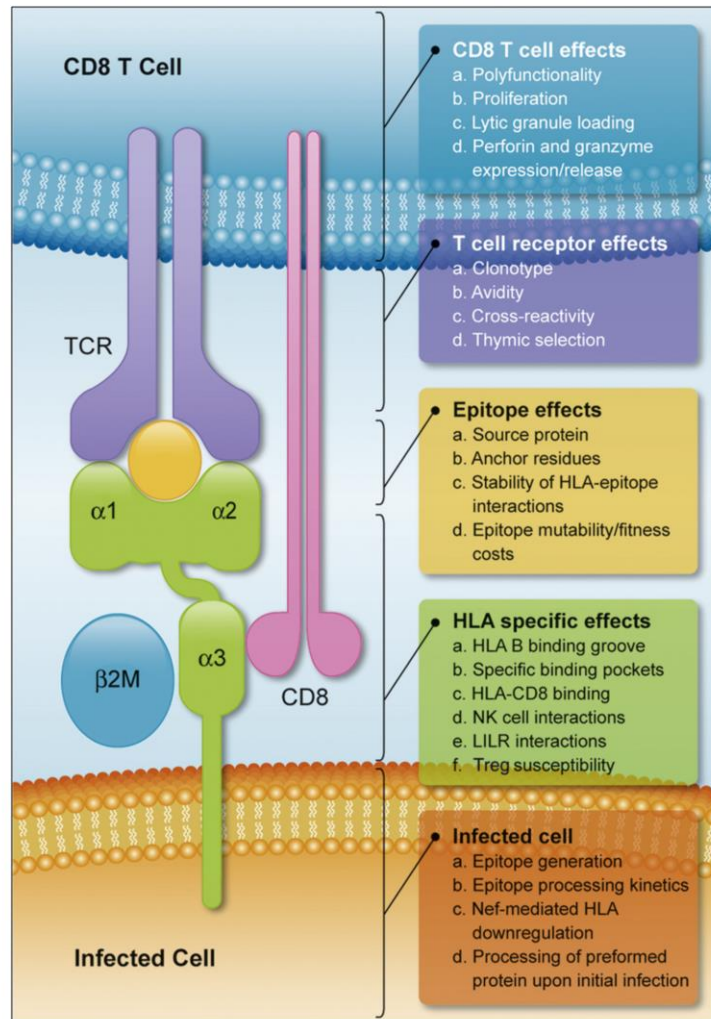


Figure 16. The potential mechanisms of HLA associated impact on viral control. Figure from Philip J.R. Goulder et al, *HIV and HLA class I: an evolving relationship*, *Immunity*. 2012 Sep 21;37(3):426-40.

3. Animal models in scientific research

Animal models play unreplacable roles in medical science research. Non-human primates such as rhesus monkeys and chimpanzees are like humans in terms of genetic background and physiological status. However, they are endangered animals with limited sources and their use is restricted by the experimental animal ethics, their expensive price also makes them difficult to promote at large scale. Small animal models such as mice, rats, tree shrews, rabbits, dogs and other animals are quite different from humans in terms of genome, metabolism and anatomy. Their species

specificity makes them are not the most optimal animal model for pre-clinical studies (Figure 17). Previous studies in these small animal models have led to divergent clinical outcomes in preclinical animal studies and authentic human clinical responses. These limitations need to be overcome to develop increasingly reliable preclinical studies.



Figure 17. The common small animal models applied to scientific research.

In recent years, with the outbreak of EBOV, MERS-CoV, SARS, H7N9 and other new or re-emerging infectious diseases globally, caused tremendous health and social harm. The development and evaluation of novel vaccines and drugs of important pathogens have become a top priority. However, many highly pathogenic microbes such as MERS, require early clinical treatment of patients after the onset of infection. However, it is difficult to obtain samples from the patients during natural infection. This hindered the studies on mechanisms and immune protection research.

3.1 Human MHC transgenic mouse models

MHC humanized mouse models are based on the strategy that human HLA molecules replaced murine H-2 molecules to execute the corresponding biological immunological function in murine immune system/ background, which could mimic human T cell responses preferably. Therefore, these new mouse models can be used to mimic human cellular immune response and thus to predict T cell responses against exogenous and endogenous antigen in human immune system, owing to the elimination of the

competitive inhibition of mouse H-2 molecules. The human HLA antigens mainly include HLA class-I and HLA class-II subsets and both subsets of HLA molecules participate in the regulation of cellular immune responses. Currently, most of the reported human MHC transgenic animal models are HLA class-I or class-II single transgenic mice which were used to study cytotoxic T cells (CTL) and helper T cell (Th) function, respectively.

Human MHC transgenic mice are promising mouse models which could replace previously traditional animal models. Construction of human MHC transgenic mice will apply to the screening and identification of MHC-restricted epitopes, the pathogenic mechanism of pathogens, the establishment of disease models and the evaluation of immunology therapies.

4. Immuno-deficient mouse models

Animal models play a critical role in scientific researches and pre-clinical experiments, such as the study of pathogenesis of diseases, the creation and evaluation of novel drugs and vaccines. The development of immuno-deficient mice was summarized in Table 5. While, some in vivo experimental studies that mimic human physiology and pathological conditions were hindered by the lack of optimal small animal models. Given that, by the respective genetic backgrounds, immune responses of human and non-human species show significant specific differences. Due to the ethical constraints[10] and higher cost of clinical trials, non-human primates (NHPs) have many limitations in researches. Although mice share up to 95% genes with human, however the physiological state and immunological state in murine are somehow different from that of the mankind, especially the MHC restriction which determined the species specificity in pre-clinical experiments which reflects the immune characteristics of humans.

Table 5. Summary of the development of immuno-deficient mice

| Strain | Year | Adaptive immunity and innate immunity | characteristics of human cell engraftment |
|--|--------------|--|--|
| SCID | 1983[11] | Deficiency of T and B cells | Low implantation efficiency |
| Rag1^{-/-} Rag2^{-/-} | 1992[12, 13] | Deficiency of T and B cells | Low implantation efficiency |
| NOD-Scid | 1995[14] | Deficiency of T and B cells; Decreased activity of NK cells | High implantation efficiency, short lifespan (8.5 months) |
| NOG | 2002[15] | Deficiency of T and B cells; Inactivity of NK cells | High implantation efficiency |
| BRG | 2004[10] | Deficiency of T and B cells; Inactivity of NK cells | High implantation efficiency, lower than NOG and NSG |
| NSG | 2005[16] | Deficiency of T, B and NK cells | High implantation efficiency, lifespan beyond 16 months |
| NSGW | 2014[17] | Deficiency of T, B and NK cells | High implantation efficiency, without prior irradiation |
| HUMAMICE | 2017[18] | Deficiency of T, B and NK cells | Human HLA transgenes, High implantation, without GvHD |

Humanized mice are immuno-deficient mice that have been transplanted with human tissues/cells, or have been genetically engineered to express transgenic human genes. The timeline for the development of immune-deficient mouse models was summarized in Figure 18. Mouse models and human cell models are complementary in pre-clinal period, and studies often need to be carried out in parallel[19]. The development history and enhancement of immune-deficient mice and humanized mouse models and their applications in hematology, HIV and tumor researches was reviewed next.

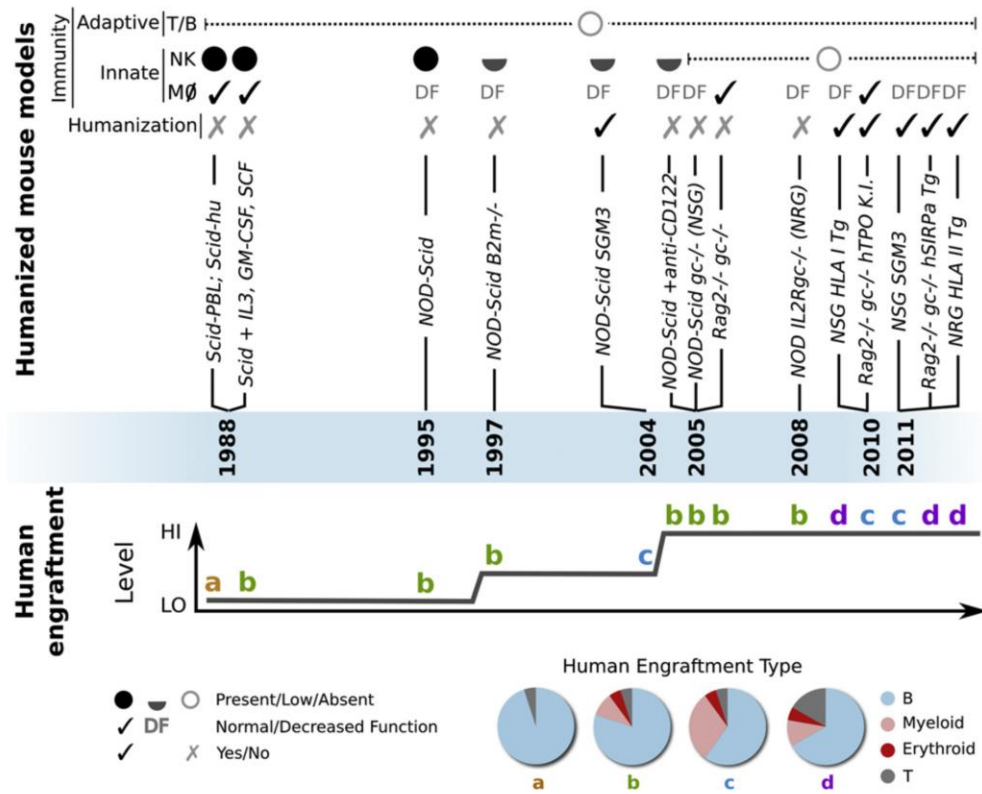


Figure 18. Timeline for the development of immune-deficient mouse models. Figure from *John E. Dick et al, Hematopoiesis: a human perspective, Cell Stem Cell, 2012 Feb 3;10(2):120-36.*

4.1 SCID (C.B-17 SCID) mice

It has been three decades since the creation of the first immune-deficient mice and that human hematopoietic cells were transplanted successfully. The breakthrough in humanized mouse models was the creation of the severe combined immuno-deficient (SCID) mouse model which was named C.B-17 SCID [11]. The partial pedigree of C.B-17 SCID mice show recessive inheritance of SCID syndrome which impaired the differentiation of both T and B lymphocytes. Consequently, the lifespan of most C.B-17 SCID mice is less than one year, which handled long-time transplantation and experiments. SCID mice represent a new model to investigate how lymphoid differentiation may be impaired in a disease state and regulated in a normal physiological state. SCID mice are broadly used in the transplantation of human peripheral blood leukocytes (PBL)[20], human fetal liver (FL) hematopoietic cells/fetal

thymus/fetal lymph node[21] and human bone marrow (BM) hematopoietic stem cell (HSC)[22], which could result in a comparable stable long-term reconstitution of a functional human immune system (HIS) in SCID mice.

Several approaches were applied to engraft human tissues/cells in SCID mice. Moiser[20] developed SCID-PBL mice model by transfer human PBL through i.v. or i.p. routes, which reconstituted human T cells, B cells, monocytes and macrophages. Specific human antibody response to tetanus toxoid was detected, which resulted in the survival of mice for at least six months. As MHC restriction in this model was still endogenous H-2 molecules, recipients generated almost mature T cells derived from donors' relative mature cells with HLA restriction, which cannot react with the antigen presenting cells (APC) of recipients. SCID-hu mice model was generated by surgical implantation of human fetal thymus, liver, lymph node or spleen into SCID mice, following with the injection of HLA-matched fetal liver cells. This resulted in a transient wave of human CD4⁺ T cells, CD8⁺ T cells and human IgG in the periphery, however no myeloid cells were detected. Namikawa established the first humanized-AIDS-mouse model by infecting the SCID-hu mice with HIV-1 virus[23].

Although human PBL and fetal liver (FL) cells were engrafted in SCID-PBL and SCID-hu mice successfully, purified human HSC transplantation need to be clarified in immune-deficient mice (to distinct from HSPC transplantation). Dick[24] transplanted human BM-derived HSC intravenously into SCID mice (SCID-repopulating cells, hu-SRC-SCID) infused with human IL-3, GM-CSF and SCF cytokines, resulted in the detection of myeloid progenitors in recipients even after 4 months, which confirmed that the transplantation was long-term and multi-potential. This model provided a criterion for the assay of human HSC activity in vivo faithfully.

SCID mice built the foundation for mouse models of human hematopoietic diseases and infectious diseases, however the engraftment was at a relatively low level, and implanted human cells could not differentiate into functional human immune cells. Since SCID mice with Prkdc mutation still have innate immune cells such as NK cells, which may bring the recovery of murine B and T lymphocytes (the occurrence over 90%).

4.2 Rag1^{-/-} and Rag2^{-/-} mice

Meanwhile, SCID mice are more sensitive to radiation than wild-type mice because of the radiation-repaired defects of SCID mice. Recombinant activation gene (Rag1 and Rag2)-deficient mice overcame the recovery of murine B and T lymphocytes which limited the studies in traditional SCID mice. The mutation in Rag1 and Rag2 prevented the production of mature T and B lymphocytes with the inability to perform V(D)J recombination, which induced higher levels of NK cells simultaneously. Nevertheless, Rag1^{-/-}[12] and Rag2^{-/-}[13] mice also restricted the implantation of human HSC to a certain extent.

4.3 NOD/SCID (NOD/LtSz-scid) mice

To generate an improved humanized mouse model with higher human engraftment level, Shultz[14] generated NOD/LtSz-scid mice by backcrossing SCID mice with non-obese diabetic (NOD/Lt) mice which defected in both adaptive immunity (B and T lymphocytes) and innate immunity (NK cells), and supported high level of human peripheral blood mononuclear cells (PBMC) engraftment. By means of this strategy, the susceptibility to HIV-1 infection was enhanced in this mouse model [25].

The activity of murine NK cells is important for the resistance to human BM HSC engraftment[26]. The level of endogenous NK cells activity in NOD/LtSz-scid mice was markedly lower than those in SCID mice, and this could remarkably facilitate the reconstitution of human hematopoietic cells. Due to the high incidence of thymic lymphoma, the lifespan of NOD/LtSz-scid mice was approximately 8.5 months under the SPF conditions.

4.4 Hu-BLT-SCID (human bone marrow-liver-thymus SCID)

Hu-BLT-SCID model was developed by the co-transplantation of human FL CD34⁺ cells and human fetal thymus/liver tissues which led to sustained human hematopoiesis and functional human immune system in NOD/SCID mice and NSG mice[27, 28]. Hu-

BLT-SCID mice showed systemic repopulation with comprehensive human lympho-hematopoietic cells, including T cells, B cells and dendritic cells (DC), high level of human IgM and IgG antibodies were detected. T cells generated in this model could undergo human thymus education and thymic selection because of the co-transplantation of human thymus[29]. Hu-BLT-SCID mice were widely used in the study of HIV biology and pathogenesis[30]. Thus, these improved mice model provided a powerful tool to study human immune function in vivo. As the MHC restriction in this model was still H-2, Hu-BLT-SCID mice were susceptible to the occurrence of Graft-versus-Host Disease (GvHD).

4.5 N/S-S/GM/3 mice and N/S- $\beta_2m^{-/-}$ -S/GM/3 mice

Hogge[31] and Eaves[32] transferred human growth factor genes Steel factor (SF), interleukin-3 (IL-3) and granulocyte macrophage-colony-stimulating factor (GM-CSF) into NOD/SCID mice and NOD/SCID- $\beta_2m^{-/-}$ mice to generate N/S-S/GM/3 mice and N/S- $\beta_2m^{-/-}$ -S/GM/3 mice, respectively. These novel models mobilized the engrafted human progenitors and improved the reconstitution of human cells, acute myeloid leukemia (AML) cells can be easily detected and quantitated.

4.6 NOG/NSG mice

Several approaches had been undertaken to improve the human cell engraftment level of NOD-Scid mice, such as the depletion of NK cells activity with anti-CD122 antibody, intra-femoral injection and the deletion or truncation of interleukin-2 (IL-2) receptor γ chain (IL-2R γ) molecule. IL-2R γ is indispensable for the signaling pathway mediated by IL-2, IL-4, IL-7, IL-9 and IL-15 [33]. The mutation of IL-2R γ gene in mice causes human X-linked severe combined immunodeficiency (XSCID) which characterized by decreased differentiation of T cells, B cells and NK cells [10, 34-36]. Based on IL-2R γ deficiency or knockout mice, NOG (NOD/SCID/ γ_c^{null}) [15], NSG (NOD/LtSz-scid IL-2R γ^{null}) [16] and NRG mice were created. 1×10^2 CD34⁺ cells could survive and differentiate in NOG mice. NSG mice generate higher humanized engraftment compared with NOG mice after the intra-femoral injection of human lineage-depleted

human umbilical cord blood (UCB) cells. The lifespan of NSG mice last beyond 16 months, the occurrence of lymphoma after sublethal irradiation was decreased, and the engraftment of human mobilized blood HSC was six-fold higher than traditional NOD/SCID mice.

The deficiency of cytokine signaling in NSG mice prevented the emergence of lymphomagenesis. Sex also affects the survival, proliferation, self-renewal and engraftment of human HSCs xenograft models, female recipients displayed much higher level of human chimerism than male recipients [37]. Brehm found that newborn immuno-deficient mice exhibited enhanced engraftment as compared to adult recipients. The immune-deficient NOD strains supported enhanced engraftment as compared to BALB/c strain [38].

The success of human HSC transplantation is also determined by the immunological compatibility which governed mainly by the MHC discrepancy between donors and recipients. However, several problems about humanized mouse models and human hematopoietic cells transplantation remain unclear, such as the histocompatibility barriers, different niches of hematopoiesis. Whether existing immuno-deficient mice could evaluate the engraftment of human HSC just like under the human physiological condition still in doubt. The other major experimental drawbacks for the studies using these above models was the rapid onset of GvHD after transplantation.

4.7 NSGS (NOD/LtSz-scid IL-2RG-SGM3)

Despite advances and improvements of human xenografts into mice, while most of the human acute myeloid leukemia (AML) samples could not engraft into mice successfully. The reasons to explain the failure may include the differences in homing, survival and expansion of human stem cells in foreign hematopoietic niche, and lack of human cytokines, human growth factors and supporting stromal cells. NSGS mice were developed by the backcross of NSG mice with N/S-S/GM/3 mice. As a result, NSGS mice constitutively express human SCF, GM-CSF and IL-3. AML xenograft level was significantly improved in NSGS mouse model[39, 40].

4.8 MITRG and MISTRG

MITRG (hM-CSF, hIL-3/hGM-CSF, hTPO⁺Rag2^{-/-}IL-2 γ ^{-/-}) and MISTRG (hM-CSF, hIL-3, hGM-CSF, hTPO⁺ Rag2^{-/-} IL-2 γ ^{-/-}hSIRP) with four genes encoding human cytokines that important for the development of innate immune cells were inserted into mouse loci[41]. SIRP is mainly expressed by macrophages, DCs, and neutrophils, and its ligand, CD47, is expressed almost ubiquitously. The SIRP-CD47 interaction is involved in regulating macrophage-mediated phagocytosis by delivering a licensing signal to macrophages. These human cytokines supported normal development of monocytes, macrophages and NK cells derived from human FL or adult CD34⁺ progenitor/stem cells implanted into mouse models. Human macrophages infiltrated human tumor xenograft in MITRG and MISTRG mice were similar with that observed in clinical patients. These humanized mouse models could be used as in vivo models for the evaluation of therapeutic candidates which were more relevant to actual human physiology.

4.9 NSGW mice

Both immune-deficient mice mentioned above need to be irradiated before transplantation. Rodewald[42] developed Rag2^{-/-}IL-2 γ c^{-/-}Kit^{W/W^v} mice which efficiently supported long-term HSC reconstitution derived from allogeneic donors without prior irradiation. Growth factor receptor-Kit is independent of HSC self-renewal in vivo. Kit mutant mice are endogenous HSC-deficient which could benefit to the implant of histocompatible or histoincompatible HSCs. Waskow[17] developed four immune-deficient mouse strains containing Kit mutations which supported robust, sustained and serially transplantation of human HSCs without irradiation. These mice were BRg Kit^{W^v/W^v} (BRgW_v), NSG Kit^{W^v/W^v}, (NSGW_v), NSG Kit^{W^v/+} (NSGW_v/+) and NSG Kit^{W⁴¹/W⁴¹} (NSGW41). Human HSCs engrafted efficiently in both newborn and adult NSGW recipients, sustained multi-lineage could contribute to series transplantation (in both first and second transplantation)[43].

5. HSC transplantation (HSCT)

The transplantation efficiency of different sources of human hematopoietic cells is variable. Freshly UCB progenitor cells showed more efficient engraftment than mobilized adult progenitor cells[44]. The higher engraftment efficiency of UCB cells may relate to the increased ability to traverse sinusoidal endothelium which is a crucial step of stem cells homing. Schoot[45] found that human UCB CD34⁺ cells showed more significant migration than BM or PB derived CD34⁺ cells did, which is possibly due to the differences in sensitivity towards SDF-1, which means that reduced number of UCB-derived CD34⁺ cells is required for human HSC transplantation. A controversial idea elaborated that the delayed reconstitution after UCBT may due to some defects of the homing-related molecules[46].

At present, HSC transplantation (HSCT) is widely used for the treatment of patients with hematological diseases and acute radiation injury in clinical. However, HSCT was limited by the inadequate numbers of HSCs in BM and UCB to some extent. Therefore, scientists had to carry out studies on in vitro expansion of HSCs and joint transplantation experiments to test the function of HSCs.

5.1 The identification of human HSC phenotypes

Current models of lineage determination in the adult Mouse and Human hematopoietic hierarchies was summarized in Figure 19. Xenogeneic engraft models are crucial to the phenotype identification of human HSCs. By transplantation of immuno-deficient mice, CD34 was discovered expressed on the surface of human hematopoietic stem and progenitor cells[47]. CD34⁺ mobilized human BM and PB cells were widely used in clinical HSC transplantation (HSCT)[48]. Dick[49] first identified human HSCs which capable of long-term multilineage engraftment at single-cell resolution, the phenotype of UCB-derived long-term (LT) HSC was **Lin⁻CD34⁺CD38⁻CD90⁺CD45RA⁻CD49f⁺Rho^{low}**, which stood out as the notable landmark in the identification and verification of human HSC at single-cell level.

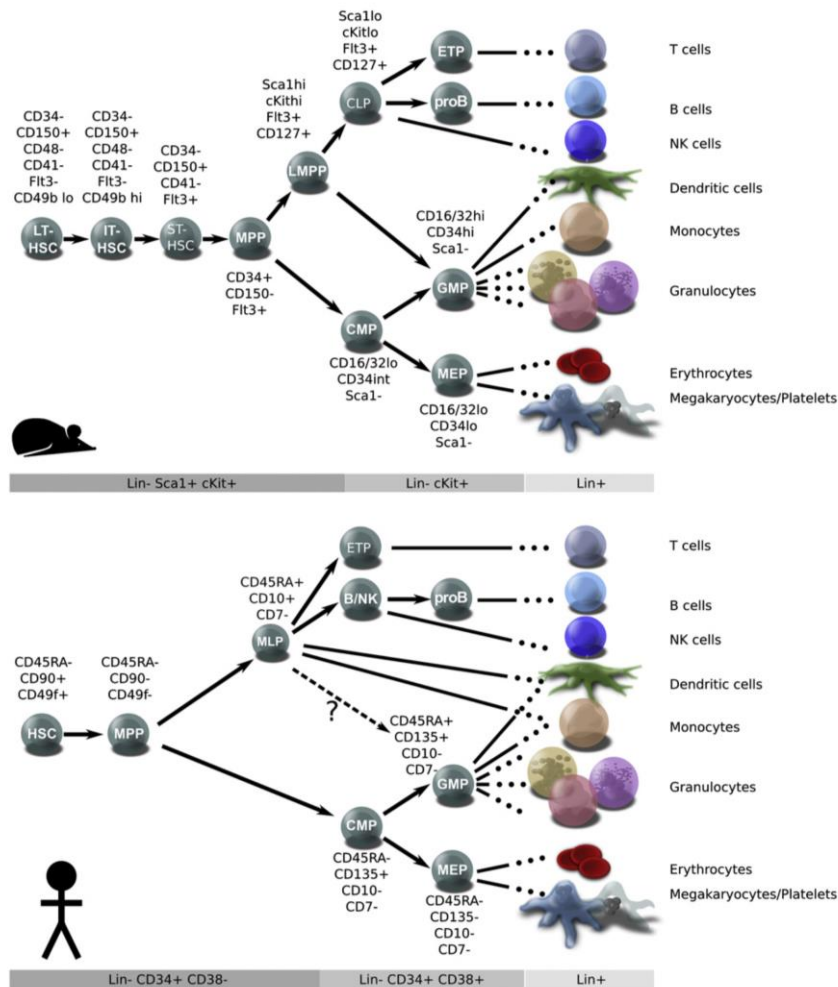


Figure 19. Current models of lineage determination in the adult mouse and human hematopoietic hierarchies. Figure from *John E. Dick et al, Hematopoiesis: a human perspective, Cell Stem Cell, 2012 Feb 3;10(2):120-36.*

The development and enhancement of immuno-deficient mice which could be engrafted with human cells have provided a powerful approach for the studies of hematopoiesis, tumorigenesis, the development and evaluation of novel drugs and vaccines. Immuno-deficient mice and humanized mice have many advantages which could be utilized to study the development, differentiation and hematopoietic reconstitution of human HSC in vivo and benefit clinical HSCT. It can also be used to evaluate the effects of drugs or cytokines on hematopoietic system. However, these mouse models also have some drawbacks, such as short lifespan, highly sensitive to irradiation and the high-price which limited the extensive application. With the rapid

progress of technology, immuno-deficient mice and humanized mouse models are continued to be developed and improved, providing more experimental evidence for clinical treatment of hematological diseases. The final aim of current animal models is to improve them so that they could mimic faithfully human physiology, particularly the human immune system.

5.2 In vitro amplification of human HSC

Among them, some small molecules compounds have good application prospect to promote human HSC expansion in vitro due to their stable properties and convenient administration. Prostaglandin E2 (PGE2) enhanced the homing, survival and proliferation of human HSC, led to long-term reconstitution[50-52]. Cooke[53] found that Stem Regenin 1 (SR1) promoted the ex vivo expansion of human CD34⁺ cells by antagonizing aryl hydrocarbon receptor (AHR), which led to 50-fold increase of human HSCs in vitro and 17-fold increase reconstitution in vivo. Sauvageau[54] found that pyrimidoindole derivatives UM171 could stimulate the expansion of human CB-derived HSCs and promote the self-renewal of HSCs, which led to human reconstitution last for at least 6 months in NSG mice.

5.3 The other factors effect human HSC transplantation

DNA methylation and histone deacetylation may also affect the proliferation of human HSC. 5aza 2' deoxycytidine (5azaD) and trichostatin A (TSA) could improve the expansion of primitive HSC/HPC in vitro[55]. Ruthardt[56] discovered that valproic acid (VPA) stimulated the proliferation and self-renewal of human HSC both in vitro and in vivo.

The optimization of micro-environment of recipients also promoted the human hematopoietic reconstitution of HSC transplantation. Antioxidant N-acetyl-L-cysteine (NAC) increased the engraftment of human HSC by decreasing the reactive oxygen species (ROS) levels in BM of NOD/SCID and NSG mice[57].

MHC restriction was critical to the human engraftment in immune-deficient mice. Lone[18] developed HUMAMICE (HLA-A2^{+/+}/DR1^{+/+}/H-2-β2m^{-/-}/IAβ^{-/-}/Rag2^{-/-}/IL-2rγ^{-/-}/Perf^{-/-} mice) expressed both human HLA class I and II molecules instead of mouse H-2 class I and II molecules, and whose immuno-deficient status was reversed by the transfer of functional HLA-matched hPBMCs, which could produce mice with an immuno-competent status with functional human immune system.

6. Vaccines

Vaccines are the biological preparations containing the antigens for artificial active immunization, which could provide active acquired immunity to specific disease/pathogen. Vaccines had undergone approximately a hundred years of development (as shown in Figure 20). Conventional vaccines include the inactivated pathogens, live attenuated pathogens and toxoids. New vaccines contain subunit vaccines, synthetic-peptides vaccines and DNA vaccines. Vaccines can also be divided according to the function as prophylactic vaccines and/or therapeutic vaccines[58].

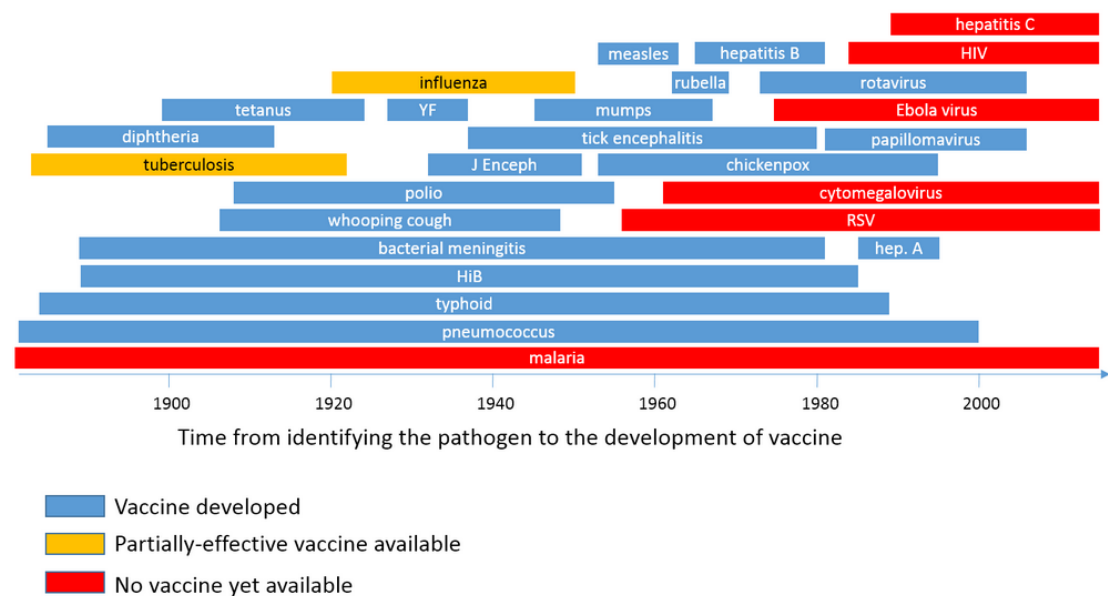


Figure 20. Timeline of vaccine development in this century.

6.1 Human oncogenic viruses, associated diseases and vaccines

Vaccines are the most frequently-used biological agents for immunoprophylaxis. Common human oncogenic viruses, associated diseases and vaccine targets are summarized in Table 6.

Table 6. Human oncogenic viruses, associated diseases and vaccine targets. Table from *Cornelis J.M. Melief et al, Therapeutic cancer vaccines, J Clin Invest. 2015 Sep;125(9):3401-12.*

| Virus | EBV | Human T lymphotropic virus I | HBV | HCV | HPV | KSV | Merkel cell carcinoma virus |
|-----------------------------|---|---------------------------------|----------------------------------|----------------------------------|---|---|---|
| Type of virus | Herpes virus | Retrovirus | Hepadna virus | RNA flavivirus | Papilloma virus | Herpes virus | Polyoma virus |
| Associated diseases | Nasopharyngeal carcinoma, B cell lymphomas, Hodgkin's disease | Adult T cell leukemia, lymphoma | Cirrhosis, hepatocellular cancer | Cirrhosis, hepatocellular cancer | Anogenital cancer, head and neck cancer | Sarcomas in immunodeficient individuals | Skin cancer |
| Therapeutic vaccine targets | LMP1 ^A , LMP2 ^A | Tax protein ^A | All HBV proteins | All HCV proteins | E6 oncoprotein ^A , E7 oncoprotein ^A | All KSV proteins | Large T protein ^A , small T protein ^A |

^AOncogenic proteins. LMP1/2, late membrane protein 1/2. KSV, Kaposi sarcoma virus.

The administration of vaccines is named as vaccination, and it is the most effective method to prevent infectious diseases up to now. Vaccinated people could acquire adaptive immunity against specific diseases after vaccination. Vaccines can stimulate the immune system to recognize pathogens as dangerous threaten and then destroy them, and even the antigens associated with these agents that may be encountered in foreseeable future. Widespread vaccination of smallpox, measles and tetanus vaccines had eliminated these diseases worldwide. Moreover, the effectiveness of influenza vaccine and HBV vaccine had been widely verified. The process of a vaccine candidate from the design to preclinical trials, to clinical trials and to final approved was time-consuming and difficult, only approximately 1% of total vaccine candidates could be validated and approved by FDA (Food and Drug Administration) (Figure 21).

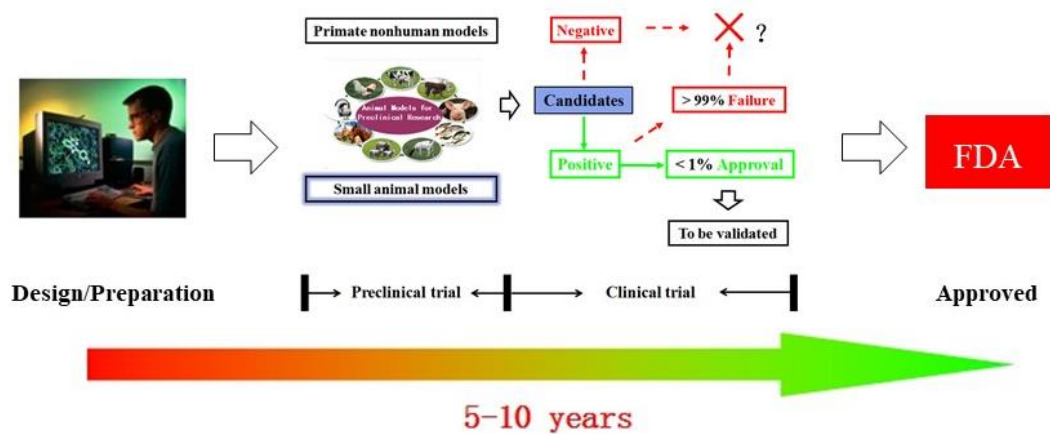


Figure 21. The process of a vaccine candidate from the design to preclinical trials, clinical trials and final approved.

6.2 Epitopes-based vaccines

In recent years, due to the progress in the fields of safety, non-toxicity and stability of epitopes-based vaccines, the research and application of epitopes and epitopes-based vaccines have been rapidly developed and the immune effect of vaccines have been greatly improved. However, there are still many challenges in immunological research and medical practice which need to be overcome.

The application of peptides-based vaccines is based on three distinct steps to create a specific anti-tumor immune response. To initiate immunity, DCs, which are taken up exogenously as part of a therapeutic vaccine differentiate into immunogenic mature DCs. DCs could enable the presentation of peptides on major histocompatibility complex (MHC) class I and II molecules (Figure 22). High affinity peptides may load onto MHC molecules directly at the cell surface of DCs. The exact mechanism of the peptide-based vaccines uptake may vary depending on the sequence of different peptides[59].

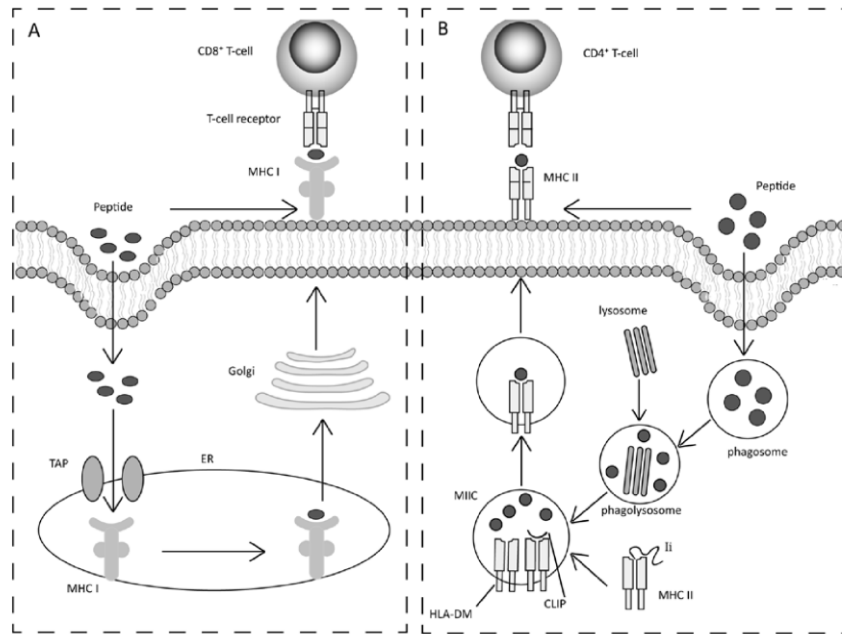


Figure 22. Entry of peptide-based vaccines through the MHC I or MHC II pathway. Figure from Zheng JN et al, *Composite peptide-based vaccines for cancer immunotherapy, Int J Mol Med.* 2015 Jan;35(1):17-23.

Gaps between clinical immune effect between epitopes-based vaccines as well as current conventional vaccines are described, due to low molecular weight of peptides and their weak immunogenicity. Moreover, the research on epitopes-based vaccines were mostly focused on linear epitopes, and conformational epitopes are still lacking[60].

In addition to some extent, adjuvants may also lead to side effects of epitopes-based vaccines. To effectively enhance the immunogenicity of epitopes-base vaccines, B cell epitopes, CTL epitopes and Th epitopes should be combined rationally, to stimulate the comprehensive specific humoral and cellular immune responses.

6.3 Personalized vaccines for cancer immunotherapy

Cancer and tumor are characterized by a gradually accumulation of genetic mutations. Somatic mutations can generate cancer-specific neoepitopes which could be recognized

by T cells as foreign antigens and to constitute the ideal candidate cancer vaccine targets. Different tumor has its own unique mutations, with only a small fraction of mutations shared between different patients. The rapid development of technological advances in genomics, proteomics and cancer immunotherapy enable the mapping of the mutations within different cancers and tumors, meanwhile, the rational selection of candidate vaccine targets, the design and production of a therapy customized to a patient. The vaccinating a patient with individual tumor mutations may become the first truly personalized treatment for cancer, which also is the implication and purpose of precision medical. Current vaccine formats explored for delivery of neoepitopes were summarized in Table 7.

Table 7. Current vaccine formats explored for delivery of neoepitopes. Table from *Türeci Ö, et al. Personalized vaccines for cancer immunotherapy. Science. 2018 Mar 23;359(6382):1355-1360.[61]*

| Vaccine format | Advantages | Challenges |
|---|--|--|
| Synthetic peptides | <ul style="list-style-type: none"> ➤ Cell-free manufacturing; ➤ Automated synthesis established; ➤ Proven clinical activity of long peptides; ➤ Compatible with a wide range of formulations to improve delivery; ➤ Transient activity and complete degradation | <ul style="list-style-type: none"> ➤ Lack of clinical-grade manufacturability of a substantial portion of sequences; ➤ High variability in the physicochemical properties of individual peptides, complicating manufacturing; ➤ Irrelevant immune responses against artificial epitopes created by peptide degradation in the extracellular space |
| Messenger RNA | <ul style="list-style-type: none"> ➤ Cell-free manufacturing; ➤ Inherent adjuvant function via TLR7, TLR8 and TLR3 signaling; ➤ Proven clinical activity; ➤ Highly efficient systemic delivery into DCs established; ➤ Transient activity and complete degradation; ➤ All types of epitopes can be encoded | <ul style="list-style-type: none"> ➤ Fast extracellular degradation of mRNA if not protected by appropriate formulation; ➤ Interpatient variability of TLR7-driven adjuvant activity |
| DNA plasmids | <ul style="list-style-type: none"> ➤ Cell-free manufacturing; Inherent adjuvant activity driven by TLR9; ➤ Cost-effective and straight forward manufacturing; ➤ All types of epitopes can be encoded | <ul style="list-style-type: none"> ➤ Potential safety risks by insertional mutagenesis; Successful transfection requires entry into nucleus, thereby limiting effective delivery of vaccines into DCs |
| Viral vectors | <ul style="list-style-type: none"> ➤ Strong immunostimulatory activity Extensive clinical experience with vector formats in the infectious disease field All types of epitopes can be encoded | <ul style="list-style-type: none"> ➤ Complex manufacturing; ➤ Immune responses against components of the viral vector backbone, limiting successful in vivo vaccine delivery and efficacy |
| Engineered attenuated bacterial vectors | <ul style="list-style-type: none"> ➤ Strong immunostimulatory activity; ➤ Could be combined with plasmid DNA; ➤ All types of epitopes can be encoded | <ul style="list-style-type: none"> ➤ Complex manufacturing and "sterility" testing; ➤ Immune responses against bacterial components, limiting vaccine delivery and vaccine immunogenicity potential safety risks due to delivery of live, replication-competent bacteria |
| Ex vivo antigen-loaded DCs | <ul style="list-style-type: none"> ➤ Strong immunostimulatory activity; ➤ Proven clinical efficacy of DC vaccines; ➤ Can be loaded with various antigen formats | <ul style="list-style-type: none"> ➤ Higher costs and resources required for adoptive cell therapy approaches |

RESULTS

Part 1. Creation of an immuno-deficient HLA-transgenic mouse (HUMAMICE) and functional validation of human immunity after transfer of HLA-matched human cells

Yang Zeng, Bingrun Liu, Marie-Thèrèse Rubio, Xinyue Wang, David M. Ojcius, Ruoping Tang, Antoine Durrbach, Zhitao Ru, Yusen Zhou, Yu-Chun Lone*

RESEARCH ARTICLE

Creation of an immunodeficient HLA-transgenic mouse (HUMAMICE) and functional validation of human immunity after transfer of HLA-matched human cells

Yang Zeng^{1,2}, Bingrun Liu², Marie-Thérèse Rubio³, Xinyue Wang², David M. Ojcius⁴, Ruoping Tang⁵, Antoine Durrbach^{2,6}, Zhitao Ru^{1,2}, Yusen Zhou¹, Yu-Chun Lone^{2*}



1 State Key Laboratory of Pathogen and Biosecurity, Beijing Institute of Microbiology and Epidemiology, Beijing, China, **2** INSERM U1197 (ex U1014), Hospital Paul Brousse, University of Paris-Sud, Université Paris-Saclay, Villejuif, France, **3** Service d'Hématologie de médecine interne, Hôpital Brabois, CHRU Nancy, Vandoeuvre les Nancy, France, **4** CNRS UMR 7365, IMoPa, Biopole de l'Université de Lorraine, Vandoeuvre les Nancy, France, **5** Department of Biomedical Sciences, University of the Pacific, Arthur Dugoni School of Dentistry, San Francisco, CA, United States of America, **6** Tumorothèque du service d'Hématologie de l'Hôpital Saint-Antoine, Assistance Publique-Hôpitaux de Paris (AP-HP), Paris, France, * yu-chun.lone@inserm.fr

OPEN ACCESS

Citation: Zeng Y, Liu B, Rubio M-T, Wang X, Ojcius DM, Tang R, et al. (2017) Creation of an immunodeficient HLA-transgenic mouse (HUMAMICE) and functional validation of human immunity after transfer of HLA-matched human cells. PLoS ONE 12(4): e0173754. <https://doi.org/10.1371/journal.pone.0173754>

Editor: Ali A. Ashkar, McMaster University, CANADA

Received: January 27, 2016

Accepted: February 27, 2017

Published: April 11, 2017

Copyright: © 2017 Zeng et al. This is an open access article distributed under the terms of the [Creative Commons Attribution License](https://creativecommons.org/licenses/by/4.0/), which permits unrestricted use, distribution, and reproduction in any medium, provided the original author and source are credited.

Data Availability Statement: All relevant data are within the paper.

Funding: This work was supported by grant from CAS President's International Fellowship Initiative (PIFI). Yusen Zhou was supported by the National Project of Infectious Disease (2012ZX10004502).

Competing interests: David Ojcius is a member of the editorial board of PLoS ONE. This does not alter our adherence to PLOS ONE policies on sharing data and materials.

Abstract

Research on human immunology has been hindered by the lack of optimal small animal models, given that the protective immune responses of human and non-human species show significant differences. However, due to ethical constraints[1] and the high cost of clinical trials, it is urgent to improve the current animal models that can mimic faithfully human physiology, particularly the human immune system (HIS). HIS mice had been generated recently by engrafting human hematopoietic stem cells (hHSCs) or human peripheral mononuclear cells (hPBMCs) into highly immuno-deficient mice such as NSG, NOG or NRG mice. However, a major experimental drawback for studies using these models is the rapid onset of Graft-versus-Host Disease (GvHD). In the present study, we overcome this limitation by generating new immuno-deficient mice named "HUMAMICE" (HLA-A2^{+/+}/DR1^{+/+}/H-2-β₂m^{-/-}/IAB^{-/-}/Rag2^{-/-}/IL2γ^{-/-}/Perf^{-/-} mice), which expressed human HLA molecules instead of mouse MHC molecules (H-2), and whose immuno-deficient status was reversed by transferring functional HLA-matched PBMCs thus producing mice with an immuno-competent status with a functional human immune system. We showed that in this HLA-matched context, the hPBMC-transfer led to high lymphocytes engraftment rates without GvHD over three months in this novel mouse model. Furthermore, to evaluate the utility of the hPBMC-HUMAMICE, we immunized them with commercial vaccine of Hepatitis B virus (HBsAg, Hepvac@) which resulted in robust and reproducible production of high levels of HBsAg-specific antibodies, implying that both transferred T and B lymphocytes were functional in HUMAMICE. These responses are comparable to those observed in human clinical trials with this identical vaccine. In conclusion, these findings indicated that the HLA-matched-hPBMC-HUMAMICE represents a promising model for dissecting human immune

Abstract

Research on human immunology has been hindered by the lack of optimal small animal models, given that the protective immune responses of human and non-human species show some differences. However, due to ethical constraints[10] and the high cost of clinical trials, it is urgent to improve current animal models that can mimic faithfully human physiology, particularly the human immune system (HIS). HIS mice had been generated recently by engrafting human hematopoietic stem cells (hHSCs) or human peripheral mononuclear cells (hPBMCs) into highly immuno-deficient mice such as NSG, NOG or NRG mice. However, a major experimental drawback for studies using these models is the rapid onset of Graft-versus-Host Disease (GvHD). In the present study, we overcame this limitation by generating new immuno-deficient mice named “HUMAMICE” (HLA-A2^{+/+}/DR1^{+/+}/H-2-β₂m^{-/-}/IAβ^{-/-}/Rag2^{-/-}/IL-2rγ^{-/-}/Perf^{-/-}), which expressed human HLA molecules instead of mouse MHC molecules (H-2), and whose immuno-deficient status was reversed by transferring functional HLA-matched PBMCs thus producing mice with an immuno-competent status with a functional human immune system. We showed that in this HLA-matched context, the hPBMC-transfer led to high lymphocytes engraftment rates without GvHD over two months in this novel mouse model. Furthermore, to evaluate the utility of the hPBMC-HUMAMICE, we immunized them with commercial vaccine of Hepatitis B virus (HBsAg, Hepvac@) which resulted in robust and reproducible production of high levels of HBsAg-specific antibodies, implying that both transferred T and B lymphocytes were functional in HUMAMICE. These responses are comparable to those observed in human clinical trials with this identical vaccine. In conclusion, these findings indicated that the HLA-matched-hPBMC-HUMAMICE represents a promising model for dissecting human immune responses in various human diseases, including infectious diseases, cancers and tumors and to facilitate the development of novel vaccines and cellular therapies.

Introduction

Mice functionally engrafted with human hematopoietic cells (hHSCs) may represent a valuable preclinical tool for basic and applied investigations in human immune system[62]. The current reference models for such humanized mice involved grafting a functional human immune system into immuno-deficient mice, for example, NSG[63], NOG, NRG, Rag2^{-/-} [64] and IL-2 γ ^{-/-} mice [65-67]. These highly immuno-deficient mice lack almost entire mouse-derived immune system, including murine B cells, T cells, and natural killer cells. These models have certain advantages for fostering the survival and expansion of human donor cells, but also have several limitations and drawbacks[68, 69]. However, the maintenance of HLA compatibility is necessary for ensuring proper function of a normal human immune system in a murine genetic background. Indeed, after hPBMC transferred, a constant and rapid onset of xenogeneic Graft-*versus*-Host Disease (xeno-GvHD[70]) was observed in all hPBMC-humanized mice. This complication caused researchers to avoid these models for studies of human immune system[71], in particular, to explore responses against infections such as human-tropic infectious diseases (caused by Epstein–Barr virus and HIV[72]). Consequently, the models are not used in the development of vaccines and cell or gene therapies[73].

Nonetheless, these PBMC-humanized mice are still an excellent xeno-GvHD model for evaluating therapeutic strategies that could interfere with xeno-GvHD development. Unfortunately, while the transfer of hPBMC leads to high lymphocytes engraftment rates, the timeframe for experimental intervention and analysis is somewhat limited, because of the rapid development of xenogeneic GvHD.

The principal host components responsible for triggering GvHD are the xenogeneic mouse MHC (H-2) class I and class II molecules. Studies with NSG mice lacking H-2 class I (β_2m null) or H-2 class II (IA β null) showed that the deletion of H-2 class I and II molecules could delay the occurrence of the diseases significantly compared with WT NSG mice, but could not abrogate it completely[74, 75]. By contrast, H-2 class I-deficient NSG mice were relatively resistant to the development of xeno-GvHD. These data indicated that both donors' CD8⁺ and CD4⁺ T cells contributed significantly to development of xenogeneic GvHD and revealed the critical role of H-2 class I and class II molecules in the development of xeno-GvHD in mice. Furthermore, in contrast to the

repopulation of NRG mice with xenogeneic human DQ8-PBMCs which resulted in rapid induction of xeno-GvHD and poor survival rate of the animals, the transfer of HLA-class II-matched human DQ8-PBMCs into NRG IA β ^{-/-}DQ8 transgenic recipients (lacking the expression of murine H-2 class-II molecules and expressing a transgenic HLA-DQ8 molecule) resulted in a milder form of xeno-GvHD, such that the mice survived significantly longer than other previous mouse models. These data showed that HLA compatibility between donors and recipients is a requirement for ensuring a proper function of human immune systems in mice without the emergence of graft rejection.

Previously, we have developed an HLA class I and class II transgenic mouse (Sure-L1 mice) (HLA-A2^{+/+}/DR1^{+/+}/H-2- β 2m^{-/-}/IA β ^{-/-}) which lacked both murine H-2 class I and II molecules, and instead expressed HLA-A2 and HLA-DR1 molecules[76]. In this humanized mouse model, murine T cells could only mount HLA-restricted responses without H-2-restricted responses, demonstrating that the expression of both transgenic HLA class I and II molecules could result in proper thymic education and differentiation of developing T lymphocytes.

In this part, we described a novel mouse strain derived from Sure-L1 mouse (HLA-A2^{+/+}/DR1^{+/+}/H-2- β 2m^{-/-}/IA β ^{-/-}), in which we additionally depleted the murine Rag 2 allele, the interleukin 2 receptor gamma chain allele (IL-2 γ) and the perforin allele (Perf), leading to the generation of immuno-deficient mice (HLA-A2^{+/+}/DR1^{+/+}/H-2- β 2m^{-/-}/IA β ^{-/-}/Rag^{2-/-}/IL-2 γ ^{-/-}/Perf^{-/-} mice) which named HUMAMICE.

Furthermore, we confirmed that the transfer of HLA-matched hPBMCs into this HUMAMICE can generate a functional human immune system without signs compatible with onset of Graft-versus-Host Disease (GvHD) including the pathological symptoms like weight loss, diarrhea, alopecia or the immunological signs like infiltration of activated human lymphocytes in liver, skin, or intestine.

Therefore, HLA-matched-hPBMC HUMAMICE model opens the possibility of studying not only normal human immune-hematopoietic development but also human disease pathogenesis for a broad range of biomedical applications.

Methods

Ethics statement

Experimental procedures were approved by the Animal Care Committee of the University Paris-Sud Network, and carried out in accordance with Animal Care Guidelines. Human PBMCs were collected from healthy volunteers (with written informed consent, that these documents are recorded in tumorothèque of Hôpital Saint Antoine) in Hospital Saint Antoine and in compliance with French and European regulations. Tumorothèque of Hôpital Saint Antoine 's review board specifically approved the study regarding the collection of Human PBMCs valid until June 30th, 2016.

Creation and generation of HUMAMICE

HUMAMICE (HLA-A2^{+/+}/DR1^{+/+}/H-2- β 2m^{-/-}/IA β ^{-/-}/Rag2^{-/-}/IL-2r γ ^{-/-}/Perf^{-/-} mice) were generated on the background of Sure-L1 mice (HLA-A2^{+/+}/DR1^{+/+}/H-2- β 2m^{-/-}/IA β ^{-/-}) to homozygosity. The construction of Sure-L1 mice was fully described previously. In brief, we established the homozygous Sure-L1 mice by intercrossing the HLA-A2.1 (HHD)-transgenic H-2 class I-KO (β 2m^{-/-}) mice (genetic background of C57BL/6 backcrossed nine generation) with HLA-DR1 transgenic H-2 class II KO (IA β ^{-/-}) mice (the genetic background of C57BL/6 backcrossed for seven generation). HUMAMICE was produced by several inter-crossings between Sure-L1 mice with Rag2^{null} (Rag2^{-/-}) mice, IL-2r γ ^{null} (IL-2r γ ^{-/-}) mice and Perf^{null} (Perf^{-/-}) mice. The obtained final homozygote HUMAMICE (HLA-A2^{+/+}/DR1^{+/+}/H-2- β 2m^{-/-}/IA β ^{-/-}/Rag2^{-/-}/IL-2r γ ^{-/-}/Perf^{-/-}) were checked by specific PCR molecular genotyping and FACS analysis after specific immune-labelling.

HUMAMICE were bred and housed under specific pathogen-free (SPF) conditions in isolators in the animal facility at the TAAM Orle'ans center and using sterile techniques and micro-isolator caging. Experimental procedures were approved by the Animal Care Committee of the University Paris-Sud Network, and carried out in accordance with Animal Care Guidelines. Six to eight-weeks-old female mice were used as transplantation recipients. The endpoint for the survival study was set when recipient

mice looked clinically ill or lost more than 15% of body weight, and mice were humanely sacrificed by cervical dislocation under general anesthetic or CO₂.

Genotype identification of HUMAMICE

The transgenic of HLA-A2 and HLA-DR1, as well as the knockout of H-2-β_{2m}, H-2-IAβ, Rag2, IL-2γ and Perf were identified by specific PCR. Murine genomic DNA was extracted as described previously[77]. The immuno-deficiency characteristic of HUMAMICE was checked by flow cytometry, while the immuno-competent C57BL/6 mice were chosen as the controls. Splenocytes were labelled with mCD3-PE and mCD19-FITC, mCD4-APC and mCD8-PE-Cy5.

The identification of the immuno-deficiency of HUMAMICE

To confirm the immuno-deficiency status of HUMAMICE, we subcutaneously engrafted the human RAMOS tumor cells (10⁷ cells) into HUMAMICE and immuno-competent parental Sure-L1 mice. Furthermore, to verify that the inability of HUMAMICE to reject RAMOS cells is due to lack of the mouse-derived immune system, 30 days after the injection of RAMOS cells, we transferred total splenocytes, purified CD8⁺ T lymphocytes or other lymphocytes derived from immuno-competent Sure-L1 mice which had rejected RAMOS cells into HUMAMICE carrying a solid tumor. Moreover, we surveyed and measured the volume of tumors constantly.

Collection and purification of human PBMC

Human PBMCs were collected from healthy volunteers in Hospital Saint Antoine and compliance with French and European regulations. PBMCs were purified by Ficoll-Hypaque density centrifugation and suspended in PBS.

HLA genotyping

HLA-A0201 (HLA-A2) positive individuals were identified by flow cytometry. And the DNA was extracted from 1×10⁶ donor hPBMCs using DNeasy Blood & Tissue Kit (Qiagen). HLA-DRB1-01 (HLA-DR1) positive individuals were identified by specific polymerase chain reaction (PCR) using Olerup SSP DR low resolution and high resolution SSP DRB1:01 kit following the instructions.

Xenogeneic hPBMC transplantation

Female 6- to 8-week-old HUMAMICE were irradiated with 3.0 Gy using a cobalt radiation source shortly the day before cell transfer (Precision X-RAD 320 Biological Irradiator) and were followed given by intravenous injection of 10^7 hPBMC cells with a total volume of 100 μ L per recipient mouse (Figure 23). After transplantation, mice were given sterile water containing prophylactic neomycin sulfate. And mice were monitored for weight and clinical symptoms twice per week. Weight loss of > 15% of original starting weight is a sign of GvHD development and necessitates euthanasia of hPBMC-engrafted mice.

Two independent experiments with two different HLA-matched (HLA-A2⁺/DR1⁺) donors were performed using a group of 5 or 4 mice. For HLA-A2⁺/DR1⁺ donor A, we transferred with five mice. Three HUMAMICE were analyzed at five weeks post hPBMC transfer, and two were sacrificed at 8 weeks post hPBMC transfer for FACS analysis. For HLA-A2⁺/DR1⁺ donor B, we transferred with 4 mice. HUMAMICE (2 at 5 weeks post hPBMC transfer, 1 mouse at 8 weeks and 1 mouse at 12 weeks post hPBMC transfer) were sacrificed for FACS analysis.

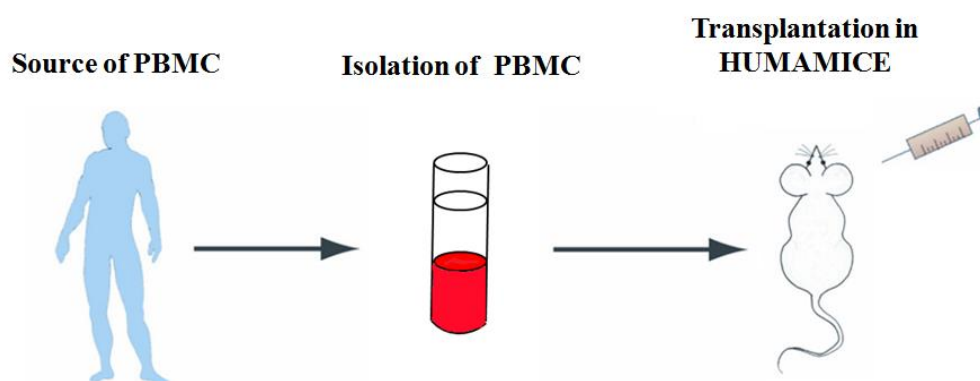


Figure 23. The schematic of human PBMC transplantation of HUMAMICE.

Immunization of HUMAMICE

14 days after the transplantation of hPBMCs, HUMAMICE received three intramuscular (i.m.) injections of recombinant HBV vaccine (10 μ g) (Pasteur Institute)

in a total injection volume of 100 μ L. Each immunization was separated by an interval of 14 days. Sera were collected both before and after each immunization boost for serological analysis. Mice were sacrificed 10 days after the final boost.

Flow cytometry

To detect human cells engrafted in HUMAMICE, multi-colors cytometric analysis was performed using *BD* LSR Fortessa, according to the manufacturer's protocol but with a minor modification. HUMAMICE were sacrificed and the spleens were removed at three different times after hPBMCs were transplanted. Splenocytes were collected and lysed by ACK lysis buffer, counted and incubated with an appropriate volume of antibodies for 1 hour at 4°C and then subjected to flow cytometry analysis.

Commonly used antibodies included: Anti-Human CD45 FITC, Clone: 2D1, (ebioscience, 9011-9459); isotype control, Mouse IgG1 K Isotype Control (ebioscience, FITC 11-4714) ; Anti-Mouse CD45 eFluor 450 (ebioscience, 48-0451-82) ; isotype control, Mouse IgG2b K Isotype Control eFluor 450 (ebioscience, 48-4732-82) ; Anti-Human CD3 APC-eFluor780, Clone: UCHT1, (ebioscience, 47-0038) ; Mouse IgG1 K Isotype Control APC-eFluor780 (ebioscience, 47-4714) ; Anti-Human CD4 PerCP-Cyanine5.5, Clone: OKT4 (OKT-4), (ebioscience, 45-0048); isotype control, Mouse IgG2b K Isotype Control PerCP-Cyanine5.5 (cat. 45-4732); Anti-Human CD8a PE-Cyanine7, Clone: SK1, (ebioscience, 25-0087); isotype control, Mouse IgG1 K Isotype Control PE-Cyanine7 (ebioscience, 25-4714); Anti-Human CD19 APC, Clone: 2H7, (ebioscience, 17-0209); isotype control, Mouse IgG1 K Isotype Control APC (ebioscience, 17-4714).

Measurement of serum antibodies by ELISA

The serum levels of antibodies specific for commercial HBsAg vaccine in immunized HUMAMICE were measured by ELISA test. The plates coated with HBsAg vaccine were blocked with PBS supplemented with 0.1% Tween 20 and 10% FCS and then washed three times. After the addition of mouse serum for 1 h, the plates were washed again, and bound antibodies were detected with Anti-Human IgG (whole molecule)-Peroxidase antibody produced in rabbit (SIGMA-ALDRICH, A8792) and Anti-Human IgM (μ -chain specific)-Peroxidase antibody produced in goat-affinity isolated antibody

(SIGMA-ALDRICH, A6907). Absorbance was then measured at 450 nm in a plate reader. The antibody titers (the mean of at least three determinations) were calculated using the serial end-point dilution method.

Statistical analysis

Each experiment was repeated at least three times, and data were expressed as the mean \pm SEM. The means or geometric means of multiple groups were compared using Student's t-test. All statistical analysis was performed using GraphPad Prism version 5.0. A P value < 0.05 was considered statistically significant.

Results

Generation and characterization of HUMAMICE

Based on the background of Sure-L1 mice (HLA-A2/DR1 transgenic mice, HLA-A2^{+/+}/DR1^{+/+}/H-2- β 2m^{-/-}/IA β ^{-/-}), we generated humanized immuno-deficient mice - "HUMAMICE". This was achieved by several rounds of backcrossing between Sure-L1 mice with Rag2^{-/-} mice, IL-2 γ ^{-/-} mice and Perf^{-/-} mice. The resulting homozygote HUMAMICE (HLA-A2^{+/+}/DR1^{+/+}/H-2- β 2m^{-/-}/IA β ^{-/-}/Rag2^{-/-}/IL-2 γ ^{-/-}/Perf^{-/-}) were determined by specific PCR molecular genotyping (Figure 24) and FACS analysis after specific immune-labelling (Figure 25).

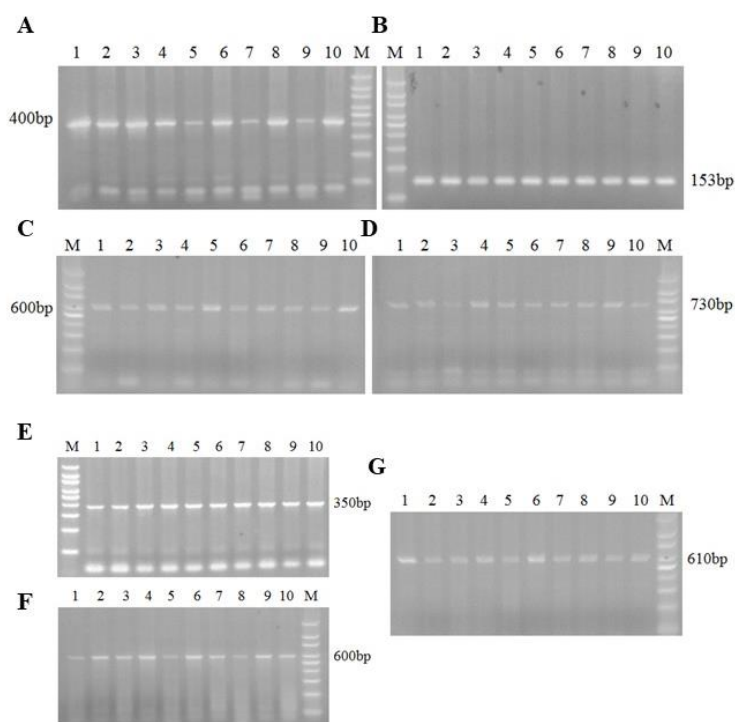


Figure 24. PCR molecular genotyping of HUMAMICE. A. HLA-A2 gene. B. HLA-DR1 gene. C. H-2- β 2m gene. D. H-2-IA β gene. E. Rag2 gene. F. IL-2 γ gene. G. Perf gene.

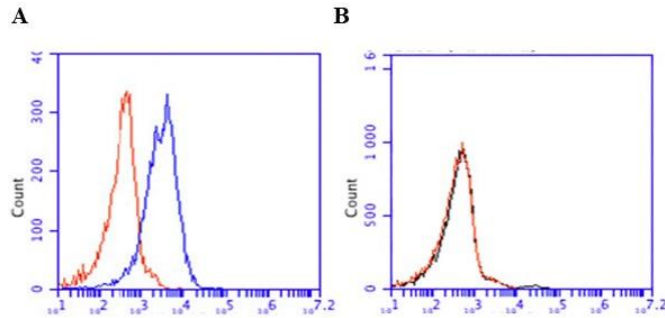


Figure 25. FACS analysis of HLA-A2 molecule in the splenocytes of HUMAMICE.

A. HUMAMICE. B. C57BL/6 mice.

We confirmed the immuno-deficiency characteristics of HUMAMICE by flow cytometry. Highly immuno-deficient mice such as *NOG/NSG* mice are characterized by the lack of almost entire mouse-derived adaptive immune system, including murine B cells, T cells and NK cells. Comparative cell analysis by flow cytometry of splenocytes from immuno-deficient HUMAMICE and immuno-competent C57BL/6 mice were shown in Figure 26. Representative immuno-competent C57BL/6 mice expressed 24.9% mCD3⁺ T cells and 52.3% mCD19⁺ B cells; while only a residual population (<0.5%) of mCD3⁺ T cells and mCD19⁺ B cells was found in immuno-deficient HUMAMICE (Figure 26A). The ratio of mCD4⁺/mCD8⁺ T cells in C57BL/6 mice was 1.85 (54.1%/29.2%) (Figure 26B, right) and there were neither CD4⁺ nor CD8⁺ T cells in HUMAMICE (Figure 26B, left). The absence of murine T cells (CD3⁺CD4⁺ T cells and CD3⁺CD8⁺ T cells) and B cells (CD19⁺CD20⁺ B cells) is an important requirement for the immuno-deficient state of these mice. Table 8 summarized the results of other cell populations in HUMAMICE and C57BL/6 mice. We noted that, the absence of NK cells in HUMAMICE (0%) compared with C57BL/6 mice (1.9% and 2.4%). The consequence of this lack of almost the entire mouse-derived immune system is the sign of severe immune-deficiency characterized by the inability to reject foreign cells.

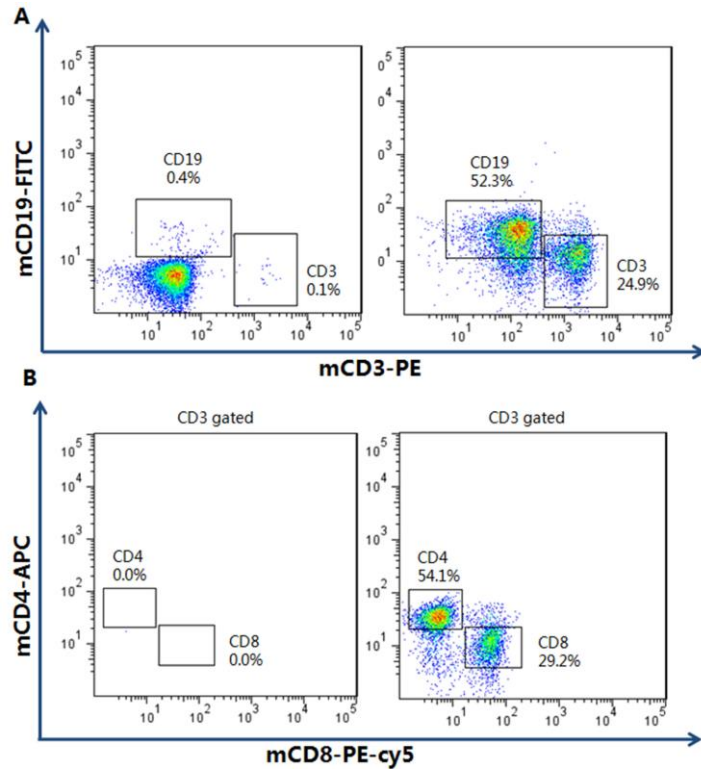


Figure 26. Flow cytometry analysis of immuno-deficient HUMAMICE. Comparative cell analysis by flow cytometry of immuno-deficient HUMAMICE (HLA-A2^{+/+}/DR1^{+/+}/H-2-β₂m^{-/-}/IAβ^{-/-}/Rag2^{-/-}/IL-2rγ^{-/-}/Perf^{-/-}) and immuno-competent C57BL/6 mice. The left panel shows the analysis of HUMAMICE and the right panel was C57BL/6 mice. A. Samples in Figure 26A were double labelled with mCD3-PE and mCD19-FITC. B. Samples in Figure 26B were labelled with mCD4-APC and mCD8-PE-Cy5 (gated in mCD3⁺ cells).

Table 8: Summary of cell analysis of HUMAMICE and C57BL/6 mice

| Cellular type | HUMAMICE-1 | HUMAMICE-2 | C57BL/6-1 | C57BL/6-2 |
|---------------------------------------|------------|------------|-----------|-----------|
| mCD45 ⁺ | 44.9% | 32.1% | 88.8% | 95% |
| mCD3 ⁺ mCD4 ⁺ | 0.4% | 0.2% | 13.5% | 27.5% |
| mCD3 ⁺ mCD8 ⁺ | 0.4% | 0.5% | 7.3% | 17.1% |
| mCD19 ⁺ mCD20 ⁺ | 0.1% | 0% | 52.3% | 32% |
| mCD19 ⁻ mCD20 ⁺ | 0.1% | 0.7% | 2.4% | 2.5% |
| NKp46 ⁺ NK1.1 ⁺ | 0% | 0% | 1.9% | 2.4% |
| mTer119 ⁺ | 18.2% | 30.8% | 5% | 5.7% |
| mCD11b ⁺ | 9.4% | 8.5% | 6.4% | 8.5% |

The populations $mCD45^+$; $mCD3^+mCD4^+$; $mCD3^+mCD8^+$; $mCD19^+mCD20^+$; $mCD19^-mCD20^+$; $NKp46^+NK1.1^+$; $mTer119^+$ and $mCD11b^+$ were presented above.

Histopathological analysis of the spleen and thymus of HUMAMICE

Through the histopathological analysis of the spleen of HUMAMICE and Sure-L1 mice (HLA-A2/DR1 mice), we found that the spleen of HUMAMICE was atrophic and no clear splenic corpuscle was observed (as shown in Figure 27). The red pulp and white pulp of HUMAMICE spleen were significantly reduced (as indicated in Figure 27B by the yellow arrow). While the spleen of Sure-L1 mice (HLA-A2/DR1 mice) with the same genetic background was normal, and the edge area between of white pulp and red pulp was clear (as shown in Figure 27A by the black arrows). The above results indicated that the spleen of HUMAMICE is immature.

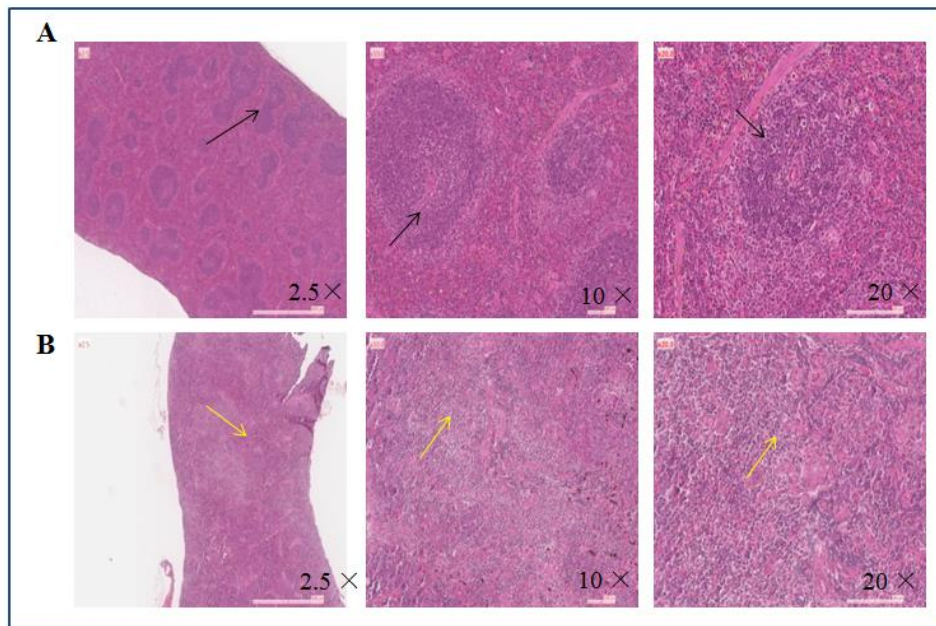


Figure 27. Histopathological analysis of spleen of HUMAMICE. A. Sure-L1 mice (HLA-A2/DR1 mice). B. HUMAMICE.

Histopathological examination of the thymus of HUMAMICE and Sure-L1 mice revealed that the thymus of HUMAMICE was underdeveloped, the boundary between the cortex and medulla was unclear, and the structure of the thymus lobules was unclear (as shown in Figure 28B). As shown in Figure 28A, immunologically normal Sure-L1

mice have structurally normal cortical and medullar structures of thymus (as indicated by the black arrows). The results showed that the thymic of HUMAMICE mice was underdeveloped, and the thymus of Sure-L1 mice (HLA-A2/DR1 mice) was normal.

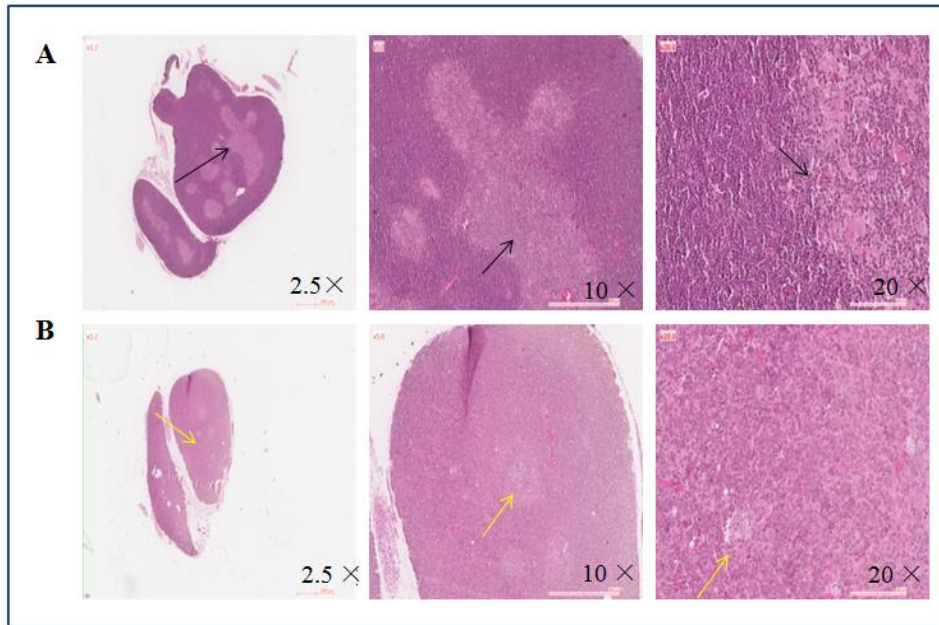


Figure 28. Histopathological analysis of thymus of HUMAMICE. A. Sure-L1 mice (HLA-A2/DR1 mice). B. HUMAMICE.

Confirmation of the immuno-deficiency of HUMAMICE

To confirm the immuno-deficiency status of HUMAMICE, we subcutaneously injected human RAMOS tumor cells (10^7 cells/mouse) into HUMAMICE and immuno-competent parental Sure-L1 mice. Figure 29A (left) showed the kinetics of RAMOS tumor growth in six HUMAMICE (mouse No.912; 926; 953; 952; 948; 950), whereas Figure 29A (right) showed the tumor size in five immuno-competent Sure-L1 mice. In addition, Figure 29B shows the RAMOS tumor cells subcutaneous development in six HUMAMICE and five Sure-L1 mice during 25 days post the injection. Overall, human RAMOS cells induced tumors in HUMAMICE, whereas they were not able to grow in Sure-L1 mice.

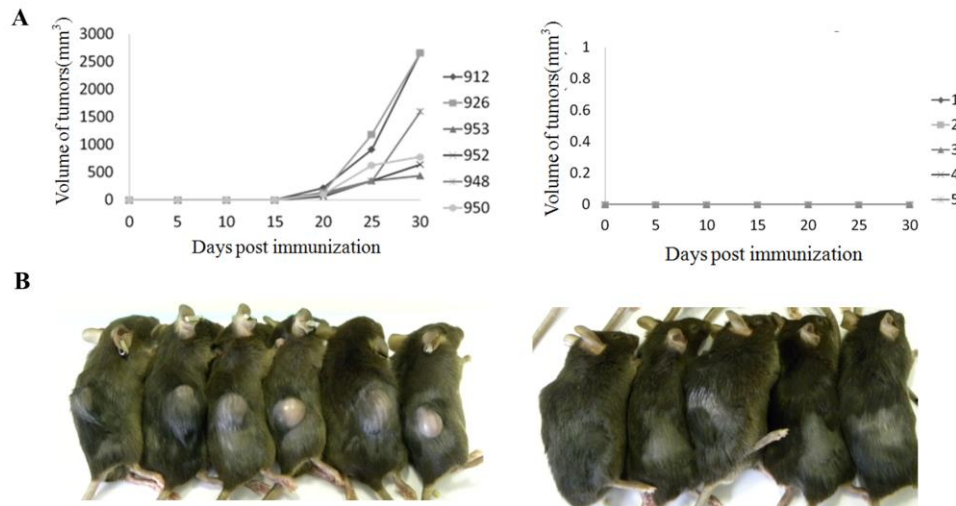


Figure 29. The tumor growth kinetics in immuno-deficient HUMAMICE and immuno-competent Sure-L1 mice after subcutaneous injection of RAMOS tumor cells. Comparative tumor growth in six immuno-deficient HUMAMICE and five immuno-competent Sure-L1 mice 25 days after the subcutaneous injection of RAMOS cells. Figure 29A (left) and B (left) show HUMAMICE, while Figure 29A (right) and B (right) show Sure-L1 mice.

Furthermore, to verify that the inability of HUMAMICE to reject RAMOS cells is due to lack of mouse-derived immune system, we transferred the total splenocytes, purified CD8⁺ T lymphocytes or purified CD8⁻ T lymphocytes derived from the immuno-competent Sure-L1 mice which had rejected RAMOS cells into HUMAMICE that developed a solid tumor. Results of the kinetics of tumor growth after the transfer of total splenocytes, purified CD8⁺ T lymphocytes or purified CD8⁻ T lymphocytes from immuno-competent tumor-primed Sure-L1 mice are shown in Figure 30 A/B/C, respectively.

In Figure 30A, three immuno-deficient HUMAMICE bearing a solid RAMOS tumor (mouse No.926; 948; 952) rejected completely their tumors 15 days after cell-transfer of total splenocytes from Sure-L1 mice, while the volume of tumor continued to grow in No.953 HUMAMICE which did not receive cell transfer. Figure 30B showed the examples of No.208 and No.326 HUMAMICE which bore solid RAMOS tumors. After the transfer of CD8⁺ purified T lymphocytes from Sure-L1 mice, only No.326 mouse could reject completely the tumors in 12 days, whereas No.208 mouse could only stop

the tumor growth at 6 days and stabilized the tumor size without total rejection, compared with control mouse No.323 which did not receive cell transfer and in which the tumor continued to grow. As shown in Figure 30C, after receiving purified CD8⁻ T lymphocytes from Sure-L1 mice, No.139, No.212 and No.337 HUMAMICE bearing a solid RAMOS tumor started to reject their tumors by reducing progressively their size from 6 days post-transfer, while the tumors continued to grow in control No.323 mouse that did not receive cell transfer. Altogether, these results confirmed that HUMAMICE are severely immuno-deficient.

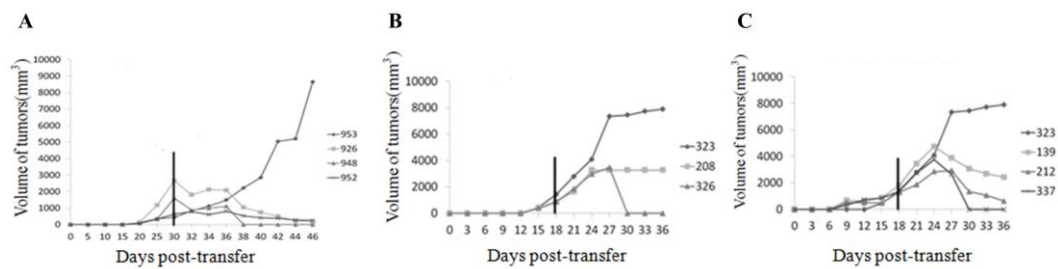


Figure 30. The tumor growth kinetics in HUMAMICE after transfer of RAMOS specific splenocytes from parental Sure-L1 mice. A. Tumor growth kinetics following transfer of tumor specific splenocytes from Sure-L1 mice in three immuno-deficient HUMAMICE bearing a solid RAMOS tumor (mouse No.926; 948; 952) and the control No.953 mouse without the transfer of tumor-bearing cells. B. Tumor growth kinetics following transfer of purified tumor specific CD8⁺ T lymphocytes from Sure-L1 mice in two immuno-deficient HUMAMICE bearing a solid RAMOS tumor (mouse No.208; 326) and the control No.323 mouse without transfer of tumor-bearing cells. C. Tumor growth kinetics following transfer of tumor specific splenocytes depleted of CD8⁺ T cells (purified CD8⁻ T lymphocytes) from Sure-L1 mice in three immuno-deficient HUMAMICE bearing a solid RAMOS tumor (mouse No.139; 212; 337) and the control No.323 mouse without transfer of tumor-bearing cells.

hPBMC engraftment in HUMAMICE

In order to evaluate the engraftment of HLA-matching hPBMCs in this new immuno-deficient HLA-humanized mouse model, we transferred 10⁷ HLA-matched (HLA-

A2⁺DR1⁺) hPBMCs intravenously into HUMAMICE after a total body irradiation and monitored the weight of mice and clinical GvHD signs once a week as described previously[78]. The experimental protocol is summarized in Figure 31.

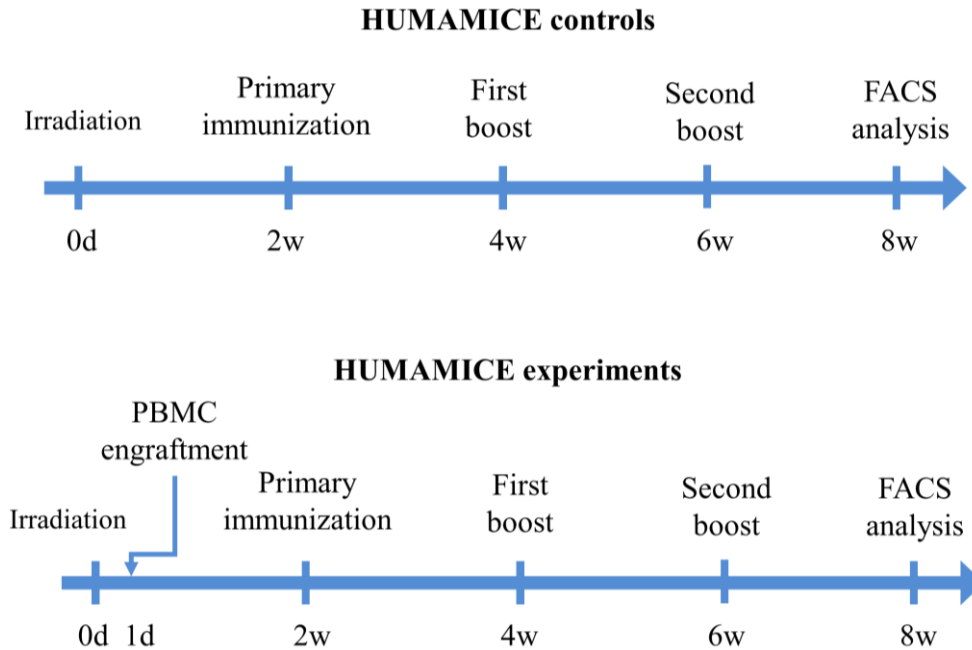


Figure 31. The experimental procedure of hPBMC transplantation and immunization with HBsAg vaccine in HUMAMICE.

Flow cytometry analysis was done at five, eight and twelve weeks after hPBMC were transferred (as shown in Table 9). Results of two representative mice (from nine analyzed mice) which analyzed at five and eight weeks after transplantation were shown in Figure 32. For the mouse that was analyzed at 5 weeks after transplantation (Figure 32A), 11.6% of splenocytes were composed by human CD45⁺ cells, with 45.2% of this population being hCD19⁺, and 17.1% of this population being hCD45⁺hCD3⁺ T lymphocytes: 29.0% of them were hCD8⁺ T lymphocytes (hCD45⁺hCD3⁺hCD8⁺) and approximately 60.9% were hCD4⁺ T lymphocytes (hCD45⁺hCD3⁺hCD4⁺). For the mouse which was analyzed at eight weeks after transplantation (Figure 32B), 9.7% of splenocytes were composed by hCD45⁺ cells, with 49.4% of this population being hCD19⁺ B cells, and 16.1% of this population being hCD45⁺hCD3⁺ T lymphocytes: 30.0% of them were hCD8⁺ T lymphocytes (hCD45⁺hCD3⁺hCD8⁺) and approximately

59.0% were hCD4⁺ T lymphocytes (hCD45⁺hCD3⁺hCD4⁺). The constitutions of splenocytes of hPBMC-transplanted HUMAMICE were shown in Table 9. Moreover, none of the HUMAMICE developed GvHD signs or weight loss (as shown in Figure 33).

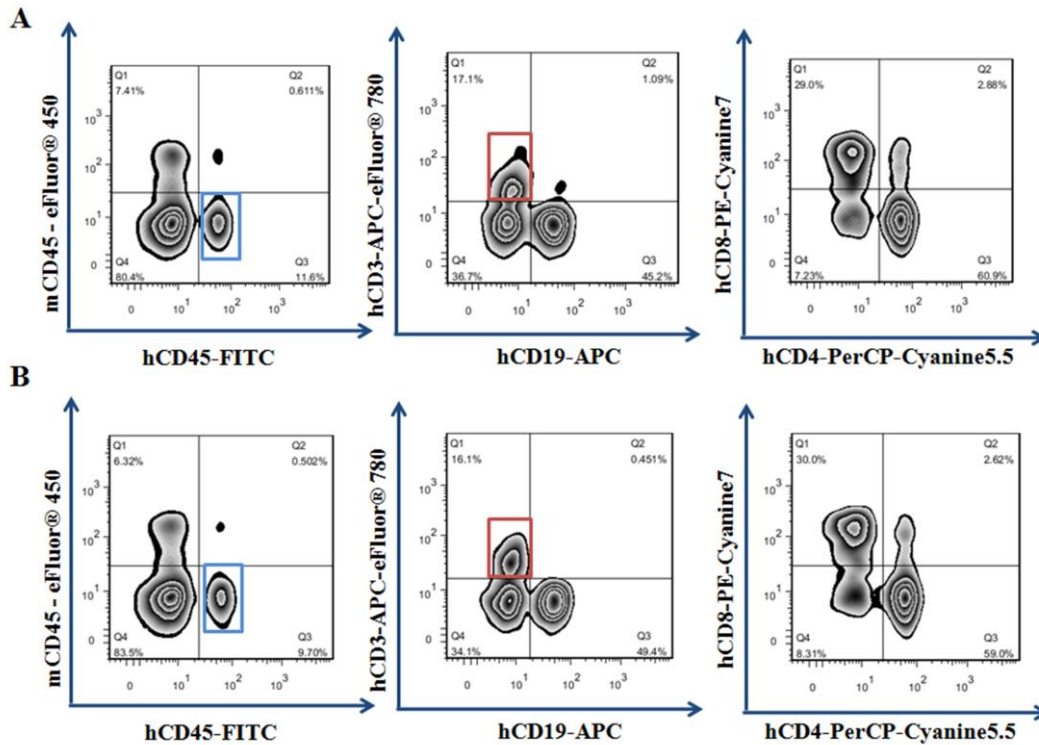


Figure 32. Flow cytometry analysis after five and eight weeks of hPBMC transplantation in HUMAMICE. Results of two representative mice (from nine analyzed mice) which were analyzed at five and eight weeks after transplantation are shown in Figure 32. A. For the mouse which was analyzed at 5 weeks after transplantation, 11.6% of splenocytes were composed by hCD45⁺ cells, with 45.2% of this population being hCD19⁺, and 17.1% being hCD45⁺hCD3⁺ T lymphocytes: 29.0% of them were hCD3⁺CD8⁺ and 60.9% were hCD3⁺CD4⁺ T cells. B. For the mouse which was analyzed at 8 weeks after transplantation, 9.7% of splenocytes were composed by hCD45⁺ cells, with 49.4% of this population being hCD19⁺, and 16.1% being T lymphocytes: 30.0% of them were hCD3⁺CD8⁺ and 59.0% were hCD3⁺CD4⁺ T lymphocytes.

Table 9. Summary of HUMAMICE transplanted with HLA-A2⁺/DR1⁺ hPBMCs.

| Donor A/mouse | mCD45 ⁻ | hCD45 ⁺ | hCD45 ⁺ | hCD3 ⁺ | hCD3 ⁺ |
|---------------------------|--------------------|--------------------|--------------------|-------------------|-------------------|
| | hCD45 ⁺ | hCD19 ⁺ | hCD3 ⁺ | hCD4 ⁺ | hCD8 ⁺ |
| Mouse 1 (5 weeks) | 11.6% | 45.2% | 17.1% | 60.9% | 29.0% |
| Mouse 2 (5 weeks) | 13.4% | 51.9% | 15.4% | 68.3% | 24.6% |
| Mouse 3 (5 weeks) | 15.2% | 56.7% | 18.9% | 52.4% | 22.8% |
| Mouse 4 (8 weeks) | 9.7% | 49.4% | 16.1% | 59.0% | 30.0% |
| Mouse 5 (8 weeks) | 7.1% | 60.8% | 13.2% | 40.9% | 15.8% |
| Donor B/Mouse | | | | | |
| Mouse 6 (5 weeks) | 19.2% | 69.2% | 14.7% | 63.1% | 20.9% |
| Mouse 7 (5 weeks) | 15.8% | 54.2% | 15.1% | 60.7% | 19.2% |
| Mouse 8 (8 weeks) | 8.9% | 51.2% | 20.7% | 40.9% | 12.1% |
| Mouse 9 (12 weeks) | 5.4% | 42.1% | 12.2% | 19.5% | 4.5% |

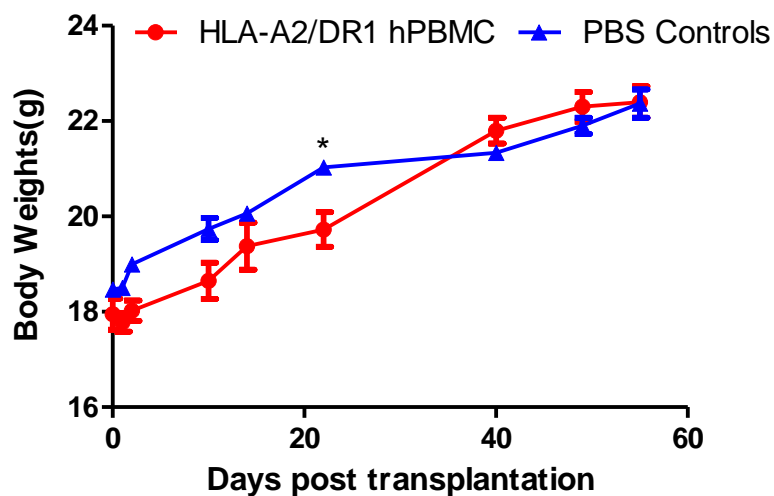


Figure 33. The evaluation of body weight of HUMAMICE after hPBMC transplantation. The average weight is shown as a percentage of starting weight. None of HUMAMICE developed weight loss after hPBMC transplantation.

The humoral immune response of HUMAMICE to a specific HBsAg vaccine

We next evaluated the functional ability of these adoptively transferred HLA-matched

hPBMCs in HUMAMICE to respond to a specific antigenic stimulus, namely HBsAg vaccine. The schedule of immunization with HBsAg vaccine was shown in Figure 31 and included the primary immunization two weeks after hPBMC transfer, followed by two immunization boosts every two weeks after primary immunization. The collected sera were analyzed with an HBsAg specific ELISA test according to the protocol described in Material and Methods. The background noise was represented by the mean of two HUMAMICE controls without transfer of hPBMCs. Figure 34 showed the HBsAg-specific-hIgG (Figure 34A) and HBsAg-specific-hIgM (Figure 34B) responses of immunized hPBMC-HUMAMICE before (0w) and every two weeks after immunization (before each immunization boost). We observed a significant HBsAg-specific hIgG response which was amplified after recall immunization boots. HBsAg-specific-IgM responses were detected after primary-immunization, while no more responses were observed after recall immunization.

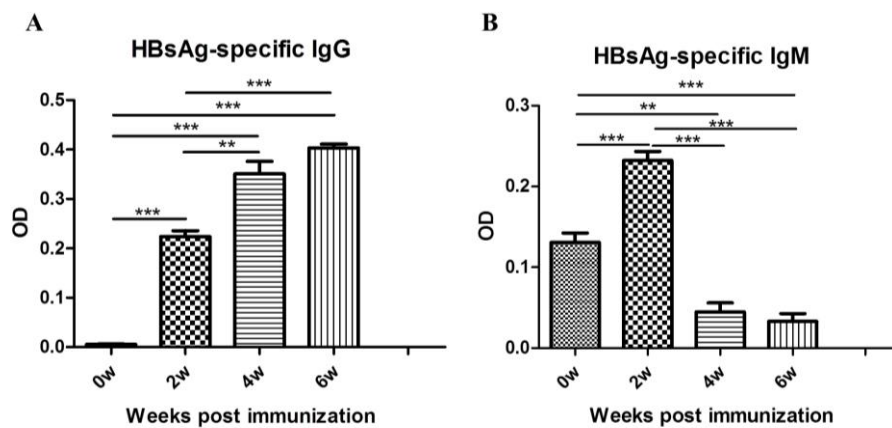


Figure 34. The humoral immune response of hPBMC-HUMAMICE after immunization with HBsAg vaccine. The HBsAg specific IgG (A) and HBsAg specific IgM (B) responses of immunized hPBMC-HUMAMICE before (0w) and every two weeks after immunization (before each immunization boost).

Discussion

The development of small animal models that could mimic human immune responses is important to evaluate novel human clinical drugs or to test new therapeutic treatments or new vaccines. In this part, we show that HUMAMICE developed by backcrossing derived Sure-L1 mice with Rag2^{-/-} mice, IL-2 γ ^{-/-} mice and Perf^{-/-} mice can be efficiently reconstitute with HLA-matched PBMCs without developing GvHD and with a functional immune system able to launch a robust human T cell-dependent response. Human adaptive immune responses are HLA-restricted, implying that maintaining HLA compatibility is a requirement for normal human immune responses. Currently, no experimental preclinical mouse model can meet this requirement, including recently developed models such NSG[79], NOG or NRG mice. Thus, after hPBMC transferred, a rapid onset of xenogeneic Graft-versus-Host Disease (xeno-GvHD) is observed in all hPBMC-NSG mice. These mice exhibited weight loss, diarrhea, alopecia and pathological infiltration of activated human lymphocytes in liver, skin, or intestine, leading finally to death after 20 to 25 days[80]. It is interesting to note that the removal of murine MHC class I activity greatly reduces human *in vitro* T cell proliferative responses to murine cells and should thus lead to reduced xenogeneic GvHD following engraftment with human PBMC[81]. After HLA-matched hPBMC transferred, our mice did not develop any evidence of GvHD during the three months follow up period. In present study, we developed a new improved immuno-deficient HUMAMICE model (HLA-A2^{+/+}/DR1^{+/+}/H-2- β 2m^{-/-}/IA β ^{-/-}/Rag2^{-/-}/IL-2 γ ^{-/-}/Perf^{-/-}) which could satisfy this requirement.

Indeed, HUMAMICE strain is an immuno-deficient strain with a humanized immune microenvironment expressing both HLA class I and class II molecules, and which overcomes the lack of central thymic and peripheral human T-cell maturation through selective interaction with HLA class I and class II molecules. The HUMAMICE lack almost all essential murine immune cells, as similarly demonstrated in NSG, NOG or NRG mouse model. It's worth noting that a significant reduction of NK cells could favor the engraftment of foreign cells.

The proliferation of RAMOS tumor cells in immuno-deficient HUMAMICE but not in the parental immuno-competent Sure-L1 mice, and the subsequent tumor elimination by the transfer of immune cells from RAMOS-rejected Sure-L1 mice, confirmed the

severe immunodeficiency status of HUMAMICE. Interestingly, HUMAMICE could also be used as a readout system—together with their parental Sure-L1 mice or Sure-L1-TGFP mice (where all T cells co-express the GFP protein) or Sure-L1-FoxP3-GFP mice (where T cells co-expressed FoxP3 protein and GFP protein as fusion protein) to dissect the contribution role of each cell population to the protective immune responses against foreign antigens like pathogens. The present data indicated that all immune cells including T cells ($CD3^+CD4^+$, $CD3^+CD8^+$), B cells and NK cells were involved in rejection of the RAMOS tumor.

After transferring 10^7 HLA-matched (HLA-A2⁺/DR1⁺) hPBMC cells intravenously into HUMAMICE, we found hCD45⁺ cells in splenocytes of HUMAMICE, which included both human B cells (hCD45⁺hCD19⁺) and human T cells (hCD45⁺hCD3⁺hCD4⁺ and hCD45⁺hCD3⁺hCD8⁺). More importantly, none of HUMAMICE developed any GvHD signs or weight loss after HLA-A2⁺/DR1⁺ hPBMC were transferred.

Because of limited availability HLA-A2⁺/DR1⁺ PBMCs from two donors, we could only perform one analysis in one mouse at 3 months after transfer of human PBMCs. At this time point, we detected around 42% hCD45⁺hCD19⁺ compared to 12% hCD45⁺hCD3⁺ cells. These B cells (42%) could optimally interact with both reconstituted hAPC and hCD4⁺ cells. In addition, they could also interact with mAPC which expressed HLA-A2 and HLA-DR1. This could explain how both HBsAg-specific hIgG and hIgM antibodies are induced in our model. Our research indicated successful engraftment of hPBMCs in this new immuno-deficient HLA-humanized mouse model-HUMAMICE.

In the model of Xeno-GvHD, after intravenous transfer of hPBMCs in Rag2^{-/-}c^{-/-} mice[82], high engraftment rates of human cells had been reported between 2 to 4 weeks after transplantation, with a T-cell chimerism of at least 20–48% in more than 90% of mice. This high engraftment rate was associated with the development of acute Xeno-GvHD and a mortality rate of 85% of the mice within 2 months. Interestingly only a small population of B cells (around 7-11%) residing in lymphoid compartments were detected in these mice explaining the detection of elevated plasma levels of IgG and IgM. In fact, it has also been reported that immunoglobulin production in hPBMC-SCID models could be high despite low numbers of B cells and was generally used as

an indication of good engraftment of the human cells[14, 20, 83, 84].

Conclusions

The HUMAMICE model represents an improvement over the traditional immunodeficient mice models like NSG and NOG mice, which have drawbacks such as development of xeno-GVHD. The HLA-compatible-hPBMC-HUMAMICE is thus a unique model that could be used to explore human immunology in a normal physiological situation (without xeno-GvHD) and could be useful for evaluation of cell-therapies, generation of human monoclonal antibodies, and production of novel vaccines.

Nonetheless, it should be noted that the new HUMAMICE mice were made on the C57BL/6 genetic background, and then backcrossed for seven generations, and not originally on the NOD background. The genetic background of the mice will impact the ability of the mice to sustain long-term engraftment of human HSCs and PBMCs in several immunodeficient strains. It was previously shown that NOD-scid mice supported higher levels of engraftment with human PBMCs than other strains tested, including C3H/HeJ-scid and C57BL/6-scid mice[14, 25].

More recently, it was shown that NSG (NOD-scid IL-2 γ^{null}) mouse model supports higher levels of human hemato-lymphoid engraftment than BALB/c-Rag1 $^{\text{null}}$ IL-2 γ^{null} mice[85], and that NOD-Rag1 $^{\text{null}}$ IL-2 γ^{null} mice also engraft with human PBMC at higher levels than NOD-scid IL-2 γ^{null} mice[86]. These data indicated that the difference of human PBMC engraftment between NOD-scid IL-2 γ^{null} and BALB/c-Rag2 $^{\text{null}}$ IL-2 γ^{null} mice is not due to SCID vs. Rag1 $^{\text{null}}$ or Rag2 $^{\text{null}}$ genes but rather to the genetic polymorphic background modifiers.

Genomic studies showed that these background modifiers are localized to the Idd13 locus, which encodes the Sirp gene. SIRP is mainly expressed by macrophages, DCs, and neutrophils, and its ligand, CD47, is expressed almost ubiquitously. The SIRP-CD47 interaction is involved in regulating macrophage-mediated phagocytosis by delivering a licensing signal to macrophages[87]. The NOD SIRP- α protein is more like the human SIRP- α protein than that of C57BL/6 mice. It shows enhanced binding to the human CD47 ligand, and its expression on mouse macrophages leads to better support of human hematopoiesis[88]. The role of murine macrophages in the rejection of human cells and prevention of human reconstitution was confirmed when more

successful engraftment rates of human cells were observed in neonate recipients that had lower macrophage activity and in adult murine hosts after depletion of macrophages following intraperitoneal injection of clodronate[89]

Moreover, NSG mice engraft with human PBMC better than H₂d-Rag2^{null} IL-2r γ ^{null} mice. The production of NSG mice provides an immunodeficient mouse model lacking host NK cells, facilitating human PBMC engraftment. NSG mice support survival of engrafted human T cells, but the human cells mount a severe xenogeneic GvHD following engraftment into NK cell-deficient hosts.

In present study, we create immuno-deficient HUMAMICE mice, which are mouse MHC Class I and Class II deficient, and express both HLA-A2 and HLA-DR1. It is interesting to note that the removal of mouse MHC class I activity greatly reduces human in vitro T cell proliferative responses to murine cells[81] and should lead to reduced xenogeneic GvHD following engraftment with human PBMC. This hypothesis was supported by experiments where PBMC were injected intravenously into NOD-SCID β_2m^{null} mice via the tail vein, resulting in transient engraftment and failing to induce xenogeneic GvHD[90]. Furthermore, it was previously shown that NOD-SCID β_2m^{null} mice support higher levels of human PBMC engraftment than NOD-SCID mice[91], because in the absence of β_2m , natural killer (NK) cell numbers and activity are severely depressed due to the lack of MHC class I expression[91]. More importantly, the absence of β_2m in host cells reduces xenogeneic GvHD responses of the human T cells. In addition, macrophages in HUMAMICE express both HLA-A2 and HLA-DR1, which are compatible with grafted human PBMC. In this HLA-matched situation, there are no allo-like or xeno-like rejection reactions, so the non-optimal mSIRP-hCD47 interaction does not affect long-term PBMC engraftment. However, it must be noted that HUMAMICE is not a good model for engraftment of non-HLA-matched PBMC or any human stem cells, including human HSCs, due to the NOD genetic background of the HUMAMICE and the lack of supporting cytokines, supporting cells such as stromal cells, and human APCs in the mice.

In conclusion, despite some of the drawbacks listed above, the HLA-matched-hPBMC-HUMAMICE model allows the possibility of studying normal human immune responses in various human diseases, including infectious diseases and cancer in the HLA-matched population. It also represents a promising model for facilitating the

development of novel vaccines and cellular therapies.

**Part 2. Generation of human MHC (HLA-A11/DR1)
transgenic mice vaccine evaluation**


Yang Zeng, Tongtong Gao, Guangyu Zhao, Yuting Jiang, Yi Yang, Hong Yu, Zhihua Kou, Yuchun Lone, Shihui Sun* & Yusen Zhou*

Generation of human MHC (HLA-A11/DR1) transgenic mice for vaccine evaluation

Yang Zeng, Tongtong Gao, Guangyu Zhao, Yuting Jiang, Yi Yang, Hong Yu, Zihua Kou, Yuchun Lone, Shihui Sun & Yusen Zhou

To cite this article: Yang Zeng, Tongtong Gao, Guangyu Zhao, Yuting Jiang, Yi Yang, Hong Yu, Zihua Kou, Yuchun Lone, Shihui Sun & Yusen Zhou (2016) Generation of human MHC (HLA-A11/DR1) transgenic mice for vaccine evaluation, Human Vaccines & Immunotherapeutics, 12:3, 829-836, DOI: [10.1080/21645515.2015.1103405](https://doi.org/10.1080/21645515.2015.1103405)

To link to this article: <http://dx.doi.org/10.1080/21645515.2015.1103405>

 Accepted author version posted online: 19 Oct 2015.

 Submit your article to this journal [↗](#)

 Article views: 84

 View related articles [↗](#)

 View Crossmark data [↗](#)

Full Terms & Conditions of access and use can be found at
<http://www.tandfonline.com/action/journalInformation?journalCode=khvi20>

Download by: [Chinese Academy of Medical Sciences]

Date: 12 May 2016, At: 01:12

Abstract

The rapid occurrence of emerging infectious diseases demonstrates an urgent need for a new preclinical experimental model that reliably replicates human immune responses. Here, a new homozygous humanized human leukocyte antigen (HLA)-A11/DR1 transgenic mouse (HLA-A11^{+/+}/DR01^{+/+}/H-2- β _{2m}^{-/-}/IA β ^{-/-}) was generated by crossing HLA-A11 transgenic mice with HLA-A2^{+/+}/DR01^{+/+}/H-2- β _{2m}^{-/-}/IA β ^{-/-} mice. The HLA-A11-restricted immune response of this mouse model was then examined. HLA-A11 transgenic mice expressed a chimeric major histocompatibility complex (MHC) molecule comprising the α 1, α 2 and β _{2m} domains of human HLA-A11 and the α 3 transmembrane and cytoplasmic domains of murine H-2D^b were generated. The correct integration of HLA-A11 and HLA-DR1 into the genome of HLA-A11/DR1 transgenic mice (which lacked the expression of endogenous H-2-I/II molecules) was then confirmed. Immunizing mice with a recombinant HBV vaccine or a recombinant HIV-1 protein resulted in the generation of IFN- γ -producing cytotoxic T lymphocyte (CTL) and antigen-specific antibodies. The HLA-A11-restricted CTL response was directed at HLA immunodominant epitopes. Furthermore, we identified two HLA-A11 restricted epitopes of EBOV GP protein and four of MERS-CoV S protein. These mice represent a versatile animal model for studying the immunogenicity of HLA CTL epitopes in the absence of murine MHC responses. The established animal model will also be useful for evaluating and optimizing T cell-based vaccines and for studying differences in antigen processing between mice and humans.

Introduction

Major histocompatibility complex (MHC) molecules play a vital role in the activation of adaptive immune system. MHC presents antigens (usually peptides) to immune cells in a MHC-specific context and participate in the differentiation and maturation of T lymphocytes in thymus[92, 93]. The incidence of diseases caused by newly emerged viruses is increasing worldwide; therefore, candidate epitopes-based vaccines are vital to provide immune protection from pathogens via the elicitation of humoral and cellular responses[94-99]. Specific cytotoxic T lymphocyte (CTL) responses would lead to a marked reduction in the viral load and may even clear the virus and cure some autoimmune diseases[100]. A protective adaptive immune response is based on the effective activation and mobilization of B cells, cytotoxic T cells and helper T cells[101]. Synergism between MHC class I and II molecules are key components of an effective host immune response.

Human MHC molecules-HLA molecules are the most polymorphic genes in human genome. HLA restriction differs markedly according to geographical region and ethnicity. Several studies based on HLA-I or HLA-II transgenic mice to illuminate the molecular mechanism(s) underlying diseases, to evaluate candidate vaccines, and to identify HLA-restricted epitopes[102, 103]. For example, Ishioka et al [104] used HLA-A2 and HLA-A11 transgenic mice to evaluate a minigene DNA vaccine encoding multiple HLA-restricted CTL epitopes derived from HIV and HBV. Pajot[105] used HLA-DR1 transgenic mice to identify novel HLA-DR1-restricted epitopes derived from HBV envelope protein. T helper cells play a vital role in boosting CTL responses and humoral immune responses against pathogens; indeed, the collaboration between T helper and cytotoxic CD8⁺ T cells is critical for an effective CTL response[106, 107]. We previously generated HLA-transgenic mice expressing both HLA class I and II molecules (e.g., HLA-A2/DR1 transgenic mice[76] and HLA-A2/DP4 transgenic mice[77]) and applied them to develop and evaluate vaccines[108-111].

HLA-A11 is one of the most common HLA class I alleles in the world, with a phenotypic frequency of about 20-30% in Chinese population and 10–15% in European and American populations[112]. The first HLA-A11/K^b mouse was generated by Alexander[113] and was applied to develop HLA-A11 restricted epitopes based vaccines[114]. However, the relevance of this model to human immune system was

overshadowed by the presence of murine H-2 class I or II molecules, which were used preferentially as restricting elements in response to antigens[115, 116]. Furthermore, HLA-A11/K^b mice did not accurately reflect human T helper cell responses because they lacked HLA-II molecules. Thus, a transgenic mouse model expressing both HLA-A11 and HLA-DR1 molecules, but lacking H-2 class I and II molecules is needed.

Here, we constructed an HLA-A11/DR1 (A11^{+/+}/DR01^{+/+}/H-2-β_{2m}^{-/-}/IAβ^{-/-}) double transgenic mouse model based on HLA-A*1101/DR01 alleles, which represented 20-25% of Chinese population, and furthermore applied it to the evaluation of commercial and candidate vaccines, and the identification of candidate epitopes.

Materials and methods

Construction of the HHD chimeric HLA-A11 transgenic plasmid

A 2873 bp chimeric HLA-A*1101 (GenBank accession number, D16841.1) monochain fragment was synthesized by GenScript and sub cloned into pUC57 plasmid to generate pUC57-HLA-A11 recombinant plasmid. Then pUC57-HLA-A11 was enzyme digestion via *Sal* I and *Bam*H I restriction sites to generate a 2900 bp fragment (Table 10).

Table 10. The enzyme digestion identification of pUC57-HLA-A11 plasmid

| Reagents | Volume (μ L) |
|----------------------------|-------------------|
| <i>Sal</i> I | 0.5 |
| <i>Bam</i> H I | 0.5 |
| pUC57-HLA-A11 | 5 |
| H ₂ O | 3 |
| 10 \times loading buffer | 1 |

Reaction condition: 37°C, 2h

The product after enzyme digestion (HLA-A11 fragment, 2900 bp) was linked with pET-32a plasmid to generated pET-32a-HLA-A11 (Table 11).

Table 11. The construction of pET-32a-HLA-A11 plasmid.

| Reagents | Volume (μ L) |
|------------------|-------------------|
| Solution I | 5 |
| HLA-A11 fragment | 4.5 |
| pET-32a | 0.5 |

Reaction condition: 16°C, 1h

A 2873 bp chimeric HLA-A11*01 mono-chain fragment sub-cloned into pET-32a plasmid via *Sal*I and *Kpn*I to generate pET-32a-HLA-A11 (Table 12), which encompassed the human HLA-A11 leader sequence, α 1 and α 2 domains, murine H-2D^b

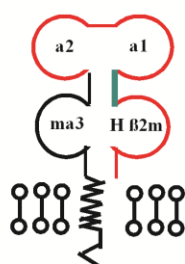
(from $\alpha 3$ domain to COOH terminus), and human $\beta 2$ -microglobulin ($\beta 2m$), which was covalently linked between the leader sequence and the 5' end of HLA-A11 ($\alpha 1$ and $\alpha 2$) domains via a 15 amino acid linker encoding Gly₄Ser₃[117] (as shown in Figure 35). Mouse $\alpha 3$ domain within the chimeric HLA-A11 molecule facilitates the interaction with mouse CD8 molecules[117].

Table 12. The enzyme digestion identification of pET-32a-HLA-A11 plasmid

| Reagents | Volume (μ L) |
|----------------------------|-------------------|
| <i>Kpn</i> I | 0.5 |
| <i>Sal</i> I | 0.5 |
| pET-32a-HLA-A11 | 5 |
| H ₂ O | 3 |
| 10 \times loading buffer | 1 |

Reaction condition: 37°C, 2h

A



B

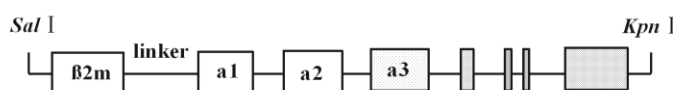


Figure 35. Schematic diagram of the chimeric human/mouse MHC class I gene. A. Schematic diagram of the monochain chimeric human/mouse MHC class I gene showing the HHD structure of the chimeric human $\alpha 1$, $\alpha 2$ and $\beta 2m$ of HLA-A11/murine H-2 $\alpha 3$ molecule. The murine H-2 $\alpha 1$ domain is covalently linked to human $\beta 2m$ via a 15-amino acid linker. B. Linear representation of final HLA-A11 construct.

Generation of HHD chimeric HLA-A11 transgenic mice

The purified HLA-A11 fragment was released from pET-32a-A11 by digestion with *SalI* and *KpnI* and microinjected into pronuclei from fertilized (C57BL/6J × C57BL/6J) F1 mouse eggs to generate transgenic embryos. The embryos were then re-implanted into pseudo pregnant female mice. HLA-A11 transgenic mice were identified by PCR of genomic DNA and by fluorescence activated cell sorting of T lymphocytes (see below).

Genotype identification

HLA-A11 and HLA-DR1 transgenes and H-2 β_2m /IA β knockout mice were identified by PCR. Murine genomic DNA was extracted using genomic DNA isolation protocols. Murine tails were digested by incubation with NaCl (100 mM), Tris-HCl (50 mM), EDTA (100 mM), 1% SDS and proteinase K (0.5 mg/mL, Merck, Germany) overnight at the 56 °C incubators. Followed by the addition of 250 mL of saturated NaCl solution and isopropanol precipitation. Pellets were washed two or three times with 70% ethanol and resuspended in 100 mL deionized water. After homogenization of DNA concentration, PCR was conducted using the following primers (Table 13-16):

Table 13. The primers of HLA-A11/DR1 and H-2 β_2m / Ia β

| Primers | Sequences |
|-------------------------|-----------------------------|
| HLA-A11-up-F | 5'-CTGGGTTTCATCCATCCG-3' |
| HLA-A11-up-R | 5'-GATCGGTCTGGCTCTGAGC-3' |
| HLA-A11-down-F | 5'- CTGGGTTTCATCCATCCG-3' |
| HLA-A11-down-R | 5'- GATCGGTCTGGCTCTGAGC-3' |
| HLA-DR1-F | 5'-GCTTCGAAATGGAAAACCTG-3', |
| HLA-DR1-R | 5'-ATGTGCCTTACAGAGGCCCC-3' |
| Mouse β_2m -F | 5'-CTGAGCTCTGTTTTTCGTCTG-3' |
| Mouse β_2m -R | 5'-CTTAACTCTGCAGGCGTATG-3' |
| Mouse H-2 IA β -F | 5'-TTCGTGTACCAGTTCATGGG-3' |
| Mouse H-2 IA β -R | 5'-TAGTTGTGTCTGCACACCGT-3' |
| Neo55a | 5'-CCTGCCGAGAAAGTATCCA-3' |

Table 14. The PCR reaction systems of HLA-A11/DR1 and H-2 β_2m / Ia β

| Genotype | 2× Taq Master Mix (μ L) | Primers (250 nm) (μ L) | DNA (μ L) | H ₂ O (μ L) |
|-----------------|---------------------------------|--------------------------------|-------------------|--------------------------------|
| HLA-A11-up | 10 | 2 | 1 | 7 |
| HLA-A11-down | 10 | 2 | 1 | 7 |
| HLA-DR1 | 10 | 2 | 1 | 7 |
| H-2- β_2m | 10 | 3 | 1 | 6 |
| H-2-Ia β | 10 | 3 | 1 | 6 |

Table 15. The PCR reaction conditions of HLA-A11/DR1 and H-2 β_2m / Ia β

| Genotype | 95°C | 94°C | Annealing °C | Annealing | 72°C | Circles | 72°C |
|-----------------|--------|--------|--------------|-----------|--------|---------|--------|
| HLA-A11-up | 5 min | 30 sec | 54 °C | 30 sec | 30 sec | 34 | 10 min |
| HLA-A11-down | 5 min | 30 sec | 54 °C | 30 sec | 30 sec | 34 | 10 min |
| HLA-DR1 | 10 min | 30 sec | 55 °C | 30 sec | 30 sec | 40 | 10 min |
| H-2- β_2m | 10 min | 30 sec | 52 °C | 30 sec | 30 sec | 40 | 10 min |
| H-2-Ia β | 10 min | 30 sec | 52 °C | 30 sec | 30 sec | 40 | 10 min |

Table 16. The PCR reaction products of HLA-A11/DR1 and H-2 β_2m / Ia β

| | HLA-A11-up | HLA-A11-down | HLA-DR1 | H-2- β_2m | H-2-Ia β |
|-----|------------|--------------|---------|-----------------|----------------|
| +/+ | 570 bp | 483 bp | 600 bp | 600 bp | 730 bp |
| +/- | 570 bp | 483 bp | 600 bp | 260 bp | 230 bp |
| -/- | / | / | / | 260 bp/600 bp | 230 bp/730 bp |

The Detection of gene copies number of HLA-A11 transgenic founder mice

The above six HLA-A11 transgenic founder mice identified by PCR were named HLA-A11 founder mice No.1-6, among them, HLA-A11 founder mice No.3 and No.5 had better vitality and better physiological state. The HLA-A11 gene copies numbers in

genome DNA of HLA-A11 founder mice No.3 and No.5 were detected by Real-time PCR. The results were shown in Figure 38, 3 copies of HLA-A11 gene in the genome of HLA-A11 founder mice No.5 is significantly higher than HLA-A11 founder mice No.3 and C57BL/6 mice.

Generation of HLA-A11/DR1 transgenic mice

HLA-A11 transgenic mice showed the highest expression of HLA-A11 were crossed with HLA-A2/DR1 (HLA-A2^{+/+}/DR1^{+/+}/β₂m⁻/IAβ⁻) transgenic mice on a C57BL/6 background, HLA-A2/DR1 transgenic mice were originally generated by Dr. Yuchun Lone[76]. Offspring with HLA-A2⁻A11^{+/+}/DR1^{+/+}/H-2-β₂m⁻/IAβ⁻ genotype were identified by PCR and flow cytometry analysis.

Mice

Mice were bred in the animal facility at the Laboratory Animal Center, Chinese Academy of Medical Sciences, Beijing, China. All experiments were performed according to the approved protocols and guidelines of the animal facility at the Institutional Animal Care and Use Committees of the Laboratory Animal Center, State Key Laboratory of Pathogen and Biosecurity, Beijing Institute of Microbiology and Epidemiology (permit number, BIME 2014-0017), and the recommendations set out in the guide for the Care and Use of Laboratory Animals.

Flow cytometry analysis

Mice from the experimental and control group were euthanized and the splenocytes were isolated. The expression of HLA-A11 and HLA-DR1 was analyzed by flow cytometry with PE-anti-human HLA-ABC and FITC-anti-human HLA-DR antibodies (anti-HLA class I and anti-HLA class II, respectively; BioLegend, San Diego, CA, USA). Splenocytes isolated from wild-type C57BL/6 and H-2-I/II knockout mice were used as controls. To determine the percentage of CD4⁺ cells and CD8⁺ cells, splenocytes were first labeled with a PE-anti-mouse CD3 antibody (BioLegend), followed by PE-Cy5-anti-mouse CD8 antibody or APC-anti-mouse CD4 antibody (BioLegend).

Immunization of HLA-A11/DR1 transgenic mice

Female HLA-A11/DR1 transgenic mice or wild-type C57BL/6 mice (6-8 weeks old) received three intramuscular (i.m.) injections of recombinant HBV S antigen (1 µg) adsorbed to 100 µg of Al(OH)₃ (alum adjuvant) in combination with 10 µg of CpG-ODNs (kindly provided by Dr. Honglin Xu[118]) (total injected volume, 100 µL). Each immunization was separated by an interval of 14 days. Sera were collected both before and after each immunization for serological analysis. Mice were sacrificed 10 days after the final boost, and the cytolytic responses to a recombinant HBsAg vaccine were examined in an IFN-γ ELISPOT assay.

Female transgenic and wild-type mice (6-8 weeks old) were anesthetized, and the tibialis anterior muscles were injected with 10 µg of recombinant HIV-1 protein in alum adjuvant; mice received three injections at 14 days intervals[119]. The immunogenicity of two known HLA-A11-restricted epitopes derived from the HIV-Pol gene (HIV-Pol₁₇₇₋₁₈₈: QMAVFIHNFKRK)[120] and the HIV-GP160 gene (HIV-GP160₃₂₋₄₅: KLWVTVYYGVPVWR)[120] was examined by measuring the amount of IFN-γ secreted by CD8⁺ T lymphocytes from HLA-A11/DR1 transgenic mice and wild-type C57BL/6 mice. Mice were sacrificed 10 days after the final boost, and the cytolytic responses and HLA-A11-restricted CTL responses to the recombinant HIV-1 protein were determined in an ELISPOT assay.

Measurement of serum antibodies by ELISA

The serum levels of antibodies specific for recombinant HBV vaccine and recombinant HIV-1 protein in immunized HLA-A11/DR1 transgenic mice and C57BL/6 mice were measured in ELISA. The plates coated with the HBV vaccine antigen or the recombinant HIV-1 protein were blocked with PBS supplemented with 0.1% Tween 20 and 10% FCS and then washed three times. After the addition of mouse serum for 1 h, the plates were washed again, and bound antibodies were detected with HRP (horseradish peroxidase)-labeled anti-mouse IgG (Santa Cruz Biotechnology, Inc.). Absorbance was then measured at 450_{nm} and 630_{nm} in a plate reader. The antibody titers (the mean of at least three determinations) were calculated using the serial end-point dilution method[121].

ELISPOT assay

An ELISPOT assay was performed to detect IFN- γ secreted by CD8⁺ T lymphocytes with BD™ ELISPOT kit (BD Biosciences, CA). Briefly, 96-well ELISPOT plates were coated with an anti-IFN- γ mAb overnight at 4°C and then blocked with blocking solution. Splenocytes (5×10^5) were added to each well and cultured in the presence of recombinant HBV vaccine, synthetic peptides, or recombinant HIV-1 protein (all at 10 μ g/ml) and incubated at 37°C/5% CO₂ for 48 h. IFN- γ -secreting cells were captured by an anti-IFN- γ mAb and detected by incubation with a biotinylated anti-IFN- γ mAb for 2 h at 37°C, followed by streptavidin-HRP for 1 h. The plates were then developed for 5-10 minutes in an ACE substrate solution (BD Biosciences, CA), washed three times, and air-dried at room temperature. Positive spots were counted using an ELISPOT plate reader (Cellular Technology Ltd).

Database resources and analysis software

The amino acid sequences of EBOV GP protein and MERS CoV S protein were obtained from Genbank database. Comprehensive bioinformatics software was used to analyze and predict the CTL epitopes of EBOV GP protein and MERS CoV S protein, such as SYFPEITHI, BIMAS, MAPPP, NetMHC (4.0), MHCpred (version 2.0) and EpiTOP, etc. The websites of these online software were shown as follows:

SYFPEITHI: <http://www.syfpeithi.de/>

NetMHC: <http://www.cbs.dtu.dk/services/NetMHCII/>

MHCpred: <http://www.ddg-pharmfac.net/mhcpred/MHCPred/>

MAPPP: <http://www.mpiib-berlin.mpg.de/MAPPP/binding.html>

BIMAS: http://www-bimas.cit.nih.gov/molbio/hla_bind/

Among the predicted epitopes with higher HLA-A11-restricted score and higher binding ability to HLA-A11 molecule, the hydrophobicity and solubility of these peptides sequences were analyzed. As a result, the peptides with conventional hydrophobicity below zero were easier to synthesize and dissolve. Twelve HLA-A11-restricted epitopes derived from EBOV GP and twelve HLA-A11-restricted CTL epitope peptides of MERS-CoV S protein were screened out and synthesized. HLA-A11/DR1 transgenic mice will be applied to identify these HLA-A11 restricted CTL epitopes (Table 17).

Table 17. HLA-A11-restricted CTL epitopes of EBOV and MERS-CoV analyzed by comprehensive prediction

| No. | Sequences | Location | Length | Conventional hydrophobicity | Score |
|--------------|------------------|----------------------------|---------------|------------------------------------|--------------|
| E-P1 | ATDVPSVTK | EBOV-GP ₇₆ | 9 | -1 | 28 |
| E-P2 | STHNTPVYK | EBOV-GP ₃₈₇ | 9 | -11.5 | 28 |
| E-P3 | ATTAAGPLK | EBOV-GP ₄₂₃ | 9 | 1.9 | 26 |
| E-P4 | NTTGKLIWK | EBOV-GP ₂₆₈ | 9 | -5.7 | 25 |
| E-P5 | EVIVNAQPK | EBOV-GP ₅₀₂ | 9 | -1.3 | 23 |
| E-P6 | VTGILQLPR | EBOV-GP ₃ | 9 | 5.6 | 22 |
| E-P7 | FTAVSNGPK | EBOV-GP ₃₀₈ | 9 | -2.1 | 22 |
| E-P8 | ATQVGQHHR | EBOV-GP ₄₀₁ | 9 | -13 | 22 |
| E-P9 | RTFSILNRK | EBOV-GP ₅₈₀ | 9 | -6.8 | 22 |
| E-P10 | QIIHDFVDK | EBO-GP ₆₂₅ | 9 | -1.6 | 22 |
| E-P11 | TSPQPPTTK | EBOV-GP ₃₇₃ | 9 | -15.1 | 21 |
| E-P12 | ETKKNLTRK | EBOV-GP ₂₉₂ | 9 | -20.8 | 20 |
| M-P1 | ASIGDIIQR | MERS-CoV-S ₁₀₄₉ | 9 | 2.6 | 28 |
| M-P2 | PSTSATIRK | MERS-CoV-S ₁₃₄ | 9 | -6.7 | 25 |
| M-P3 | GTNCMGKLK | MERS-CoV-S ₁₃₂₄ | 9 | -4.6 | 25 |
| M-P4 | SVGNFSDGK | MERS-CoV-S ₁₅₂ | 9 | -6.3 | 24 |
| M-P5 | SVIYDKETK | MERS-CoV-S ₆₆₀ | 9 | -8.9 | 24 |
| M-P6 | SSLFVEDCK | MERS-CoV-S ₇₂₀ | 9 | 0.8 | 24 |
| M-P7 | STLTPRSVR | MERS-CoV-S ₇₄₃ | 9 | -5.6 | 24 |
| M-P8 | LTITKPLK | MERS-CoV-S ₄₈₈ | 9 | 0.6 | 22 |
| M-P9 | SSTMSQYSR | MERS-CoV-S ₆₈₃ | 9 | -11.3 | 21 |
| M-P10 | AIEDLLFDK | MERS-CoV-S ₈₈₉ | 9 | 2.3 | 21 |
| M-P11 | TTTNEAFRK | MERS-CoV-S ₁₀₁₃ | 9 | -12.9 | 21 |
| M-P12 | AALSAQLAK | MERS-CoV-S ₁₀₉₂ | 9 | 6.6 | 19 |

Statistical analysis

Each experiment was repeated at least three times, and data were expressed as the mean

± SEM. The means or geometric means of multiple groups were compared using Student's t-test. All statistical analysis was performed using GraphPad Prism version 5.0. A P value <0.05 was considered statistically significant.

Results

Identification of HLA-A11 transgenic vector

A 2873 bp chimeric HLA-A11*01 mono-chain fragment sub-cloned into the pET-32a plasmid (5841 bp) via *SalI* and *KpnI* to generate pET-32a-HLA-A11 recombinant vector (Figure 36A). We confirmed the HLA-A11 transgenic vector pET-32a-A11 recombinant plasmid by enzyme digestion (Figure 36B) and PCR amplification (Figure 36C).

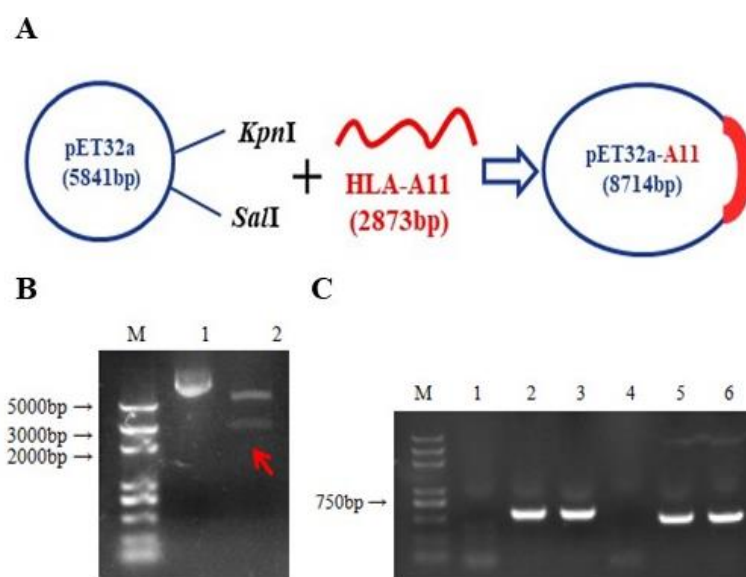


Figure 36. The identification of pET-32a-A11 recombinant plasmid. A. The construction schematic of pET-32a-A11. B. Identification of pET-32a-A11 recombinant plasmid by enzyme digestion. M: Trans 2K Plus DNA Marker; 1: pET-32a-A11 recombinant plasmid control; 2: pET-32a-A11 recombinant plasmid digested by *KpnI/SalI*. C. Identification of pET-32a-A11 recombinant plasmid. HLA-A11-up primers: 1: NC; 2: pET-32a-A11; 3: 10^{-3} * pET-32a-A11. HLA-A11-Down; 4: NC; 5: pET-32a-A11; 6: 10^{-3} * pET-32a-A11; M: Trans 2K Plus DNA Marker.

Microinjection of HLA-A11 transgenic vector and identification of HLA-A11 transgenic founder mice

The purified HLA-A11 fragment was released from pET-32a-A11 by digestion with

SalI and *KpnI* and microinjected into pronuclei from fertilized (C57BL/6J × C57BL/6J) F1 mouse eggs to generate transgenic embryos, a total of 421 transgenic embryos were obtained. The embryos were then re-implanted into 16 pseudo pregnant female mice, among them 12 mice were pregnant, the success rate of transplant was 75%. 76 neonatal mice were born. Six mice (No.44, 47, 55, 56, 69 and 71) were positive for HLA-A11 by PCR identification. The positive rate was 7.89%. Figure 37 showed the results of PCR identification of six HLA-A11 transgenic founder mice.

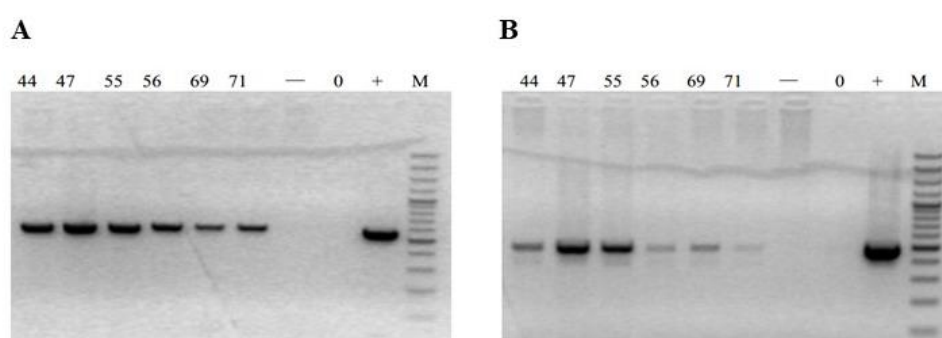


Figure 37. PCR identification of HLA-A11 transgenic founder mice. A. HLA-A11 up primers. B. HLA-A11 down primers.

The detection of gene copies number of HLA-A11 transgenic founder mice

Six HLA-A11 transgenic founder mice identified by PCR were named as No.1-No.6 HLA-A11 transgenic founder mouse, among them No.3 and No.5 were more active and dynamically. Real-time PCR was used to detect the copy numbers of the HLA-A11 transgene in the genomic DNA of the HLA-A11 transgenic mice No.3 and No.5. As shown in Figure 38, the copy numbers of HLA-A11 gene in the genome of No. 3 and No. 5 HLA-A11 transgenic founder mice were significantly higher than that of C57BL/6 mice. Among them, the copy number of the gene of No.5 HLA-A11 transgenic founder mice were relatively stable, and the results of two HLA-A11 transgenic founder mice were statistically different from those of C57BL/6 mice.

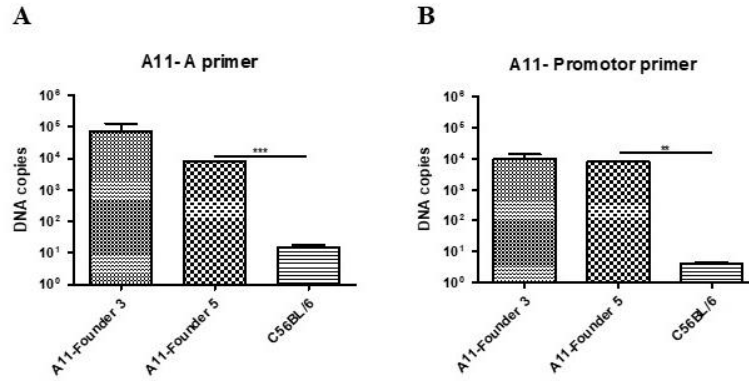


Figure 38. Real-time PCR analysis of gene copies number of HLA-A11 transgenic founder mice. A. HLA-A primers. B. HLA-Promotor primers.

Generation of homozygous HLA-A11/DR1 (HLA-A11^{+/+}/DR1^{+/+}/H-2β_{2m}^{-/-}/IAβ^{-/-}) transgenic mice

The construction of the recombinant gene encoding chimeric HLA-A11 mono-chain illustrated in Figure 35 and Figure 36. Transgenic mice expressing the integrated HLA-A11 fragment were identified by PCR (data not shown). HLA-A11/DR1 (HLA-A11^{+/+}/DR1^{+/+}/H-2β_{2m}^{-/-}/IAβ^{-/-}) transgenic mice were obtained by backcrossing the parental HLA-A11^{+/+} (HLA-A11) transgenic mice with HLA-A2^{+/+}/DR1^{+/+}/H-2β_{2m}^{-/-}/IAβ^{-/-} (HLA-A2/DR1) transgenic mice (as shown in Figure 39).

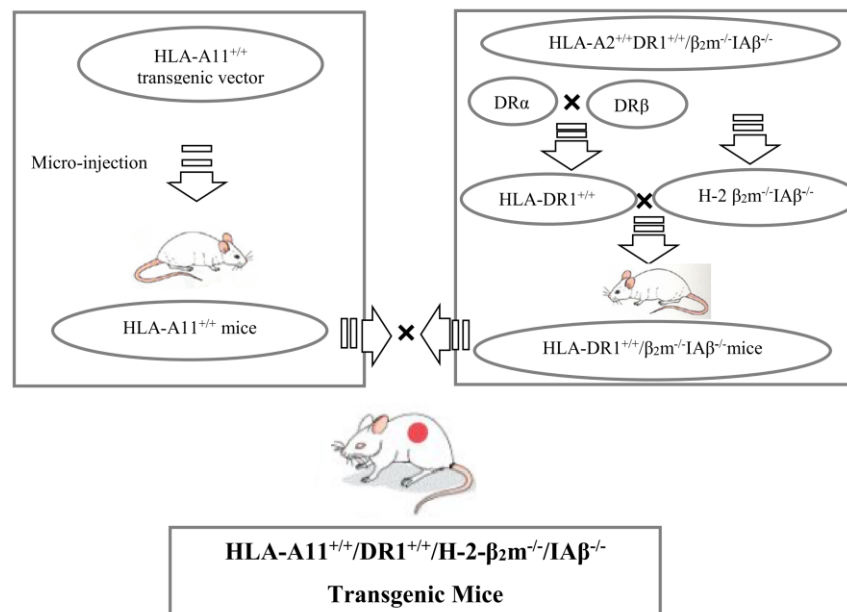


Figure 39. The construction of HLA-A11/DR1 double transgenic mice.

The genotype of HLA-A11/DR1 transgenic mice was confirmed by PCR, with offspring-derived genomic DNA as a template. The exogenous HLA-A11 and HLA-DR1 fragments were integrated into mouse genome (Figure 40A), and the endogenous H-2- β_2m and H-2-IA β (Figure 40B) genes were knocked out.

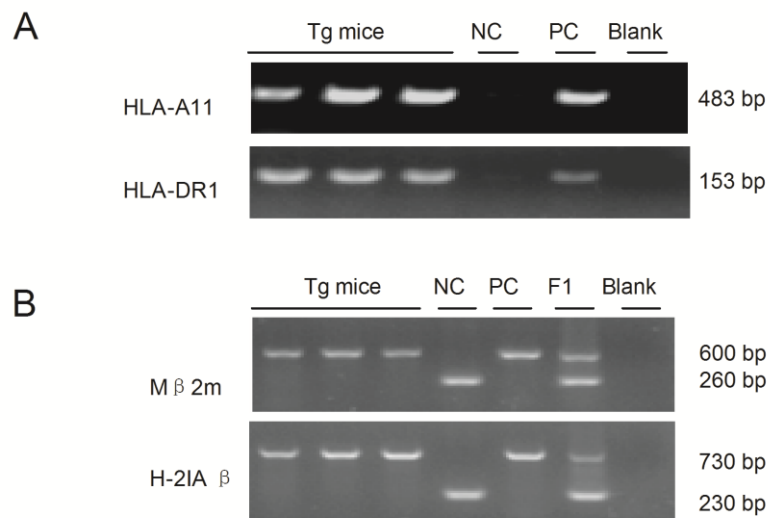


Figure 40. Genotype identification of HLA-A11/DR1 transgenic mice. Genomic DNA purified from HLA-A11/DR1 transgenic mice was analyzed by PCR using primers specific for HLA-A11, HLA-DR1, mouse β_2m , and H-2 IA β . A. Identification of HLA-A11 (upper panel) and HLA-DR1 (lower panel). Tg mice, HLA-A11/DR1 transgenic mice; NC, Negative control; PC, Positive control; Blank, dH₂O. B. Identification of mouse H-2- β_2m (upper panel) and H-2-IA β (lower panel). Tg mice, HLA-A11/DR1 transgenic mice; NC, Negative control; PC, Positive control; F1, Heterozygote control; Blank, dH₂O.

Identification of homozygous HLA-A11/DR1 transgenic mice

Male and female HLA-A11/DR1 transgenic mice (genotypes of HLA-A11 and HLA-DR1 were “+/+” or “+/-”) were mated with female or male C57BL/6 mice. According to ten offspring, the genotypes of their parents could be confirmed to be “+/+” or “+/-”.

As shown in Figure 41, if ten progenies are all positive for HLA-A11 or HLA-DR1, it means that the parental HLA-A11/DR1 male and female mice are homozygous for the target gene, which is “+/+”. On condition that negative results appeared among ten progenies indicated that the genotypes of HLA-A11 and HLA-DR1 in parental mice was “+/-”, which need to be further self-crossed to achieve homozygous. Through self-crossing for more than 10 generations, homozygous HLA-A11/DR1 double transgenic mice transgenic mice (HLA-A11^{+/+}/DR1^{+/+}/H-2-β₂m^{-/-}/IAβ^{-/-}) were successfully constructed and stably obtained.

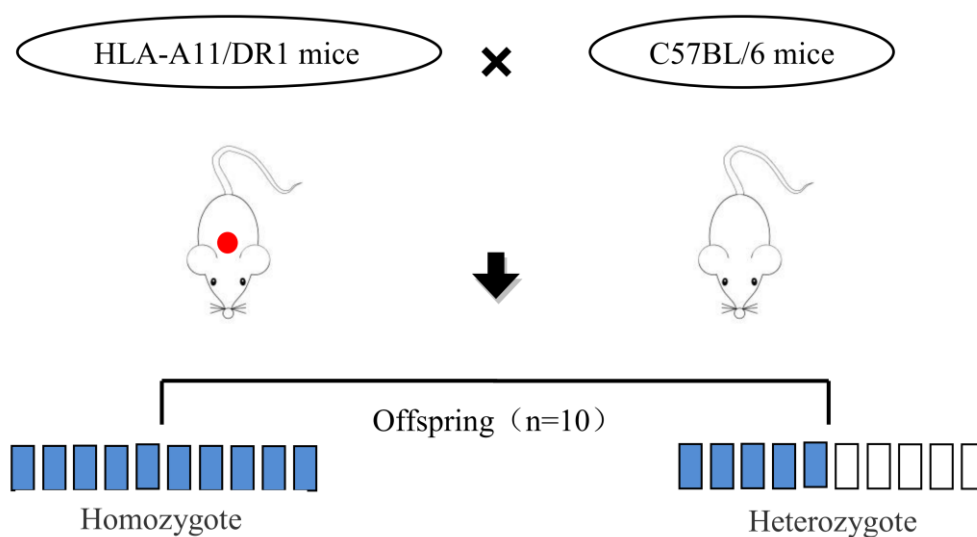


Figure 41. Schematic representation of HLA-A11/DR1 transgenic homozygous and heterozygote mice.

Analysis of HLA expression in immune cells of HLA-A11/DR1 transgenic mice

Expression of HLA-A11 and HLA-DR1 in splenocytes isolated from HLA-A11/DR1 transgenic mice was detected by flow cytometry. HLA-A11/DR1 transgenic mice expressed both HLA-A11 (Figure 42A) and HLA-DR1 (Figure 42B), whereas no HLA transgenes were expressed in wild-type C57BL/6 mice or H-2-I/II knockout mice.

Taken together, these results demonstrated that HLA-A11 and HLA-DR1 transgenes had integrated into the mouse genome and were expressed by splenocytes of HLA-

A11/DR1 transgenic mice, while the competitive inhibition by mouse endogenous H-2-I/II molecules had been eliminated. Thus, the mouse model could be used to examine cooperation between human HLA-I/II molecules without interference from mouse H-2 molecules.

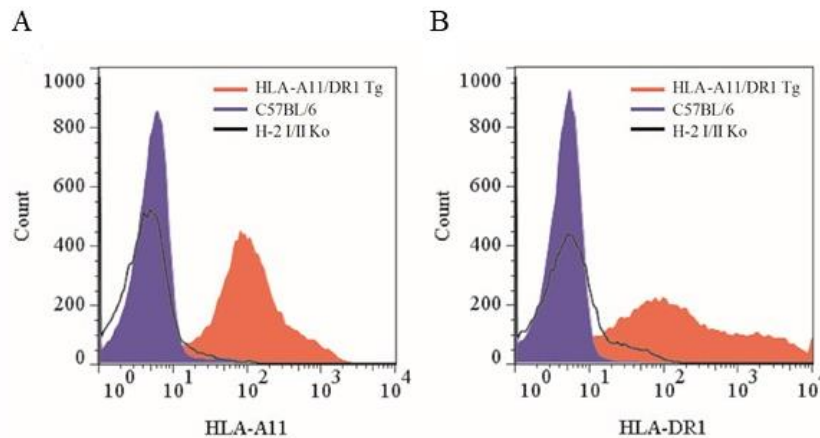


Figure 42. Flow cytometric analysis of transgenic HLA molecules expressed on the surface of immune cells of HLA-A11/DR1 transgenic mice. Splenocytes of HLA-A11/DR1 (red histogram), H-2-I/II knockout mice (black histogram), and wild-type C57BL/6 (blue histogram) mice were isolated and stained with a PE-anti-human HLA-ABC antibody (A) or an FITC-anti-human-HLA-DR antibody (B) to detect HLA-A11 and HLA-DR1 expression, respectively.

Proportions of CD8⁺ and CD4⁺ T lymphocytes in the splenocytes of HLA-A11/DR1 transgenic mice

To test whether the expression of exogenous HLA transgenes would still allow positive and negative selection of CD4⁺ and CD8⁺ T lymphocytes in HLA-A11/DR1 transgenic mice, we next examined the populations of HLA-regulated T lymphocytes in the periphery. The numbers of CD3⁺CD4⁺ and CD3⁺CD8⁺ T lymphocytes were counted by flow cytometry.

The isolated splenocytes were labeled with a PE-anti-mouse CD3 antibody, followed by a PE-Cy5-anti-mouse CD8 antibody. Figure 43 A-D showed that 1.48% of lymphocytes in HLA-A11/DR1 transgenic mice, 3.32% of lymphocytes in HLA-A11

transgenic mice, and 1.16% of lymphocytes in HLA-DR1 transgenic mice were CD8⁺ T cells. By contrast, 11.7% of lymphocytes in C57BL/6 mice were CD8⁺ T cells. Peripheral CD4⁺ T lymphocytes were labeled with a PE-anti-mouse CD3 antibody, followed by an APC-anti-mouse CD4 antibody. Figure 43 E-H shows that 92.2% of lymphocytes in HLA-A11/DR1 transgenic mice, 62.6% in HLA-A11 transgenic mice, and 94.8% in HLA-DR1 transgenic mice were CD4⁺ T cells, compared with 64.6% in C57BL/6 mice. Results were summarized in Table 18.

These results showed that the percentage of CD4⁺ T cells in HLA-A11/DR1 transgenic mice were similar with that of C57BL/6 mice, while the number of CD8⁺ T cells in HLA-A11/DR1 transgenic mice was lower than that in C57BL/6 mice. However, the lower percentage of CD8⁺ T cell was in accordance with that in HLA-A2/DR1 transgenic mice or HLA-A2/DP4 transgenic mice in which efficient humoral and cellular immune responses could be developed[76, 77]. Thus, HLA transgenes enabled the differentiation and maturation of CD4⁺ and CD8⁺ T lymphocytes in transgenic mice.

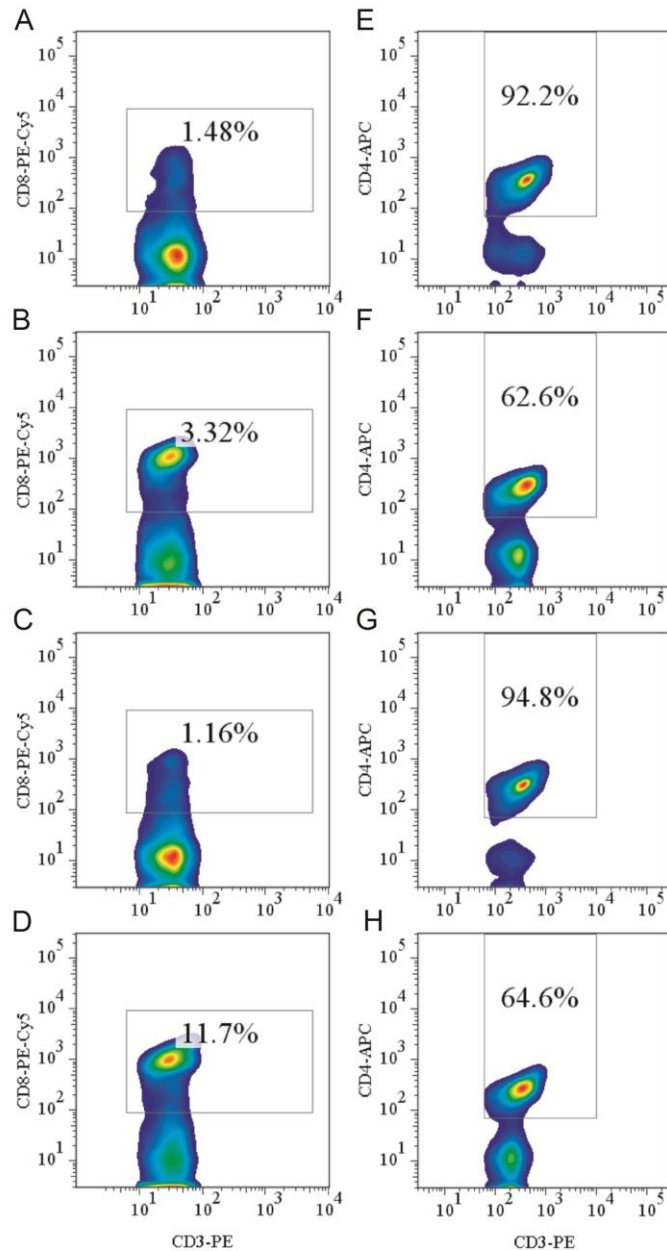


Figure 43. Flow cytometric analysis of peripheral CD8⁺ and CD4⁺ (T) lymphocytes. (A-D) Splenocytes of HLA-A11/DR1 mice (A), HLA-A11 mice (B), HLA-DR1 mice (C), and C57BL/6 mice (D) were isolated. CD3⁺ T lymphocytes were gated by staining with an FITC-anti-CD3 mAb and CD8⁺ T lymphocytes were gated by staining with a PE-cy5-anti-CD8 mAb. (E-H) Splenocytes of HLA-A11/DR1 mice (E), HLA-A11 mice (F), HLA-DR1 mice (G), and C57BL/6 mice (H) were isolated. CD3⁺ T lymphocytes were gated by staining with a PE-anti-CD3 mAb, and CD4⁺ T lymphocytes were gated by staining with an APC-anti-CD4 mAb.

Table 18. Ratio of CD8⁺ and CD4⁺ T lymphocytes to peripheral lymphocytes in HLA-A11/DR1 transgenic Mice.

| Cell types | HLA-A11/DR1 mice | HLA-A11 Mice | HLA-DR1 Mice | C57BL/6 Mice |
|---------------------------------|-------------------------|---------------------|---------------------|---------------------|
| mCD4⁺ T cells | 92.2% | 62.6% | 94.8% | 64.6% |
| mCD8⁺ T cells | 1.48% | 3.32% | 1.16% | 11.7% |

HLA-A11/DR1 transgenic mice show HLA-A11-restricted cytotoxic responses

To verify that HLA-A11/DR1 transgenic mice mount a fully functional immune response, two known immunodominant HLA-A11-restricted epitopes, one derived from HIV-Pol₁₇₇₋₁₈₈ (QMAVFIHNFKRK)[120] and the other derived from HIV-GP160₃₂₋₄₅ (KLWVTVYYGVPVWR)[120], were used to measure IFN- γ production by CD8⁺ T lymphocytes from HLA-A11/DR1 mice immunized with a recombinant HIV-1 protein vaccine.

Compared with those from C57BL/6 mice, CD8⁺ T lymphocytes from HLA-A11/DR1 mice were functionally restricted by the transgenic human MHC class I molecules (HLA-A11). HLA-A11-restricted HIV-specific CTL immune responses were specific for HLA-A11-restricted-epitopes HIV-Pol₁₇₇₋₁₈₈ (Figure 44A and B) and HIV-GP160₃₂₋₄₅ (Figure 44C and D). Collectively, these data showed that HLA-A11/DR1 transgenic mice mount a functional HLA-A11 restricted immune response.

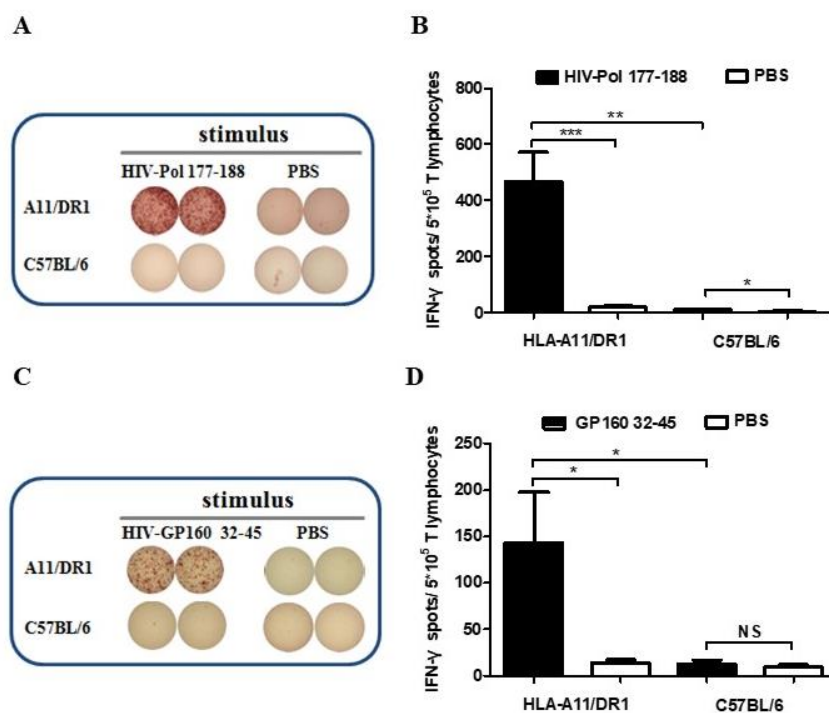


Figure 44. HLA-A11 restricted cytotoxic responses in HLA-A11/DR1 transgenic mice. Responses to HLA-A11-restricted epitope HIV-Pol₁₇₇₋₁₈₈ (A and B), and to HLA-A11-restricted epitope, HIV-GP₃₂₋₄₅ (C and D), were assessed in immunized HLA-A11/DR1 mice and C57BL/6 mice by counting the number of IFN- γ -secreting spots in ELISPOT assays.

HLA-A11/DR1 transgenic mice mount effective humoral and cellular responses

To examine the specific humoral and cellular responses to vaccination in HLA-A11/DR1 transgenic mice, mice were immunized with a recombinant HBV vaccine (derived from HBV envelope protein[118]) or with a multi-epitope HIV-1-based candidate vaccine[119].

The amount of HBsAg-specific IgG antibodies in the serum of HLA-A11/DR1 mice was similar with that in C57BL/6 mice (Figure 45A). It is worth noting that HLA-A11/DR1 mice generated 4-5-fold more IFN- γ than wild-type mice, indicating a satisfactory cellular immune response and an ability to mimic human cytotoxic response (Figure 45B).

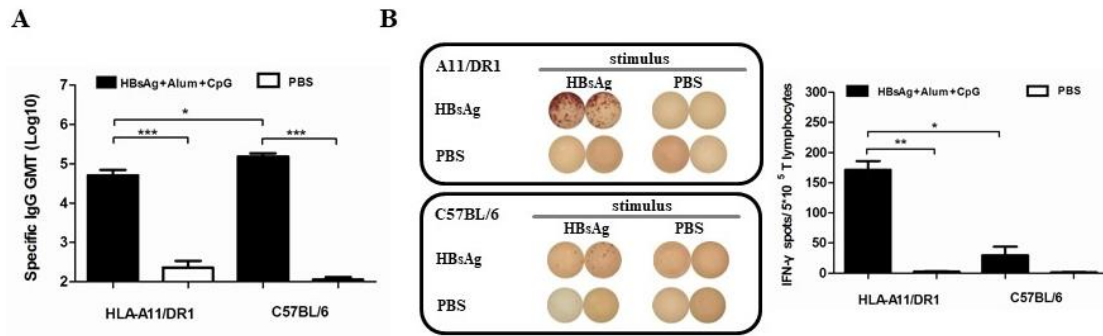


Figure 45. HBs-specific antibody and cell-mediated responses after immunization with a recombinant HBsAg vaccine. A. Sera were collected from immunized HLA-A11/DR1 transgenic mice and wild-type C57BL/6 mice, and the titers of anti-HBs (IgG) antibodies were compared with those of PBS-immunized (hollow bar) mice in an ELISA test. B. HBs epitope-specific IFN- γ production by cytotoxic T lymphocytes was examined by measuring the response of both HLA-A11/DR1 mice and C57BL/6 mice to a recombinant HBs vaccine or PBS.

The amount of HIV-specific IgG antibodies and the amount of IFN- γ secreted by CD8⁺ T lymphocytes was measured respectively. The results revealed an increase ($p < 0.05$) in the levels of specific IgG antibodies in HLA-A11/DR1 mice (Figure 46A). HLA-A11/DR1 mice also secreted more IFN- γ than wild-type mice (Figure 46B). These results suggested that HLA-A11/DR1 mice show stronger cellular immune responses than C57BL/6 mice and are therefore a suitable model for evaluating vaccines.

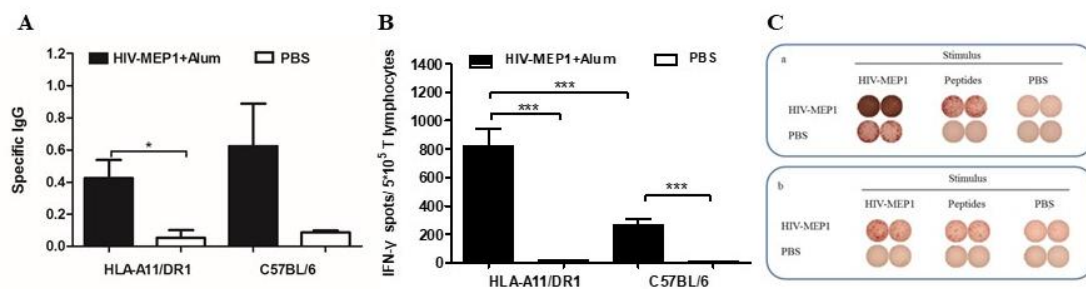


Figure 46. HIV-specific antibody and CD8⁺ T cell responses after immunization with a recombinant HIV-1 protein. A. HIV-specific antibody titers in HLA-A11/DR1 mice and C57BL/6 mice immunized with a recombinant HIV-1 protein or PBS. B and C. HIV-specific IFN- γ production by cytotoxic T lymphocytes was examined by

measuring responses to the recombinant HIV-1 protein in immunized mice (PBS-immunized mice were used as control) (a. HLA-A11/DR1 mice; b. C57BL/6 mice).

The identification of novel HLA-A11 restricted CTL epitopes of EBOV and MERS-CoV

We predicted twelve HLA-A11-restricted epitopes of EP protein of EBOV virus with the comprehensive bioinformation analysis, to identify the specific CTL response of these HLA-A11-restricted epitopes, HLA-A11/DR1 mice and C57BL/6 mice were immunized with every single peptide. ELISPOT results showed that the specific CTL responses induced by E-P1 (EBOV-GP₇₆₋₈₄, ATDVPSVTK) and E-P3 (EBOV-GP₄₂₃₋₄₃₁, ATTAAGPLK) in HLA-A11/DR1 mice was 44 SFU/5*10⁵ cells and 38 SFU/5*10⁵ cells, respectively, which was significantly stronger than that of C57BL/6 mice (3 SFU/5*10⁵ cells and 2 SFU/5*10⁵ cells) (Figure 47).

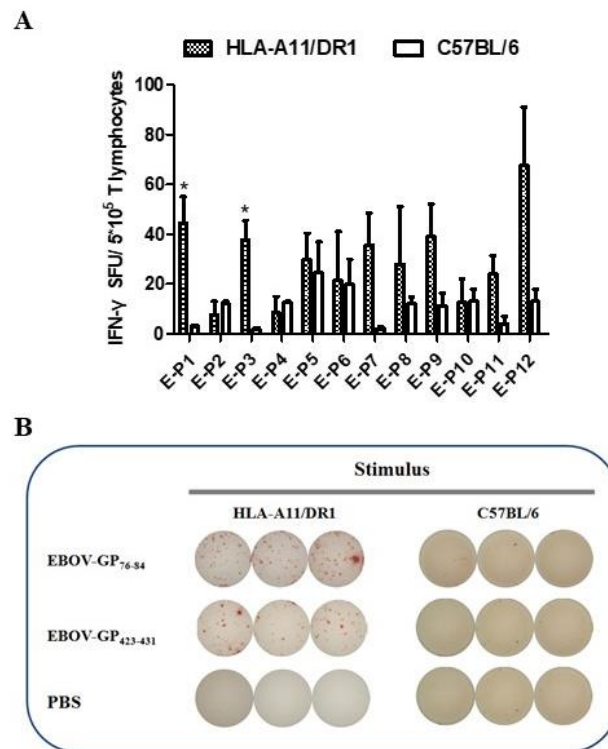


Figure 47. ELISPOT analysis of HLA-A11 restricted epitopes of EBOV virus in HLA-A11/DR1 mice.

As shown in Figure 48, HLA-A11/DR1 mice generated specific HLA-A11 CTL responses in four HLA-A11 restricted epitopes of MERS-CoV virus, which were M-P4 (MERS-S₁₅₂₋₁₆₀, SVGNFSDGK), M-P6 (MERS-S₇₂₀₋₇₂₈, SSLFVEDCK), and M-P10 (MERS-S₈₈₉₋₈₉₇, AIEDLLFDK) and M-P12 (MERS-S₁₀₉₂₋₁₁₀₀, AALSAQLAK). The specific IFN- γ produced by four HLA-A11-restricted CTL peptides in HLA-A11/DR1 mice was 30 SFU/5*10⁵ cells, 43 SFU/5*10⁵ cells, 35 SFU/5*10⁵ cells and 34 SFU/5*10⁵ cells, respectively. Whereas, the IFN- γ produced by C57BL/6 mice were 1 SFU/5*10⁵ cells, 1 SFU/5*10⁵ cells, 1 SFU/5*10⁵ cells, 1 SFU/5*10⁵ cells, respectively.

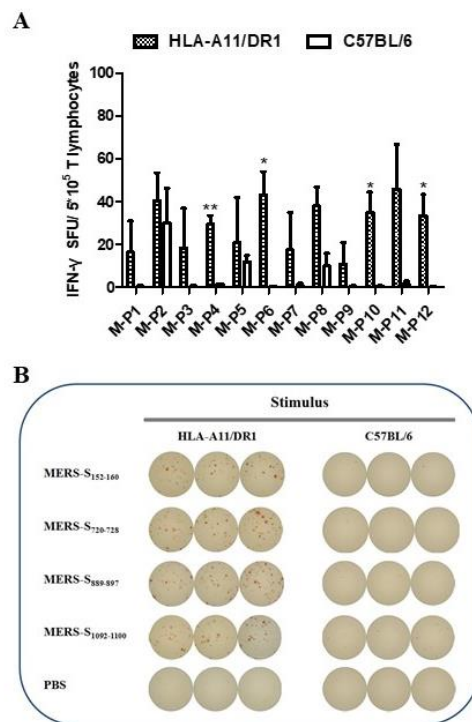


Figure 48. ELISPOT analysis of HLA-A11 restricted epitopes of MERS-CoV virus in HLA-A11/DR1 mice.

Discussion

Vaccines based on multiple epitopes can be used to target well-defined ethnic populations and could prime robust immune responses[120, 122]. To facilitate the evaluation and development of novel candidate epitopes-based vaccines, we constructed a novel humanized HLA-A11/DR1 transgenic mouse model expressing both HLA-A11 and HLA-DR1 molecules, while in the absence of H-2 class I/II molecules. Different from previous HLA-A2/DR1[76] transgenic mice and HLA-A2/DP4 transgenic mice [77], HLA-A11/DR1 transgenic mice showed combined expression of HLA-I allele-A11 and HLA-II allele-DR1, which are prevalent in Chinese population. Because a quarter of Chinese population express HLA-A11 and HLA-DR1 alleles[112], this novel animal model could be used to predict and evaluate the cellular responses of this Chinese population more accurately than previous transgenic mouse models.

HLA system is the most polymorphic gene cluster in human beings. HLA class I and II alleles are expressed in a co-dominant manner in any individual. Competition among different HLA molecules results in the selection of different immunodominant epitopes that recognize and present processed antigens to immune cells. Research on the function of an independent HLA molecule in the absence of competitive inhibition of other HLA alleles is a real challenge. Humanized mice have allowed the investigation of individual HLA molecules due to the integration of specific HLA alleles into the mouse genome. Indeed, HLA double-transgenic mice (expressing both human HLA class I and class II molecules) in the absence of murine H-2 molecules have been developed [76, 77].

The phenotypic frequency of HLA-A11 in Chinese population is about 20–30% compared with 10–15% in European, American, and Middle Eastern populations[112]. Thus, more and more research are focused on HLA-A11 transgenic mice to evaluate HLA-A11-restricted epitope-based vaccines[123, 124].

To ensure that the transgenes are functioned within the mouse genome, we designed an HLA-A11 HHD chimeric monochain expressing the $\alpha 1/\alpha 2/\beta_2m$ domains of HLA-A11 and the $\alpha 3$ domain of endogenous H-2. Replacing human $\alpha 3$ domain with mouse $\alpha 3$ domain preserved the species-specific binding affinity between HLA-A11 chimeric

monochain and mouse CD8 molecule. Inactivating important components of endogenous H-2 molecule could prevent H-2 molecules from competing with transgenic HLA molecules. Through this strategy, HLA transgenic mice could only mount HLA-restricted immune responses without H-2-restricted immune responses.

Conclusions

We confirmed the cell surface expression of HLA-I and HLA-II molecules in immune cells of HLA-A11 transgenic mice. Although the percentage of CD8⁺ T lymphocytes in HLA-A11/DR1 transgenic mice was lower than that in C57BL/6 mice, the transgenic HLA molecules efficiently presented antigens to immune cells to generate functional humoral and cellular immune responses. The low percentage of CD8⁺ T lymphocytes in HLA-A11/DR1 mice is in accordance with that in HLA-A2/DR1 mice[76], HLA-A2/DP4 mice[77], and other HLA class I transgenic mice models which also could develop efficient humoral and cellular immune responses similar to those in humans[125, 126]. Furthermore, several studies show that the lower percentage of CD8⁺ T lymphocytes does not preclude the use of HLA-A2/DR1 mice to study the immune responses to pathogens such as HBV and HIV[125, 127]. Interesting, it is now well documented by several comparative studies that transgenic HLA class I molecules in chimeric monochain form are superior than traditional transgenic HLA class I molecule mice to induce more efficient T cell responses, even though the number of CD8⁺ T cell is lower[116, 128].

We also confirmed that HLA-A11/DR1 transgenic mice mount efficient and functional humoral and cellular immune responses to a recombinant HBV vaccine and a recombinant HIV-1 protein, and especially mount the specific A11-restricted cellular immune response to a recombinant HIV-1 protein. In our HLA-A11/DR1 transgenic mice, the HLA-DR1 genes were derived from HLA-A2/DR1 transgenic mice in which the HLA-DR1-restricted CD4⁺ T cell responses were described with HLA-DR1-restricted epitope HBsAg₁₇₉₋₁₉₄[76]. Furthermore, by using HLA-A2/DR1 transgenic mice, Pajot [127] identified two new HLA-DR1-restricted HIV-1 Gag p24-derived epitopes (Gag₃₂₁₋₃₄₀ and Gag₃₃₁₋₃₅₀) and confirmed the immunogenicity of seven epitopes that had been described previously. In addition, it is well documented that in the absence of MHC class II expression, there are no CD4⁺ T cells and more interesting, there were also no humoral responses in the case of vaccination against HBV, as shown in HLA-A2 single transgenic H-2 class I/class II knock-out (KO) mice[127]. In the present HLA-A11/DR1 transgenic mice, we confirmed the HLA-DR1-restricted epitope HBsAg₁₇₉₋₁₉₄ responses as reported in HLA-A2/DR1 mice (data not shown). Furthermore, we show an efficient specific antibodies response (Figure 45) which were

reported highly protective against HBV infection. The results indicated that the novel HLA-A11/DR1 transgenic mice model has the potential to evaluate both T cells (CD8 and CD4) and B cells activities as in HLA-A2/DR1 transgenic mice, but covering different population. Two models mentioned above are equally important to evaluate available commercial vaccines and novel vaccine candidates. Furthermore, we identified two HLA-A11 restricted epitopes of EBOV GP protein and four of MERS-CoV S protein.

In summary, we generated a novel HLA-A11/DR1 transgenic mouse strain that faithfully reproduced a human immune response and may be useful for identifying protective epitopes, designing human vaccine and for evaluating vaccination strategies. The humanized HLA-A11/DR1 transgenic mouse is a promising and versatile preclinical model that will facilitate the study of human immune responses to a variety of antigens.

**Part 3. A novel helper-dependent adenovirus-based cell
culture model for Hepatitis C virus replication and
production**

Xiaojun Zhou[#], **Yang Zeng[#]**, Junfeng Li, Yan Guo, Yuanhui Fu, Jinsheng He, Shihui Sun* and Yusen Zhou*

By using the Hepatitis C virus (HCV) genotype 2a JFH-1 or its chimeric strains, a HCV infection system had been previously developed through several methods— such as in vitro-transcribed JFH1-RNA transfection or stable transfection of the JFH1 cDNA into human hepatoma Huh-7 cell line or its derivatives. However, other reliable methods for delivery of the HCV genome into cells are still worth trying. The helper-dependent adenovirus (HDAd) is devoid of all viral coding sequences and has a package capacity of 37 kb, which is suitably large for the delivery of the HCV genome. Here we report a new method for delivery of the HCV genome into Huh-7 and HepG2 cells by using the HDAd vector. Our results demonstrated that the infection of Huh-7 cells with the HDAdJFH1 virus led to efficient HCV replication and virion production. We found that the HCV viral RNA levels could reach 10^7 copies per milliliter in the culture medium. HDAdJFH1-infected Huh-7 cells could be cultured for 8 passages with the culture medium remaining infectious for naïve Huh-7 cells throughout this period. This infection system proved effective for evaluating the anti-HCV effects of IFN- α in Huh-7 cells. Co-infection of HepG2 cells with the HDAdJFH1 and HDAdmiR-122 virus also resulted in HCV expression and replication. This is the first report of an HDAd-based strategy for HCV replication and production in vitro.

RESEARCH

Open Access

A novel helper-dependent adenovirus-based cell culture model for Hepatitis C virus replication and production

Xiaojun Zhou^{1,2}, Yang Zeng^{1†}, Junfeng Li¹, Yan Guo¹, Yuanhui Fu³, Jinsheng He³, Shihui Sun^{1*} and Yusen Zhou^{1*}

Abstract

Background: By using the hepatitis C virus (HCV) genotype 2a JFH1 or its chimeric strains, a HCV infection system has been previously developed through several methods— such as *in vitro*-transcribed JFH1-RNA transfection or stable transfection of the JFH1 cDNA into human hepatoma Huh-7 cell line or its derivatives. However, other reliable methods for delivery of the HCV genome into cells are still worth trying. The helper-dependent adenovirus (HDAd) is devoid of all viral coding sequences and has a package capacity of 37 kb, which is suitably large for the delivery of the HCV genome. Here we report a new method for delivery of the HCV genome into Huh-7 and HepG2 cells by using the HDAd vector.

Results: Our results demonstrated that the infection of Huh-7 cells with the HDAdJFH1 virus led to efficient HCV replication and virion production. We found that the HCV viral RNA levels could reach 107 copies per milliliter (ml) in the culture medium. HDAdJFH1-infected Huh-7 cells could be cultured for 8 passages with the culture medium remaining infectious for naïve Huh-7 cells throughout this period. This infection system proved effective for evaluating the anti-HCV effects of IFN- α in Huh-7 cells. Co-infection of HepG2 cells with the HDAdJFH1 and HDAdmiR-122 virus also resulted in HCV expression and replication.

Conclusion: This is the first report of an HDAd-based strategy for HCV replication and production *in vitro*.

Keywords: Hepatitis C virus, Cell-culture model, Helper-dependent adenovirus

Background

Hepatitis C virus (HCV) is a 9.6 kb positive-strand RNA virus and a member of the flavivirus family [1]. It is estimated that approximately 170 million people worldwide are persistently infected by HCV, which can result in hepatic fibrosis, cirrhosis and hepatocellular carcinoma [2]. Current interferon- α based therapy, in combination with ribavirin, has limited efficacy in only approximately 50% of patients and has severe side effects [3]. HCV replication takes place in the cytoplasm, and the 9.6 kb RNA genome encodes a polyprotein localized to the rough endoplasmic reticulum (ER), where it is cleaved into at least 10 structural (C, E1, E2, and P7) and

nonstructural (NS2, NS3, NS4A, NS4B, NS5A, and NS5B) proteins that play important roles in virus replication, assembly and pathogenesis [4].

HCV research has been hampered by the lack of adequate *in vitro* and *in vivo* model systems. Replicons have been utilized for studying HCV RNA replication, but these are not useful for studying aspects of virion production and infection [5]. In 2005, researchers discovered a genotype 2a isolate JFH1 from a Japanese patient with fulminant hepatitis that could exhibit complete the virus life cycle after transfection of *in vitro* transcribed full-length JFH1 RNA into Huh-7 or Huh-7.5 cells. This system is also able to produce infectious viral particles in cell culture (HCVcc) [6,7]. Furthermore, it was found that stable human hepatoma cell lines containing a chromosomally integrated cDNA copy of

* Correspondence: sunsh01@163.com; yzzhou@nic.bmi.ac.cn

†Equal contributors

¹State Key Laboratory of Pathogen and Biosecurity, Beijing Institute of Microbiology and Epidemiology, Beijing, China

Full list of author information is available at the end of the article



the JFH1 genome with a hepatitis delta virus ribozyme at the 3' end can constitutively produce infectious viral particles [8]. These methods have proven to be effective in generating infectious HCV cell culture models in Huh-7 cell line and its derivatives.

In contrast to Huh-7 cells, the hepatocellular carcinoma derived HepG2 cells polarize and would thus permit the investigation of how cell polarization impacts the HCV life cycle [9]. However, HepG2 cells does not express endogenous miR-122, a liver-expressed miRNA which is required to support HCV RNA replication [10], and weakly supports HCV replication [11]. Although a recent study has indicated that HepG2 cells expressing miR-122 can support the entire HCV life cycle [11], the efficiency of HCV replication and virion production still needs increasing. Thus other potential methods besides transfection for delivery of the HCV genome into cells are still worth trying especially when the cells, such as HepG2 cells, possess a relatively lower transfection efficiency.

Adenoviruses (Ads) are non-enveloped double-stranded DNA viruses, which can mediate efficient transduction and expression of foreign genes in cells [12]. The helper-dependent adenovirus (HDAd) possesses the same ability to deliver foreign DNA into cells as earlier generation adenoviruses (Ads); furthermore, HDAd vectors are devoid of all viral coding sequences and have cloning capacities of up to 37 kb [13], which makes it possible to introduce large genes into cells using HDAd vectors. Lacking all viral coding sequences, it displays only minimal immunogenicity and negligible side-effects and allows for long-term transgene expression in animal models for delivery of transgenes into the liver, skeletal muscle, myocardium or brain [14]. Furthermore, it does not integrate into the host genome, which makes them a promising class of potential delivery vehicles for human gene therapy [15].

In this study, we developed a HDAd vector containing the full-length JFH1 genome and an HDV ribozyme sequence located at the 3' end of the JFH1 genome. Our results demonstrate that the HDAd vector was able to efficiently deliver the HCV genome into Huh-7 cells and HepG2 cells, in which infectious HCV particles could be produced *in vitro*. To our knowledge, an efficient HDAd-based method for introducing the full-length 9.6 kb HCV RNA genome into hepatocytes has not been previously described. Therefore, this is the first report of an *in vitro* HDAd-mediated HCV genomic replication and production system.

Results

Construction of a helper-dependent adenoviral vector expressing the HCV RNA genome

An Ad5 vector has been previously used for the introduction of the hepatitis B viral genome into cultured

cells and mice, and it was found that high-titer hepatitis B virions were secreted into the culture medium of infected hepatoma cells and the sera of infected mice [16]. However, the size of the transgene that can be delivered by the conventional Ad5 vector is limited to 8.1-8.2 kb [17], which is nearly the size of the HCV replicon. Although an Ad5/35 chimera vector was recently used to generate a HCV subgenomic-replicon construct [18], there have been no reports of the packaging and transfer of the full 9.6 kb HCV genome *in vitro* or *in vivo*. In this study, we aimed to develop a simple and reliable method for packaging and delivering the HCV genome into cells to establish a novel HCV infection system. To this end, we chose to utilize the genotype 2a JFH1 HCV clone due to its efficient replication in human hepatoma [19] and mouse cells [20]. The full-length JFH1 RNA genome is under the control of a 5' minimal CMV promoter in the HDAd vector, and the 3' terminus of the transcript is processed by an HDV ribozyme sequence. The helper-dependent adenovirus plasmid also contained a GFP expression cassette (Figure 1a).

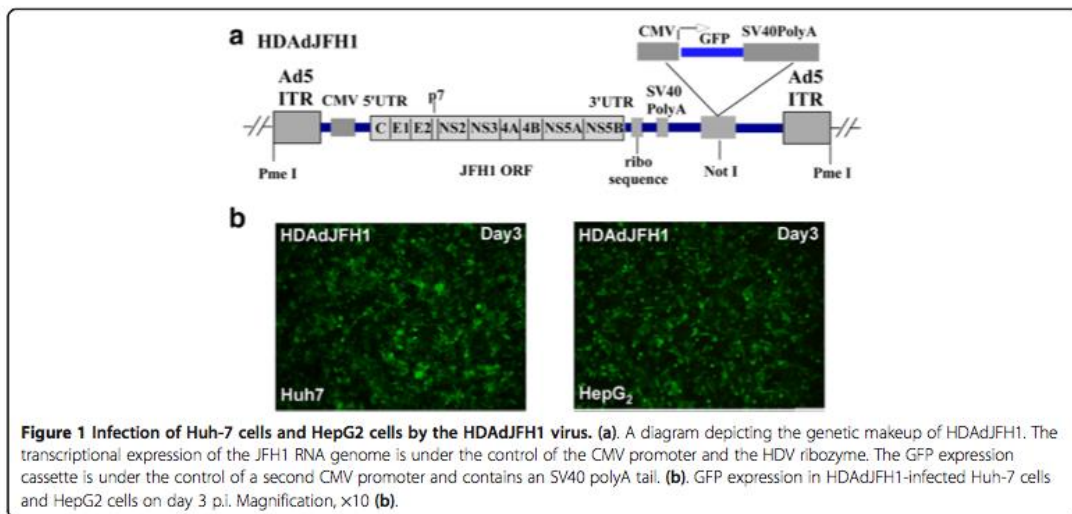
Amplification of the HDAdHCV virus and infection of cells

As quantified by absorbance, the titer of the amplified and purified HDAdJFH1, HDAdJFH1/GND, HDAdmiR-122 and HDAdGFP virus were found to be 2×10^{11} , 3×10^{11} , 1×10^{11} , 2×10^{11} viral particles/ml, respectively. Huh-7 cells and HepG2 cells were infected by the HDAds at a ratio of 200 viral particles/cell. GFP expression was observed in the infected Huh-7 and HepG2 cells at 3 days p.i. (Figure 1b). At 3 days p.i., nearly all the Huh-7 and HepG2 cells were infected with the HDAdJFH1 virus and had high levels of GFP expression.

Detection of HDAd-mediated HCV protein expression and RNA replication

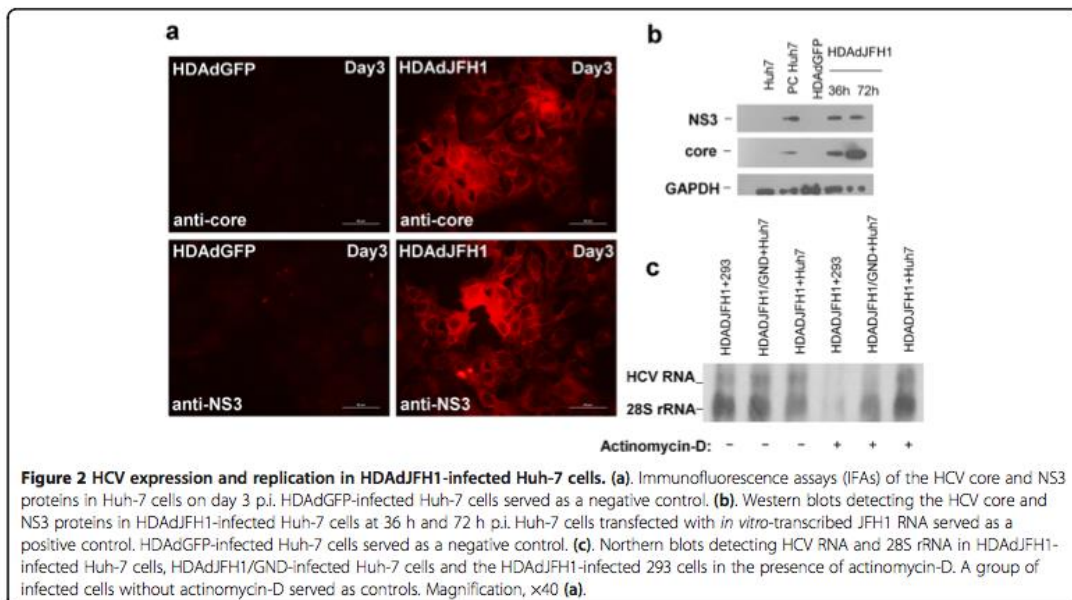
HDAd can mediate the efficient delivery and strong expression of foreign DNA sequences *in vitro* [21]. Our results indicate that HDAd can also mediate the efficient expression of HCV proteins in HDAdJFH1-infected Huh-7 cells. The expression of HCV core and NS3 proteins was confirmed by immunofluorescence staining and western blotting using core- and NS3-specific monoclonal antibodies. At 3 days p.i., immunofluorescence staining for HCV core and NS3 were both positive (Figure 2a). High levels of HCV core and NS3 proteins were also detected by western blotting at 36 h and 72 h p.i., respectively (Figure 2b). The expression of HCV NS3 protein was still detectable at 20 days p.i. (data not shown), demonstrating the long-term expression of the HCV genome.

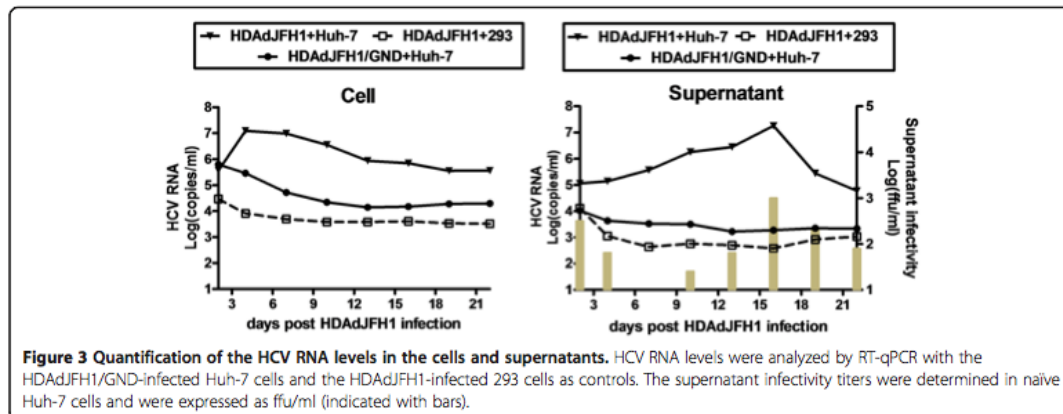
Actinomycin-D has been shown to have the ability to inhibit transcription [22]. Thus, actinomycin-D was added in the cell culture medium and northern blot was



performed to confirm replication of HCV genome. The concentration of actinomycin-D was maintained 5 µg/ml in the medium for 16 hours in HDAdJFH1, HDAdJFH1/GND-infected Huh-7 cells and HDAdJFH1-infected 293 cells since 6 hours p.i. After actinomycin-D treatment, expression of intracellular HCV RNA can be detected in the HDAdJFH1-infected Huh-7 cells, compared with those in the HDAdJFH1/GND-infected Huh-7 cells and HDAdJFH1-infected 293 cells (Figure 2c). The results

indicated that actinomycin-D inhibited the HDAd-mediated HCV genome transcription in HDAdJFH1/GND-infected Huh-7 cells and HCV replicated in the HDAdJFH1-infected Huh-7 cells. Quantitative RT-PCR analysis also showed an increase of HCV RNA levels in the cell culture medium since HDAdJFH1 infection of Huh-7 cells (Figure 3). Together, these results demonstrated the replication of HCV genome in the HDAdJFH1-infected Huh-7 cells.

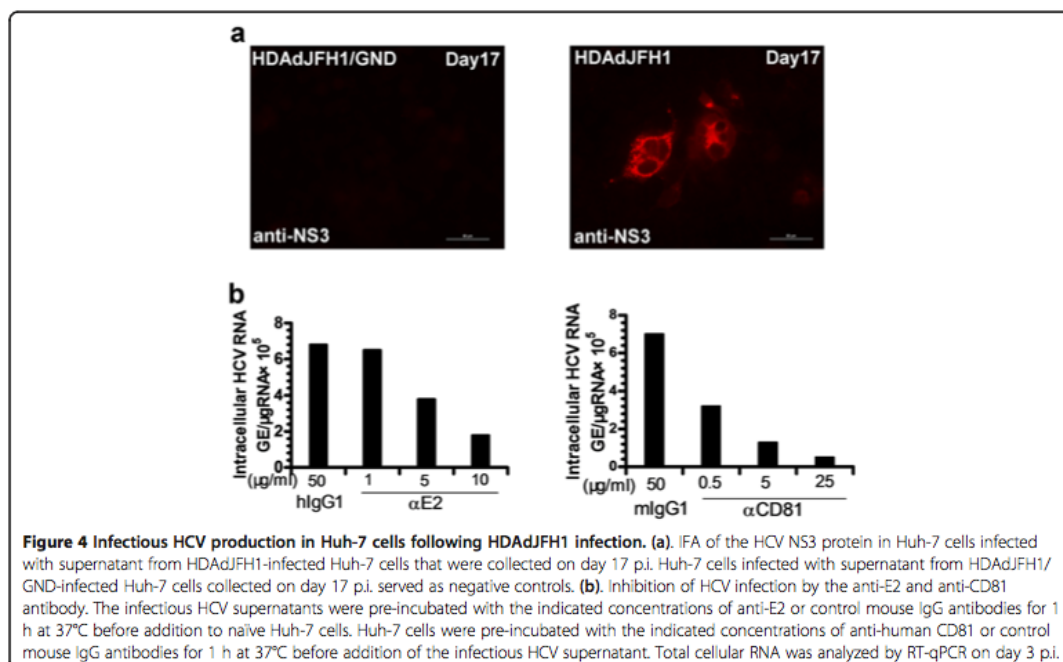




Determination of the infectivity of HDAdJFH1-infected Huh-7 cell culture medium

We found that HCV RNA levels in the cell culture medium of the HDAdJFH1-infected Huh-7 cells first increased to a maximal level at 16 days p.i. and then decreased in the following days. While HCV RNA levels in the supernatant of the HDAdJFH1/GND-infected Huh-7 cells decreased gradually (Figure 3). Based on these findings, we wondered whether HDAd-mediated HCV virions were present in the cell culture medium. To

HDAdJFH1-infected Huh-7 cells, we infected naïve Huh-7 cells with the medium for 1 h at 37°C; we subsequently determined the expression levels of the HCV NS3 protein using IFA. As shown in Figure 4a, naïve Huh-7 cells were infected with medium collected at day 17 p.i., cultured for another 3 days and then assayed for HCV NS3 protein expression using IFA. Naïve Huh-7 cells served as a negative control. Huh-7 cells were also infected with medium from HDAdJFH1/GND-infected Huh-7 cells to confirm that HDAdJFH1 infection



mediated HCV replication and infectious HCV secretion into the medium of HDAdJFH1-infected Huh-7 cells.

To determine in more detail the infectious titer of HCV, the medium was serially diluted in 10-fold increments and used to infect Huh-7 cells. The infectious titer was determined by counting the number of cell foci that stained positive for HCV NS3 protein at the lowest dilution point, which was then multiplied by the dilution factor (n-fold) [6]. The infectious HCV titer of the medium reached a maximal level of 1×10^3 ffu/ml at 16 days p.i. (Figure 3) and was comparable to the infectious HCV titer in Huh-7 cell by conventional transfection of *in vitro* transcribed JFH1 RNA, which normally only reaches $10^2 \sim 10^3$ ffu/ml.

HCV infection is inhibited by anti-E2 and anti-CD81 antibodies

Previous studies using pseudotyped viruses expressing HCV E1/E2 have suggested that the interaction between E2 and CD81 is crucial for viral entry [23,24]. To further investigate the infectivity of the HCV virions, we performed infectivity-neutralization and inhibition experiments using monoclonal antibodies specific for HCV E2 and CD81. Prior to addition to the Huh-7 cells, the infectious HCV supernatant was pre-incubated with a dilution series of a mouse monoclonal antibody specific for HCV E2. An irrelevant human IgG1 antibody served as a negative control. In another experiment, the Huh-7 cells were pre-incubated with CD81 antibodies before the infectious HCV supernatant was added. The irrelevant mouse IgG1 antibody served as a negative control. For both the E2 and CD81 antibody treatments, the intracellular HCV RNA levels were observed to decrease in a dose-dependent manner by 3 days p.i. A concentration of 5 $\mu\text{g/ml}$ of anti-E2 antibody was sufficient to cause a 50% reduction in the intracellular HCV RNA level by 3 days p.i., whereas only 0.5 $\mu\text{g/ml}$ of anti-CD81 antibody was sufficient to cause the same reduction

(Figure 4b). These results are consistent with the previously reported findings [6,7] and confirm the infectivity of the cell culture medium.

To characterize the produced HCV virions, the culture medium of the HDAdJFH1-infected Huh-7 cells was subjected to sucrose density gradient centrifugation. The fractions were analyzed for HCV RNA levels, as well as the infectivity titers. As shown in Figure 5a, a peak for HCV RNA level and infectivity titer was found in fraction 4, which has a density of 1.15 g/ml. This density is almost consistent with the published density of HCV virions [8,25]. The infection kinetics assay showed that the cellular HCV RNA levels increased to 10^7 copies within 7 days p.i. (Figure 5b). These results further confirm the production of infectious HCV virions in this HDAd-mediated system.

Inhibition of HCV replication by IFN- α

Previous studies have shown that IFN- α can successfully inhibit HCV replication both in Huh-7 cells transfected with JFH1 RNA [6] and in Huh-7 cells with a stably integrated HCV genome [8]. Therefore, we investigated the inhibitory effects of IFN- α on HCV replication in our HDAd-mediated infection system. Beginning at 8 days p.i., HDAdJFH1-infected Huh-7 cells were incubated with DMEM containing different concentrations of IFN- α for 3 days, and levels of the NS3 protein were determined by western blotting. IFN- α efficiently inhibited HCV replication in HDAdJFH1-infected Huh-7 cells (Figure 6). Therefore, it is likely that this HDAd-mediated HCV infection system is suitable for the evaluation of new anti-HCV drugs and therapeutic strategies.

HDAdJFH1 and HDAdmiR-122 virus co-infection mediate HCV expression and replication in HepG2 cells

HepG2 cells does not express endogenous miR-122, a liver-expressed miRNA which is required to support HCV RNA replication [10], and weakly supports HCV

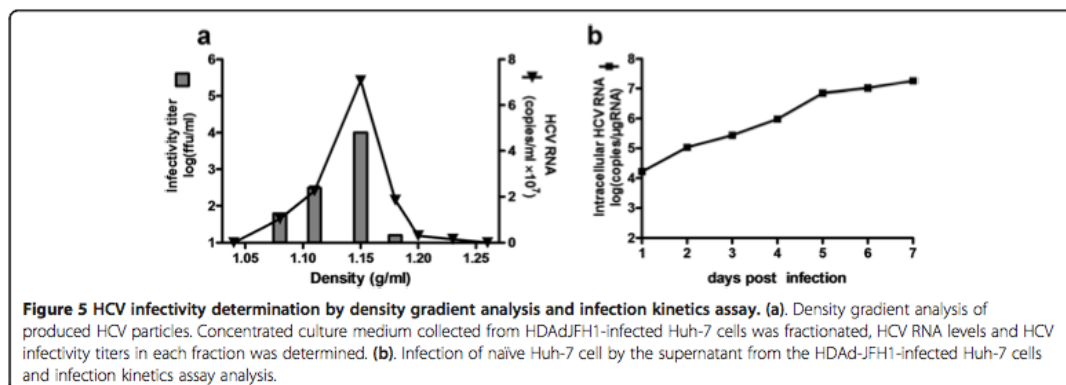
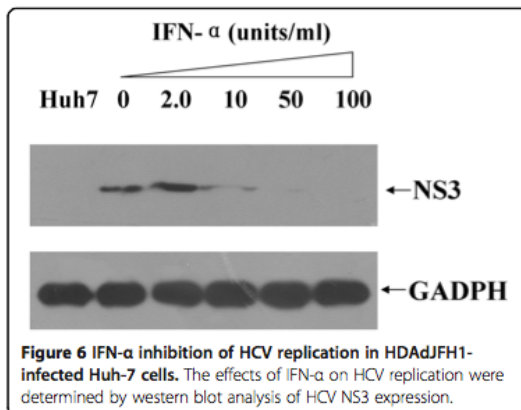


Figure 5 HCV infectivity determination by density gradient analysis and infection kinetics assay. (a). Density gradient analysis of produced HCV particles. Concentrated culture medium collected from HDAdJFH1-infected Huh-7 cells was fractionated, HCV RNA levels and HCV infectivity titers in each fraction were determined. (b). Infection of naive Huh-7 cell by the supernatant from the HDAdJFH1-infected Huh-7 cells and infection kinetics assay analysis.

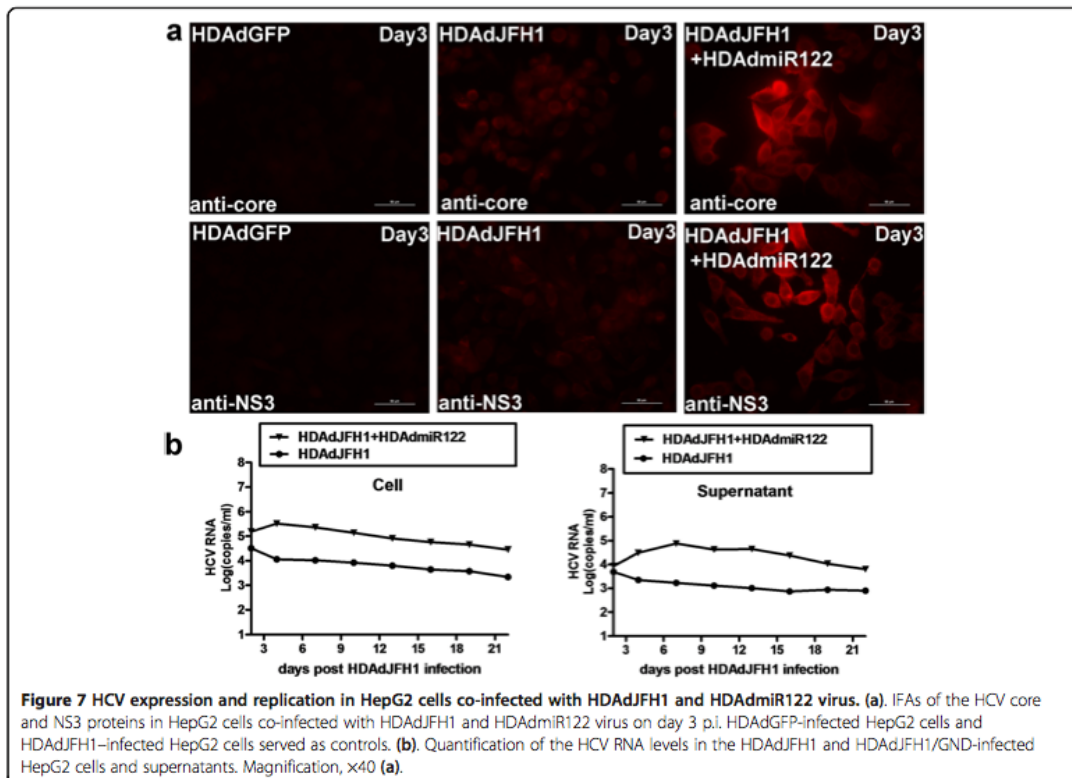


replication [11]. A recent study has indicated that HepG2 cells expressing miR-122 can support the entire HCV life cycle [11]. In this study, we tested whether the HDAd system can work in HepG2 cells. Results showed that co-infection of HepG2 cells with HDAdJFH1 and HDAdmiR-122 virus enhances HCV core and NS3

protein expression (Figure 7a). Kinetic analysis of HCV RNA levels in the co-infected HepG2 cells and culture medium were performed. Compared with the HDAdJFH1/GND infection control, HDAdJFH1 and HDAdmiR-122 co-infection resulted in relatively weak replication of HCV genome, as shown in Figure 7b.

Discussion

Hepatitis C virus (HCV) is a positive-strand RNA virus that was first identified in 1989. Since then, both basic and pharmaceutical research on HCV has been hampered by a lack of viral culturing systems [4]. Early studies on HCV mainly focused on the structure and function of the individual viral genes, and later studies utilized HCV subgenomic replicons, which were more effective for HCV RNA replication research and antiviral development [20,26]. However, the replicon system is not suitable for HCV life-cycle research due to this system's inability to produce infectious HCV virions. In 2005, it was reported that RNA generated from the JFH1 viral genome can produce infectious HCV virions when transfected into Huh-7 cells [7]. Both transient and stable transfections with DNA vectors expressing the



full-length HCV genome have also been investigated [8,25] and in these studies it was found that the HDV ribozyme plays an important role in cleavage of the HCV RNA product.

It appears that efficient delivery of the HCV RNA genome, for example by electroporation or stable transfection, is vital for the efficient replication and production of the HCV virus. Here, we report on the use of the helper-dependent adenoviral (HDAd) vector, which can mediate high-efficiency transduction of one or more foreign genes into cells [27]. Adenoviruses (Ads) are non-enveloped double-stranded DNA viruses, replication and assembly of which take place in the nucleus. Adenovirus vectors are most effective at mediating the transfer of foreign DNA into immortalized and primary cells. In the liver, they predominantly infect hepatocytes [21], where hepatitis-virus replication and infection take place. Adenoviral vectors have been used for the transfer of the genome of the hepatitis B virus into cultured cells and mice [16]. However, the 9.6 kb HCV RNA genome was too large to be introduced into early generation Ad vectors. HDAds are constructed by removing all viral sequences from earlier generation Ad vectors except for the packaging sequences and the inverted terminal repeats, which eliminates viral gene expression, liver toxicity, and the cellular immune responses elicited by Ad vectors [28]. As most of the viral coding sequences are deleted, HDAds have a large delivery capacity of up to 37 kb [29]. As a comparison, the upper size limit of transgenes that can be delivered with the conventional Ad5 vector is 8.1-8.2 kb [17] – approximately the size of the HCV replicon. Thus, it has been difficult to package the HCV replicon into Ad5, although an Ad5/35 chimera vector has recently been used to generate an HCV subgenomic-replicon construct [11]. To our knowledge, a convenient and efficient method for transferring the 9.6 kb HCV RNA genome into cells by HDAds has not been previously reported.

In this study, we developed an HDAd vector containing the full-length JFH1 genome and an HDV ribozyme sequence. HDAdJFH1 virus with a high infectious titer was prepared and used to infect Huh-7 cells *in vitro*, and we observed both long-term expression and replication of HCV genome (Figures 2 and 3). HCV replication was confirmed by de novo RNA synthesis in the presence of actinomycin-D. The HCV RNA levels in the supernatants increased to a maximal level of about 10^7 copies/ml at 16 days p.i. when many cells became rounded and floated in the culture medium, a similar cytopathic effect that can be observed on the JFH1-transfected Huh-7 cells [30]. Ten days after infection, the supernatant from HDAdJFH1-infected Huh-7 cells was found to be infectious and the infectivity of HCV could be inhibited by anti-E2 and anti-CD81 antibodies

in a dose-dependent manner (Figure 4b). As the interaction between E2 and CD81 is vital for HCV entry [31,32], we believed that HCV particles were being secreted into the supernatant of HDAdJFH1-infected Huh-7 cells. Sucrose density gradient analysis showed that the virus produced owns a density which is similar to published data for HCV virions [25]. Furthermore, we found that IFN- α efficiently inhibited HCV replication (Figure 6), further validating the potential of this system for the evaluation of HCV antiviral drugs. Taken together, our findings demonstrate long-term replication of the HCV genome and production of infectious HCV virions in this helper-dependent adenovirus-mediated system in Huh-7 cells.

MicroRNAs (miRNA) are 21~22 nucleotide RNA molecules that are expressed in a wide range of eukaryotic organisms that are predicted to downregulate the expression of the endogenous target genes by reducing mRNA stability or translation [33]. MiR-122 is liver-specific and required for efficient HCV RNA replication [10,34]. HepG2 cells does not express endogenous miR-122 and weakly supports HCV replication [11]. A recent study has indicated that HepG2 cells expressing miR-122 can support the entire HCV life cycle [11]. In this study, our results also showed that HDAd-mediated miR-122 expression was necessary for the HDAd-mediated efficient HCV expression and replication (Figure 7).

Although the method based on *in vitro*-transcribed JFH1-RNA transfection is very well established so far, it is less efficient for primary hepatocytes which are difficult to transfect. Helper-dependent adenovirus can infect a variety of different cell types, including hepatic cell lines, primary hepatocytes [35], as well as quiescent, non-dividing, or terminally differentiated somatic cells [36], with high expression efficiency. Thus, by using this HDAd system, HCV replication or infection can be studied in the above cell types *in vitro*. So far, HCV can only infect human and chimpanzees *in vivo* and the host range for HCV infection is narrow. Although human liver chimeric mice can be infected by HCV, it is immunodeficient with a high mortality rate and the source of human primary hepatocytes is limited. And it is important to generate a novel immunocompetent mouse model which can support HCV replication and infection. Although expression of the four humanized HCV receptors in mice enhance its susceptibility to HCV infection [37,38], it is still not successful for mediating HCV infection in mice. Several studies have shown that HDAds are able to mediate high-level and long-term transgene expression in animal models, especially for the liver-targeted gene therapy [13,14]. So it is probable that HDAd can mediate efficient delivery of the HCV genome into the mouse livers, but whether HDAd can mediate HCV genomic replication or even virion

production in mice is worth being investigated. Also, since extrahepatic manifestations caused by hepatitis C virus infection exists clinically [39], animal model for studying HCV extrahepatic manifestations still lacks. And this HDAd-mediated HCV genomic replication system provides a possible strategy for generating an HCV extrahepatic replication model *in vivo*.

Conclusion

This is the first report of an *in vitro* HDAd-mediated HCV genomic replication and production system, which would allow a broader examination of interactions between HCV and host cell biology, as well as provide tools for anti-HCV drug evaluation.

Methods

Helper-dependent adenoviral vector construction

The plasmid pJFH1 contains the full-length JFH1 cDNA downstream of the T7 RNA promoter [7]. To replace the T7 promoter from pJFH1 with CMV promoter, a PCR fragment, amplified 5' partial sequence of the HCV genome in pJFH1 using the chimeric forward primer 5'-ccgaattcgagctcggtaccggg-3' which consists of two segments lying beside the upstream and downstream of T7 promoter and reverse primer 5'-caccgggtccgcagaccac-3', was inserted into pJFH1 between the restriction enzyme sites for *EcoR* I and *Age* I that locates upstream and downstream of the T7 promoter respectively. The resulting construct was designated pJFH1(Δ T7). A hepatitis delta virus (HDV) ribozyme DNA sequence was synthesized and placed at the immediate 3' end of pJFH1(Δ T7), to get pJFH1-ribo(Δ T7). The JFH1-ribo sequence was then inserted between the CMV promoter and SV40PolyA of the pSC11 plasmid by the restriction enzyme sites for *EcoR* I and *Hind* III. And this expression cassette was finally inserted into the HDAd vector between the restriction enzyme sites for *I-Ceu* I and *I-Sce* I. The resulting construct, HDAdJFH1, also contains a cassette for the expression of green fluorescent protein (GFP) [40]. HDAdJFH1/GND was constructed with the same strategy. And an empty HDAd plasmid expressing GFP (HDAdGFP) served as a control.

Using the Huh-7 cells derived total RNA-reverse transcribed cDNA as a template, the human genomic miR-122 precursor sequence was amplified by RT-PCR using the forward and reverse primers 5'-ccggaattctctggctacagagttt-3' and 5'-cccaagcttttatcgaggggaaggatt-3', and then inserted into the pSC11 plasmid by the restriction enzyme sites for *EcoR* I and *Hind* III. And this expression cassette was finally inserted into the HDAd vector between the restriction enzyme sites for *I-Ceu* I and *I-Sce* I. The resulting construct was designated HDAdmiR-122.

Cells and cell culture methods used in this study

A modified version of the 293 cell line that expresses high levels of the Cre enzyme – known as the 116 cell line (kindly provided by Dr. Li-min Liu) – was maintained in MEM supplemented with 10% fetal bovine serum (FBS), 0.1 mg/ml hygromycin, 100 U/ml penicillin, 100 μ g/ml streptomycin, and 2 mM L-glutamine (Invitrogen) [41]. The hepatoma cell lines Huh-7, HepG2, as well as non-hepatic 293 cell line, were obtained from ATCC (Manassas, VA) and maintained in DMEM supplemented with 100 U/ml penicillin, 100 μ g/ml streptomycin, nonessential amino acids, and 10% FBS (Invitrogen).

Amplification of the HDAdHCV virus and infection of cells

The helper-dependent adenoviral plasmids, including HDAdJFH1, HDAdJFH1/GND, HDAdmiR-122, HDAdGFP, were digested with the restriction enzyme *Pme*I to release both inverted terminal repeats and were then transfected into 116 cells with the calcium phosphate method, respectively [42]. Helper-dependent adenoviral particles were prepared by repeated amplification cycles in 116 cells with the helper virus AdNG163 (a kind gift of Dr. Li-min Liu; see above). After 4–6 rounds of amplification in 150-mm dishes, 116 cells suspended in a 3 L spinner flask were infected for large-scale preparation of HDAdJFH1, HDAdJFH1/GND, HDAdmiR-122, HDAdGFP. The viral particles were isolated by centrifugation in a cesium chloride gradient, followed by dialysis with three exchanges of 10 mM Tris-HCl (pH 8.0) at 4°C [43]. Virus particles were quantified by measuring the absorbance at 260 nm [44]. Huh-7, HepG₂ and 293 cells were infected with the purified HDAds at 80% confluency with an MOI of 200 viral particles/cell and were passaged every 2 or 3 days.

Western blot analysis

The HDAdJFH1-infected Huh-7 cells were lysed in protein sample buffer containing 50 mM Tris-HCl, 150 mM NaCl, 5 mM EDTA, 0.2 mM sodium orthovanadate, 1% Triton X-100, 1% sodium deoxycholate, and 1% sodium dodecyl sulfate; the buffer was also supplemented with aprotinin (2 μ g/ml), pepstatin A (0.7 μ g/ml), leupeptin (0.5 μ g/ml), and PMSF (1 mM). For each sample, 30 μ g of total protein was electrophoresed through a 10% sodium dodecyl sulfate-polyacrylamide gel and transferred onto a nitrocellulose membrane. The membrane was blocked by pre-incubation with 5% skim milk. The levels of the HCV core and NS3 proteins were determined using monoclonal antibodies specific to the core and NS3 proteins (Thermo Scientific), which were detected with a horseradish peroxidase-conjugated goat anti-mouse immunoglobulin G antibody (IgG, Pierce) and visualized with a chemiluminescent substrate (Pierce). The level of the GAPDH protein served as an internal control, and this

protein was detected with an anti-GAPDH monoclonal antibody (Sigma).

Immunofluorescence assays (IFAs)

The HDAdJFH1-infected Huh-7 and HepG2 cells were grown overnight on coverslips in a 6-well culture plate. Cells were washed with 1× phosphate-buffered saline (PBS), fixed with chilled acetone, and blocked with 1% bovine serum albumin and 1% goat serum in PBS. The localizations of the HCV core and NS3 proteins were visualized in the fixed cells by incubation with core- and NS3-specific monoclonal antibodies and a secondary goat anti-mouse IgG antibody conjugated to DyLight™594 fluorescein (used at a 1:800 dilution) (Beijing Golden Bridge Biotechnology, Beijing, China). The HDAdGFP-infected Huh-7 and HepG2 cells served as a negative control. The coverslips were then mounted onto slides, and the HCV proteins were visualized with a Zeiss Axioplan 2 fluorescence microscope.

Quantification of HCV RNA levels

Total cellular RNA was extracted from infected cells using the RNeasy RNA isolation kit (Qiagen). Total RNA was extracted from the supernatants of the infected cells using the QIAamp Viral RNA Mini Kit (Qiagen). The RNA concentration was determined by spectrophotometry. RT-qPCR was performed as described elsewhere [6], and the HCV levels were determined relative to a standard curve created using serial dilutions of a plasmid containing the HCV JFH1 cDNA.

Northern blot analysis of intracellular viral RNA levels

To confirm the replication of HCV genome, actinomycin-D (Sigma) was maintained in the cell culture medium at a concentration of 5 µg/ml for 16h in HDAdJFH1, HDAdJFH1/GND-infected Huh-7 cells and HDAdJFH1-infected 293 cells since 6 hours p.i.. Total cellular RNA was extracted from infected Huh-7 cells using the RNeasy RNA isolation kit (Qiagen). Four micrograms of isolated RNA was separated using a 1% agarose gel containing formaldehyde, blotted onto a positively charged nylon membrane (Hybond-N+, GE), and immobilized with a Stratalinker UV crosslinker (Stratagene). The DNA probes complementary to a region of the HCV 5'UTR and human 28S rRNA was synthesized using the DIG High Prime DNA Labeling and Detection Starter Kit II (Roche).

HCV infection and infectivity neutralization

Naïve Huh-7 cells in a 6-well culture plate were infected with 1 ml of cultured supernatant from HDAdJFH1-infected Huh-7 cells. At 3 h postinfection (p.i.), the supernatants were replaced with 2 ml of DMEM containing 10% FBS, and the cells were incubated at 37°C for 3 days prior to the protein and RNA analysis. At 3 days p.i., the

HCV infectivity was determined by IFA for the HCV core and NS3 proteins using core- and NS3-specific monoclonal antibodies, respectively. Titration of infectious HCV was performed by focus forming assay. Cell supernatants were serially diluted 10-fold in complete DMEM and used to infect naïve Huh-7 cells. The level of infectious HCV titer was determined by the average number of NS3-positive foci detected at highest dilutions at 3 days p.i.. For the infectivity-neutralization experiments, monoclonal antibodies specific to HCV E2 and CD81 (Santa Cruz Biotechnology) were diluted with the HCV-containing culture medium at 3 days p.i.; normal mouse IgG1 (Santa Cruz Biotechnology) antibodies were used as negative controls. The effects of the E2 and CD81 monoclonal antibodies on HCV infectivity and replication were determined by RT-qPCR.

Sucrose density gradient analysis

We collected the cell culture medium of the HDAdJFH1-infected Huh-7 cells at 16 days p.i. using low-speed centrifugation and passed it through a 0.45-µm filter. Then the filtrate was layered on a sucrose gradient (60%~10%, wt/vol) and centrifuged it for 16 h. The fractions were harvested and analyzed for the HCV RNA levels and infectivity titers.

IFN-α inhibition of HCV replication in HDAdJFH1-infected Huh-7 cells

For the IFN-α inhibition experiments, Huh-7 cells were infected with HDAdJFH1 and incubated with DMEM containing increasing concentrations of IFN-α (Sigma) for 3 days. The effects of IFN-α on HCV replication were determined using western blot analysis of HCV NS3 expression.

Abbreviations

HCV: Hepatitis C virus; cDNA: Complementary DNA; HCVcc: infectious HCV in cell culture; HDAd: Helper-dependent adenovirus; ml: milliliter; IFN-α: Interferon-α; RNA: Ribonucleic acid; ER: Endoplasmic reticulum; UTR: Untranslated region; ORF: Open reading frame; miRNA: microRNA; IFA: Immunofluorescence assay; RT-PCR: Reverse transcription-polymerase chain reaction; ffu: foci forming unit; pi: postinfection; DMEM: Dulbecco's Modified Eagle Medium; CMV: Cytomegalovirus; FBS: Fetal bovine serum; ATCC: American type culture collection; MOI: Multiplicity of infection; EDTA: Ethylenediaminetetraacetic acid; PMSF: Phenylmethanesulfonyl fluoride; RT-qPCR: Real-time quantitative polymerase chain reaction; DIG: Digoxigenin.

Competing interests

The authors have declared that no competing interests exist.

Authors' contributions

Conceived and designed the experiments: YZ and S-hS. Performed the experiments: X-jZ, YZ, JL, YG, and Y-hf. Analyzed the data: X-jZ and YZ. Wrote and revised the manuscript: X-jZ, J-shH, and Y-sZ. All authors read and approved the final manuscript.

Acknowledgments

We are grateful to Professor Yue Wang (Chinese Center for Disease Control and Prevention) for providing the pJFH1 and pJFH1/GND plasmid, to Dr. Li-min Liu (McMaster University) for providing the Cre-expressing 293 cell line and the HDAd vector, and to Professor Jing-sheng He (Beijing Jiaotong University) for assistance in production of HDAdJFH1 virus.

Funding

This work was supported by National Program of Infectious Diseases (No.2012ZX10004-502) and The National High Technology Research and Development Program ("863" Program) of China (No.2007AA02Z151).

Author details

¹State Key Laboratory of Pathogen and Biosecurity, Beijing Institute of Microbiology and Epidemiology, Beijing, China. ²Laboratory Animal Center of the Academy of Military Medical Science, Beijing, China. ³College of Life Sciences & Bioengineering, Beijing Jiaotong University, Beijing, China.

Received: 28 December 2012 Accepted: 26 August 2013

Published: 30 August 2013

References

- Alter MJ, Margolis HS, Krawczynski K, Judson FN, Mares A, Alexander WJ, Hu PY, Miller JK, Gerber MA, Sampliner RE, The Sentinel Counties Chronic non-A, non-B Hepatitis Study Team: The natural history of community-acquired hepatitis C in the United States. *N Engl J Med* 1992, **327**:1899-1905.
- Sarbah SA, Younossi ZM: Hepatitis C: an update on the silent epidemic. *J Clin Gastroenterol* 2000, **30**:125-143.
- Hoofnagle JH, di Bisceglie AM: The treatment of chronic viral hepatitis. *N Engl J Med* 1997, **336**:347-356.
- Reed KE, Rice CM: Overview of hepatitis C virus genome structure, polyprotein processing, and protein properties. *Curr Top Microbiol Immunol* 2000, **242**:55-84.
- Lohmann V, Korner F, Koch JO, Heریان U, Theilmann L, Bartenschlager R: Replication of subgenomic hepatitis C virus RNAs in a hepatoma cell lines. *Science* 1999, **285**:110-113.
- Zhong J, Gastaminza P, Cheng G, Kapadia S, Kato T, Burton DR, Wieland SF, Uprichard SL, Wakita T, Chisari FV: Robust hepatitis C virus infection *in vitro*. *Proc Natl Acad Sci USA* 2005, **102**:9294-9299.
- Wakita T, Pietschmann T, Kato T, Date T, Miyamoto M, Zhao Z, Murthy K, Habermann A, Krausslich HG, Mizokami M, Bartenschlager R, Liang TJ: Production of infectious hepatitis C virus in tissue culture from a cloned viral genome. *Nat Med* 2005, **11**:791-796.
- Cai ZH, Zhang C, Chang KS, Jiang JY, Ahn BC, Wakita T, Liang TJ, Luo GX: Robust production of infectious hepatitis C virus (HCV) from stably HCV cDNA-transfected human hepatoma cells. *J Virol* 2005, **79**:13963-13973.
- Decaens C, Durand M, Grosse B, Cassio D: Which *in vitro* models could be best used to study hepatocyte polarity? *Biol Cell* 2008, **100**:387-398.
- Jopling CL, Yi M, Lancaster AM, Lemon SM, Sarnow P: Modulation of hepatitis C virus RNA abundance by a liver-specific microRNA. *Science* 2005, **309**:1577-1581.
- Narbus CM, Israelow B, Sourisseau M, Michta ML, Hopcraft SE, Zeiner GM, Evans MJ: HepG2 cells expressing miR-122 support the entire hepatitis C virus life cycle. *J Virol* 2011, **85**(2):12087-12092.
- Davis AR, Wivel NA, Palladino JL, Tao L, Wilson JM: Construction of adenoviral vectors. *Mol Biotechnol* 2001, **18**:63-70.
- Vetrini F, Philip N: Gene therapy with helper-dependent adenoviral vectors: current advances and future perspectives. *Viruses* 2010, **2**:1886-1917.
- Jozkowicz A, Dulak J: Helper-dependent adenoviral vectors in experiment gene therapy. *Acta Biochim Pol* 2005, **52**:589-599.
- Adam E, Nasz I: Adenovirus vectors and their clinical application in gene therapy. *Orv Hetil* 2001, **142**:2061-2070.
- Sprinzl MF, Oberwinkler H, Schaller H, Protzer U: Transfer of hepatitis B virus genome by adenovirus vectors into cultured cells and mice: crossing the species barrier. *J Virol* 2001, **75**:5108-5118.
- Bett AJ, Prevec L, Graham FL: Packaging capacity and stability of human adenovirus type 5 vectors. *J Virol* 1993, **67**:5911-5921.
- Yoshida T, Kondoh M, Ojima M, Mizuguchi H, Yamagishi Y, Sakamoto N, Yagi K: Adenovirus vector-mediated assay system for hepatitis C virus replication. *Nucleic Acids Res* 2011, **39**:e1-8.
- Kato T, Date T, Miyamoto M, Furusaka A, Tokushige K, Mizokamo M, Wakita T: Efficient replication of the genotype 2a hepatitis C virus subgenomic replicon. *Gastroenterology* 2003, **125**:1808-1817.
- Uprichard SL, Chung J, Chisari FV, Wakita T: Replication of a hepatitis C virus replicon clone in mouse cells. *Viral J* 2006, **3**:89.
- Palmer DJ, Ng P: Helper-dependent adenoviral vectors for gene therapy. *Hum Gene Ther* 2005, **16**:1-16.
- Sobell H: Actinomycin and DNA transcription. *Proc Natl Acad Sci USA* 1985, **82**:5328-5331.
- Hsu M, Zhang J, Flint M, Logvinoff C, Cheng-Mayer C, Rice CM, McKeating JA: Hepatitis C virus glycoproteins mediate pH-dependent cell entry of pseudotyped retroviral particles. *Proc Natl Acad Sci USA* 2003, **100**:7271-7276.
- Zhang J, Randall G, Higginbottom A, Monk P, Rice CM, McKeating JA: CD81 is required for hepatitis C virus glycoprotein-mediated viral infection. *J Virol* 2004, **78**:1448-1455.
- Heller T, Saito S, Auerbach J, Williams T, Moreen TR, Jazwinski A, Cruz B, Jeurkar N, Sapp R, Luo G, Liang TJ: An *in vitro* model of hepatitis C virus production. *Proc Natl Acad Sci USA* 2005, **102**:2579-2583.
- Bartenschlager RA, Kaul SS: Replication of the hepatitis C virus in cell culture. *Antiviral Res* 2003, **60**:91-102.
- Sullivan DE, Dash S, Du H, Hiramatsu N, Aydin F, Kolls J, Blanchard J, Baskin G, Gerber MA: Liver-directed gene transfer in non-human primates. *Hum Gene Ther* 1997, **8**:1195-1206.
- Muruve DA, Cotter MJ, Zais AK, White LR, Liu Q, Chan T, Clark SA, Ross PJ, Meulenbroek RA, Maelandsmo GM, Parks RJ: Helper-dependent adenovirus vectors elicit intact innate but attenuated adaptive host immune responses *in vivo*. *J Virol* 2004, **78**:5966-5972.
- Kochanek S: High-capacity adenoviral vectors for gene transfer and somatic gene therapy. *Hum Gene Ther* 1999, **10**:2451-2459.
- Zhong J, Gastaminza P, Chung J, Stamataki Z, Isogawa M, Cheng GF, McKeating JA, Chisari FV: Persistent hepatitis C virus infection in vitro: coevolution of virus and host. *J Virol* 2006, **80**:11082-11093.
- Cormier EG, Tsamis F, Kajumo F, Durso RJ, Gardner JP, Dragic T: CD81 is an entry coreceptor for hepatitis C virus. *Proc Natl Acad Sci USA* 2004, **101**:7270-7274.
- Pileri P, Uematsu Y, Campagnoli S, Galli G, Falugi F, Petracca R, Weiner AJ, Houghton M, Rosa D, Grandi G, Abrignani S: Binding of hepatitis C virus to CD81. *Science* 1998, **282**:938-942.
- Ambros V: The functions of animal microRNAs. *Nature* 2004, **431**:350-355.
- Jangra RK, Yi M, Lemon SM: Regulation of hepatitis C virus translation and infectious virus production by the microRNA miR-122. *J Virol* 2010, **84**:6615-6625.
- Salucci V, Lu M, Aurisicchio L, La Monica N, Roggendorf M, Palombo F: Expression of a new woodchuck IFN-alpha gene by a helper-dependent adenoviral vector in woodchuck hepatitis virus-infected primary hepatocytes. *J Interferon Cytokine Res* 2002, **22**:1027-1034.
- Kubo S, Seleme MC, Soiffer HS, Perez JL, Moran JY, Kazanian HH Jr, Kasahara N: L1 retrotransposition in nondividing and primary human somatic cells. *Proc Natl Acad Sci USA* 2006, **103**:8036-41.
- Dorner M, Horwitz JA, Robbins JB, Barry WT, Feng Q, Mu K, Jones CT, Schoggins JW, Catanese MT, Burton DR, Law M, Rice CM, Ploss A: A genetically humanized mouse model for hepatitis C virus infection. *Nature* 2011, **474**:208-211.
- Hikosaka K, Noritake H, Kimura W, Sultana N, Sharkar MT, Tagawa Y, Uezato T, Kobayashi Y, Wakita T, Miura N: Expression of human factors CD81, claudin-1, scavenger receptor, and occluding in mouse hepatocytes does not confer susceptibility to HCV entry. *Biomedical Res* 2011, **32**:143-150.
- Zignego AL, Ferri C, Pileri SA, Caimi P, Bianchi FB: Extrahepatic manifestations of hepatitis C virus infection: a general overview and guidelines for a clinical approach. *Dig Liver Dis* 2007, **39**:2-17.
- Shi CX, Graham FL, Hitt MM: A convenient plasmid system for construction of helper-dependent adenoviral vectors and its application for analysis of the breast-cancer-specific mamoglobin promoter. *J Gene Med* 2006, **8**:442-451.
- Liu L, Shi CX, Ghayur A, Zhang C, Su JY, Hoff CM, Margetts PJ: Prolonged peritoneal gene expression using a helper-dependent adenovirus. *Perit Dial Int* 2009, **29**:508-516.
- Graham FL, van der Eb AJ: A new technique for the assay of infectivity of human adenovirus 5 DNA. *Virology* 1973, **52**:456-467.
- Parks RJ, Chen L, Anton M, Sankar U, Rudnicki MA, Graham FL: A helper-dependent adenovirus vector system: removal of helper virus by Cre-mediated excision of the viral packaging signal. *Proc Natl Acad Sci USA* 1996, **93**:13565-13570.
- Ng P, Parks RJ, Graham FL: Preparation of helper-dependent adenoviral vectors. *Methods Mol Med* 2002, **69**:371-388.

doi:10.1186/1743-422X-10-273

Cite this article as: Zhou et al.: A novel helper-dependent adenovirus-based cell culture model for Hepatitis C virus replication and production. *Virology Journal* 2013 **10**:273.

**Part 4. Upregulation of MicroRNA-146a by hepatitis B virus
x protein contributes to hepatitis development by
downregulating complement factor H**

Junfeng Li, Xiaopeng Dai, Wei Zhang, Shihui Sun, **Yang Zeng**, Guangyu Zhao, Zhihua Kou, Yan Guo, Hong Yu, Lannyng Du, Shibo Jiang, Yusen Zhou

Hepatic injuries in hepatitis B virus (HBV) patients are caused by immune responses of the host. In our previous study, microRNA-146a (miR-146a), an innate immunity-related miRNA, and complement factor H (CFH), an important negative regulator of the alternative pathway of complement activation, were differentially expressed in HBV-expressing and HBV free hepatocytes. Here, the roles of these factors in HBV-related liver inflammation were analyzed in detail. The expression levels of miR-146a and CFH in HBV-expressing hepatocytes were assessed via analyses of hepatocyte cell lines, transgenic mice, adenovirus-infected mice, and HBV-positive human liver samples. The expression level of miR-146a was upregulated in HBV expressing Huh-7 hepatocytes, HBV-expressing mice, and patients with HBV infection. Further results demonstrated that the HBV X protein (HBx) was responsible for its effects on miR-146a expression through NF- κ B-mediated enhancement of miR-146a promoter activity. HBV/HBx also downregulated the expression of *CFH* mRNA in hepatocyte cell lines and the livers of humans and transgenic mice. Furthermore, overexpression and inhibition of miR-146a in Huh-7 cells downregulated and upregulated *CFH* mRNA levels, respectively. Luciferase reporter assays demonstrated that miR-146a downregulated *CFH* mRNA expression in hepatocytes via 3'-untranslated-region (UTR) pairing. The overall effect of this process *in vivo* is to promote liver inflammation. These results demonstrate that the HBx-miR-146a-CFH- complement activation regulation pathway might play an important role in the immunopathogenesis of chronic HBV infection. These findings have important implications for understanding the immunopathogenesis of chronic hepatitis B and developing effective therapeutic interventions. HBV remains an important pathogen and can cause severe liver diseases, including hepatitis, liver cirrhosis, and hepatocellular carcinoma. Although HBV was found in 1966, the molecular mechanisms of pathogenesis are still poorly understood. In the present study, we found that the HBx promoted the expression of miR-146a, an innate immunity-related miRNA, through the NF- κ B signal pathway and that increasingly expressed miR-146a downregulated its target CFH, an important negative regulator of the complement alternative pathway, leading to the promotion of liver inflammation. We demonstrated that the HBx-miR-146a-CFH- complement activation regulation pathway is potentially an important mechanism of immunopathogenesis caused by chronic HBV infection. Our data provide a novel molecular mechanism of HBV pathogenesis and thus help to understand the correlations between the complement system, an important part of innate immunity,

and HBV-associated disease. These findings will also be important to identify potential therapeutic targets for HBV infection.

Upregulation of MicroRNA-146a by Hepatitis B Virus X Protein Contributes to Hepatitis Development by Downregulating Complement Factor H

Jun-Feng Li,^a Xiao-Peng Dai,^a Wei Zhang,^a Shi-Hui Sun,^a Yang Zeng,^a Guang-Yu Zhao,^a Zhi-Hua Kou,^a Yan Guo,^a Hong Yu,^a Lan-Ying Du,^b Shi-Bo Jiang,^{b,c} Yu-Sen Zhou^a

The State Key Laboratory of Pathogen and Biosecurity, Beijing Institute of Microbiology and Epidemiology, Beijing, China^a; Laboratory of Viral Immunology, Lindsley F. Kimball Research Institute, New York Blood Center, New York, New York, USA^b; Key Laboratory of Medical Molecular Virology of Ministries of Education and Health, Shanghai Medical College, Fudan University, Shanghai, China^c

ABSTRACT Hepatic injuries in hepatitis B virus (HBV) patients are caused by immune responses of the host. In our previous study, microRNA-146a (miR-146a), an innate immunity-related miRNA, and complement factor H (CFH), an important negative regulator of the alternative pathway of complement activation, were differentially expressed in HBV-expressing and HBV-free hepatocytes. Here, the roles of these factors in HBV-related liver inflammation were analyzed in detail. The expression levels of miR-146a and CFH in HBV-expressing hepatocytes were assessed via analyses of hepatocyte cell lines, transgenic mice, adenovirus-infected mice, and HBV-positive human liver samples. The expression level of miR-146a was upregulated in HBV-expressing Huh-7 hepatocytes, HBV-expressing mice, and patients with HBV infection. Further results demonstrated that the HBV X protein (HBx) was responsible for its effects on miR-146a expression through NF- κ B-mediated enhancement of miR-146a promoter activity. HBV/HBx also downregulated the expression of CFH mRNA in hepatocyte cell lines and the livers of humans and transgenic mice. Furthermore, overexpression and inhibition of miR-146a in Huh-7 cells downregulated and upregulated CFH mRNA levels, respectively. Luciferase reporter assays demonstrated that miR-146a downregulated CFH mRNA expression in hepatocytes via 3'-untranslated-region (UTR) pairing. The overall effect of this process *in vivo* is to promote liver inflammation. These results demonstrate that the HBx-miR-146a-CFH-complement activation regulation pathway might play an important role in the immunopathogenesis of chronic HBV infection. These findings have important implications for understanding the immunopathogenesis of chronic hepatitis B and developing effective therapeutic interventions.

IMPORTANCE Hepatitis B virus (HBV) remains an important pathogen and can cause severe liver diseases, including hepatitis, liver cirrhosis, and hepatocellular carcinoma. Although HBV was found in 1966, the molecular mechanisms of pathogenesis are still poorly understood. In the present study, we found that the HBV X protein (HBx) promoted the expression of miR-146a, an innate immunity-related miRNA, through the NF- κ B signal pathway and that increasingly expressed miR-146a downregulated its target complement factor H (CFH), an important negative regulator of the complement alternative pathway, leading to the promotion of liver inflammation. We demonstrated that the HBx-miR-146a-CFH-complement activation regulation pathway is potentially an important mechanism of immunopathogenesis caused by chronic HBV infection. Our data provide a novel molecular mechanism of HBV pathogenesis and thus help to understand the correlations between the complement system, an important part of innate immunity, and HBV-associated disease. These findings will also be important to identify potential therapeutic targets for HBV infection.

Received 12 December 2014 Accepted 18 February 2015 Published 24 March 2015

Citation Li J-F, Dai X-P, Zhang W, Sun S-H, Zeng Y, Zhao G-Y, Kou Z-H, Guo Y, Yu H, Du L-Y, Jiang S-B, Zhou Y-S. 2015. Upregulation of microRNA-146a by hepatitis B virus X protein contributes to hepatitis development by downregulating complement factor H. *mBio* 6(2):e02459-14. doi:10.1128/mBio.02459-14.

Invited Editor John M. Taylor, Fox Chase Cancer Center **Editor** Michael J. Imperiale, University of Michigan

Copyright © 2015 Li et al. This is an open-access article distributed under the terms of the [Creative Commons Attribution-NonCommercial-ShareAlike 3.0 Unported license](https://creativecommons.org/licenses/by-nc-sa/4.0/), which permits unrestricted noncommercial use, distribution, and reproduction in any medium, provided the original author and source are credited.

Address correspondence to Yu-Sen Zhou, yszhou@bmi.ac.cn.

Hepatitis B virus (HBV) infection is a global public health problem that affects more than 400 million people worldwide (1). HBV infects hepatocytes but is not directly cytopathic; instead, the resulting hepatic injuries are believed to be caused by immune responses of the host. The immunopathogenesis of hepatitis B depends on a complex interplay of host factors, such as age, gender, and immune status. More than 50% of people with chronic hepatitis B (CHB) are lifetime asymptomatic, whereas 15 to 40% develop liver cirrhosis and hepatocellular carcinoma

(HCC) (2), which has been attributed to repeated immune responses characterized by continuous cycles of low-level liver cell destruction and regeneration (3). Although great effort has been invested in understanding the molecular mechanisms that determine HBV pathogenesis, some major questions remain unanswered (1, 3, 4).

One of the major objectives of the CHB research community is to identify the molecular determinants of CHB progression that could facilitate prognosis and management of the disease. A range

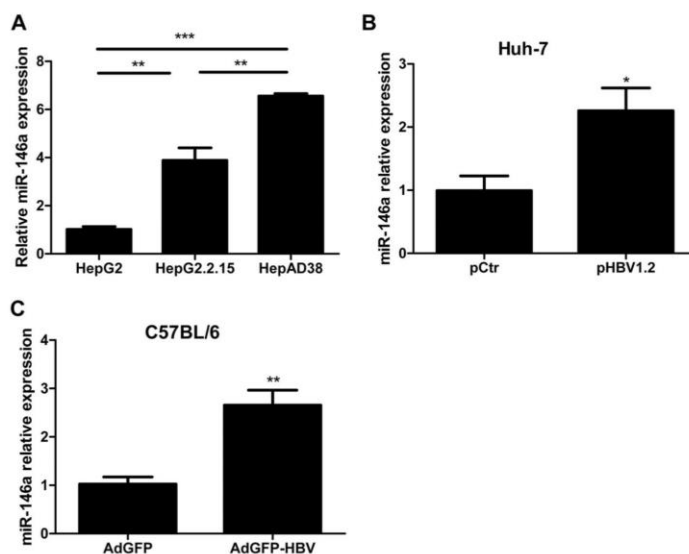


FIG 1 miR-146a is upregulated in HBV-replicating hepatocytes and livers of HBV-infected mice. (A) Quantitative RT-PCR analyses of the relative expression levels of endogenous miR-146a in HepG2, HepG2.2.15, and HepAD38 cells. Huh-7 cells transiently transfected with pHBV1.2 or a control vector (pCtr) (B) and liver tissues of C57BL/6 mice 7 days after receiving a hydrodynamic injection of AdGFP-HBV or AdGFP (C). Each assay was performed in triplicate, and the expression level of miR-146a was normalized to that of U6 snRNA. Data are presented as the means \pm SEM. *, $P < 0.05$; **, $P < 0.01$; ***, $P < 0.001$, versus control or as indicated.

of host molecules have been studied, including cytokines, chemokines, complements, and, in recent years, microRNAs (miRNAs). miRNAs are short (approximately 22 nucleotides), endogenously expressed, noncoding RNAs that regulate gene expression at the posttranscriptional level by pairing with the 3' untranslated regions (UTRs) of target transcripts, leading to translational inhibition and/or mRNA degradation (5). In fact, miRNAs represent a universal regulatory mechanism (6).

Several groups have studied the roles of miRNAs in HBV pathogenesis (7). We previously have demonstrated that miRNA-15b modulates HBV replication through targeting hepatocyte nuclear factor 1 α (8). To identify the key molecules involved in HBV-induced hepatitis, we systematically analyzed the miRNA and mRNA expression profiles of HepG2, HepG2.2.15 (a stable cell line with low HBV replication), and HepAd38 (a stable cell line with higher inducible HBV replication than HepG2.2.15) cells (8). We found that the miR-146a expression level was positively correlated with the HBV replication level. miR-146A modulates both the innate and adaptive immune responses via negative feedback loops involving downregulation of its target genes (9). It could target tumor necrosis factor (TNF) receptor-associated factor 6 and other key effectors of various Toll-like receptor (TLR) signaling pathways (10); however, different cells and disease conditions, such as various tumors (11), rheumatoid arthritis (12), and stressed neural cells (13), are associated with the use of different miR-146a effectors.

It has been reported that the plasma levels of complement component 3 (C3) and C4 are significantly lower in more severe CHB cases than in normal or mild CHB cases (14, 15). Our labo-

ratory has been studying the involvement of complements in the immunopathogenesis of CHB for a number of years. Based on our analysis of the mRNA expression profiles in HBV-expressing hepatocytes and prediction of the potential targets of miR-146a *in silico*, complement factor H (CFH) was selected for further study. CFH is a major inhibitor of the alternative pathway of complement activation (16). To examine their possible mechanisms of regulation and impact on liver inflammation during HBV infection, the hepatic expression levels of miR-146a and CFH were determined both *in vitro* and *in vivo*. Our results reveal an inverse relationship between the expression levels of miR-146a and CFH and demonstrate that both of them play important roles in the pathogenesis of HBV-induced hepatitis.

RESULTS

miR-146a is upregulated in HBV-replicating hepatocytes and hepatic tissues of HBV-expressing mice. In our previous study, we used microarrays to analyze the miRNA expression profiles of HBV-replicating (HepG2.2.15 and HepAd38 cells) and HBV-free (HepG2) hepatocytes (8) and demonstrated that the expression level of miR-146a is positively correlated with the level of HBV replication. The finding was confirmed by quantitative reverse transcription-PCR (qRT-PCR) (Fig. 1A). Furthermore, an HCC cell line (Huh-7) transfected with a vector containing a 1.2-fold HBV genome (pHBV1.2) had a higher level of miR-146a than cells transfected with a control vector (Fig. 1B), suggesting that HBV induces overexpression of miR-146a directly. Next, we performed hydrodynamic injection of an adenovirus containing green fluorescent protein (AdGFP)-HBV or AdGFP into C56BL/6 mice and

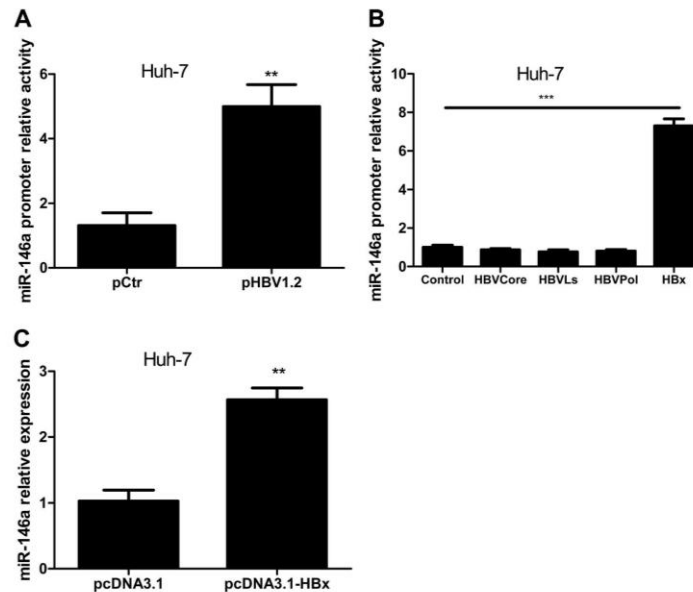


FIG 2 HBx induces miR-146a expression by enhancing its promoter activity. (A and B) The activity of a luciferase reporter gene under the control of the miR-146a promoter in cells that were cotransfected with pGL3-146aP and pHBV1.2 (A) or a pcDNA3.1-based vector expressing HBc (HBVCore), large surface protein (HBVLS), viral polymerase (HBVPol), or HBx (B). (C) Quantitative RT-PCR analyses of miR-146a expression in Huh-7 cells that were transiently transfected with pcDNA3.1-HBx or empty vector. The expression level of miR-146a was normalized to that of U6 snRNA. Data are presented as the means \pm SEM from $n = 3$ replicates. **, $P < 0.01$; ***, $P < 0.001$, versus control.

found that miR-146a expression in mouse liver was significantly higher in the AdGFP-HBV group than in the AdGFP group (Fig. 1C). Taken together, these data indicate that HBV infection of hepatocytes enhances miR-146a expression significantly.

HBV X protein induces miR-146a expression by enhancing its promoter activity. To determine whether HBV enhances miR-146a expression by acting on its promoter, Huh-7 cells were cotransfected with a luciferase reporter plasmid containing the miR-146a promoter (pGL3-146aP) and pHBV1.2. As shown in Fig. 2A, HBV expression enhanced the activity of the miR-146 promoter. To identify which HBV component caused this effect, Huh-7 cells were cotransfected with pGL3-146aP and a pcDNA3.1 vector containing the gene encoding the HBV core protein (HBc), large surface protein, viral polymerase, or X protein (HBx). Overexpression of HBx enhanced the activity of the miR-146 promoter, but overexpression of the other proteins had no effect (Fig. 2B). Furthermore, a qRT-PCR analysis revealed that the expression level of miR-146a was higher in Huh-7 cells transfected with pcDNA3.1-HBx than in those transfected with empty pcDNA3.1 vector (Fig. 2C). Overall, these results suggest that HBV promotes miR-146a expression through upregulation of miR-146a promoter activity by HBx.

The NF- κ B signaling pathway mediates HBx-induced upregulation of miR-146a. To study the mechanism of HBx-mediated upregulation of miR-146a promoter activity, we generated luciferase reporter plasmids containing the 5' (pGL3-146aP1) and 3' (pGL3-146aP2) segments of the miR-146a pro-

moter and tested their activities in Huh-7 cells. The reporter activity of pGL3-146aP1 was minimal, while the activity of pGL3-146aP2 was similar to that of the full-length miR146a promoter (Fig. 3A). In addition, overexpression of HBx by cotransfection with pcDNA3.1-HBx enhanced the activities of the full-length and 3' segment of the miR-146a promoter significantly but had no effect on that of the 5' segment (Fig. 3B). Scanning of the 3' segment of the miR-146a promoter (nucleotides -481 to $+21$ relative to the start of transcription) identified two NF- κ B binding sites (Fig. 3A), as described previously (17). HBx reportedly regulates NF- κ B activity (18); therefore, we hypothesized that HBx promotes binding of NF- κ B to its consensus sites in the miR-146a promoter, thereby upregulating the promoter activity. Mutation of the two NF- κ B binding sites in the 3' segment of the miR-146a promoter (Fig. 3A) abolished the upregulation effect on miR-146a promoter activity of HBx (Fig. 3B). Furthermore, treatment of transfected Huh-7 cells with pyrrolidine dithiocarbamate, an inhibitor of NF- κ B signaling, inhibited the HBx-mediated enhancement of miR-146a promoter activity (Fig. 3C) and upregulation of miR-146a expression (Fig. 3D). These experiments provide further evidence that HBx mediates upregulation of miR-146a via the NF- κ B signaling pathway.

HBx downregulates CFH expression in hepatocytes and hepatic tissue. As mentioned earlier, in a previous study we systematically analyzed the mRNA expression profiles of HBV-expressing (HepAD38 and HepG2.2.15) and HBV-free (HepG2) hepatocytes (unpublished data). Here, *CFH*, an important nega-

Li et al.

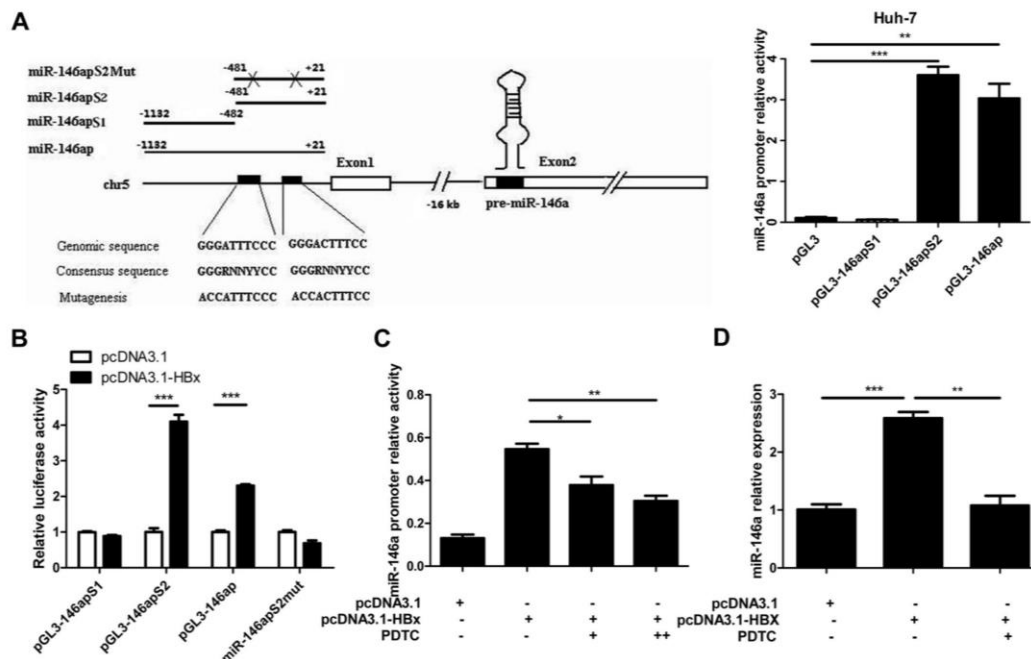


FIG 3 HBx upregulates the activity of the miR-146a promoter through NF- κ B. (A) The left panel shows a schematic illustration of the miR-146a promoter segments used to generate the PGL3 luciferase reporter constructs. The wild-type and mutated NF- κ B binding sites are also shown. The right panel shows the luciferase activities of the PGL3 reporter constructs containing the miR-146a promoter regions. The assays were performed 48 h after transfection of Huh-7 cells. (B) Effect of transient overexpression of HBx on the activities of the miR-146a promoter reporter constructs shown in panel A; (C and D) effects of pyrrolidine dithiocarbamate (PDC), an NF- κ B signaling inhibitor, on the HBx-mediated increases in miR-146a promoter activity (C) and miR-146a expression (D) in transiently transfected Huh-7 cells. Data are presented as the means \pm SEM from $n = 3$ replicates. *, $P < 0.05$; **, $P < 0.01$; ***, $P < 0.001$, versus control or as indicated.

tive regulator of the alternative pathway of complement activation that was identified as an mRNA whose expression showed an inverse relationship with HBV replication level, was selected for further analysis. This finding was confirmed by real-time PCR (Fig. 4A), and the expression level of *CFH* mRNA was significantly lower in Huh-7 cells transfected with pHBV1.2 (Fig. 4B) or pcDNA3.1-HBx (Fig. 4C) than in Huh-7 cells transfected with control plasmids. Finally, *CFH* mRNA and protein levels were significantly lower in the liver tissues of 7- or 16-month-old HBx transgenic mice than those of 7-month-old wild-type mice (Fig. 4D and E).

miR-146a mediates HBx-induced downregulation of *CFH* expression. To determine whether the inhibition of *CFH* expression by HBx occurs via an effect on the *CFH* promoter, we constructed a pGL3 reporter plasmid containing the luciferase gene under the control of the *CFH* promoter and cotransfected Huh-7 cells with this plasmid and pcDNA3-HBx. In these experiments, overexpression of HBx had no effect on the activity of the *CFH* promoter (data not shown); therefore, we hypothesized that HBx-mediated downregulation of *CFH* expression occurs via mRNA degradation. To test this proposal, the 3' UTR of *CFH* or its miR-146a binding site mutant was cloned

into pMIR-luciferase, a vector used to identify miRNA targets, to generate pMIR-*CFH*3' UTR. In cotransfected Huh-7 cells, overexpression of HBx inhibited the reporter activity of pMIR-*CFH*3' UTR but did not affect that of the control vector (Fig. 5A), suggesting that HBx acts on the 3' UTR of *CFH* in hepatocytes, possibly via an miRNA-mediated mechanism. In fact, it has been reported previously that miR-146a acts directly on the 3' UTR of *CFH* in human neural cells to inhibit *CFH* mRNA and protein expression (19).

Transient overexpression of miR-146a in Huh-7 cells downregulated *CFH* mRNA and protein expression (Fig. 5B and C) and the reporter activity of pMIR-*CFH*3' UTR (Fig. 5D) significantly but did not influence the reporter activity of the mutant (pMIR-*CFH*3' UTR-M) (Fig. 5D). In contrast, transfection of Huh-7 cells with an miR-146a antisense RNA vector (pSD14-miR-146a) resulted in a dramatic increase in the reporter activity of pMIR-*CFH*3' UTR (Fig. 5D). The inhibition effect of HBx on the reporter activity of pMIR-*CFH*3' UTR was also abrogated when the miR-146a binding site of the *CFH* 3' UTR was mutated (Fig. 5E). Overexpression of HBx in Huh-7 cells also suppressed the reporter activity of pMIR-*CFH*3' UTR, and coexpression of pSD14-miR-146a abrogated this effect (Fig. 5F). These experi-

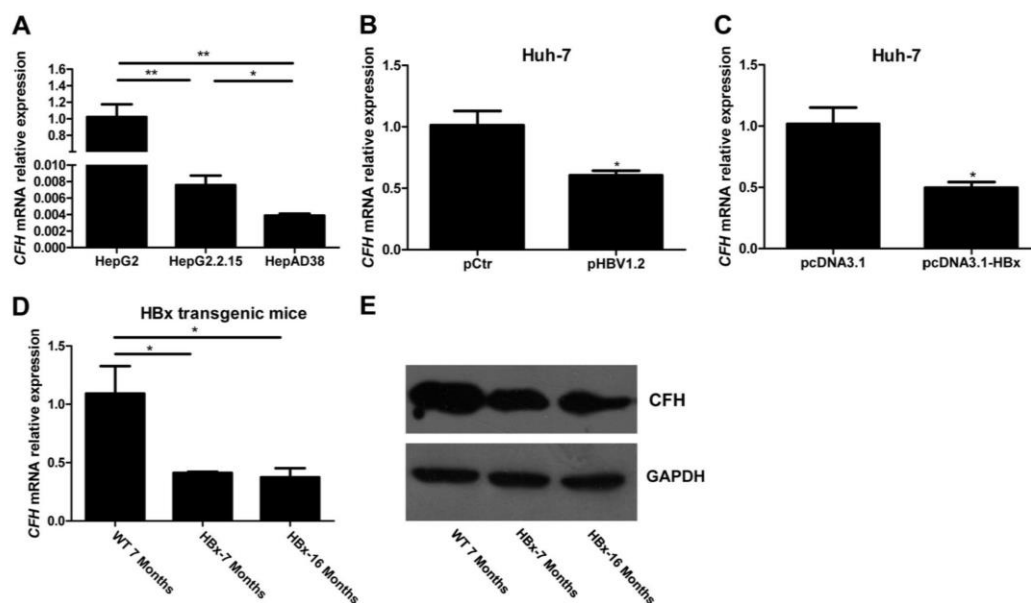


FIG 4 HBx downregulates *CFH* expression in hepatocytes and hepatic tissues. (A to D) Quantitative RT-PCR analyses of *CFH* mRNA levels in HepG2, HepG2.2.15, and HepAD38 cells (A), Huh-7 cells that were transiently transfected with a control vector, pHBV1.2 (B) or pcDNA3.1-HBx (C), and liver tissues of 7-month-old wild-type (WT) mice and 7- and 16-month-old p21-HBx-transgenic mice (D). (E) Immunoblot analyses of *CFH* protein in liver tissues of WT and p21-HBx-transgenic mice. The expression level of GAPDH was used as the internal control. Data are presented as the means \pm SEM from $n = 3$ replicates. *, $P < 0.05$; **, $P < 0.01$, versus control (A to C) or WT (D) mice.

ments indicate that suppression of *CFH* expression by HBx occurs through an miR-146a-mediated effect.

Reduced *CFH* expression is associated with HBV/HBx-induced liver inflammation. HBV can cause acute or chronic inflammation of the human liver, and mice can also present liver damage and inflammation (20–22). Hydrodynamic transfection of normal C57BL/6 mice with a recombinant adenovirus carrying the HBV genome or HBx, AdGFP-HBV or AdGFP-HBx, resulted in decreased hepatic levels of *CFH* mRNA (Fig. 6A) and protein (Fig. 6B). The sequence of mouse mature miR-146a is the same as that of human, and the 3' UTR of mouse *CFH* also has miR-146a binding sites. Together with the results described above, these findings supported that HBV/HBx causes downregulation of *CFH* expression through upregulation of miR-146a in a mouse model.

The serum levels of alanine aminotransferase (ALT) and aspartate transaminase (AST) were significantly higher in the AdGFP-HBV- and AdGFP-HBx-infected C57BL/6 mice than in those infected with AdGFP only (Fig. 6C). A histological examination also revealed marked inflammatory responses in mice infected with AdGFP-HBV or AdGFP-HBx (Fig. 6D). In contrast, C3-deficient mice infected with AdGFP-HBV showed a subdued inflammatory response in the liver, despite some localized necrosis (Fig. 6D). Combined with the finding that HBV/HBx expression in mice causes downregulation of *CFH*, these results suggest that the complement system is the effector of the inflammatory response in HBV-related hepatitis.

Cirrhosis is the advanced stage of hepatitis. To support our

results obtained using hepatic cell lines and mouse models, we examined the expression levels of miR-146a and *CFH* mRNA in liver samples from human liver transplant patients who were diagnosed with HBV-related cirrhosis ($n = 9$). As a control, samples from normal (HBV-negative) liver transplant donors ($n = 8$) were also examined. The expression level of miR-146a was significantly higher in HBV-related cirrhosis patients than in normal controls (Fig. 7A). In contrast, the *CFH* mRNA expression level was significantly lower in HBV-related cirrhosis patients than in normal controls (Fig. 7B). These data from human patients are consistent with the observations made in mouse models, indicating that HBV-related liver inflammation is associated with enhanced expression of miR-146a and decreased expression of *CFH*.

DISCUSSION

The findings presented here reveal the underlying molecular mechanism by which HBx, the major regulatory protein of HBV, downregulates complement factor H, a key host inhibitory modulator of the alternative pathway of complement activation. The results described above support a regulatory cascade in which (i) HBx enhances miR-146a promoter activity through an NF- κ B-mediated effect and (ii) HBx-induced miR-146a downregulates *CFH* by targeting its 3' UTR. The resulting reduced inhibition of complement activation by *CFH* would lead to tissue inflammation. Thus, we propose that the HBx-miR-146a-*CFH*-complement regulation axis may underlie chronic HBV infection-related immunopathogenesis (Fig. 8).

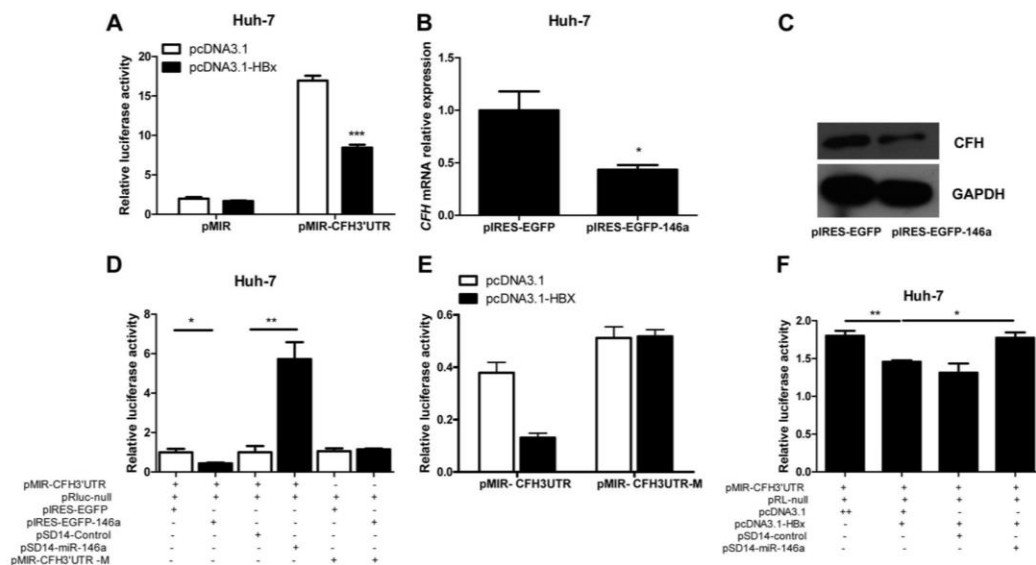


FIG 5 HBx-mediated downregulation of *CFH* expression requires miR-146a. (A) The effect of overexpression of HBx on the activity of a reporter gene under the control of the *CFH* 3' UTR. Dual-luciferase reporter assays of Huh-7 cells that were cotransfected with pcDNA3.1 or pcDNA3.1-HBx and pMIR or pMIR-CFH3'UTR were performed 48 h after transfection. Quantitative RT-PCR (B) and immunoblot analyses (C) of the effect of transient overexpression of miR-146a (pIRES-EGFP-146a) on *CFH* mRNA levels in Huh-7 cells. The effects of overexpression (pIRES-EGFP-146a) (C) or inhibition (pSD14-146a) (D) of miR-146a, or overexpression of HBx (pcDNA3.1-HBx) with or without inhibition of miR-146a (E and F), on the activity of pMIR-CFH3' UTR or pMIR-CFH3' UTR-M in transiently cotransfected Huh-7 cells. The reporter activities were determined at 48 h posttransfection. (A to D) Data are presented as the means \pm SEM from $n = 3$ replicates. *, $P < 0.05$; **, $P < 0.01$; ***, $P < 0.001$.

To our knowledge, the molecular details of NF- κ B-dependent upregulation of miR-146a by HBx and downregulation of *CFH* by miR-146a in hepatocytes are reported here for the first time. Previous studies have demonstrated that NF- κ B-dependent activation of miR-146a is involved in the regulation of factors such as lipopolysaccharide (17) and interleukin 1 β (23) and also occurs during vesicular stomatitis virus (24), human T-cell lymphotropic virus 1 (25), and Epstein-Barr virus (26, 27) infections. The results presented here demonstrate that the NF- κ B signaling pathway mediates HBV/HBx-induced upregulation of miR-146a. Downregulation of *CFH* by miR-146a has been reported previously in human neural cells (13, 19); the results presented here demonstrate that this regulation also occurs in hepatocytes. HBx reportedly induces NF- κ B activation in hepatocytes through physical interaction with p22-FLIP and NEMO (18); in combination with our observations, this finding presents the complete molecular picture of HBx-mediated upregulation of miR-146a and downregulation of *CFH* in hepatocytes.

miR-146a has emerged as a master regulator of the immune system and is involved in innate and adaptive immunity, various viral infections, cancers, and some nonimmune human diseases (9–11). Multiple targets of miR-146a have been identified to date (9). A most notable example is that in lipopolysaccharide-induced cross-tolerance, miR-146a acts as a central tuning mechanism to prevent an overstimulated acute inflammatory response (28). In HBV-related studies, miR-146a was reported to suppress the sensitivity of HCC cells to interferon alpha through SMAD4 (29), and

the CC genotype of the miR-146a rs2910164 G/C polymorphism is associated with susceptibility for acute-on-chronic hepatitis B liver failure (30), while the GG genotype is associated with higher expression of miR-146a and higher risk of HCC, especially in Asian and male populations (31, 32). It is possible that the higher miR-146a expression level found in individuals with the GG genotype leads to enhanced suppression of the acute immune responses that involve activation of the NF- κ B pathway, resulting in reduced susceptibility to acute liver failure. However, the results presented here suggest that higher miR-146a expression leads to a more severe suppression of *CFH* in hepatocytes, resulting in enhanced chronic complement-mediated cytotoxicity and subsequent liver fibrosis, cirrhosis, and HCC. Therefore, miR-146a appears to be a key molecule that has the potential to influence the direction of progressive HBV infection; as such, further investigation of the roles of miR-146a expression in HBV-related innate immunity and tumorigenesis is warranted.

The pathogenesis of HBV-induced hepatitis is complicated. The complement system, which plays an important role in various inflammatory conditions, reportedly plays a pivotal role in chemical-induced hepatitis (33) and liver-specific autoantibody-mediated hepatitis (34). It has long been known that plasma C3 and C4 levels are significantly lower in patients with severe CHB than in healthy individuals or those with mild CHB (14). However, an in-depth mechanistic study of the involvement of the complement system in HBV-induced hepatitis is lacking. *CFH* is produced mainly in the liver. *CFH* competes with B or Bb for

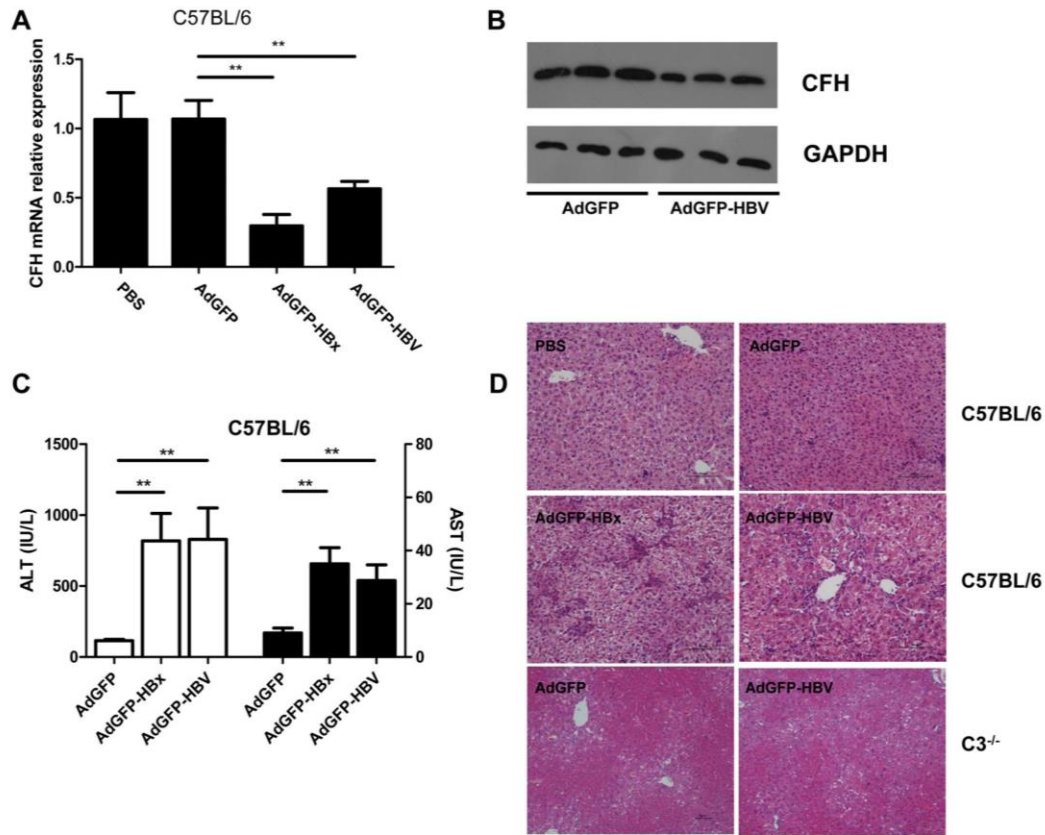


FIG 6 Reduced *CFH* expression is associated with HBV/HBx-induced liver inflammation. (A) Quantitative RT-PCR of the expression levels of *CFH* mRNA in C57BL/6 mice infected with AdGFP-HBx, AdGFP-HBV, AdGFP, or phosphate-buffered saline (PBS) via hydrodynamic injection; (B) immunoblot analyses of *CFH* protein in C57BL/6 mice infected with AdGFP or AdGFP-HBV; (C) the serum levels of ALT and AST in C57BL/6 mice infected with AdGFP, AdGFP-HBx, or AdGFP-HBV; (D) hematoxylin- and eosin-stained sections of the livers of C57BL/6 and C3^{-/-} mice infected with the indicated adenoviruses or PBS. The mice were euthanized 7 days after the injection. Data are presented as the means \pm SEM from $n = 5$ replicates. **, $P < 0.01$. Scale bar, 100 μ m.

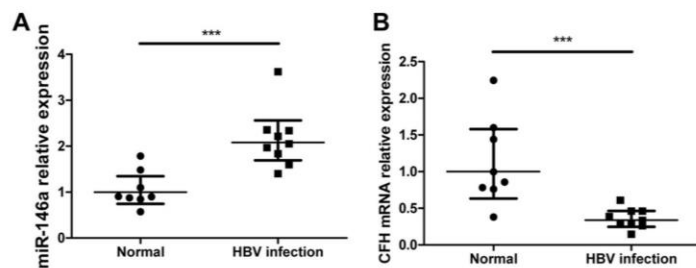


FIG 7 miR-146a and *CFH* are up- and downregulated, respectively, in HBV-positive cirrhotic human liver tissues. (A and B) The relative miR-146a (A) and *CFH* mRNA (B) expression levels in liver tissues from HBV-positive liver transplant patients with cirrhosis ($n = 9$) and healthy transplant donors ($n = 8$). Data are presented as the geometric mean with 95% CI. ***, $P < 0.001$.

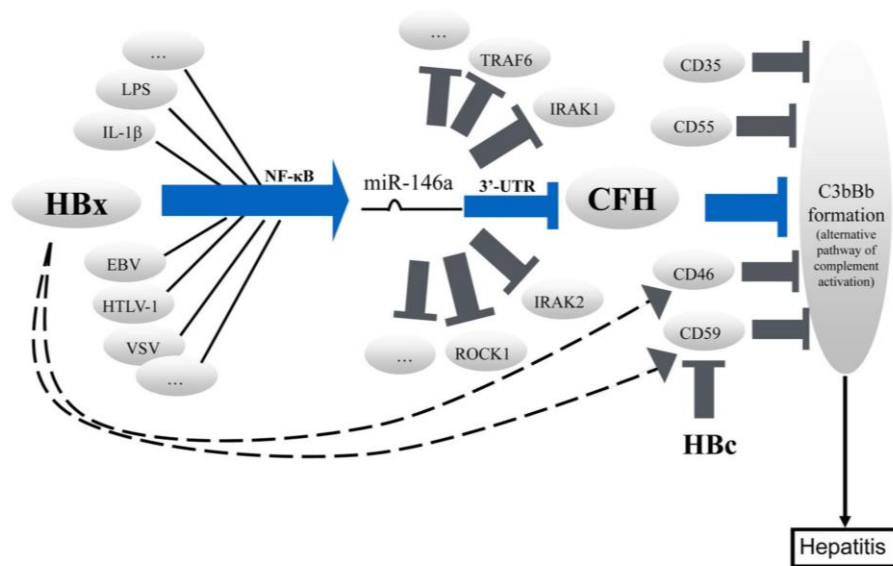


FIG 8 Overview of the regulation pathway from HBV infection to complement activation. HBx/HBV and several other viruses, such as Epstein-Barr virus (EBV), human T-cell lymphotropic virus 1 (HTLV-1), and vesicular stomatitis virus (VSV), as well as immune activators such as lipopolysaccharide (LPS) and interleukin 1 β (IL-1 β), can induce miR-146a expression by activating NF- κ B signaling. miR-146a suppresses the expression of *CFH*, as well as multiple other genes, by binding to the 3' UTRs of its targets. Together with several other negative regulators of complement activation, CFH inhibits the formation of C3 convertase (C3bBb), thus inhibiting constitutive complement activation via the alternative pathway. HBx may also enhance the expression of CD59 and CD46, while HBc may inhibit CD59 expression. The HBx-miR-146a-CFH-complement activation pathway could play a central role in chronic HBV infection-related liver inflammation.

binding to C3b and accelerates the displacement of Bb from C3b, thereby inhibiting the formation of C3 convertase (C3bBb) in the alternative pathway (16). Constitutive high expression of CFH has been detected in the eye, and a *CFH* polymorphism is strongly associated with age-related macular degeneration (35); furthermore, CFH protects the eyes through recruiting to the surface of apoptotic cells, where it neutralizes the proinflammatory properties of these cells and halts complement activation (36). These reports imply a strong association of reduced levels of CFH at local sites with increased inflammation. Here, HBV infection of mice resulted in significantly lower *CFH* levels in hepatocytes and significant liver inflammation. Considering its role as an inhibitor of the alternative pathway of complement activation, we consider the lower *CFH* levels in hepatocytes to be a direct cause of the liver inflammation. Hepatic *CFH* expression was also reduced by HBx-induced overexpression of miR-146a. In agreement with our explanation of the connection between lower *CFH* levels and increased inflammation, we also observed increased liver inflammation in mice overexpressing HBx via a recombinant adenovirus vector (Fig. 5A and 6C). In addition, *CFH* expression was significantly lower in the livers of HBV-related cirrhosis liver transplant patients than in those of normal donors. Taken together, these results showed that reduced *CFH* expression induced by HBx plays a pivotal role in HBV-induced hepatitis.

The alternative pathway of complement activation has several negative regulators, including CFH, CD46, CD59, CD55, and

CD35. HBV up- or downregulates several complement regulatory molecules (see Fig. 8). HBc sensitizes hepatocytes to complement-dependent cytotoxicity by downregulating CD59 (37, 38). In contrast, HBx upregulates CD46 (39) and CD59 (40) in hepatocytes to protect against inflammation. Such complicated and delicate interactions indicate the importance of complement activation in HBV immunopathogenesis; in addition, for complement regulators that are regulated by HBV proteins in opposing directions, such as the respective up- and downregulation of CD59 by HBx and HBc, it must be considered that either one might involve different degrees of regulation or require different cofactors. The overall effect of these regulations in the context of HBV infection might be related to the stage of disease progression. The balance between complement activation and inhibition by HBV might tilt at a certain point of CHB progression to favor complement activation rather than inhibition, resulting in the commencement of tissue damage. Generating a more complete understanding of the positive and negative regulation of complement activation might provide tools or methods to control complement-mediated liver injuries. In terms of therapeutic intervention for HBV-related hepatitis, the results presented here suggest that inhibiting complement activation in CHB patients would help to control chronic liver injuries. This subject will be the focus of future studies.

In summary, this study demonstrates that HBx upregulates miR-146a in HBV-infected hepatocytes by promoting NF- κ B binding to the miR-146a promoter. Subsequently, miR-146a

TABLE 1 Oligonucleotides used for qRT-PCR of viral genomic and subgenomic RNA

| Gene product or description | Application | Type | Sequence (5'→3') | |
|-----------------------------|-----------------------------------|---------------------------------|--|---|
| U6 | Reverse transcription | Stem-loop RT | GTCGTATCCAGTGCAGGGTCCGAGGTATTCCGACTGGTACGACAAAAATATG | |
| | Real-time PCR | Forward | CGCAAAATTCGTGAAGCGTTC | |
| miR-146a | Real-time PCR | Universal reverse | GTGCAGGGTCCGAGGTATTCC | |
| | Pri-miR-146a clone | Forward | AGATCTTCAAGCGATCCTCCACACAG | |
| | Pri-miR-146a clone | Reverse | CTGCAGCATGAAAGCACTACAACAGTACCTG | |
| | Reverse transcription | Stem-loop RT | GCCTGGTCCACACCCTGAGCCCGCACGACCAGGCAACCCATG | |
| | Real-time PCR | Forward | AACGGCGGTGAGAACTGAATT | |
| | Real-time PCR | Reverse | Universal reverse primer as above | |
| | Promoter (-1132 to +21) | Forward | GCAGCTAGCTTTCGGTCCATGAGCACGT | |
| | Promoter (-1132 to +21) | Reverse | GCAAAGCTTAGCGGTCAAGCGTCTTGG | |
| | PromoterS1 (approx -1132 to -482) | Forward | GCAGCTAGCTTTCGGTCCATGAGCACGT | |
| | PromoterS1 (approx -1132 to -482) | Reverse | CTCGAGAAGTGCAGCGCAGGCTGAGTTTC | |
| | PromoterS2 (-481 to +21) | Forward | GGTACCGAAAAGCCAACAGGCTCATTG | |
| | PromoterS2 (-481 to +21) | Reverse | GCAAAGCTTAGCGGTCAAGCGTCTTGG | |
| | Mutation in NF-κB binding sites | 146aS2mut | Forward | ACAGCAAAAGCCCGAGCGACCTTCGGTACCGAAAAGCCAACAGGCTCATTG |
| | | 146aS2mut | Reverse | CTTTCTCCAAGACGCTTGACCGCTAAGCTTGTAAGCGGATGCCGGGAGCAGAC |
| 146aS2mut | | Mutant1 | AGCCGATAAAGCTCTCACCATTTCGCCGCGGGGCTG | |
| 146aS2mut | | Mutant2 | GCGCCGAGGAGGGATCTAGAAACCATTTCAGAGAGGGTTAGCG | |
| CFH | | Real-time PCR for humans | Forward | AACAGATTGTCTCAGTTTACCTAGC |
| | | Real-time PCR for humans | Reverse | ACCGGCCTTATACACATCCCTTC |
| | | CFH-3'UTR | Forward | GAATCAATCATAAAGTGACACACC |
| | | CFH-3'UTR | Reverse | GTTTTCCAGGATTTAATATGGTGC |
| | | CFH-3'UTRmut | Forward | ACAGCAAAAGCCCGAGCGACCTTCGAATTTCGAATCAATCATAAAGTGACAC |
| | | CFH-3'UTRmut | Reverse | CCATATTAATCCTGGAAAACCTCGAGCGGCTAAGGCCAGCGCCACTTTT |
| | CFH-3'UTRmut | Mutant | TTAGTATTAACCTTCTGACTAATTTTCATTTTTAAG | |
| | Real-time PCR for mice | Forward | CTCGCTGTGTTGGACTTCCTT | |
| | Real-time PCR for mice | Reverse | GTATGTAACCTCTTCCCATGTTG | |
| | Promoter | Forward | GGTACCTCAGCATTTCAAATTTGTTGATTTTG | |
| Promoter | Reverse | AAGCTTGGATCTTTTAAGAGGACATTACCAG | | |
| GAPDH | Real-time PCR for humans | Forward | TGGGTGTGAACCATGAGAAGTATG | |
| | Real-time PCR for humans | Reverse | ACTGTGGTCATGAGTCCCTCCA | |
| | Real-time PCR for mice | Forward | TGCACCACCAACTGCTTAGC | |
| | Real-time PCR for mice | Reverse | GTCTTCTGGGTGGCAGTGATG | |

downregulates *CFH* expression via 3'-UTR targeting. *In vivo*, the overall effect of this process is the promotion of liver inflammation. The HBx-miR-146a-CFH-complement activation regulation pathway might be the central mechanism of CHB-related immunopathogenesis. These findings might have important implications for the immunopathogenesis of CHB and the development of effective interventions.

MATERIALS AND METHODS

Plasmids and recombinant adenoviruses. The expression vector containing a 1.2-fold HBV genome (pHBV1.2), the pcDNA3.1-based expression plasmids containing the HBV genes encoding HBc, large surface protein, viral polymerase, or HBx, and the recombinant adenoviruses expressing HBV (AdGFP-HBV) and HBx (AdGFP-HBx) were generated as described previously (8). The PGL3-based promoter reporter plasmids (Promega) were generated by inserting the full-length human miR-146a promoter (nucleotides -1132 to +21 relative to the transcription start site), the 5' (S1) segment of the human miR-146a promoter (nucleotides -1132 to -482), the 3' (S2) segment of the human miR-146a promoter (nucleotides -481 to +21) (27), or the *CFH* promoter (nucleotides -553 to +110) (41) amplified from HepG2 cells. Site-directed mutagenesis of the two NF-κB binding sites in S2

was performed using the Multipoints mutagenesis kit (TaKaRa Biotechnology) (17). The pMIR-CFH3' UTR and pMIR-CFH3' UTR-M reporter plasmids were constructed by inserting the 3' UTR (nucleotides +3748 to +3936) of *CFH* or its miR-146a binding site mutant into the pMIR-luciferase vector (8). The internal control reporter vector pRL-UBI was constructed by replacing the TK promoter region of the pRL-TK vector (Promega) with the ubiquitin promoter. The miR-146a expression plasmid (pIRES-EGFP-146a [where EGFP is enhanced green fluorescent protein]) was constructed by inserting an amplified pri-miR-146a sequence into the pIRES2-EGFP vector (Clontech). The antisense miR-146a expression plasmid (pSD14-miR-146a) was constructed by inserting an antisense oligonucleotide of mature miR-146a into the pSD14 vector (GeneChem Shanghai). The primers used in this study were synthesized by Invitrogen (Beijing) and are listed in Table 1.

Cell culture and transfection. HepG2, HepG2.2.15, HepAD38, and Huh-7 cells were cultured and transfected with plasmids as described previously (8). For the experiments shown in Fig. 3C and D, 30 μM (Fig. 3C and D) or 60 μM (Fig. 3C) pyrrolidine dithiocarbamate was added to the cells 6 h after transfection.

Quantitative real-time PCR. Total RNA was extracted and reverse transcribed as described previously (8). A 2-μl aliquot of reverse transcription product was used as the template for qPCR reactions using

GoTaq qPCR master mix (Promega). U6 snRNA and GAPDH were used for normalization of miRNAs and mRNAs, respectively. Data analysis was performed using the $2^{-\Delta\Delta Ct}$ method (42).

Reporter assays. For the experiments shown in Fig. 2 and 3, Huh-7 cells were cotransfected with the pGL3-146P, pRL-UBI, and pHBV1.2 plasmids or a pcDNA3.1-based plasmid containing the specific HBV gene; for the experiments shown in Fig. 5, Huh-7 cells were cotransfected with pMIR-CFH3' UTR, pRL-UBI, and pIRES-EGFP-146a, pSD14-miR-146a, or pcDNA3.1-HBx. Dual-luciferase assays were performed as described previously (8).

Animals and ethics statement. The methods used to generate AdGFP-HBx- and AdGFP-HBV-infected mice and extract liver tissues of p21-HBx gene knock-in transgenic mice (C57BL/6) and control mice have been described previously (8). $C3^{-/-}$ mice (B6.129S4-C3^{tm1Cre}/J) have also been described previously (43). All animal-related procedures were approved by the Institutional Animal Care and Use Committee of the Beijing Institute of Microbiology and Epidemiology (permit no. BIME 2013-16), and relevant guidelines were strictly followed. Clinical liver tissue RNA samples were obtained from Dexi Chen of Beijing You'an Hospital. The study protocol was approved by the ethics committees of Beijing You'an Hospital.

Immunoblotting. Standard protocols were followed utilizing 8% denaturing gels, antibodies against human CFH (Genematrix) and GAPDH (Cell Signaling Technology), a horseradish peroxidase (HRP)-conjugated secondary antibody, and ECL Western blotting substrate (Pierce).

Biochemical and histological analyses to evaluate liver injury. The test of levels of alanine aminotransferase (ALT) and aspartate amino transferase (AST) in mouse serum and histological analysis (hematoxylin and eosin staining) of mouse liver tissues were performed as described previously (43), and the extent of the liver damage was assessed by two independent observers who were blinded to the groups.

Statistical analysis. Each experiment was repeated at least three times. Comparisons of relative luciferase activity, as well as expression levels of miRNAs, mRNAs, and proteins between the two groups, were performed using Student's *t* tests (Fig. 1 to Fig. 6) or a Mann-Whitney test (Fig. 7). Quantitative values are, respectively, expressed as the means \pm standard errors of the means (SEM) or geometric means with 95% confidence intervals (CI). *P* values of <0.05 were considered statistically significant.

ACKNOWLEDGMENTS

This work was supported by the National Program of Infectious Diseases (no. 2012ZX10004-502), an NSFC grant (no. 30900753), and 973 Project (no. 2012 CB 518905).

REFERENCES

- Tang CM, Yau TO, Yu J. 2014. Management of chronic hepatitis B infection: current treatment guidelines, challenges, and new developments. *World J Gastroenterol* 20:6262–6278. <http://dx.doi.org/10.3748/wjg.v20.i20.6262>.
- Fattovich G, Stroffolini T, Zagni I, Donato F. 2004. Hepatocellular carcinoma in cirrhosis: incidence and risk factors. *Gastroenterology* 127: S35–S50. <http://dx.doi.org/10.1053/j.gastro.2004.09.014>.
- Chisari FV, Iisogawa M, Wieland SF. 2010. Pathogenesis of hepatitis B virus infection. *Pathol Biol* 58:258–266. <http://dx.doi.org/10.1016/j.patbio.2009.11.001>.
- Dandri M, Locarnini S. 2012. New insight in the pathobiology of hepatitis B virus infection. *Gut* 61(Suppl 1):i6–i17. <http://dx.doi.org/10.1136/gutjnl-2012-302056>.
- Murchison EP, Hannon GJ. 2004. miRNAs on the move: miRNA biogenesis and the RNAi machinery. *Curr Opin Cell Biol* 16:223–229. <http://dx.doi.org/10.1016/j.cob.2004.04.003>.
- Wang Y, Li X, Hu H. 2011. Transcriptional regulation of co-expressed microRNA target genes. *Genomics* 98:445–452. <http://dx.doi.org/10.1016/j.ygeno.2011.09.004>.
- Thirion M, Ochiya T. 2013. Roles of microRNAs in the hepatitis B virus infection and related diseases. *Viruses* 5:2690–2703. <http://dx.doi.org/10.3390/v5112690>.
- Dai X, Zhang W, Zhang H, Sun S, Yu H, Guo Y, Kou Z, Zhao G, Du L, Jiang S, Zhang J, Li J, Zhou Y. 2014. Modulation of HBV replication by microRNA-15b through targeting hepatocyte nuclear factor 1alpha. *Nucleic Acids Res* 42:6578–6590. <http://dx.doi.org/10.1093/nar/gku260>.
- Labbaye C, Testa U. 2012. The emerging role of MIR-146A in the control of hematopoiesis, immune function and cancer. *J Hematol Oncol* 5:13. <http://dx.doi.org/10.1186/1756-8722-5-13>.
- Rusca N, Monticelli S. 2011. miR-146a in immunity and disease. *Mol Biol Int* 2011:437301. <http://dx.doi.org/10.4061/2011/437301>.
- Li L, Chen XP, Li YJ. 2010. MicroRNA-146a and human disease. *Scand J Immunol* 71:227–231. <http://dx.doi.org/10.1111/j.1365-3083.2010.02383.x>.
- Abou-Zeid A, Saad M, Soliman E. 2011. MicroRNA 146a expression in rheumatoid arthritis: association with tumor necrosis factor-alpha and disease activity. *Genet Test Mol Biomarkers* 15:807–812. <http://dx.doi.org/10.1089/gtmb.2011.0026>.
- Pogue AI, Li YY, Cui JG, Zhao Y, Kruck TP, Percy ME, Tarr MA, Lukiw WJ. 2009. Characterization of an NF-kappaB-regulated, miRNA-146a-mediated down-regulation of complement factor H (CFH) in metal-sulfate-stressed human brain cells. *J Inorg Biochem* 103:1591–1595. <http://dx.doi.org/10.1016/j.jinorgbio.2009.05.012>.
- Joshi N, Ayesha Q, Habibullah CM. 1990. Immunological studies in HBV-related chronic liver diseases. *Indian J Pathol Microbiol* 33:351–354.
- Ozer FT, Barut A, Inal A, Hacibektaşoğlu A. 1992. Complement C3 and C4 levels in serum from acute viral hepatitis. *Mikrobiyol Bul* 26:314–319.
- Makou E, Herbert AP, Barlow PN. 2013. Functional anatomy of complement factor H. *Biochemistry* 52:3949–3962. <http://dx.doi.org/10.1021/bi4003452>.
- Taganov KD, Boldin MP, Chang KJ, Baltimore D. 2006. NF-kappaB-dependent induction of microRNA miR-146, an inhibitor targeted to signaling proteins of innate immune responses. *Proc Natl Acad Sci U S A* 103:12481–12486. <http://dx.doi.org/10.1073/pnas.0605298103>.
- Lim KH, Choi HS, Park YK, Park ES, Shin GC, Kim DH, Ahn SH, Kim KH. 2013. HBx-induced NF-kappaB signaling in liver cells is potentially mediated by the ternary complex of HBx with p22-FLIP and NEMO. *PLoS One* 8:e57331. <http://dx.doi.org/10.1371/journal.pone.0057331>.
- Lukiw WJ, Zhao Y, Cui JG. 2008. An NF-kappaB-sensitive microRNA-146a-mediated inflammatory circuit in Alzheimer disease and in stressed human brain cells. *J Biol Chem* 283:31315–31322. <http://dx.doi.org/10.1074/jbc.M805371200>.
- Von Freyend MJ, Untergasser A, Arzberger S, Oberwinkler H, Drebber U, Schirmacher P, Protzer U. 2011. Sequential control of hepatitis B virus in a mouse model of acute, self-resolving hepatitis B. *J Viral Hepat* 18: 216–226. <http://dx.doi.org/10.1111/j.1365-2893.2010.01302.x>.
- Huang LR, Gabel YA, Graf S, Arzberger S, Kurts C, Heikenwalder M, Knolle PA, Protzer U. 2012. Transfer of HBV genomes using low doses of adenovirus vectors leads to persistent infection in immune competent mice. *Gastroenterology* 142:1447–1450. e3. <http://dx.doi.org/10.1053/j.gastro.2012.03.006>.
- Xia YJ, Zeng D, Xia LM, Yu F, Lin HH, Zhou L, Tian DA, Liu M. 2012. Role of monokine induced by interferon-gamma in liver injury induced by hepatitis B virus in mice. *J Viral Hepat* 19:509–518. <http://dx.doi.org/10.1111/j.1365-2893.2011.01581.x>.
- Perry MM, Moschos SA, Williams AE, Shepherd NJ, Larner-Svensson HM, Lindsay MA. 2008. Rapid changes in microRNA-146a expression negatively regulate the IL-1beta-induced inflammatory response in human lung alveolar epithelial cells. *J Immunol* 180:5689–5698. <http://dx.doi.org/10.4049/jimmunol.180.8.5689>.
- Hou J, Wang P, Lin L, Liu X, Ma F, An H, Wang Z, Cao X. 2009. MicroRNA-146a feedback inhibits RIG-I-dependent type I IFN production in macrophages by targeting TRAF6, IRAK1, and IRAK2. *J Immunol* 183:2150–2158. <http://dx.doi.org/10.4049/jimmunol.0900707>.
- Tomita M, Tanaka Y, Mori N. 2012. MicroRNA miR-146a is induced by HTLV-1 tax and increases the growth of HTLV-1-infected T-cells. *Int J Cancer* 130:2300–2309. <http://dx.doi.org/10.1002/ijc.25115>.
- Motsch N, Pfuhl T, Mrazek J, Barth S, Grässer FA. 2007. Epstein-Barr virus-encoded latent membrane protein 1 (LMP1) induces the expression of the cellular microRNA miR-146a. *RNA Biol* 4:131–137. <http://dx.doi.org/10.4161/rna.4.3.5206>.
- Cameron JE, Yin Q, Fewell C, Lacey M, McBride J, Wang X, Lin Z, Schaefer BC, Flemington EK. 2008. Epstein-Barr virus latent membrane protein 1 induces cellular microRNA miR-146a, a modulator of lympho-

- cyte signaling pathways. *J Virol* 82:1946–1958. <http://dx.doi.org/10.1128/JVI.02136-07>.
28. Nahid MA, Pauley KM, Satoh M, Chan EK. 2009. miR-146a is critical for endotoxin-induced tolerance: implication in innate immunity. *J Biol Chem* 284:34590–34599. <http://dx.doi.org/10.1074/jbc.M109.056317>.
 29. Tomokuni A, Eguchi H, Tomimaru Y, Wada H, Kawamoto K, Kobayashi S, Marubashi S, Tanemura M, Nagano H, Mori M, Doki Y. 2011. miR-146a suppresses the sensitivity to interferon alpha in hepatocellular carcinoma cells. *Biochem Biophys Res Commun* 414:675–680. <http://dx.doi.org/10.1016/j.bbrc.2011.09.124>.
 30. Jiang H, He X, Li J, Xie Q, Lin J, Chang Y. 2013. Association of a single-nucleotide polymorphism within the miR-146a gene with susceptibility for acute-on-chronic hepatitis B liver failure. *Immunogenetics* 65:257–263. <http://dx.doi.org/10.1007/s00251-012-0675-4>.
 31. Xu T, Zhu Y, Wei QK, Yuan Y, Zhou F, Ge YY, Yang JR, Su H, Zhuang SM. 2008. A functional polymorphism in the miR-146a gene is associated with the risk for hepatocellular carcinoma. *Carcinogenesis* 29:2126–2131. <http://dx.doi.org/10.1093/carcin/bgn195>.
 32. Xu Y, Li L, Xiang X, Wang H, Cai W, Xie J, Han Y, Bao S, Xie Q. 2013. Three common functional polymorphisms in microRNA encoding genes in the susceptibility to hepatocellular carcinoma: a systematic review and meta-analysis. *Gene* 527:584–593. <http://dx.doi.org/10.1016/j.gene.2013.05.085>.
 33. Losser MR, Payen D. 1996. Mechanisms of liver damage. *Semin Liver Dis* 16:357–367. <http://dx.doi.org/10.1055/s-2007-1007249>.
 34. Tu Z, Li Q, Chou HS, Hsieh CC, Meyerson H, Peters MG, Bu H, Fung JJ, Qian S, Lu L, Lin F. 2011. Complement mediated hepatocytes injury in a model of autoantibody induced hepatitis. *Immunobiology* 216:528–534. <http://dx.doi.org/10.1016/j.imbio.2010.08.004>.
 35. Klein RJ, Zeiss C, Chew EY, Tsai JY, Sackler RS, Haynes C, Henning AK, SanGiovanni JP, Mane SM, Mayne ST, Bracken MB, Ferris FL, Ott J, Barnstable C, Hoh J. 2005. Complement factor H polymorphism in age-related macular degeneration. *Science* 308:385–389. <http://dx.doi.org/10.1126/science.1109557>.
 36. Weismann D, Hartvigsen K, Lauer N, Bennett KL, Scholl HP, Charbel Issa P, Cano M, Brandstätter H, Tsimikas S, Skerka C, Superti-Furga G, Handa JT, Zipfel PF, Witztum JL, Binder CJ. 2011. Complement factor H binds malondialdehyde epitopes and protects from oxidative stress. *Nature* 478:76–81. <http://dx.doi.org/10.1038/nature10449>.
 37. Qu Z, Liang X, Liu Y, Du J, Liu S, Sun W. 2009. Hepatitis B virus sensitizes hepatocytes to complement-dependent cytotoxicity through downregulating CD59. *Mol Immunol* 47:283–289. <http://dx.doi.org/10.1016/j.molimm.2009.09.022>.
 38. Liu D, Ni B, Wang L, Zhang M, Liu W, Wu Y. 2013. Hepatitis B virus core protein interacts with CD59 to promote complement-mediated liver inflammation during chronic hepatitis B virus infection. *FEBS Lett* 587:3314–3320. <http://dx.doi.org/10.1016/j.febslet.2013.08.044>.
 39. Zhang S, Shan C, Cui W, You X, Du Y, Kong G, Gao F, Ye L, Zhang X. 2013. Hepatitis B virus X protein protects hepatoma and hepatic cells from complement-dependent cytotoxicity by up-regulation of CD46. *FEBS Lett* 587:645–651. <http://dx.doi.org/10.1016/j.febslet.2013.01.019>.
 40. Shan C, Zhang S, Cui W, You X, Kong G, Du Y, Qiu L, Ye L, Zhang X. 2011. Hepatitis B virus X protein activates CD59 involving DNA binding and let-7i in protection of hepatoma and hepatic cells from complement attack. *Carcinogenesis* 32:1190–1197. <http://dx.doi.org/10.1093/carcin/bgr106>.
 41. Wu Z, Lauer TW, Sick A, Hackett SF, Campochiaro PA. 2007. Oxidative stress modulates complement factor H expression in retinal pigmented epithelial cells by acetylation of FOXO3. *J Biol Chem* 282:22414–22425. <http://dx.doi.org/10.1074/jbc.M702321200>.
 42. Livak KJ, Schmittgen TD. 2001. Analysis of relative gene expression data using real-time quantitative PCR and the 2⁻(Delta Delta C(T)) method. *Methods* 25:402–408. <http://dx.doi.org/10.1006/meth.2001.1262>.
 43. Sun S, Guo Y, Zhao G, Zhou X, Li J, Hu J, Yu H, Chen Y, Song H, Qiao F, Xu G, Yang F, Wu Y, Tomlinson S, Duan Z, Zhou Y. 2011. Complement and the alternative pathway play an important role in LPS/D-GalN-induced fulminant hepatic failure. *PLoS One* 6:e26838. <http://dx.doi.org/10.1371/journal.pone.0026838>.

**Part 5. Multi-organ damage in human dipeptidyl peptidase 4
transgenic mice infected with Middle East Respiratory
Syndrome-Coronavirus**

Guangyu Zhao[#], Yuting Jiang[#], Hongjie Qiu, Tongtong Gao, **Yang Zeng**, Yan Guo,
Hong Yu, Junfeng Li, Zihua Kou, Lanying Du, Wenjie Tan, Shibo Jiang, Shihui Sun*,
Yusen Zhou*

The Middle East Respiratory Syndrome Coronavirus (MERS-CoV) causes severe acute respiratory failure and considerable extrapulmonary organ dysfunction with substantial high mortality. For the limited number of autopsy reports, small animal models are urgently needed to study the mechanisms of MERS-CoV infection and pathogenesis of the disease and to evaluate the efficacy of therapeutics against MERS-CoV infection. In this study, we developed a transgenic mouse model globally expressing codon-optimized human dipeptidyl peptidase 4 (hDPP4), the receptor for MERS-CoV. After intranasal inoculation with MERS-CoV, the mice rapidly developed severe pneumonia and multi-organ damage, with viral replication being detected in the lungs on day 5 and in the lungs, kidneys and brains on day 9 post-infection. In addition, the mice exhibited systemic inflammation with mild to severe pneumonia accompanied by the injury of liver, kidney and spleen with neutrophil and macrophage infiltration. Importantly, the mice exhibited symptoms of paralysis with high viral burden and viral positive neurons on day 9. Taken together, this study characterizes the tropism of MERS-CoV upon infection. Importantly, this hDPP4-expressing transgenic mouse model will be applicable for studying the pathogenesis of MERS-CoV infection and investigating the efficacy of vaccines and antiviral agents designed to combat MERS-CoV infection.

RESEARCH ARTICLE

Multi-Organ Damage in Human Dipeptidyl Peptidase 4 Transgenic Mice Infected with Middle East Respiratory Syndrome-Coronavirus

Guangyu Zhao¹*, Yuting Jiang¹*, Hongjie Qiu¹, Tongtong Gao¹, Yang Zeng¹, Yan Guo¹, Hong Yu¹, Junfeng Li¹, Zhihua Kou¹, Lanying Du², Wenjie Tan⁴, Shibo Jiang^{2,3}, Shihui Sun^{1*}, Yusen Zhou^{1*}

1 State Key Laboratory of Pathogen and Biosecurity, Beijing Institute of Microbiology and Epidemiology, Beijing, 100071, China, **2** Lindsley F. Kimball Research Institute, New York Blood Center, New York, New York, 10065, United States of America, **3** Key Laboratory of Medical Molecular Virology of Ministries of Education and Health, Shanghai Medical College, Fudan University, Shanghai, 200433, China, **4** Key Laboratory of Medical Virology, Ministry of Health, National Institute for Viral Disease Control and Prevention, China CDC, Beijing, 102206, China

* These authors contributed equally to this work.

* yszhou@bmi.ac.cn (Y. Zhou); sunsh01@163.com (SS)



OPEN ACCESS

Citation: Zhao G, Jiang Y, Qiu H, Gao T, Zeng Y, Guo Y, et al. (2015) Multi-Organ Damage in Human Dipeptidyl Peptidase 4 Transgenic Mice Infected with Middle East Respiratory Syndrome-Coronavirus. *PLoS ONE* 10(12): e0145561. doi:10.1371/journal.pone.0145561

Editor: Stefan Pöhlmann, Deutsches Primatenzentrum GmbH - Leibniz-Institut für Primatenforschung, GERMANY

Received: July 31, 2015

Accepted: December 4, 2015

Published: December 23, 2015

Copyright: © 2015 Zhao et al. This is an open access article distributed under the terms of the [Creative Commons Attribution License](https://creativecommons.org/licenses/by/4.0/), which permits unrestricted use, distribution, and reproduction in any medium, provided the original author and source are credited.

Data Availability Statement: All relevant data are within the paper.

Funding: This work was supported by the National Project of Infectious Disease (2014ZX10004001004, 2012ZX10004502), the Basic Research 973 Project (2011CB504706), and the National Natural Science Foundation of China (81371805). The funders had no role in study design, data collection and analysis, decision to publish, or preparation of the manuscript.

Abstract

The Middle East Respiratory Syndrome Coronavirus (MERS-CoV) causes severe acute respiratory failure and considerable extrapulmonary organ dysfunction with substantial high mortality. For the limited number of autopsy reports, small animal models are urgently needed to study the mechanisms of MERS-CoV infection and pathogenesis of the disease and to evaluate the efficacy of therapeutics against MERS-CoV infection. In this study, we developed a transgenic mouse model globally expressing codon-optimized human dipeptidyl peptidase 4 (hDPP4), the receptor for MERS-CoV. After intranasal inoculation with MERS-CoV, the mice rapidly developed severe pneumonia and multi-organ damage, with viral replication being detected in the lungs on day 5 and in the lungs, kidneys and brains on day 9 post-infection. In addition, the mice exhibited systemic inflammation with mild to severe pneumonia accompanied by the injury of liver, kidney and spleen with neutrophil and macrophage infiltration. Importantly, the mice exhibited symptoms of paralysis with high viral burden and viral positive neurons on day 9. Taken together, this study characterizes the tropism of MERS-CoV upon infection. Importantly, this hDPP4-expressing transgenic mouse model will be applicable for studying the pathogenesis of MERS-CoV infection and investigating the efficacy of vaccines and antiviral agents designed to combat MERS-CoV infection.

Competing Interests: The authors have declared that no competing interests exist.

Introduction

The highly pathogenic Middle East respiratory syndrome-coronavirus (MERS-CoV) was first documented in the Middle East in 2012. As of November 13, 2015, a total of 1618 cases had been reported by the World Health Organization, including 579 fatalities (<http://www.who.int/csr/don/13-november-2015-mers-saudi-arabia/en/>). The mortality rate of MERS-CoV is as high as 35%, far higher than that of the SARS coronavirus (8–10%) [1]. Although milder and asymptomatic presentation does occur, a portion of patients develop severe respiratory disease identified as viral pneumonia and acute respiratory distress syndrome (ARDS) accompanied by leucopenia and lymphopenia, similar to patients infected with SARS-CoV. In addition, at least one-third of patients exhibit gastrointestinal symptoms and in some severe cases, renal failure develops concurrently with MERS-CoV infection [2, 3]. More recently, severe neurologic syndrome was also reported in critically cases [4]. Although the limited clinical data available indicate that systemic infection can occur, the pathological mechanism of multi-organ damage caused by MERS-CoV infection is not well understood.

Receptor specificity appears to be a key factor in the tropism of MERS-CoV [5], and dipeptidyl peptidase 4 (DPP4) has been identified as the functional cellular receptor for MERS-CoV [6]. In humans, DPP4 is constitutively expressed in epithelial cells in the liver, intestine, prostate, kidneys and in activated leukocytes [7]. MERS-CoV may infect human tracheobronchial epithelium, primary renal epithelium, alveolar adenocarcinoma, liver cells (Huh-7) and bronchiolar epithelial cells [8]. Because they do not express human DPP4, mice, hamsters and ferrets cannot be infected with MERS-CoV [9–12]. However, rhesus macaques can be infected with MERS-CoV. Following infection, rhesus macaques develop transient clinical symptoms with histopathologically evident multifocal mild-to-moderate interstitial pneumonia on day 3 post-infection [13]. Common marmosets infected with high doses of MERS-CoV develop more severe disease than rhesus macaques, with sometimes fatal pneumonia [14]. In MERS-CoV-infected common marmosets, clinical disease was more severe and viral loads in the lungs were higher than in the rhesus macaque lungs. However, while viral RNA was detected in kidney samples from five out of seven common marmosets, no histological abnormalities were observed. Furthermore, the ethics, higher expense and sophisticated operation limited their application for the studies on the pathogenesis of the disease and efficient evaluation of vaccines or drugs to treat MERS-CoV infection.

Stanley Perlman's research group developed an Ad5-hDPP4-transduced mouse able to maintain MERS-CoV infection [15]. Although this model may be used efficiently for evaluating the efficacy of vaccines and drugs, it is still limited in its ability to recapitulate the pathogenesis of the disease for its transient and self-limited viral infection. To develop a more susceptible, stable and efficient model, Chien-Te K. Tseng's group successfully established a transgenic mice model stably expressing hDPP4 that exhibited progressive pneumonia and lethal outcome after MERS-CoV infection [16]. In the model, although no tissue damage was observed in the brain, viral replication was reported. More recently, another hDPP4 mouse model was developed by replacing 79 kb mouse DPP4 genomic DNA with that encoding 82 kb human genomic DPP4 using the VelociGene technology. Although no mortality or clinical signs of disease was observed up to day 4, robust viral replication and pathology in the lungs were detected. No specific MERS-CoV RNA and information was detected in brain [17]. In this study, we generated a transgenic mouse model also that globally expresses codon-optimized-hDPP4. This MERS-CoV infected optimized-hDPP4 transgenic mice developed severe pneumonia with multi-organ injury including liver, kidney and brain damages.

Methods

Ethics statement

All procedures involving animals were approved by the Laboratory Animal Center, State Key Laboratory of Pathogen and Biosecurity, Beijing Institute of Microbiology and Epidemiology IACUC's (The permit number is BIME 2014-0017). Animal studies were carried out in strict accordance with the recommendations in the Guide for the Care and Use of Laboratory Animals. All experimental operations to mice were performed under sodium pentobarbital anesthesia, and mice were euthanized with overdose inhalational carbon dioxide. All efforts were made to minimize suffering of animals.

Determination of hDPP4 expression in cell lines

Considering the species differences, the hDPP4-coding sequence was codon-optimized and synthesized (GenScript, Nanjing, China) according to the mRNA sequence (Accession number NM_001935.3) and cloned into the multiple cloning site (MCS) of a pCAGGS plasmid, leading to strong expression of the gene. The recombinant plasmid pCAGGS-hDPP4 contained the hCMV IE Enhancer (hCMVIEE), the CAG promoter (chicken β -actin promoter/intron), a codon-optimized open reading frame (ORF) of hDPP4 and rabbit β -globin polyA (Fig 1A). Expression of the codon-optimized hDPP4 was achieved by transfection of the pCAGGS-hDPP4 plasmid into Cos-7 cells, followed by confirmation of expression using anti-human CD26 monoclonal antibody (R&D Systems, Minneapolis, MN, USA). To confirm the binding of hDPP4 to the MERS-CoV receptor-binding domain (RBD), transfected Cos-7 cells were incubated with a recombinant protein expressing the RBD of MERS-CoV fused to human IgG Fc (RBD-Fc) [18], followed by addition of DyLight 549-conjugated goat anti-human IgG to detect binding.

Determination of hDPP4 copy number and transcription levels in transgenic mice

The purified 5861bp fragment generated from ApaI digestion of pCAGGS-hDPP4 was used as the transgene for injection into the pronuclei of fertilized F1 (C57BL/6 \times C57BL/6) mouse eggs to generate transgenic embryos. The mice used in this study were backcrossed two to three times onto a C57BL/6 background. All animal studies were performed in strict accordance with the recommendations outlined in the Guide for the Care and Use of Laboratory Animals.

Genomic DNA from each transgenic founder line and from wild-type C57BL/6 mice was isolated from the liver tissue using DNAzol reagent (Qiagen, Valencia, CA, USA) according to the manufacturer's instructions. The hDPP4 DNA copy numbers were determined by quantitative PCR using Power SYBR[®] Green PCR Master Mix (Life Technologies, Carlsbad, CA, USA). Total hDPP4 DNA was normalized using a single-copy reference gene (PKD1) as an endogenous control. The primers specific for hDPP4 were forward 5' CTACAGCTCCTGGG CAACGTGCTG 3' and reverse 5' AGATGTCGTAAGTGGCGGTGTAAG 3'. The primers specific for mPKD1 were forward 5' GGCTGCTGAGCGTCTGGTA 3' and reverse 5' CCAGGTCTGCGTGTCTGA 3'.

To detect the expression of optimized hDPP4 in the tissues of our transgenic mice model, samples were harvested and stored immediately in RNeasy lysis reagent (Qiagen, Valencia, CA, USA) until total RNA was extracted and purified using an RNeasy Extraction kit (Qiagen, Valencia, CA, USA). For each sample, 2 μ g of total RNA was used as template for first-strand cDNA synthesis. The resulting cDNA was subjected to quantitative PCR using Power SYBR[®] Green PCR Master Mix (Life Technologies, Carlsbad, CA, USA) to determine

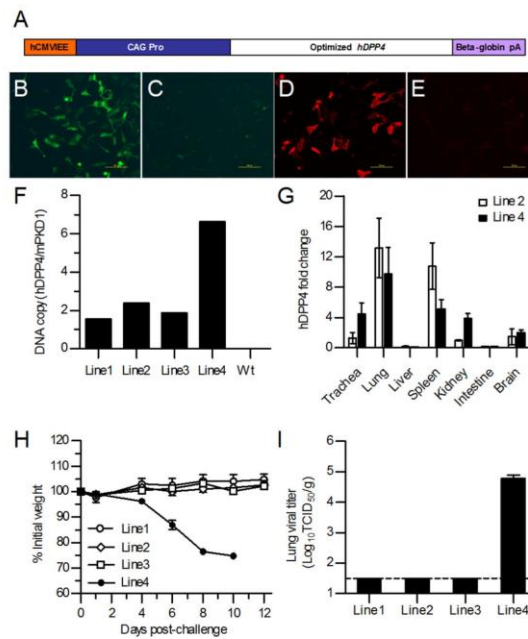


Fig 1. Generation and characterization of hDPP4 transgenic mice. (A) Schematic diagram of the optimized hDPP4 expression vector cassette. The optimized hDPP4 was cloned into a pCAGGS plasmid in which hDPP4 expression was driven by the CAG promoter. hDPP4 expression was confirmed *in vitro* by transfection of Cos-7 cells with the pCAGGS-hDPP4 (B) or pCAGGS (C) plasmids and detected by direct immunofluorescence assay with FITC-labeled anti-human CD26-Fluorescein antibody. Confirmation of the binding between DPP4 and MERS-CoV RBD was achieved by transfecting Cos-7 cells with pCAGGS-hDPP4 (D) or pCAGGS (E) plasmid followed by indirect immunofluorescence assay with MERS-RBD-Fc protein and DyLight 549-conjugated goat anti-human IgG antibody. (F) Determination of the copy numbers of hDPP4 cDNA in four transgenic founder lines by qPCR. (G) Expression of hDPP4 mRNA in the indicated tissues of transgenic mice in two founder lines as determined by qRT-PCR. Results are mean±SEM ($n = 3$). (H) Four lines of hDPP4 transgenic mice were infected with MERS-CoV and monitored for body weight changes. Results are mean±SEM ($n = 6$). (I) Lung viral titer at day 5 postinfection was determined for four lines of hDPP4 transgenic mice. The data are expressed as mean±SEM ($n = 3$). The dotted line indicates the limit of detection.

doi:10.1371/journal.pone.0145561.g001

the relative abundances of hDPP4 in the tissues. The forward and reverse primers for hDPP4 amplicons were as the same as those noted above. The relative amount of hDPP4 in different tissues was obtained by normalizing mRNA expression to that of the endogenous control gene GAPDH [19].

Infection of hDPP4 transgenic mice with MERS-CoV and sample collection

MERS-CoV (HCoV-EMC/2012 strain) was propagated and titered on Vero cells in an approved biosafety level 3 laboratory. Following intraperitoneal anesthetization with sodium pentobarbital (5 mg/kg of body weight), mice under virus infection were intranasally inoculated with MERS-CoV ($10^{4.3}$ TCID₅₀) in 20 μ l Dulbecco's modified Eagle's medium (DMEM),

and mice in sham group were treated with the same volume of DMEM. Mice were monitored for weight loss and survival for 12 days. We have taken special precautions and followed standard guidelines outlined in the Guide for the Care and Use of Laboratory Animals to ensure that ample food and water as well as sanitary cage conditions with enrichment devices were present in order to maximize the animal's comfort. Humane endpoints were used during the survival experiments. After virus infection, mice were closely monitored by daily observation and weighing of trained animal caretaker, and the monitoring will raise to twice per day once mice lost more than 10% of their initial body weight, or exhibited lethargy, ruffled hair coat, or hunched posture. Animals were deemed gravely ill and were euthanized by overdose inhalation of carbon dioxide if they lost more than 25% of their weight, or lost ability to ambulate and access food or water. Sera were collected on day 5 and inactivated at 56°C for 30 min before the levels of cytokines and chemokines were measured. To assess viral replication and histopathologic damage following MERS-CoV infection, mice were euthanized with overdose inhalational carbon dioxide, and tissues included lungs, kidneys, livers, spleens, intestines and brains were harvested on indicated time points.

Detection of MERS-CoV RNA in hDPP4 transgenic mouse tissues

The viral RNA copies in tissues were determined by qRT-PCR according to the protocol described elsewhere [20]. Briefly, total RNA was extracted from 20mg of collected tissues using RNeasy Extraction Kits (Qiagen, Valencia, CA, USA) following the manufacturer's instructions. MERS-CoV RNA was quantified in a 25 μ l mixture containing 5 μ l RNA using the Invitrogen SuperScript[™] III One-Step RT-PCR system with Platinum[®] Taq (Life Technologies, Carlsbad, CA, USA). The primers and probes specific for the upE envelope gene of the MERS-CoV virus were as follows: forward 5' GCAACGCGCGATTTCAGTT 3' ; reverse 5' GCCTCTACACGGGACCCATA 3' ; fluorescence probe /56-FAM/ CTCTTCACATAATCGCCCCGAGCTCGCG/36-TAMSp/ [21]. Mouse GAPDH was used as a housekeeping gene control. A standard curve was generated for PCR reaction using 10-10⁷ copies of quantified RNA transcripts to calculate copy numbers for each reaction. The results were considered positive at C_T values below 35 for primer and probe set, and were calculated as viral RNA copies per gram of tissues.

Viral titer in tissue

The tissues of infected mice were harvested aseptically at indicated time points and homogenized in minimal essential medium (MEM) plus antibiotics to produce 10% (w/v) suspensions. Tissue homogenates were centrifuged and titered on the monolayer of Vero cells. The cytopathic effects (CPE) were daily observed under phase-contrast microscopy for 3 days. The viral titer was determined as TCID₅₀ by CPE-based assay, and calculated using the Reed and Muench method. The viral titer in tissue was expressed as Log₁₀ TCID₅₀/g of tissue.

Histopathology and immunohistochemistry

Collected tissue samples were immediately fixed in 10% neutral buffered formalin, sectioned at 4 μ m thickness, and stained with hematoxylin and eosin (H&E) to examine histopathology as described previously [22]. The expression of virus antigens and infiltration of neutrophils and macrophages in organs after MERS-CoV infection was detected by immunohistochemistry. Briefly, formalin-fixed, paraffin-embedded lung sections were deparaffinized and hydrated using graded alcohols. Expression of virus antigen and inflammatory cell infiltration was assessed using rabbit polyclonal antibody to MERS-CoV nucleoprotein (NP) (Sino Biological Inc., Beijing, China), neutrophil marker NIMP-14, (Santa Cruz Biotechnology, Paso Robles, CA, USA) and CD68 (Abcam, Cambridge, MA, USA). The reaction was detected using a

standard streptavidin-biotin detection system (Beijing Zhongshan Biotechnology Co., Ltd., Beijing, China) and visualized using DAB with hematoxylin counterstaining.

Detection of inflammatory cytokines and chemokines

Cytokines and chemokines in mouse sera were quantified using a commercial Milliplex Mouse Cytokine/Chemokine Magnetic Panel kit (Merck Millipore, USA.). A panel of inflammatory cytokines and chemokines (IFN- γ , IP-10, IL-1 β , IL-17, IL-6, TNF- α , GM-CSF, KC, MCP-1, MIP-1 α , MIP-1 β and RANTES) was measured according to the manufacturer's protocols.

Statistics

Statistical analyses were performed using GraphPad Prism version 5.01. To compare the groups in terms of hDPP4 copies, inflammatory cytokine/chemokine levels, and tissue viral RNA copies, Student's *t* test with Welch's correction was used. The significance between survival curves was analyzed by Kaplan-Meier survival analysis with log-rank test. *p* values lower than 0.05 were considered statistically significant.

Results

Generation and characterization of transgenic mice expressing hDPP4

DPP4 is constitutively expressed in human parenchyma cells in tissues including the liver, intestines and kidneys as well as in T and B cells [7]. We developed transgenic mice in which hDPP4 expression was driven by the chicken β -actin promoter in the pCAGGS plasmid (Fig 1A). Expression of hDPP4 *in vitro* was achieved by transfection of the pCAGGS-hDPP4 plasmid into Cos-7 cells and detected by immunofluorescence analysis. The results showed that hDPP4 was expressed in Cos-7 cells and that it effectively bound MERS-CoV (Fig 1B–1E). After microinjection of linearized DNA, founder lines that transferred the hDPP4 gene to their progeny were established. The levels of transgenic DNA in the founder lines ranged from 2 to 6 copies per genome, as determined by qPCR (Fig 1F). In addition, the mRNA levels of hDPP4 in the trachea, lung, liver, spleen, kidney, intestine and brain in two of the founder lines were measured by qRT-PCR. The data showed that hDPP4 expression was higher in the trachea, lung, spleen, kidney and brain in both lines, and the expressions were relative higher in trachea and kidney in line 4 compared with that in line 2 (Fig 1G). In order to determine the effective infection of MERS-CoV in different lines of transgenic mice, 6 mice in each line were infected with MERS-CoV and the changes of body weight were monitored. The results showed that all mice in line 1, 2 and 3 survived with no significant changes in body weight but all mice in line 4 died by day 10 following MERS-CoV inoculation (Fig 1H). In order to confirm the virus replications in transgenic mice, three mice of each line were sacrificed on day 5 after MERS-CoV infection for the detection of viral titer and viral antigen expression in lungs. As expected, compared with high level of lung viral titers in line 4 mice, no viral titer were detected (Fig 1I) in lungs of line 1, 2 and 3 mice, which also confirmed by the negative results of viral antigen expression detected by immunohistochemistry in lung (data not shown).

Multi-organ tissue damage in hDPP4 transgenic mice infected with MERS-CoV

Wild-type mice, such as BALB/c, 129/SvEv and STAT1 mice, are not permissive to MERS-CoV infection, and Syrian hamsters do not support replication of MERS-CoV [9–12]. Macaques have been confirmed to develop mild to marked interstitial pneumonia upon MERS-CoV infection [23], but fail to progress to the extent observed in human subjects. Marmoset model,

which has the same interaction characteristic between its DPP4 and MERS-CoV spike protein, was partially lethal and developed a progressive severe pneumonia after MERS-CoV infection [14]. In this study, we found that hDPP4 transgenic mice infected with MERS-CoV exhibited decreased activity and significant weight loss from day 6 after infection, and all of the infected mice died by day 10 (Fig 2A and 2B). Importantly, symptoms of neural defects with paralysis were observed on day 9 in the infected transgenic mice.

Compared to the sham-infected group (Fig 3A, 3D, 3G and 3J), the histopathological analysis of the tissues in transgenic mice on days 5 and 9 after MERS-CoV infection showed the presence of inflammatory tissue damage in the kidney, liver and spleen, with mild inflammatory responses in the lungs but no significant changes in the intestines. On day 5 after inoculation, the hDPP4 transgenic mice exhibited mild inflammation in the lungs with focal exudation and hemorrhage (Fig 3B), and by day 9, the damage was more severe, with evidence of diffused alveolar damage, alveolar septal thickening, hemorrhage and activated macrophage infiltration (Fig 3C). In the kidneys, mild interstitial inflammation with inflammatory cell infiltration was observed in the interstitium and exudates of renal tubules on day 5 (Fig 3E). By day 9, more renal tubular epithelial cells were injured, with evidence of focal hemorrhage in the renal interstitium (Fig 3F). In the liver, mild to moderate liver damage was seen in the transgenic mice infected with MERS-CoV on day 5, including scattered hepatocyte necrosis and numerous activated kupffer cells and macrophage infiltrates in hepatic sinusoid (Fig 3H), and on day 9, fatty change in hepatocytes with less hepatocyte necrosis was observed (Fig 3I). In spleens, necrosis of splenic cells and increased reticulum cells in red pulp with significant hemosiderin deposition was observed on both day 5 and day 9 (Fig 3K and 3L). Typical characteristics of viral encephalitis were observed in the brain at day 9, with perivascular cuffs (Fig 3M) and neuronal cell necrosis in the cerebral cortex (Fig 3N), including hippocampal neurons (Fig 3O). There was no apparent damage in the intestines after MERS-CoV infection on day 5 or day 9 (data not shown).

Determination of virus antigen expression and viral replication in hDPP4 transgenic mice infected with MERS-CoV

To evaluate MERS-CoV infection in the hDPP4 transgenic mice, distribution of the viral antigen NP protein was assessed in mouse tissues by immunohistochemical staining. The results showed that type I and type II pneumocytes in the lungs and renal tubular epithelial cells in the kidneys expressed viral antigen on day 5 after MERS-CoV infection and that the expression was more abundant on day 9, and no viral antigen was detected in sham-infected group (Fig 4A–4F). Strong viral antigen expression was evident not only in neuronal cell bodies, but also in dendrites, axons and some microglia in the cerebral cortex (Fig 4H) including the hippocampus (Fig 4I). No viral antigen expression was observed in the brains of mice in the sham-infected group (Fig 4G). Viral RNA copies in lung and brain were detectable on day 5 postinfection and increased to a higher level on day 9 (Fig 4J). Lower level of viral RNA copies can be also detected in kidney collected on day 9. In order to further confirm the effective replication of MERS-CoV, the dynamic changes of viral titer in organs were detected. The results showed that on day 3 after infection, only lower viral titer was detected in lung and not detectable in other organs. However, on day 5, viral titer was also detected in brain. On day 7 and day 9, increased viral titers were detected in both lung and brain, and lower level viral titer in kidney was detectable (Fig 4K). These results indicate that the transgenic mice had been successfully infected and that MERS-CoV exhibited cell and tissue tropism especially for pneumocytes and neurons. Furthermore, synapses may be one of the structures by which viruses diffuse through the brain after MERS-CoV infection.

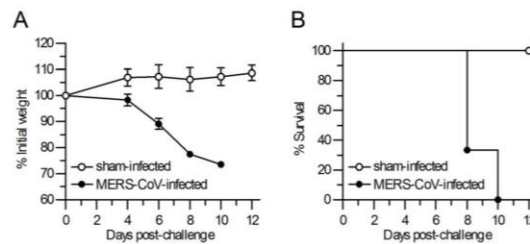


Fig 2. MERS-CoV infection resulted in lethal disease in hDPP4 transgenic mice. Transgenic mice were infected intranasally with MERS-CoV and monitored for 12 days. (A) Body weight changes of MERS-CoV- and sham-infected mice. Results are mean \pm SEM ($n = 3$) on indicated time post-infection. (B) Survival curves of mice in MERS-CoV- and sham-infected mice ($n = 3$). * $p < 0.05$.

doi:10.1371/journal.pone.0145561.g002

Increased inflammatory response in MERS-CoV-infected hDPP4 transgenic mice

To date, only limited data on the immune response of MERS patients are available [24]. Because of the clinical similarity between the symptoms of MERS-CoV and those of patients infected with SARS-CoV [1], the aberrant immune response may be related to the pathogenesis of MERS-CoV infection. In our mouse model, an aberrant inflammatory response was confirmed by infiltration of neutrophils in the lung, liver and spleen (Fig 5A–5F) and macrophages in the lung, liver and kidney (Fig 5G–5L). In addition, deposition of hemosiderin in the spleen (Fig 3K and 3L) indicated an increase in activated macrophages, and a systemic inflammatory response after virus infection was demonstrated by a significant increase in cytokines such as IFN- γ , IP-10, and IL-17 in the serum on day 5 after MERS-CoV infection (Fig 5M).

Discussion

Although several species, such as rhesus macaques and common marmosets are reported to be sensitive to MERS-CoV infection and to develop mild to marked broncho-interstitial pneumonia, small animal models are urgently needed to study the pathogenesis of this disease and evaluate the effects of vaccines and antiviral agents. A MERS-CoV-infection mouse model was generated by transducing mice with a recombinant non-replicating adenovirus expressing hDPP4; however, while the mice exhibit viral antigen expression and progress to interstitial pneumonia, there is no mortality after virus infection [15]. Although a transgenic mouse model expressing human DPP4 was also established, and its immune response was studied after infection with MERS-CoV [16], the transgenic mice in the study died on day 6 with only progressive pneumonia and mild perivascular cuffing in brain, and no neurological disorder or other multi-organ damage was observed. Different from the aforementioned transgenic mice, our hDPP4 transgenic mice experienced a longer incubation period post-infection and developed progressive pneumonia and neurological disorders accompanied by histological damage to the lungs, brain, spleen and liver, which more closely resembles the clinical cases.

The results from this study indicate that MERS-CoV infection was lethal in hDPP4 transgenic mice with higher transgene copy number, while lines with lower levels of hDPP4 expressed especially in trachea had no significant clinical symptoms (data not shown), suggesting that the copy number of the transgene was closely related to the efficiency of MERS-CoV infection. Although the expression level of optimized hDPP4 was not highest in the brains, the tissues had higher viral titers following MERS-CoV infection, revealing the tropism of

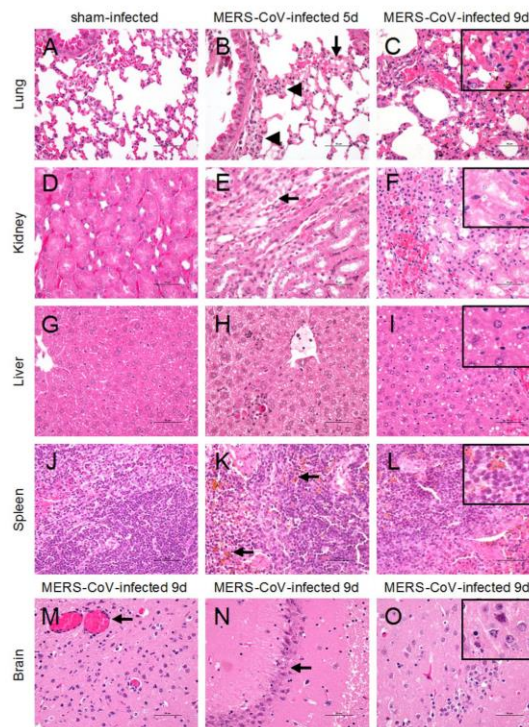


Fig 3. Histopathological analysis of hDPP4 transgenic mice after MERS-CoV infection. The hDPP4 transgenic mice were infected intranasally with MERS-CoV. Lungs, kidneys, liver, spleen and brain were collected on day 5 or day 9 after MERS-CoV infection, fixed in neutral formaldehyde solution and stained with hematoxylin and eosin. Histopathological analysis of hDPP4 transgenic mice was performed using sham-infected mice as controls (A, D, G, J). (B-C) In the lungs, mild inflammation was observed, with inflammatory cell infiltration (arrowheads) and focal hemorrhage and exudation (arrow) on day 5. Damage was more severe on day 9, with increased inflammatory cell infiltration, focal hemorrhage (inset) and exudation. (E-F) In the kidney, MERS-CoV-infected hDPP4 transgenic mice showed focal interstitial inflammation with inflammatory cell infiltration in the interstitium and exudates in renal tubules (arrow) on day 5. On day 9, degeneration and necrosis in the renal tubular epithelial cells (inset) and focal hemorrhage were observed. (H-I) In the liver, MERS-CoV-infected hDPP4 transgenic mice showed scattered hepatocyte necrosis and numerous activated kupffer cells and infiltrated macrophages in the hepatic sinusoid on day 5. Fatty change of hepatocytes (inset) was observed in the liver on day 9. (K-L) In the spleen, necrotic splenic cells and increased reticulum cells in the red pulp with significant amounts of hememosiderin deposition were observed in hDPP4 transgenic mice on days 5 and 9 (arrow and inset). (M-O) Neurological damage with perivascular cuffs (M) and neuronal cell necrosis in the cerebral cortex (N) including damaged neurons (inset) in the hippocampus (O) was observed in the brains of hDPP4 transgenic mice infected with MERS-CoV. ($n = 2$, scale bars = 50 μm).

doi:10.1371/journal.pone.0145561.g003

MERS-CoV for both lungs and brains, tissues in which pneumocytes and neurons may be the main target cells (Fig 4). However, MERS-CoV infection in brain via blood or olfactory nerves needs to be further studied due to the strong expression of viral antigens in dendrites and axons.

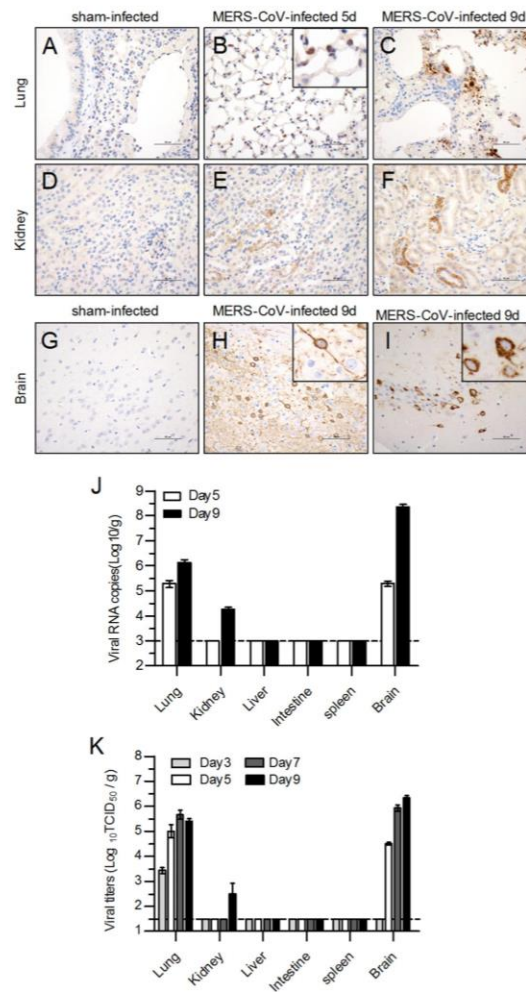


Fig 4. Detection of virus antigen expression and viral replications in the tissues of hDPP4 transgenic mice infected with MERS-CoV. Transgenic mice were infected intranasally with MERS-CoV and sacrificed to access the expression of viral antigens by immunohistochemical staining ($n = 2$). No viral antigens were detected in the sham-infected mice (A, D, G), but viral antigens were detected in type I and type II pneumocytes and infiltrated macrophages in the lungs (B-C), renal tubular epithelial cells in the kidneys (E-F), and neuron cell bodies as well as in dendrites and axons in the brain (H-I), including the hippocampus (I). (J) Viral load was detected by qRT-PCR and expressed as viral RNA copies/g of tissues. The detection limit shown as dotted line is 1×10^3 copies/g. Results are mean \pm SEM ($n = 2$). (K) Viral titers in tissues of infected hDPP4 transgenic mice were determined by CPE-based assay and expressed as $\text{Log}_{10}\text{TCID}_{50}/\text{g}$ of tissues. Results are mean \pm SEM ($n = 5$). The dotted line indicates the detection limit.

doi:10.1371/journal.pone.0145561.g004

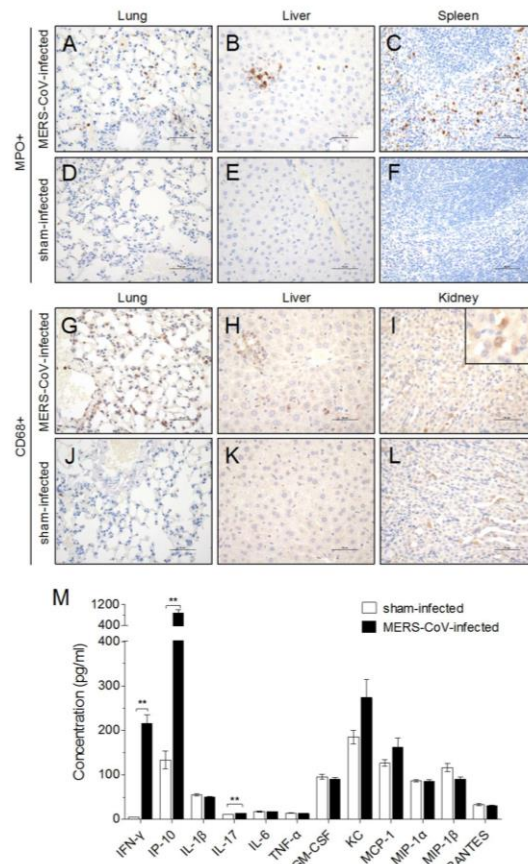


Fig 5. Detection of inflammatory cell infiltration and proinflammatory cytokines in the serum of hDPP4 transgenic mice infected with MERS-CoV. Neutrophil infiltration in the lungs, liver and spleen was evaluated 5 days after MERS-CoV infection (A-C) or sham infection (D-F). Macrophage infiltration in the lung, liver and kidney was detected 5 days after MERS-CoV (G-I) or sham infection (J-L) ($n = 2$). (M) Sera from the two groups of mice were collected on day 5 and assayed for levels of IFN- γ , IP-10, IL-1 β , IL-17, IL-6, TNF- α , GM-CSF, KC, MCP-1, MIP-1 α , MIP-1 β and RANTES. Results are mean \pm SEM ($n = 4$). * $p < 0.05$.

doi:10.1371/journal.pone.0145561.g005

Although few autopsy reports exist on fatal MERS-CoV cases and atypical pneumonia and respiratory failure are suspected the causes of death [24], other types of extrapulmonary organ dysfunction have also been documented in MERS critically ill patients with abnormal clinical manifestations [25–27]. For example, acute renal failure was described in a number of MERS cases [28–32]. In addition, renal epithelial cells may produce almost 1000-fold more infectious MERS-CoV progeny than bronchial epithelial cells [33]. More recently, severe neurologic syndrome including altered level of consciousness from confusion to coma, ataxia and focal motor deficit was also reported in three critically cases by Balkhy H et al [4]. According to the

neurologic manifestations and distinct imaging patterns, an important question was raised on the pathogenic mechanisms that underlie the occurrence of neurologic injury in patients. It has been studied that corona virus such as SARS-CoV are generally known for causing respiratory illness, and the strong tropism of SARS-CoV to CNS and causing neuronal injury had also been demonstrated both in clinical and experimental studies [34–38], which suggested the possible relations of MERS-CoV infection with brain injury. As to the extensive expression of hDPP4 in the lung, kidney, placenta, liver, skeletal muscle, brain, endothelium, pancreasour and T cell in human, our globally expressed hDPP4 transgenic mouse manifested with multi-organ damage infected with MERS-CoV could be a suitable model for the pathogenic mechanisms study.

Systemic inflammation is believed to be a primary reason for the severe outcome in MERS-CoV infections [14, 24]. Although the transgenic mice model died after MERS-CoV infection with multi-organ damages, it is still uncertain whether these mice are mainly dying from lung damage. In our transgenic mice, aberrant immune response such as elevated IP-10, IFN- γ and IL-17, which are closely related to acute virally-mediated lung injury [39–42], was also a specific manifestation after MERS-CoV infection. So, as to the mechanism of lethal which was due to the virus replication directly or induced by the aberrant inflammatory response need to be further studied. The mechanism of MERS-CoV infection caused death is complex and complicated. Aberrant immune response after MERS-CoV infection may be one of main reasons which need to be further studied. We have added more discussions on this issue in the revised manuscript.

In summary, the transgenic mouse model developed in this study was efficiently infected by MERS-CoV and exhibited severe acute respiratory injury and considerable extrapulmonary organ damage. This model will be useful for studying the pathogenesis of MERS-CoV infection and evaluating the efficacy of MERS vaccines and therapeutic agents.

Author Contributions

Conceived and designed the experiments: GZ SS Y. Zhou. Performed the experiments: GZ YJ HQ TG Y. Zeng YG HY SS. Analyzed the data: GZ SS JL ZK LD WT. Wrote the paper: GZ SS LD SJ Y. Zhou.

References

1. Gralinski LE, Baric RS. Molecular pathology of emerging coronavirus infections. *J Pathol.* 2015; 235(2):185–95. doi: [10.1002/path.4454](https://doi.org/10.1002/path.4454) PMID: [25270030](https://pubmed.ncbi.nlm.nih.gov/25270030/)
2. Group TWM-CR. State of Knowledge and Data Gaps of Middle East Respiratory Syndrome Coronavirus (MERS-CoV) in Humans. *PLoS Curr.* 2013; 5. doi: [10.1371/currents.outbreaks.0bf719e352e7478f8ad85fa30127ddb8](https://doi.org/10.1371/currents.outbreaks.0bf719e352e7478f8ad85fa30127ddb8)
3. Assiri A, McGeer A, Perl TM, Price CS, Al Rabeeah AA, Cummings DA, et al. Hospital outbreak of Middle East respiratory syndrome coronavirus. *N Engl J Med.* 2013; 369(5):407–16. doi: [10.1056/NEJMoa1306742](https://doi.org/10.1056/NEJMoa1306742) PMID: [23782161](https://pubmed.ncbi.nlm.nih.gov/23782161/)
4. Arabi YM, Harthi A, Hussein J, Bouchama A, Johani S, Hajeer AH, et al. Severe neurologic syndrome associated with Middle East respiratory syndrome corona virus (MERS-CoV). *Infection.* 2015; 43(4):495–501. doi: [10.1007/s15010-015-0720-y](https://doi.org/10.1007/s15010-015-0720-y) PMID: [25600929](https://pubmed.ncbi.nlm.nih.gov/25600929/)
5. van Doremalen N, Miazgowiec KL, Milne-Price S, Bushmaker T, Robertson S, Scott D, et al. Host species restriction of Middle East respiratory syndrome coronavirus through its receptor, dipeptidyl peptidase 4. *J Virol.* 2014; 88(16):9220–32. doi: [10.1128/JVI.00676-14](https://doi.org/10.1128/JVI.00676-14) PMID: [24899185](https://pubmed.ncbi.nlm.nih.gov/24899185/)
6. Raj VS, Mou H, Smits SL, Dekkers DH, Muller MA, Dijkman R, et al. Dipeptidyl peptidase 4 is a functional receptor for the emerging human coronavirus-EMC. *Nature.* 2013; 495(7440):251–4. doi: [10.1038/nature12005](https://doi.org/10.1038/nature12005) PMID: [23486063](https://pubmed.ncbi.nlm.nih.gov/23486063/)
7. Boonacker E, Van Noorden CJ. The multifunctional or moonlighting protein CD26/DPPIV. *Eur J Cell Biol.* 2003; 82(2):53–73. PMID: [12647932](https://pubmed.ncbi.nlm.nih.gov/12647932/)

8. Mackay IM, Arden KE. Middle East respiratory syndrome: An emerging coronavirus infection tracked by the crowd. *Virus Res.* 2015.
9. Coleman CM, Matthews KL, Goicochea L, Frieman MB. Wild-type and innate immune-deficient mice are not susceptible to the Middle East respiratory syndrome coronavirus. *J Gen Virol.* 2014; 95(Pt 2):408–12. doi: [10.1099/vir.0.060640-0](https://doi.org/10.1099/vir.0.060640-0) PMID: [24197535](https://pubmed.ncbi.nlm.nih.gov/24197535/)
10. Scobey T, Yount BL, Sims AC, Donaldson EF, Agnihothram SS, Menachery VD, et al. Reverse genetics with a full-length infectious cDNA of the Middle East respiratory syndrome coronavirus. *Proc Natl Acad Sci U S A.* 2013; 110(40):16157–62. doi: [10.1073/pnas.1311542110](https://doi.org/10.1073/pnas.1311542110) PMID: [24043791](https://pubmed.ncbi.nlm.nih.gov/24043791/)
11. de Wit E, Prescott J, Baseler L, Bushmaker T, Thomas T, Lackemeyer MG, et al. The Middle East respiratory syndrome coronavirus (MERS-CoV) does not replicate in Syrian hamsters. *PLoS One.* 2013; 8(7):e69127. doi: [10.1371/journal.pone.0069127](https://doi.org/10.1371/journal.pone.0069127) PMID: [23844250](https://pubmed.ncbi.nlm.nih.gov/23844250/)
12. Raj VS, Smits SL, Procvacia LB, van den Brand JM, Wiersma L, Ouwendijk WJ, et al. Adenosine deaminase acts as a natural antagonist for dipeptidyl peptidase 4-mediated entry of the Middle East respiratory syndrome coronavirus. *J Virol.* 2013; 88(3):1834–8. doi: [10.1128/JVI.02935-13](https://doi.org/10.1128/JVI.02935-13) PMID: [24257613](https://pubmed.ncbi.nlm.nih.gov/24257613/)
13. de Wit E, Rasmussen AL, Falzarano D, Bushmaker T, Feldmann F, Brining DL, et al. Middle East respiratory syndrome coronavirus (MERS-CoV) causes transient lower respiratory tract infection in rhesus macaques. *Proc Natl Acad Sci U S A.* 2013; 110(41):16598–603. doi: [10.1073/pnas.1310744110](https://doi.org/10.1073/pnas.1310744110) PMID: [24062443](https://pubmed.ncbi.nlm.nih.gov/24062443/)
14. Falzarano D, de Wit E, Feldmann F, Rasmussen AL, Okumura A, Peng X, et al. Infection with MERS-CoV causes lethal pneumonia in the common marmoset. *PLoS Pathog.* 2014; 10(8):e1004250. doi: [10.1371/journal.ppat.1004250](https://doi.org/10.1371/journal.ppat.1004250) PMID: [25144235](https://pubmed.ncbi.nlm.nih.gov/25144235/)
15. Zhao J, Li K, Wohlford-Lenane C, Agnihothram SS, Fett C, Zhao J, et al. Rapid generation of a mouse model for Middle East respiratory syndrome. *Proc Natl Acad Sci U S A.* 2014; 111(13):4970–5. doi: [10.1073/pnas.1323279111](https://doi.org/10.1073/pnas.1323279111) PMID: [24599590](https://pubmed.ncbi.nlm.nih.gov/24599590/)
16. Agrawal AS, Garron T, Tao X, Peng BH, Wakamiya M, Chan TS, et al. Generation of a transgenic mouse model of middle East respiratory syndrome coronavirus infection and disease. *J Virol.* 2015; 89(7):3659–70. doi: [10.1128/JVI.03427-14](https://doi.org/10.1128/JVI.03427-14) PMID: [25589660](https://pubmed.ncbi.nlm.nih.gov/25589660/)
17. Pascal KE, Coleman CM, Mujica AO, Kamat V, Badithe A, Fairhurst J, et al. Pre- and postexposure efficacy of fully human antibodies against Spike protein in a novel humanized mouse model of MERS-CoV infection. *Proc Natl Acad Sci U S A.* 2015; 112(28):8738–43. doi: [10.1073/pnas.1510830112](https://doi.org/10.1073/pnas.1510830112) PMID: [26124093](https://pubmed.ncbi.nlm.nih.gov/26124093/)
18. Du L, Zhao G, Yang Y, Qiu H, Wang L, Kou Z, et al. A conformation-dependent neutralizing monoclonal antibody specifically targeting receptor-binding domain in Middle East respiratory syndrome coronavirus spike protein. *J Virol.* 2014; 88(12):7045–53. doi: [10.1128/JVI.00433-14](https://doi.org/10.1128/JVI.00433-14) PMID: [24719424](https://pubmed.ncbi.nlm.nih.gov/24719424/)
19. Livak KJ, Schmittgen TD. Analysis of relative gene expression data using real-time quantitative PCR and the 2(-Delta Delta C(T)) Method. *Methods.* 2001; 25(4):402–8. PMID: [11846609](https://pubmed.ncbi.nlm.nih.gov/11846609/)
20. Lu X, Whitaker B, Sakthivel SK, Kamili S, Rose LE, Lowe L, et al. Real-time reverse transcription-PCR assay panel for Middle East respiratory syndrome coronavirus. *J Clin Microbiol.* 2014; 52(1):67–75. doi: [10.1128/JCM.02533-13](https://doi.org/10.1128/JCM.02533-13) PMID: [24153118](https://pubmed.ncbi.nlm.nih.gov/24153118/)
21. Corman VM, Eckerle I, Bleicker T, Zaki A, Landt O, Eschbach-Bludau M, et al. Detection of a novel human coronavirus by real-time reverse-transcription polymerase chain reaction. *Euro Surveill.* 2012; 17(39).
22. Sun S, Zhao G, Liu C, Wu X, Guo Y, Yu H, et al. Inhibition of complement activation alleviates acute lung injury induced by highly pathogenic avian influenza H5N1 virus infection. *Am J Respir Cell Mol Biol.* 2013; 49(2):221–30. doi: [10.1165/rcmb.2012-0428OC](https://doi.org/10.1165/rcmb.2012-0428OC) PMID: [23526211](https://pubmed.ncbi.nlm.nih.gov/23526211/)
23. Falzarano D, de Wit E, Rasmussen AL, Feldmann F, Okumura A, Scott DP, et al. Treatment with interferon-alpha2b and ribavirin improves outcome in MERS-CoV-infected rhesus macaques. *Nat Med.* 2013; 19(10):1313–7. doi: [10.1038/nm.3362](https://doi.org/10.1038/nm.3362) PMID: [24013700](https://pubmed.ncbi.nlm.nih.gov/24013700/)
24. van den Brand JM, Smits SL, Haagmans BL. Pathogenesis of Middle East respiratory syndrome coronavirus. *J Pathol.* 2015; 235(2):175–84. doi: [10.1002/path.4458](https://doi.org/10.1002/path.4458) PMID: [25294366](https://pubmed.ncbi.nlm.nih.gov/25294366/)
25. Assiri A, Al-Tawfiq JA, Al-Rabeeah AA, Al-Rabiah FA, Al-Hajjar S, Al-Barrak A, et al. Epidemiological, demographic, and clinical characteristics of 47 cases of Middle East respiratory syndrome coronavirus disease from Saudi Arabia: a descriptive study. *Lancet Infect Dis.* 2013; 13(9):752–61. doi: [10.1016/S1473-3099\(13\)70204-4](https://doi.org/10.1016/S1473-3099(13)70204-4) PMID: [23891402](https://pubmed.ncbi.nlm.nih.gov/23891402/)
26. Al-Abdallat MM, Payne DC, Alqasrawi S, Rha B, Tohme RA, Abedi GR, et al. Hospital-associated outbreak of Middle East respiratory syndrome coronavirus: a serologic, epidemiologic, and clinical description. *Clin Infect Dis.* 2014; 59(9):1225–33. doi: [10.1093/cid/ciu359](https://doi.org/10.1093/cid/ciu359) PMID: [24829216](https://pubmed.ncbi.nlm.nih.gov/24829216/)

27. Arabi YM, Arifi AA, Balkhy HH, Najm H, Aldawood AS, Ghabashi A, et al. Clinical course and outcomes of critically ill patients with Middle East respiratory syndrome coronavirus infection. *Ann Intern Med*. 2014; 160(6):389–97. doi: [10.7326/M13-2486](https://doi.org/10.7326/M13-2486) PMID: [24474051](https://pubmed.ncbi.nlm.nih.gov/24474051/)
28. Zaki AM, van Boheemen S, Bestebroer TM, Osterhaus AD, Fouchier RA. Isolation of a novel coronavirus from a man with pneumonia in Saudi Arabia. *N Engl J Med*. 2012; 367(19):1814–20. doi: [10.1056/NEJMoa1211721](https://doi.org/10.1056/NEJMoa1211721) PMID: [23075143](https://pubmed.ncbi.nlm.nih.gov/23075143/)
29. Memish ZA, Zumla AI, Al-Hakeem RF, Al-Rabeeh AA, Stephens GM. Family cluster of Middle East respiratory syndrome coronavirus infections. *N Engl J Med*. 2013; 368(26):2487–94. doi: [10.1056/NEJMoa1303729](https://doi.org/10.1056/NEJMoa1303729) PMID: [23718156](https://pubmed.ncbi.nlm.nih.gov/23718156/)
30. Drosten C, Seilmaier M, Corman VM, Hartmann W, Scheible G, Sack S, et al. Clinical features and virological analysis of a case of Middle East respiratory syndrome coronavirus infection. *Lancet Infect Dis*. 2013; 13(9):745–51. doi: [10.1016/S1473-3099\(13\)70154-3](https://doi.org/10.1016/S1473-3099(13)70154-3) PMID: [23782859](https://pubmed.ncbi.nlm.nih.gov/23782859/)
31. Pollack MP, Pringle C, Madoff LC, Memish ZA. Latest outbreak news from ProMED-mail: novel coronavirus—Middle East. *Int J Infect Dis*. 2013; 17(2):e143–4. doi: [10.1016/j.ijid.2012.12.001](https://doi.org/10.1016/j.ijid.2012.12.001) PMID: [23270612](https://pubmed.ncbi.nlm.nih.gov/23270612/)
32. Guery B, Poissy J, el Mansouf L, Sejourne C, Ettahar N, Lemaire X, et al. Clinical features and viral diagnosis of two cases of infection with Middle East Respiratory Syndrome coronavirus: a report of nosocomial transmission. *Lancet*. 2013; 381(9885):2265–72. doi: [10.1016/S0140-6736\(13\)60982-4](https://doi.org/10.1016/S0140-6736(13)60982-4) PMID: [23727167](https://pubmed.ncbi.nlm.nih.gov/23727167/)
33. Eckerle I, Muller MA, Kallies S, Gotthardt DN, Drosten C. In-vitro renal epithelial cell infection reveals a viral kidney tropism as a potential mechanism for acute renal failure during Middle East Respiratory Syndrome (MERS) Coronavirus infection. *Virology*. 2013; 10:359. doi: [10.1186/1743-422X-10-359](https://doi.org/10.1186/1743-422X-10-359) PMID: [24364985](https://pubmed.ncbi.nlm.nih.gov/24364985/)
34. Lau KK, Yu WC, Chu CM, Lau ST, Sheng B, Yuen KY. Possible central nervous system infection by SARS coronavirus. *Emerg Infect Dis*. 2004; 10(2):342–4. PMID: [15030709](https://pubmed.ncbi.nlm.nih.gov/15030709/)
35. Xu J, Zhong S, Liu J, Li L, Li Y, Wu X, et al. Detection of severe acute respiratory syndrome coronavirus in the brain: potential role of the chemokine mig in pathogenesis. *Clin Infect Dis*. 2005; 41(8):1089–96. PMID: [16163626](https://pubmed.ncbi.nlm.nih.gov/16163626/)
36. Gu J, Gong E, Zhang B, Zheng J, Gao Z, Zhong Y, et al. Multiple organ infection and the pathogenesis of SARS. *J Exp Med*. 2005; 202(3):415–24. PMID: [16043521](https://pubmed.ncbi.nlm.nih.gov/16043521/)
37. Gu J, Korteweg C. Pathology and pathogenesis of severe acute respiratory syndrome. *Am J Pathol*. 2007; 170(4):1136–47. PMID: [17392154](https://pubmed.ncbi.nlm.nih.gov/17392154/)
38. Yamashita M, Yamate M, Li GM, Ikuta K. Susceptibility of human and rat neural cell lines to infection by SARS-coronavirus. *Biochem Biophys Res Commun*. 2005; 334(1):79–85. PMID: [15992768](https://pubmed.ncbi.nlm.nih.gov/15992768/)
39. Baskin CR, Bielefeldt-Ohmann H, Tumpey TM, Sabourin PJ, Long JP, Garcia-Sastre A, et al. Early and sustained innate immune response defines pathology and death in nonhuman primates infected by highly pathogenic influenza virus. *Proc Natl Acad Sci U S A*. 2009; 106(9):3455–60. doi: [10.1073/pnas.0813234106](https://doi.org/10.1073/pnas.0813234106) PMID: [19218453](https://pubmed.ncbi.nlm.nih.gov/19218453/)
40. Wong GW, Li AM, Ng PC, Fok TF. Severe acute respiratory syndrome in children. *Pediatr Pulmonol*. 2003; 36(4):261–6. PMID: [12950037](https://pubmed.ncbi.nlm.nih.gov/12950037/)
41. Cameron MJ, Ran L, Xu L, Danesh A, Bermejo-Martin JF, Cameron CM, et al. Interferon-mediated immunopathological events are associated with atypical innate and adaptive immune responses in patients with severe acute respiratory syndrome. *J Virol*. 2007; 81(16):8692–706. PMID: [17537853](https://pubmed.ncbi.nlm.nih.gov/17537853/)
42. Cao B, Hayden FG. Therapy of H7N9 pneumonia: current perspectives. *Expert Rev Anti Infect Ther*. 2013; 11(11):1123–6. doi: [10.1586/14787210.2013.847787](https://doi.org/10.1586/14787210.2013.847787) PMID: [24151830](https://pubmed.ncbi.nlm.nih.gov/24151830/)

Part 6. Differences in the pathogenicity and inflammatory responses induced by avian influenza A/H7N9 Virus infection in BALB/c and C57BL/6 mouse models

Guangyu Zhao[#], Chenfeng Liu[#], Zhihua Kou[#], Tongtong Gao, Ting Pan, Xiaohong Wu, Hong Yu, Yan Guo, **Yang Zeng**, Lanying Du, Shibo Jiang, Shihui Sun*, Yusen Zhou*

Avian influenza A/H7N9 virus infection causes pneumonia in humans with a high case fatality rate. However, virus-induced modulation of immune responses is being recognized increasingly as a factor in the pathogenesis of this disease. In this study, we compared the pathogenicity of A/H7N9 infection in BALB/c and C57BL/6 mouse models and investigated the putative involvement of proinflammatory cytokines in lung injury and viral clearance. In both mouse strains, A/Anhui/1/2013 (H7N9) infection with 10^6 TCID₅₀ resulted in viral replication in lung, severe body weight loss and acute lung injury. During the early infection stage, infected C57BL/6 mice exhibited more severe lung injury, slower recovery from lung damage, less effective viral clearance, higher levels of IL-6, MCP-1, and IL-1b, and lower levels of TNF-a and IFN-c than infected BALB/c mice. These results suggest that TNF-a and IFN-c may help suppress viral gene expression and increase viral clearance, and that IL-6 and MCP-1 may contribute to lung injury in A/H7N9-infected individuals. In addition, lung damage and the distribution of virus antigen in tissues were similar in young and middle-aged mice. These results suggest that the more serious lung injury in middle-aged or older H7N9 cases is not mainly caused by differences in viral replication in the lung but probably by a dysregulated immune response induced by underlying comorbidities. These results indicate that the extent of dysregulation of the host immune response after H7N9 virus infection most probably determines the outcome of H7N9 virus infection.

Differences in the Pathogenicity and Inflammatory Responses Induced by Avian Influenza A/H7N9 Virus Infection in BALB/c and C57BL/6 Mouse Models

Guangyu Zhao^{1,3}, Chenfeng Liu^{1,3}, Zhihua Kou^{1,3}, Tongtong Gao¹, Ting Pan¹, Xiaohong Wu¹, Hong Yu¹, Yan Guo¹, Yang Zeng¹, Lanying Du², Shibo Jiang^{2,3}, Shihui Sun^{1*}, Yusen Zhou^{1*}

1 State Key Laboratory of Pathogen and Biosecurity, Beijing Institute of Microbiology and Epidemiology, Beijing, China, **2** Lindsley F. Kimball Research Institute, New York Blood Center, New York, United States of America, **3** Key Laboratory of Medical Molecular Virology of Ministries of Education and Health, Shanghai Medical College and Institute of Medical Microbiology, Fudan University, Shanghai, China

Abstract

Avian influenza A/H7N9 virus infection causes pneumonia in humans with a high case fatality rate. However, virus-induced modulation of immune responses is being recognized increasingly as a factor in the pathogenesis of this disease. In this study, we compared the pathogenicity of A/H7N9 infection in BALB/c and C57BL/6 mouse models, and investigated the putative involvement of proinflammatory cytokines in lung injury and viral clearance. In both mouse strains, A/Anhui/1/2013(H7N9) infection with 10^6 TCID₅₀ resulted in viral replication in lung, severe body weight loss and acute lung injury. During the early infection stage, infected C57BL/6 mice exhibited more severe lung injury, slower recovery from lung damage, less effective viral clearance, higher levels of interleukine (IL)-6, monocyte chemoattractant protein (MCP)-1, and IL-1 β , and lower levels of tumor necrosis factor (TNF)- α and interferon (IFN)- γ than infected BALB/c mice. These results suggest that TNF- α and IFN- γ may help suppress viral gene expression and increase viral clearance, and that IL-6 and MCP-1 may contribute to lung injury in A/H7N9-infected individuals. In addition, lung damage and the distribution of virus antigen in tissues were similar in young and middle-aged mice. These results suggest that the more serious lung injury in middle-aged or older H7N9 cases is not mainly caused by differences in viral replication in the lung but probably by a dysregulated immune response induced by underlying comorbidities. These results indicate that the extent of dysregulation of the host immune response after H7N9 virus infection most probably determines the outcome of H7N9 virus infection.

Citation: Zhao G, Liu C, Kou Z, Gao T, Pan T, et al. (2014) Differences in the Pathogenicity and Inflammatory Responses Induced by Avian Influenza A/H7N9 Virus Infection in BALB/c and C57BL/6 Mouse Models. PLoS ONE 9(3): e92987. doi:10.1371/journal.pone.0092987

Editor: Yuxian He, Chinese Academy of Medical Sciences, China

Received: December 18, 2013; **Accepted:** February 27, 2014; **Published:** March 27, 2014

Copyright: © 2014 Zhao et al. This is an open-access article distributed under the terms of the Creative Commons Attribution License, which permits unrestricted use, distribution, and reproduction in any medium, provided the original author and source are credited.

Funding: This work was supported by grants from the Project on Human H7N9 from the Ministry of Science and Technology of China (KJYJ-2013-01-04), the National Projects of Infectious Disease (2012ZX10004502), the NSFC of China (81371805), and Shanghai Joint Research Projects on the Prevention and Control of Avian Influenza H7N9 Virus (2013QLG010). The funders had no role in study design, data collection and analysis, decision to publish, or preparation of the manuscript.

Competing Interests: The authors have declared that no competing interests exist.

* E-mail: yzshou@bmi.ac.cn (Y. Zhou); sunsh01@163.com (SS)

† These authors contributed equally to this work.

Introduction

During March 2013, a novel avian influenza A/H7N9 virus was identified in Shanghai and Anhui, China [1]. By November 6, 2013, 139 laboratory confirmed human cases of A/H7N9 infection, including 45 deaths (a case fatality rate of 32%), had been reported to the World Health Organization [2]. Most of the A/H7N9-infected patients suffered from pneumonia, but some of them exhibited acute respiratory distress syndrome (ARDS) with respiratory failure [1].

The dysregulation of proinflammatory cytokines and chemokines, or a “cytokine storm”, a severe adverse reaction created by the secretion of large amounts of proinflammatory cytokines, may aggravate lung injury observed in A/H5N1- and A/H7N9-infected patients [3,4]. Chi et al. [5] reported that the serum concentrations of IFN γ -inducible protein 10 (IP-10), IL-6, IL-17, and IL-2 were significantly higher in A/H7N9-infected patients than in normal individuals and that those of IP-10 and IL-6 were much higher in severe A/H7N9 patients than in non-sever

patients. Chen et al. [6] showed that the serum IL-10 level in a patient who died from A/H7N9 infection was much higher than that in a patient who survived A/H7N9 infection. Zhou et al. [7] also found that the levels of IP-10, monokine induced by γ interferon (MIG), macrophage inflammatory protein 1 beta (MIP-1 β), MCP-1, IL-6, IL-8 and IFN- α were significantly higher in patients with A/H7N9 than in healthy subject controls. With the exception of MIG and MIP-1 β levels, there were no significant differences in the levels of these cytokines and chemokines in patients infected with A/H7N9 or H5N1 viruses. Mok et al. [8] reported that A/H7N9-infected BALB/c mice exhibited mild, self-limited disease with higher lung titers of H7N9 virus and higher serum levels of several proinflammatory cytokines and chemokines during the early stage of viral infection. However, the cytokines potentially involved in lung injury and viral clearance are not known.

Clinical data show that the fatality risks of patients admitted to hospital differ substantially depending on age. Increasing age is

associated with greater disease severity in patients infected with seasonal influenza [9]. In contrast to the skewed age distribution of young people with highly pathogenic avian (HPAI) influenza A H5N1 virus infection, middle-aged or older patients with underlying medical conditions were among the severe cases of H7N9 virus infection. However, it is still unclear whether disease severity of patients is related to their susceptibility to H7N9 virus infection or to differences in the activities of host factors after virus infection.

BALB/c and C57BL/6 mice have been used widely to study the pathogenesis of infectious diseases and exhibit different susceptibilities and immune responses to invading pathogens. For example, Otte et al. [10] reported that C57BL/6 mice were more susceptible to pH1N1 influenza virus infection than BALB/c mice and that HPAI H5N1 virus was more virulent in BALB/c mice than in C57BL/6 mice. C57BL/6 mice show increased Th1 activity and a strong Th1 cytokine response upon infection. BALB/c mice show increased Th2-type cell activity [11]. In the present study, we used BALB/c and C57BL/6 mice infected with A/Anhui/1/2013(H7N9) influenza virus to study the pathogenesis of A/H7N9 infection in two strains and to determine the potential effects of proinflammatory cytokine dysregulation.

Materials and Methods

Ethics statement

All of the procedures involving animals were approved by the Laboratory Animal Center, State Key Laboratory of Pathogen and Biosecurity, Beijing Institute of Microbiology and Epidemiology (Permit number BIME 2013-15). The animal studies were conducted in strict accordance with the recommendations in the Guide for the Care and Use of Laboratory Animals. All of the procedures involving live A/H7N9 viruses were carried out in an approved biosafety level 3 facility.

Mice and viruses

Specific pathogen-free young C57BL/6 and BALB/c mice (6-week-old males and females) and female middle-aged BALB/c mice (10 months old) were obtained from the Laboratory Animal Center, Academy of Military Medical Sciences, Beijing, China. A/Anhui/1/2013 (H7N9) virus (Anhui/1/H7N9) was initially isolated by the National Institute for Viral Diseases Control and Prevention, Chinese Center for Diseases Control and Prevention (CDC) from a throat-swab specimen of the third case of laboratory-confirmed A/H7N9 virus [1], and was authorizedly provided by Chinese CDC. Anhui/1/H7N9 virus used in this study was harvested-allantoic fluid following two passages in Madin-Darby canine kidney (MDCK) cells and two subsequent propagations in the allantoic cavity of embryonated eggs. The sequence of the virus was confirmed by sequencing the entire genome using a Genome Sequencer Junior (Roche).

Experimental infection of C57BL/6 mice and BALB/c mice

The juvenile C57BL/6 and BALB/c mice and the middle-aged BALB/c mice were anesthetized via intraperitoneal injection of ketamine (80 mg/kg) and then inoculated intranasally (i.n.) with a 50% tissue culture infective dose (TCID₅₀) of 10⁶ H7N9 virus in a volume of 20 μ l. The infected mice were sacrificed at the times indicated and the lung, spleen, liver, kidney, brain, and intestine were harvested for virological and pathological analyses. Mouse sera were also collected for cytokine analysis. In addition, the young C57BL/6 and BALB/c mice were monitored daily to assess weight loss following H7N9 virus infection.

Analysis of serum cytokines

Sera were collected from the infected mice at the times indicated and stored at -20°C before being analyzed. The levels of IL-1 β , TNF- α , IL-6, IFN- γ , MCP-1, and keratinocyte-derived cytokine (KC) (a mouse homologue of IL-8) in the mouse sera were determined quantitatively using an enzyme-linked immunosorbent assay (ELISA) (Neobioscience, China), according to the manufacturer's protocol. Briefly, 100 μ l of diluted mouse serum was added to a plate precoated with a monoclonal antibody specific for individual mouse cytokines and incubated at 37 $^{\circ}\text{C}$ for 90 min. After washing, biotinylated-detection antibodies specific to each cytokine were added and incubated at 37 $^{\circ}\text{C}$ for 1 h. Plates were then washed and incubated for 1 h with 100 μ l of HRP-conjugate streptavidin. The reactions were developed with 3,3',5,5'-tetramethylbenzidine (TMB) substrate (Invitrogen, Carlsbad, CA) at 37 $^{\circ}\text{C}$ for 30 min, followed by adding 1 N H₂SO₄ to stop the reactions. Plates were then read on an ELISA plate reader (Synergy 2, BioTek) at 450 nm. The levels of mouse serum cytokines were determined using standard curves.

Viral titers in lung tissues

The tissues of infected mice were harvested at the times indicated and homogenized in minimal essential medium (MEM) plus antibiotics to produce 10% (w/v) suspensions. The viral titers in tissues were determined as the TCID₅₀, as described previously [12]. In brief, monolayers of MDCK cells were inoculated with tenfold serial dilutions of mouse organ homogenates in quadruplicate. Two hours after inoculation, the supernatants were removed and replaced with MEM plus antibiotics and 2 μ g/ml TPCK-trypsin (Sigma, Shanghai, China). The viral cytopathic effect was observed for 3 days before viral infectivity in MDCK cells was measured using a hemagglutination assay with 0.5% turkey erythrocytes. The tissue viral titers were calculated using the Reed and Muench method and expressed as log₁₀ TCID₅₀/g of tissue [13].

Histological analysis of lung damage

A portion of lung tissue was excised, fixed with 10% neutral buffered formalin, dehydrated, and then embedded in paraffin before performing routine histology. Sections measuring 6 μ m in thickness were stained with hematoxylin and eosin (H&E) and examined by light microscopy. The extent of lung injury was scored according to the levels of degeneration and necrosis of the bronchi and bronchiolar epithelium, infiltration of inflammatory cells, alveoli degeneration and collapse, expansion of parenchymal wall, hemorrhage, and interstitial edema [14].

Immunohistochemical staining of a neutrophil marker and the hemagglutinin (HA) protein of H7N9 virus in lung tissue

Formalin-fixed, paraffin-embedded lung sections were deparaffinized with xylene and hydrated using a graded alcohol series. The changes in the levels of HA protein of A/H7N9 virus and infiltrating neutrophils were assessed using a rabbit polyclonal antibody to A/H7N9 HA (Sino Biological Inc., China) and neutrophil marker NIMP-R14 (Santa Cruz Biotechnology Inc, Santa Cruz, CA), respectively. Antibodies were detected using a standard streptavidin-biotin detection system (Beijing Zhongshan Biotechnology Co. Ltd, Beijing, China), according to the manufacturer's instructions.

Neutrophil infiltration was assessed semi-quantitatively by examining in a blinded manner for the presence of neutrophils in 10 arbitrarily selected 40 \times objective fields of lung parenchyma

in each lung section by light microscopy. The cumulative scores for each animal were expressed as the number of positive fields per 100 fields (%) [14].

Statistical analysis

All of the analyses were performed using Graphpad Prism version 5.01. The differences in the gross lesion areas between mouse strains were analyzed using a nonparametric Mann-Whitney test. The differences between mouse groups at the times indicated were analyzed using a two-way ANOVA and a Bonferroni post test.

Results

Lung injury in A/H7N9-infected C57BL/6 and BALB/c mice

To determine whether the pathogenicity H7N9 virus infection differed between mouse strains, healthy 6-week-old C57BL/6 and BALB/c mice were infected i.n. with 10^6 TCID₅₀ of AH/1/H7N9 virus. Both C57BL/6 and BALB/c mice exhibited ruffled fur and hunched backs during the days following infection (data not shown). Although none of the mice died after infection with AH/1/H7N9 virus, body weight loss was clearly observed in all of the infected mice. Compared with BALB/c mice, which had an average body weight loss of 25% on day 8 postviral infection, C57BL/6 mice exhibited more severe weight loss, particularly on days 9–10 postviral infection. Moreover, infected C57BL/6 mice recovered body weight loss more slowly than infected BALB/c mice (Fig. 1A).

During necropsy, the gross pathologies of the lungs from the two mouse strains after A/H7N9 virus infection were similar with respect to multifocal consolidation and dark red discolorations, but the gross lesion areas were significantly different ($P < 0.05$), with mean gross lesion areas of 28% and 45% in BALB/c mice and C57BL/6 mice, respectively. Gross presentations in both mice after A/H7N9 virus infection indicated more severe lung damage in C57BL/6 mice than in BALB/c mice (Fig. 1B).

Histopathological analysis of mouse lung, spleen, brain, intestine, and kidney at different time points after AH/1/H7N9 virus infection showed no significant changes in the histology of mouse spleen, brain, intestine, or kidney. However, significant lung injury was detected in C57BL/6 and BALB/c mice infected with AH/1/H7N9. On days 1 and 3 postviral infection, lung damage in the form of vacuolated bronchial epithelial cells on day 1 and necrosis on day 3 was similar in C57BL/6 and BALB/c mice. In addition, a patchy inflammatory response was observed around the bronchioles and blood vessels (Fig. 2A–D). On days 5 and 7 postviral infection, lung damage was noticeably more severe in C57BL/6 mice than in BALB/c mice, as evidenced by alveolar and interstitial flooding of inflammatory cells, severe widening of lung septa, interstitial edema, fibrin, focal hemorrhage in parenchyma, and scattered bronchiolar and terminal airway epithelial degeneration and necrosis (Fig. 2E–H), as well as a higher lung damage score (Fig. 2K). In particular, on day 7 postviral infection, regeneration of the bronchial epithelium and cells around blood vessels was observed in the lungs of BALB/c mice, but not in the lungs of C57BL/6 mice (Fig. 2H). On day 14 postviral infection, the parenchyma regeneration was observed in both strains, but cell proliferation was higher around the blood vessels of BALB/c mice (Fig. 2I–J). These results demonstrate that C57BL/6 mice were more susceptible to A/H7N9 infection than BALB/c mice, and that A/H7N9-infected C57BL/6 mice had more severe lung injury than A/H7N9-infected BALB/c mice. Furthermore, BALB/c mice exhibited more rapid restoration of lung tissue than C57BL/6 mice.

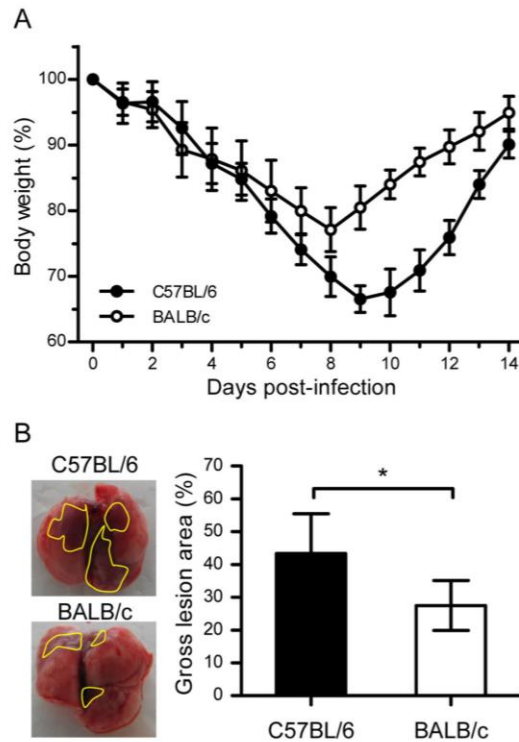


Figure 1. Weight change and gross pathology of the lungs in C57BL/6 and BALB/c mice infected with H7N9 virus. (A) Weight changes in C57BL/6 and BALB/c mice after challenge with AH/1/H7N9 virus. Healthy young C57BL/6 and BALB/c mice (equal numbers of males and females) were infected intranasally with 10^6 TCID₅₀ of AH/1/H7N9 virus and monitored for 14 days. The body weights were measured daily ($n = 12$) and the data are expressed as the mean \pm standard deviation (SD). (B) Gross pathology of the lungs from C57BL/6 and BALB/c mice at day 3 postviral infection. The gross lesion area percentage is indicated on the right ($n = 6$) and the data are expressed as the mean \pm SD (bar). *, **, and *** indicate $P < 0.05$, 0.01 , and 0.001 , respectively. doi:10.1371/journal.pone.0092987.g001

To further investigate and compare the recovery of C57BL/6 and BALB/c mice from A/H7N9 virus infection, we stained cells for proliferating cell nuclear antigen (PCNA), an indicator of cell proliferation. The number of PCNA-positive cells was similar in the two strains of mice at 0, 3, and 5 days after virus infection (data not shown). On days 7 and 14 after viral infection, however, the number of regenerative cells among bronchial epithelial cells and in the interstitial tissues of the lungs of BALB/c mice was higher than that in the lungs of C57BL/6 mice (Fig. 3), thereby further confirming that BALB/c mice recover more effectively than C57BL/6 mice from A/H7N9 infection.

Virus infection and viral clearance in C57BL/6 mice and BALB/c mice

To determine whether an association existed between the severity of lung injury and the tissue distribution of A/H7N9 virus, the distribution of the virus was followed at different time points after viral inoculation. The results demonstrated that many

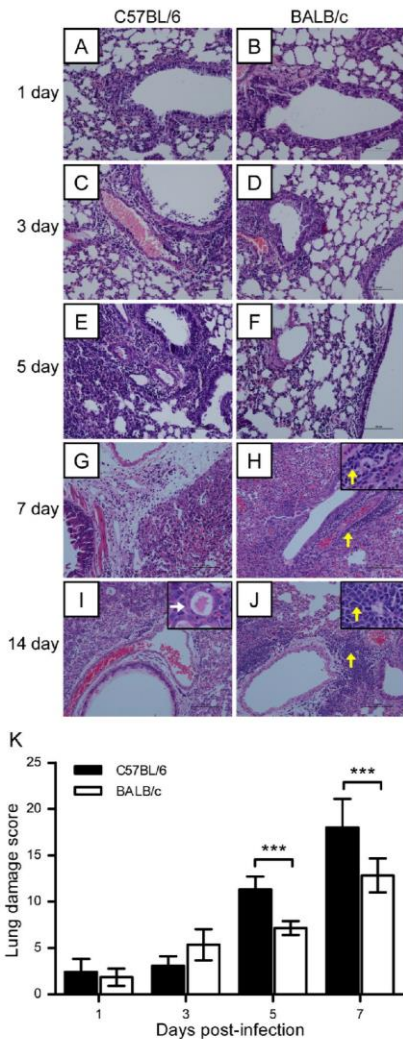


Figure 2. Lung injury in C57BL/6 and BALB/c mice following H7N9 virus infection. C57BL/6 and BALB/c mice were challenged intranasally with 10^6 TCID₅₀ of AH1/H7N9 virus and euthanized on days 0, 1, 3, 5, 7, and 14 after viral infection. (A–J) Histological changes in mouse lung tissues on days 0, 1, 3, 5, 7, and 14 postviral challenge. White and yellow arrows indicate the regeneration of pneumocytes and dissociation cells, respectively. (K) Semiquantitative assessments of lung lesions in mice on days 1, 3, 5, and 7 postviral infection ($n=6$). The data are expressed as the mean \pm SD (bar). *, **, and *** indicate $P<0.05$, 0.01, and 0.001, respectively. doi:10.1371/journal.pone.0092987.g002

bronchial epithelial cells, but few pneumocytes or terminal bronchiole cells, were infected on day 1 postviral infection in either mouse (Fig. 4A–B). On day 5 postviral infection, antigen-positive cells appeared in the bronchioles, bronchioles terminalis, and lung tissues of both mice, but there were more of these cells in

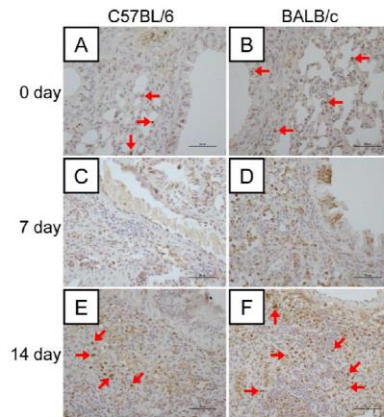


Figure 3. Regeneration of lung tissues in mice following H7N9 virus infection. (A–F) Immunohistochemical staining of proliferating cell nuclear antigen (PCNA)-positive cells in the lung tissues of C57BL/6 and BALB/c mice on days 0, 7, and 14 postviral infection. Positive cells were more abundant in the bronchial epithelial cells and interstitial tissues in the lungs. Red arrows indicate PCNA-positive cells. doi:10.1371/journal.pone.0092987.g003

C57BL/6 mice than in BALB/c mice (Fig. 4C–D). On day 7 postviral infection, the tissue distribution of the virus in C57BL/6 mice was similar to that on day 5, whereas in BALB/c mice, only necrotic cells were observed in the bronchial epithelium and antigen distribution was limited to the interstitial tissue of the lungs (Fig. 4E–F). No virus antigen was observed in either mouse strain at 14 days postviral infection (Fig. 4G–H). The viral titers in the lung tissues were then measured. As shown in Figure 4I, viral titers in both groups increased after infection, reaching a peak on day 3 in BALB/c mice and on day 5 in C57BL/6 mice. Although viral titers dropped dramatically thereafter in both BALB/c and C57BL/6 mice, the drop in the lungs of BALB/c mice was greater than that in the lungs of C57BL/6 mice (Fig. 4A–H). Thus, H7N9 virus could replicate equally well in the lungs of both mouse strains, but BALB/c mice were more proficient in viral clearance than C57BL/6 mice, as evidenced by the earlier clearance of the virus.

Levels of proinflammatory cytokines and cytokines in C57BL/6 mice and BALB/c mice infected with H7N9

The dysregulation of proinflammatory cytokines and chemokines, which is sometimes referred to as a cytokine storm, is associated with lung injury and pneumonia in H7N9-infected patients [5–7]. To investigate whether this was also the case for the two mouse strains used in this study, we measured the levels of several representative proinflammatory cytokines and chemokines in the sera of C57BL/6 and BALB/c mice following A/H7N9 virus challenge. The results showed that the serum levels of cytokines and chemokines were significantly different on days 3 and 5 postviral infection in C57BL/6 and BALB/c mice, although their levels increased similarly in both mouse strains, reaching a peak on day 3 after H7N9 virus infection. In particular, on day 3, the levels of cytokines IL-1 β and IL-6 were significantly higher in C57BL/6 mice than in BALB/c mice (Fig. 5A and C), whereas the levels of TNF- α and IFN- γ were significantly higher in BALB/c mice than in C57BL/6 mice on days 3 and 5, respectively (Fig. 5B and D). On day 3, the level of chemokine MCP-1 was also

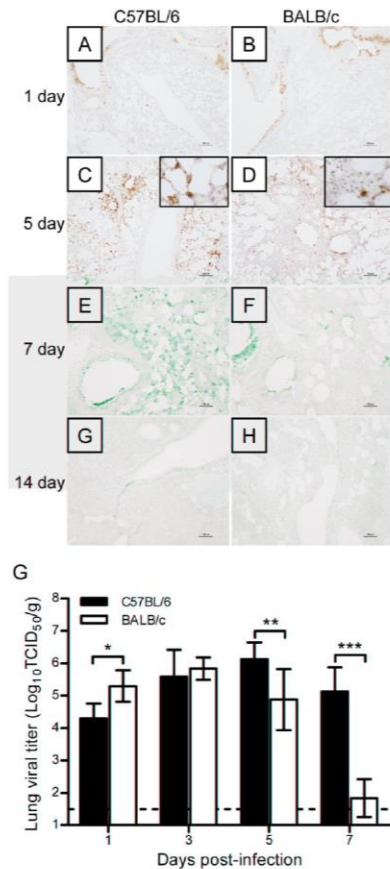


Figure 4. H7N9 virus antigen distribution in lung tissues after H7N9 virus infection. (A–H) Immunohistochemical staining of H7N9 virus antigen in the lungs of C57BL/6 and BALB/c mice on days 1, 5, 7, and 14 postviral infection. (I) Dynamic changes in the viral titers in the lungs of C57BL/6 and BALB/c mice on days 1, 3, 5, and 7 postviral infection ($n=6$). The data are expressed as the mean \pm SD (bar). *, **, and *** indicate $P<0.05$, 0.01, and 0.001, respectively. doi:10.1371/journal.pone.0092987.g004

significantly higher in C57BL/6 mice than in BALB/c mice (Fig. 5E). However, there was no significant difference in the serum concentration of KC between C57BL/6 and BALB/c mice (Fig. 5F). Thus, these results suggest that lung injury was more severe and occurred more slowly in H7N9-infected C57BL/6 mice than in H7N9-infected BALB/c mice, which was probably a consequence of the more dysregulated immune response in H7N9-infected C57BL/6 mice.

Levels of neutrophil infiltration in the lungs of H7N9-infected C57BL/6 mice and H7N9-infected BALB/c mice during the early stage of infection

Neutrophil infiltration was observed as early as day 1 and it reached a peak on day 5 after A/H7N9 virus infection. Neutrophils were present mainly in the parenchyma around

bronchi on days 1 and 3, whereas they were found mainly in the necrotic areas of lungs on day 5 postviral challenge. Neutrophil infiltration disappeared at 14 days postviral infection. During the early stage of viral infection, however, more neutrophils were observed in the parenchyma around the bronchi and lung tissues of BALB/c mice than in the parenchyma of C57BL/6 mice, whereas there was no significant difference in this respect between the two mouse strains on day 14 (Fig. 6). These results suggest that appropriate neutrophil infiltration, especially during the early stage of H7N9 virus infection, may be critical for suppressing virus replication and enhancing viral clearance.

Lung lesions and virus replication in young and middle-aged mice

To clarify whether the clinical severity of lung injury in elderly patients is related to virus replication, we examined the lung lesions in healthy naive young and middle-aged BALB/c mice infected with H7N9 virus after H&E staining. The lung tissue distribution of the H7N9 virus was also followed by the HA antigen detection assay. The results showed that lung lesions were similar in middle-aged and young mice on day 5 postviral infection (Fig. 7A–B). The HA viral antigen was found mainly in bronchi on day 1 postviral infection, with patches appearing in the lung parenchyma on day 5 (Fig. 7C–F). There were no apparent differences in the distribution of the HA antigen or in the level of neutrophil infiltration between young and middle-aged mice (Fig. 7G–I). These results suggest that more serious lung injury in middle-aged or older H7N9 cases is not mainly caused by differences in virus replication in the lungs, but instead, it is probably a consequence of a dysregulated immune response induced by underlying comorbidities.

Discussion

The novel avian influenza H7N9 virus has caused outbreaks of influenza in China, which have resulted in 139 infected cases and a high case fatality rate (32%) [1,2]. Most of the patients died of severe pneumonia and ARDS with respiratory failure [6,7]. A cytokine storm, or the upregulation of proinflammatory cytokines and chemokines, such as IL-6, IL-8, IFN- α , IP-10, MIG, MIP-1 β , and MCP-1, is reported to have contributed to the lung injury and severe pneumonia in these H7N9-infected patients [5,7]. H7N9-infected BALB/c mice produced higher levels of proinflammatory cytokines and chemokines, including IP-10, TNF- α , MCP-1, MCP-3, IFN- α , MIP-1 β , KC, and regulated upon activation normal T cell expressed and secreted (RANTES), at an early stage of infection (day 3 post-infection) than BALB/c mice infected with the H9N2 virus, but lower levels than those produced when BALB/c mice were infected with H5N1 [8]. H7N9 virus replicates effectively in the nasal cavity and lung tissues of BALB/c mice, but its infection causes mild focal inflammation, with minimal involvement of the bronchial or bronchiolar epithelium [8]. These results suggest that H7N9 virus can replicate and cause disease in mice, but that it is less pathogenic than H5N1 virus.

Previous reports show that BALB/c and C57BL/6 mice differ in their susceptibility and immune responses to infection by HPAI H5N1 and pandemic H1N1 (pH1N1) viruses [10]. In this study, we performed a series of experiments to compare the pathogenicity of H7N9 infection in BALB/c and C57BL/6 mice. Despite causing severe disease and even fatal outcome, different isolates of avian influenza A H7N9 virus may have a little bit of difference on pathogenicity. Zhou et al. [7] reported a more productive replication of Anhui/1/H7N9 in lung tissues than that of Shanghai/1/H7N9 was observed. In our experiments, C57BL/6

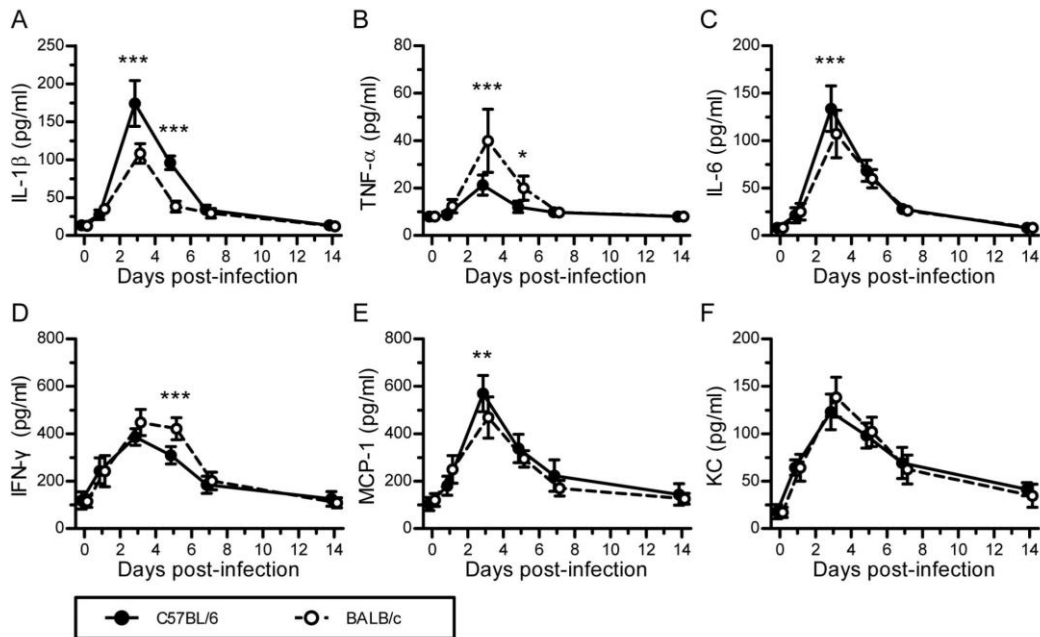


Figure 5. Innate immune responses induced by H7N9 virus infection in C57BL/6 and BALB/c mice. The experimental setup was the same as that described in Figure 2. (A–F) Levels of IL-1 β , TNF- α , IL-6, IFN- γ , MCP-1, and KC in mouse sera on days 0, 1, 3, 5, 7, and 14 postviral infection, which were measured by ELISA ($n=6$). The data are expressed as the mean \pm SD (bar). *, **, and *** indicate $P<0.05$, 0.01, and 0.001, respectively. doi:10.1371/journal.pone.0092987.g005

and BALB/c mice were infected with Anhui/1/H7N9 virus, and C57BL/6 exhibited a more severe body weight loss than BALB/c mice (35% *vs* 25%, Fig. 1A). The gross lesion areas in the lungs of H7N9-infected C57BL/6 mice were significantly larger than those in the lungs of H7N9-infected BALB/c mice (45% *vs* 28%, Fig. 1B). The lung damage in C57BL/6 mice at days 5 and 7 postviral infection was more severe than that in BALB/c mice (Fig. 2), and the lung injury recovery time was longer in H7N9-infected C57BL/6 mice than in H7N9-infected BALB/c mice (Fig. 3). The numbers of viral antigen-positive cells in the bronchioles and lungs of both strains of H7N9-infected mice, as well as the viral titers in their lungs, were similar during the early stage of viral infection (1–3 days postviral infection). However, the decline in the number of virus-infected cells and viral titers was more rapid in the lungs of H7N9-infected BALB/c mice than in the lungs of H7N9-infected C57BL/6 mice (Fig. 4), suggesting that the immune system of BALB/c mice is more proficient in clearing H7N9 virus.

It is widely believed that proinflammatory cytokine and chemokine dysregulation, referred to as a cytokine storm, contributes to lung injury and severe pneumonia during the progression of a viral infection. In the present study, we compared the levels of proinflammatory cytokines in C57BL/6 and BALB/c mice infected with A/H7N9 at different time points after viral infection. We found that the levels of proinflammatory cytokines, including IL-6, MCP-1, IL-1 β , TNF- α , and IFN- γ , increased immediately after infection and peaked on day 3 postviral infection, before returning to their baseline levels about 7–10 days after infection in both mouse strains. However, A/H7N9-

infected C57BL/6 mice exhibited higher levels of IL-6, MCP-1, and IL-1 β , but lower levels of TNF- α and IFN- γ , than A/H7N9-infected BALB/c mice at day 3 postviral infection (Fig. 5). These findings suggest that dysregulated cytokine expression may mediate lung injury in H7N9-infected hosts. Zhou et al. [7] reported that, in the absence of any other differences between the two groups, the levels of IL-6 and MCP-1 are significantly higher in H7N9- and H5N1-infected patients than in healthy subjects. Thus, it was suggested that hypercytokinemia in H7N9-infected patients may increase clinical severity, as observed previously in patients infected by H5N1 virus [3,4].

MCP-1 plays an important role in the inflammatory and fibrotic responses to influenza A virus infection under neonatal hyperoxia [15], and van Helden et al. [16] demonstrated that the migration of NK cells to the site of influenza virus infection is MCP-1-dependent. IL-6 is an important mediator of the acute phase response and fever because it crosses the blood-brain barrier [17] and promotes PGE₂ synthesis in the hypothalamus, resulting in a change in the body temperature set point. The overexpression of IL-6 during the early stage of H1N1 infection has been reported to contribute to airway inflammation and bronchial hyper-reactivity in infected children [18]. To the best of our knowledge, the present study is the first to report that the serum IL-1 β level is increased in H7N9-infected mice during the early stage of H7N9 infection and that it is higher in H7N9-infected C57BL/6 mice than in H7N9-infected BALB/c mice (Fig. 5A). However, the role of IL-1 β in the pathogenesis of H7N9 infection remains controversial. Schmitz et al. [19] showed that IL-1 α/β mediated acute pulmonary inflammatory pathology and increased the survival rate of

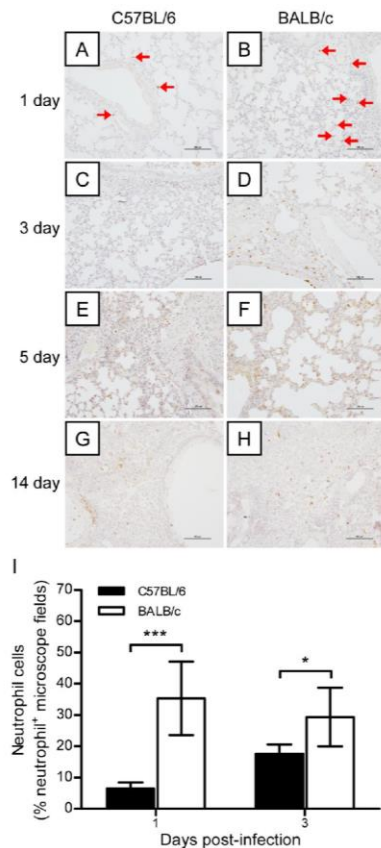


Figure 6. Dynamic changes in neutrophil infiltration in the lung tissues of mice after H7N9 virus challenge. The experimental setup was the same as that described in Figure 2. (A–H) Immunohistochemical staining of neutrophils in the lungs of BALB/c and C57BL/6 mice on days 1, 3, 5, and 7 postviral infection. The red arrows indicate infiltrating neutrophils. (I) Semiquantitative assessments of neutrophil infiltration in the lungs on days 1 and 3 postviral infection ($n=6$). The data are expressed as the mean \pm SD (bar). * and *** indicate $P<0.05$ and 0.001 , respectively. doi:10.1371/journal.pone.0092987.g006

influenza virus-infected mice. They suggested that IL-1 β may enhance IgM antibody responses and the recruitment of CD4+ T cells to viral infection sites. However, although the levels of cytokines were increased after H7N9 virus infection, the post-infection serum levels were much lower than those observed after HPAI H5N1 virus infection, especially on day 3 [8], which may explain why lung damage and illness are less severe in clinical H7N9 virus-infected patients. In the present study, the cytokine expression levels of BALB/c mice were different from those of C57BL/6 mice, which might explain the difference in lung lesions between the two mouse strains.

TNF- α , which is generally considered to be a proinflammatory and proimmune cytokine, plays an important role in the early stages of host defense against influenza infection [20,21]. In

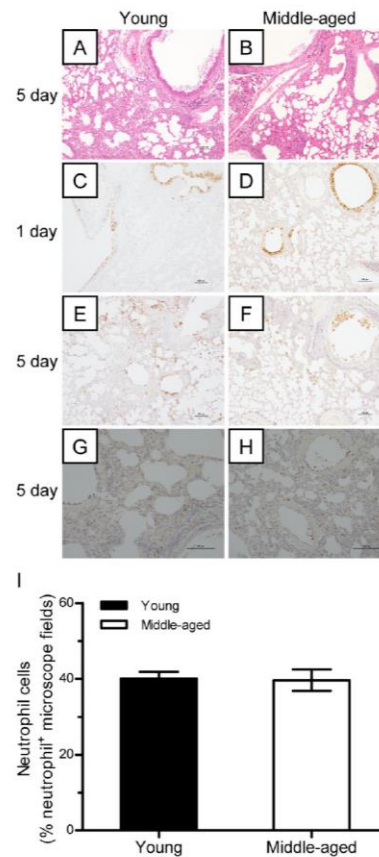


Figure 7. Lung lesion and virus replication in young and middle-aged mice. (A–B) Young and middle-aged BALB/c mice were challenged intranasally with 10^6 TCID₅₀ virus and euthanized at days 1 and 5 postviral infection. (A–B) Histological analysis of the lung tissues of mice on days 1 and 5 postviral infection. (C–F) Virus antigen distribution in the lungs on days 1 and 5 postviral infection ($n=5$). (G–I) Neutrophil infiltration in the parenchyma of the lungs on days 1 and 5 postviral infection ($n=5$). doi:10.1371/journal.pone.0092987.g007

addition, TNF- α has an immune regulatory function that controls Th1 cell activation and immunopathology following pulmonary mycobacterial infection [22], and it is also a negative regulator of CD4 and CD8 T-cell responses to lymphocytic choriomeningitis virus infection [23,24]. Recently, Damjanovic et al. [25] reported that TNF- α was critical for controlling the extent of lung immunopathology, particularly when influenza viral clearance was near completion and lung homeostasis needed to be restored during the later phases of infection. Furthermore, intrinsic TNF/TNFR2 interactions fine tune the immune response to influenza virus infection in the lung via modest enhancements of effector functions that may function to limit the damage that could be caused by a prolonged and inefficient effector response [26]. IFN- γ , which is produced by NK cells and/or Th1 cells, enhances overall development of cell-mediated immunity, macrophage

activation, antigen presentation, and chemokine gene expression. IFN- γ is a key mediator of the effect of inactivated paravoxvirus ovis against HBV and HSV infections, and the neutralization of IFN- γ by anti-IFN- γ antibodies abolish its *in vivo* antiviral effects [27]. More recently, IFN- γ was shown to play a pivotal role in controlling virus infection and in resolving acute inflammation [28,29]. In the present study, the lower level of lung damage as well as the more effective and earlier recovery of BALB/c mice may be due to the higher levels of TNF- α and IFN- γ in the serum of BALB/c mice on days 3 and 5.

Neutrophils, which migrate readily into lung tissues in response to inflammatory stimuli, occur at higher levels in pulmonary capillaries than in systemic blood. Thus, neutrophils are considered to be the host immune system's first line of defense against infection. Tumpney et al. [30] demonstrated that neutrophils and alveolar macrophages control the replication and spread of a lethal recombinant influenza virus bearing 1918 H1N1 virus HA and NA, because the depletion of neutrophils and alveolar macrophages before viral challenge resulted in uncontrolled virus replication and increased mortality in mice. Tate et al. [31] also showed that neutrophils could limit virus replication and ameliorate lung injury. Furthermore, Fujisawa [32] reported that neutrophils protect against and aid recovery from influenza virus infection in the lungs of mice. In the present study, we showed that neutrophil infiltration increased during the early stage of A/H7N9 virus infection, but decreased during the later stage, in both C57BL/6 and BALB/c mice. The lower level of neutrophil infiltration during the early stage of infection in the lungs of C57BL/6 mice may be one of the reasons why H7N9-infected

C57BL/6 mice exhibited more severe pulmonary damage and slower lung injury recovery than H7N9-infected BALB/c mice.

Epidemiological studies of human A/H7N9 virus infections show that the most severe cases occur among middle-aged and elderly patients and the age distribution differs from that of HPAI H5N1-infected cases [33,34]. However, it is still unclear whether severity of lung injury in middle-aged or older cases is immediately related to more viral replication, or to the activity of host factors after viral infection. In the present study, we found that there was no significant difference in HA antigen distribution between young and middle-aged mice during the first few days after infection, indicating that young and middle-aged mice have similar susceptibility to H7N9 virus infection. Thus, more serious lung injury in older H7N9 cases is probably attributable to differences in the host immune response. The immune responses to pathogen invasion differ with age and aged patients are considered to be at an increased risk for influenza complications because of age-related decreases in immunity or underlying medical conditions [35–37]. In the present study, the lung lesions were similar between healthy influenza-naïve BALB/c young and middle-aged mice on day 5 postviral infection. Thus, the severe nature of the disease in aged patients is probably due to an existing dysregulated immune response induced by underlying medical conditions.

Author Contributions

Conceived and designed the experiments: GZ SS Y. Zhou. Performed the experiments: GZ CL ZK TG TP XW HY YG Y. Zeng SS. Analyzed the data: GZ LD SS. Wrote the paper: GZ SJ SS Y. Zhou.

References

- Gao R, Cao B, Hu Y, Feng Z, Wang D, et al. (2013) Human infection with a novel avian-origin influenza A (H7N9) virus. *N Engl J Med* 368: 1888–1897.
- WHO (2013) Human infection with avian influenza A(H7N9) virus - update. Available: http://www.who.int/csr/don/2013_11_06/en/index.html. Accessed 16 November 2013.
- de Jong MD, Simmons CP, Thanh TT, Hien VM, Smith GJ, et al. (2006) Fatal outcome of human influenza A (H5N1) is associated with high viral load and hypercytokinemia. *Nat Med* 12: 1203–1207.
- Peiris JS, Yu WC, Leung CW, Cheung CY, Ng WF, et al. (2004) Re-emergence of fatal human influenza A subtype H5N1 disease. *Lancet* 363: 617–619.
- Chi Y, Zhu Y, Wen T, Cui L, Ge Y, et al. (2013) Cytokine and chemokine levels in patients infected with the novel avian influenza A (H7N9) virus in China. *J Infect Dis* 208: 1962–1967.
- Chen Y, Liang W, Yang S, Wu N, Gao H, et al. (2013) Human infections with the emerging avian influenza A H7N9 virus from wet market poultry: clinical analysis and characterisation of viral genome. *Lancet* 381: 1916–1925.
- Zhou J, Wang D, Gao R, Zhao B, Song J, et al. (2013) Biological features of novel avian influenza A (H7N9) virus. *Nature* 499: 500–503.
- Mok CK, Lee HH, Chan MC, Sia SF, Lestra M, et al. (2013) Pathogenicity of the novel A/H7N9 influenza virus in mice. *MBio* 4: e00362–00313.
- Yu H, Cowling BJ, Feng L, Lau EH, Liao Q, et al. (2013) Human infection with avian influenza A H7N9 virus: an assessment of clinical severity. *Lancet* 382: 138–145.
- Otte A, Sauter M, Alleva L, Baumgarte S, Klingel K, et al. (2011) Differential host determinants contribute to the pathogenesis of 2009 pandemic H1N1 and human H5N1 influenza A viruses in experimental mouse models. *Am J Pathol* 179: 230–239.
- Heinzel FP, Sadick MD, Holaday BJ, Coffman RL and Locksley RM (1989) Reciprocal expression of interferon gamma or interleukin 4 during the resolution or progression of murine leishmaniasis. Evidence for expansion of distinct helper T cell subsets. *J Exp Med* 169: 59–72.
- Zhao G, Lin Y, Du L, Guan J, Sun S, et al. (2010) An M2e-based multiple antigenic peptide vaccine protects mice from lethal challenge with divergent H5N1 influenza viruses. *Virology* 401: 7–9.
- Reed LJ and Muench H (1938) A simple method of estimating fifty per cent endpoints. *Am J Hyg* 27: 493–497.
- Sun S, Zhao G, Liu C, Wu X, Guo Y, et al. (2013) Inhibition of complement activation alleviates acute lung injury induced by highly pathogenic avian influenza H5N1 virus infection. *Am J Respir Cell Mol Biol* 49: 221–230.
- Buczynski BW, Yee M, Martin KC, Lawrence BP and O'Reilly MA (2013) Neonatal hyperoxia alters the host response to influenza A virus infection in adult mice through multiple pathways. *Am J Physiol Lung Cell Mol Physiol* 305: L282–290.
- van Helden MJ, Zaiss DM and Sijts AJ (2012) CCR2 defines a distinct population of NK cells and mediates their migration during influenza virus infection in mice. *PLoS One* 7: e52027.
- Banks WA, Kastin AJ and Gutierrez EG (1994) Penetration of interleukin-6 across the murine blood-brain barrier. *Neurosci Lett* 179: 53–56.
- Chiaretti A, Pulitano S, Conti G, Barone G, Buonsenso D, et al. (2013) Interleukin and neurotrophin up-regulation correlates with severity of H1N1 infection in children: a case-control study. *Int J Infect Dis* 17: e1186–1193.
- Schmitz N, Kurrer M, Bachmann MF and Kopf M (2005) Interleukin-1 is responsible for acute lung immunopathology but increases survival of respiratory influenza virus infection. *J Virol* 79: 6441–6448.
- Szretter KJ, Gangappa S, Lu X, Smith C, Shieh WJ, et al. (2007) Role of host cytokine responses in the pathogenesis of avian H5N1 influenza viruses in mice. *J Virol* 81: 2736–2744.
- Belisle SE, Tisoncik JR, Korh MJ, Carter VS, Proll SC, et al. (2010) Genomic profiling of tumor necrosis factor alpha (TNF-alpha) receptor and interleukin-1 receptor knockout mice reveals a link between TNF-alpha signaling and increased severity of 1918 pandemic influenza virus infection. *J Virol* 84: 12576–12588.
- Zganiacz A, Santosuosso M, Wang J, Yang T, Chen L, et al. (2004) TNF-alpha is a critical negative regulator of type 1 immune activation during intracellular bacterial infection. *J Clin Invest* 113: 401–413.
- Suresh M, Singh A and Fischer C (2005) Role of tumor necrosis factor receptors in regulating CD8 T-cell responses during acute lymphocytic choriomeningitis virus infection. *J Virol* 79: 202–213.
- Singh A, Wuthrich M, Klein B and Suresh M (2007) Indirect regulation of CD4 T-cell responses by tumor necrosis factor receptors in an acute viral infection. *J Virol* 81: 6502–6512.
- Damjanovic D, Divangahi M, Kugathasan K, Small CL, Zganiacz A, et al. (2011) Negative regulation of lung inflammation and immunopathology by TNF-alpha during acute influenza infection. *Am J Pathol* 179: 2963–2976.
- Wortzman ME, Lin GH and Watts TH (2013) Intrinsic TNF/TNFR2 interactions fine-tune the CD8 T cell response to respiratory influenza virus infection in mice. *PLoS One* 8: e68911.
- Weber O, Siegfing A, Friebe A, Limmer A, Schlapp T, et al. (2003) Inactivated paravoxvirus ovis (Orf virus) has antiviral activity against hepatitis B virus and herpes simplex virus. *J Gen Virol* 84: 1843–1852.
- Decker T, Stockinger S, Karaghiosoff M, Muller M and Kovarik P (2002) IFNs and STATs in innate immunity to microorganisms. *J Clin Invest* 109: 1271–1277.

29. McLoughlin RM, Witowski J, Robson RL, Wilkinson TS, Hurst SM, et al. (2003) Interplay between IFN-gamma and IL-6 signaling governs neutrophil trafficking and apoptosis during acute inflammation. *J Clin Invest* 112: 598–607.
30. Tumpy TM, Garcia-Sastre A, Taubenberger JK, Palese P, Swayne DE, et al. (2005) Pathogenicity of influenza viruses with genes from the 1918 pandemic virus: functional roles of alveolar macrophages and neutrophils in limiting virus replication and mortality in mice. *J Virol* 79: 14933–14944.
31. Tate MD, Deng YM, Jones JE, Anderson GP, Brooks AG, et al. (2009) Neutrophils ameliorate lung injury and the development of severe disease during influenza infection. *J Immunol* 183: 7441–7450.
32. Fujisawa H (2008) Neutrophils play an essential role in cooperation with antibody in both protection against and recovery from pulmonary infection with influenza virus in mice. *J Virol* 82: 2772–2783.
33. Smallman-Raynor M and Cliff AD (2007) Avian influenza A (H5N1) age distribution in humans. *Emerg Infect Dis* 13: 510–512.
34. Li Q, Zhou L, Zhou M, Chen Z, Li F, et al. (2013) Epidemiology of human infections with avian influenza A(H7N9) virus in China. *N Engl J Med* 370: 520–532.
35. Liang S, Domon H, Hosur KB, Wang M and Hajshengallis G (2009) Age-related alterations in innate immune receptor expression and ability of macrophages to respond to pathogen challenge in vitro. *Mech Ageing Dev* 130: 538–546.
36. Maue AC, Yager EJ, Swain SL, Woodland DL, Blackman MA, et al. (2009) T-cell immunosenescence: lessons learned from mouse models of aging. *Trends Immunol* 30: 301–305.
37. Zaghouani H, Hoeman CM and Adkins B (2009) Neonatal immunity: faulty T-helpers and the shortcomings of dendritic cells. *Trends Immunol* 30: 585–591.

**Part 7. Manuscript “Identification of novel HLA-A11-
restricted T-cell epitopes in the Ebola virus nucleoprotein**

Dan Li, Pei Li, Nianping Song, Yuting Jiang, **Yang Zeng**, Guangyu Zhao, Yunzhi Fa,
Huahu Ye, Yuchun Lone, Yusen Zhou, Shihui Sun, Lin Zeng

The Ebola virus (EBOV) is a very contagious virus that is highly fatal in humans and animals. The largest epidemic was in West Africa in 2014, in which over 11,000 people died. However, to date, there are no licensed vaccines against it. Studies show that CD4⁺ and CD8⁺ T-cell responses, especially cytotoxic T-lymphocyte (CTL) responses, play key roles in protecting individuals from EBOV infection. Since HLA-restricted epitope vaccines are likely to be effective and safe immunization strategies for infectious diseases, the present study screened for CTL epitopes in the EBOV-nucleoprotein that are restricted by HLA-A11 (a common allele in Chinese people). Predictive computer analysis of the amino-acid sequence of EBOV-nucleoprotein identified ten putative HLA-A11-restricted epitopes. ELISPOT assay of immunized HLA-A11/DR1 transgenic mice showed that five (GR-9, VR-9, EK-9, PK-9, and RK-9) induced effective CTL responses. Additional epitope analyses will aid the design of epitope vaccines against EBOV.

1 ORIGINAL ARTICLE

2 Identification of novel HLA-A11-restricted T-cell epitopes in
3 the Ebola virus nucleoprotein

4 Dan Li^{1,2}, Pei Li², Nianping Song², Yuting Jiang², Yang Zeng³, Guangyu Zhao², Yunzhi Fa¹,
5 Huahu Ye¹, Yuchun Lone³, Yusen Zhou^{2*}, Shihui Sun^{2*}, Lin Zeng^{1*}

6 **Author affiliations:**

7 ¹ *Laboratory Animal Center of the Academy of Military Medical Science, Beijing, 100071,*
8 *China*

9 ² *State Key Laboratory of Pathogen and Biosecurity, Beijing Institute of Microbiology and*
10 *Epidemiology, Beijing, 100071, China*

11 ³ *INSERM U1197 (ex U1014), University of Paris-Sud, Hospital Paul Brousse, Villejuif,*
12 *France*

13 *Correspondence should be addressed to Yusen Zhou (yszhou@bmi.ac.cn), Shihui Sun
14 (sunsh01@163.com) and Lin Zeng (zenglin1965@126.com)

15

16 Abstract

17 The Ebola virus (EBOV) is a very contagious virus that is highly fatal in humans and
18 animals. The largest epidemic was in West Africa in 2014, in which over 11,000 people died.
19 However, to date, there are no licensed vaccines against it. Studies show that CD4⁺ and CD8⁺
20 T-cell responses, especially cytotoxic T-lymphocyte (CTL) responses, play key roles in
21 protecting individuals from EBOV infection. Since HLA-restricted epitope vaccines are likely
22 to be effective and safe immunization strategies for infectious diseases, the present study
23 screened for CTL epitopes in the EBOV-nucleoprotein that are restricted by HLA-A11 (a
24 common allele in Chinese people). Predictive computer analysis of the amino-acid sequence
25 of EBOV-nucleoprotein identified ten putative HLA-A11-restricted epitopes. ELISPOT assay
26 of immunized HLA-A11/DR1 transgenic mice showed that five (GR-9, VR-9, EK-9, PK-9,
27 and RK-9) induced effective CTL responses. Additional epitope analyses will aid the design
28 of epitope vaccines against EBOV.

29 **Key words:** Ebola virus; HLA-A11-restricted epitope; Vaccine

30

31 1. Introduction

32 Ebola virus (EBOV) disease (EVD) is a highly contagious disease that is caused by
33 EBOV infection. EVD mortality rates in humans and primates vary from 50% to 90% [1, 2].
34 The most recent Ebola epidemic was in 2014 and it was the largest in recorded history: over
35 28,616 people were infected and over 11,310 died [3-5]. However, to date, a licensed vaccine
36 that prevents and/or controls Ebola virus infections is still not available.

37 Several studies suggest that CD4⁺ and CD8⁺ T cells, especially cytotoxic T-lymphocytes
38 that are specific for the glycoprotein or nucleoprotein (NP) of EBOV infection play critical
39 roles in protection from EBOV [6-8]. For example, when Sullivan *et al.* [9] immunized non-
40 human primates with an adenoviral vector vaccine that encoded the EBOV glycoprotein and
41 NP genes, the animals were protected from challenge with EBOV, and this response
42 associated with the generation of EBOV-specific CD8⁺ T cells and antibodies.

43 Vaccines can be a highly effective method of preventing and controlling infectious
44 diseases. One approach is to use whole inactivated or attenuated microbes. However, these
45 vaccines can cause inflammation and other serious immunological problems [10]. A much
46 safer alternative is peptide-based vaccines, which consist of one or more immunogenic T-cell
47 epitopes from the proteins of the microbe in question. Such proteins are dogged by two
48 problems. One is epitope polymorphism: even single amino-acid change in the microbe
49 epitope can allow the microbe to escape from immune surveillance [11, 12]. To avoid this, it

50 is necessary to map the microbe epitopes that generate protective immune responses in
51 humans and then assess the effect of common polymorphisms in wild strains on the immune
52 responses. The second problem is lack of promiscuous MHC binding by the microbe
53 epitope(s). This problem can be overcome by identifying the immunogenic microbe epitopes
54 that bind to the most common HLAs in the populations that are at risk. The design of such
55 vaccines has been greatly facilitated by the recent explosion in microbe proteome information
56 [13, 14].

57 Since the EBOV glycoprotein and NP confer protective immunity [15, 16], a desirable
58 EBOV vaccine would be one that bears the CTL epitopes from these proteins that can be
59 presented by common MHC-I molecules. Multiple peptide-screening studies have been
60 conducted to delineate these epitopes on EBOV glycoprotein and NP. The CTL epitopes on
61 EBOV-NP are of particular interest in the present study because internal viral proteins such as
62 EBOV-NP are more likely to induce protective CTL responses [6]. One study showed that
63 there are three CTL epitopes on EBOV-NP that binds to HLA-A2.1 [15]. Two other studies
64 then used immunoinformatics to screen for HLA-A2-, HLA-B7-, and HLA-B40-restricted T-
65 cell epitopes in EBOV-NP [17, 18]. However, although many EBOV peptides have been
66 confirmed to bind to the predicted HLA, only a few are actually immunogenic for T cells [19].

67 The HLA-A11 allele is found in approximately 18.2% of the Asian population. In the
68 Chinese population, its phenotypic frequency is about 20–30%. It is much more common in

69 this population than in Europeans (5.9%) and blacks (1.1%) [20-22]. The present study was
70 conducted to identify the epitopes in the EBOV-NP that both bind to HLA-A11 and can
71 induce specific CTL responses. The EBOV-NP sequence that we used was that of the Ebola-
72 Makona strain, which was responsible for the extensive viral outbreak in West Africa in
73 2014–2015. To identify the HLA-A11-restricted epitopes, we employed the HLA-A11/DR1
74 double-transgenic mice that we reported previously [23]. These mice lack murine H-2
75 molecules and mount robust humoral and cellular immune responses to antigens in a HLA-
76 A11- or HLA-DR1-dependent manner [23]. The protective immune responses especially CTL
77 response against pathogens usually requires the cooperation of cytotoxic CD8⁺ T cells and T
78 helper cells. However, single transgenic mice which only have the HLA class I- or HLA class
79 II- molecule could not monitor effective immune responses due to the absence of the
80 collaboration of the HLA class I- and HLA class II- molecules [24-26]. Thus, we used HLA-
81 A11/DR1 double transgenic mice in the presence of HLA-A11 and HLA-DR1 molecules to
82 screen for candidate immunogenic T-cell epitopes.

83

84 **2. Materials and methods**

85 *2.1. Ethics statement*

86 All procedures involving animals were improved by the Institutional Animal Care and Use

87 Committees of the Laboratory Animal Center, State Key Laboratory of Pathogen and
88 Biosecurity, the Beijing Institute of Microbiology and Epidemiology (Permit Number:
89 BIME20170916). The animal studies were carried out in strict accordance with the
90 recommendations in the Guide for the Care and Use of Laboratory Animals of the National
91 Institutes of Health.

92 2.2. Construction of a recombinant adenovirus that expresses EBOV-NP

93 The EBOV-NP gene (GenBank: KY401672.1) was first synthesized and cloned in the pET32a
94 vector and then subcloned into the shuttle vector pShuttle-CMV (Stratagene, USA). The
95 positive clones were selected by PCR and validated by sequencing. The shuttle vector was
96 linearized with *Pme* I and then transformed to BJ5183-AD-1 bacteria (Stratagene, USA),
97 which carry the AdEasy-1 plasmid that encodes the adenovirus-5 (Ad5) genome.
98 Recombinant Ad5 plasmids were designated as Ad5-EBOV-NP and were digested with *Pac* I
99 and then used to transfect the AD-293 packaging cell line (stored in our laboratory). The
100 transfected cells were identified on the basis of the adenovirus-related cytopathic effects. The
101 recombinant Ad5-EBOV-NP viruses were then reamplified in AD-293 cells and purified. To
102 check the expression of the recombinant virus, AD-293 cells were infected with the purified
103 Ad5-EBOV-NP preparation and observed 48 h later under a fluorescence microscope.

104 2.3. Western blotting analysis

105 The expression of EBOV-NP protein by infected AD-293 cells was validated by Western
106 blotting. Briefly, AD-293 cells plated in 6-well plates (Corning, USA) were infected with
107 Ad5-EBOV-NP or Ad5 and incubated for 48 h in a humidified atmosphere at 37°C and 5%
108 CO₂. The cells were then lysed, after which the lysates were separated on a SDS-PAGE gel
109 and transferred onto polyvinylidene difluoride (PVDF) membranes. After blocking, the
110 membranes were first incubated with anti-EBOV-NP antibodies (Sino biological, China) and
111 then with horseradish peroxidase (HRP)-conjugated goat-anti-rabbit secondary antibodies
112 (TransGen Biotech, China). The proteins were visualized by using Pierce™ ECL Western
113 Blotting Substrate.

114 2.4. *Animals and immunizations*

115 Female HLA-A11^{+/+}/DR01^{+/+}/H-2-β2m^{-/-}/IAB^{-/-} transgenic mice and wild-type C57BL/6 mice
116 were immunized three times with 10⁸ pfu of Ad5-EBOV-NP or Ad5 by intramuscular (i.m.)
117 injection at intervals of three weeks. Ten days after each immunization, serum was collected
118 and frozen until use. The mice were sacrificed 2 weeks after the last immunization and the
119 spleens were harvested for further analyses.

120 2.5. *ELISAs*

121 ELISAs were performed to measure the total IgG antibody responses to EBOV-NP protein by
122 the mice. Briefly, 96-well microplates (Corning, USA) were pre-coated with recombinant

123 Zaire EBOV-NP protein (Sino biological, China) by an overnight incubation at 4°C. The
124 plates then were washed four times with PBS containing 0.1% Tween 20 and blocked for 1 h
125 at room temperature with PBS containing 3% fetal bovine serum. Serial dilutions of serum
126 (1:10, 1:40, 1:160, 1:640, 1:2560, 1:10,240 and 1:40,960) in PBS containing 3% fetal bovine
127 serum were added to the wells. The plates were incubated for 1 h at room temperature,
128 washed, and incubated 1 h at room temperature with a HRP-conjugated goat anti-mouse IgG
129 (Southern Biotech, Birmingham). The ELISA was performed according to the manufacturer's
130 instructions. The titers in each mouse were determined on the basis of the plots and the titers
131 of the mouse groups were expressed as geometric mean \log_{10} titers.

132 *2.6. Computational prediction of candidate epitopes in EBOV-NP and synthesis of the*
133 *peptides*

134 The potential HLA-A11-binding epitopes in the EBOV-NP protein were predicted by using
135 NetMHC[27], ProPred-I[28], and SYFPEITHI[29]. The ten candidate epitopes were
136 synthesized commercially (GenScript, China) and then purified to >95% purity. All peptides
137 were dissolved with sterile phosphate-buffered saline (PBS) to a concentration of 200 g/ml.
138 They were then frozen at -80°C until use.

139 *2.7. ELISPOT assay*

140 Mice were sacrificed 2 weeks after the third immunization. The spleens were pushed through
141 a 70- μ m cell strainer in complete RPMI 1640 medium (RPMI 1640 with 10% FBS,

142 penicillin/streptomycin, and L-glutamine) to form a single cell suspension. The splenocytes
143 were harvested and the red blood cells were removed with ACK lysing buffer. After washing,
144 the cells were counted and diluted to 10^7 cells/ml. The enzyme-linked immunospot (ELISPOT)
145 assay was performed to detect the interferon- γ (IFN- γ)-secreting antigen-stimulated
146 splenocytes from the immunized mice: this is a measure of CTL activation. IFN- γ ELISPOT
147 was performed by using a commercially available kit according to the manufacturer's
148 instructions (BD Biosciences, CA). Briefly, an ELISPOT plate was pre-coated with the
149 purified anti-mouse IFN- γ antibody overnight at 4°C. After blocked, the murine splenocytes
150 were dispensed at 5×10^5 cells per well. Each peptide was diluted to 10 μ g/ml and added 50 μ l
151 to each well to stimulate the cells. After 48 h stimulation, biotinylated anti-IFN- γ mAb was
152 diluted and incubated for another 2 h at room temperature. Diluted enzyme conjugate was
153 then added and incubated for 1 h at room temperature. Then, ACE substrate solution was
154 added and followed by the stop substrate. Spots were counted by using an automatic
155 ELISPOT reader (Cellular Technology Ltd, USA).

156 2.8. Statistical analysis

157 All statistical analyses were performed by using GraphPad Prism version 5.0. Unpaired
158 Student's two-tailed *t*-tests were used to compare the treatment groups and calculate the *p*
159 values. *P* values of <0.05 were considered to indicate statistically significant differences.

160

161 **3. Results**

162 *3.1 Construction and verification of Ad5-EBOV-NP*

163 The recombinant adenoviral vector system has been widely used in the development of
164 vaccines [30-32]. We cloned and sequenced the NP of the Ebola-Makona strain and used it to
165 construct the recombinant adenovirus vector EBOV-NP (Fig. 1A). The green fluorescent
166 protein marker in the shuttle vector pAdTrack-CMV helped to track the expression of Ad5-
167 EBOV-NP in infected AD-293 cells. Moreover, 48 h after infection, the AD-293 cells started
168 to exhibit the cytopathic effect of the infection with Ad5-EBOV-NP and began to detach from
169 the surface of the flasks (Fig. 1B). The expression of NP was also identified by western blot
170 analysis. These data show that EBOV-NP protein was effectively expressed in this system
171 (Fig. 1C).

172 *3.2 Immunization of HLA-A11/DR1 transgenic mice with Ad5-EBOV-NP*

173 To test whether Ad5-EBOV-NP immunization can raise immune responses in HLA-A11/DR1
174 transgenic mice, these mice and their wild type C57BL/6 controls were given three i.m.
175 injections of Ad5-EBOV-NP or Ad5 at intervals of 3 weeks. The sera were collected 10 days
176 after each immunization. ELISAs showed that the EBOV-NP-immunized transgenic mice
177 started raising detectable IgG antibody responses to EBOV-NP around the third vaccination.
178 These antibodies were already detectable in the EBOV-NP-immunized wild-type mice after

179 the second immunization. However, ten days after the third immunization, the EBOV-NP-
180 specific IgG antibody levels of the EBOV-NP-immunized wild-type and transgenic mice were
181 similarly high (as indicated by the OD₄₅₀ values) and significantly different from the blank
182 ELISA control (Fig. 2A). Indeed, when the anti-EBOV-NP levels were expressed as geometric
183 mean log₁₀ EBOV-NP-specific IgG titers, the EBOV-NP-immunized strains had similar titers
184 after the final immunization. The titers of the EBOV-NP-immunized transgenic mice were
185 significantly greater than the titers of the Ad5-immunized transgenic mice (Fig. 2B). Thus,
186 HLA-A11/DR1 mice immunized three times with Ad5-EBOV-NP produced similar levels of
187 anti-EBOV-NP antibodies as the wild-type mice.

188 *3.3 Prediction of EBOV-NP epitopes*

189 Since the HLA-A11/DR1 double transgenic mice produced a robust and specific IgG antibody
190 after Ad5-EBOV-NP vaccination, we used prediction programs available on the internet to
191 predict the HLA-A11-restricted epitopes in the EBOV-NP protein from the Ebola-Makona
192 strain. On the basis of the degree of predicted HLA-A11 binding and conventional
193 hydrophobicity values (low values indicate good solubility in PBS), ten epitopes were
194 selected for screening in our HLA-A11/DR1 transgenic mouse model (Table 1).

195 *3.4 Identification of HLA-A11-restricted CD8⁺ T-cell epitopes in EBOV-NP*

196 To determine whether the predicted HLA-A11-binding EBOV-NP epitopes do bind to this

197 HLA and induce T-cell responses, the HLA-A11/DR1 transgenic mice were immunized with
198 Ad5-EBOV-NP or Ad5. The primed splenocytes were harvested 2 weeks after the third
199 immunization and the T-cell reactivity to each peptide was analyzed by IFN- γ ELISPOT
200 assays. Compared to the responses of the splenocytes from the Ad5-immunized transgenic
201 mice, six of the ten peptides, namely, GR-9, VR-9, QR-9, EK-9, PK-9, and RK-9, induced
202 significant IFN- γ production by the splenocytes from the Ad5-EBOV-NP-immunized mice: on
203 average, 5×10^5 splenocytes from the Ad5-EBOV-NP-immunized transgenic mice produced
204 78, 79, 99, 88, 89, and 88 spots to GR-9, VR-9, QR-9, EK-9, PK-9, and RK-9, respectively,
205 while the splenocytes from the Ad5-immunized transgenic mice produced 16, 16, 18, 18, 17,
206 and 17 spots, respectively. The remaining four peptides did not induce a response (Fig. 3).

207 To confirm that the six epitopes are restricted by HLA-A11 and can serve as T-cell
208 epitopes, the HLA-A11/DR1 and C57BL/6 mice were immunized three times with Ad5-
209 EBOV-NP and the splenocytes were harvested 2 weeks after the third immunization and
210 subjected to ELISPOT assays with the six peptides. All of the peptides except QR-9 induced
211 strong CD8⁺ T-cell responses by the Ad5-EBOV-NP-immunized transgenic mice: on average,
212 5×10^5 cells generated 78, 78, 88, 89, and 88 spots to GR-9, VR-9, EK-9, PK-9, and RK-9,
213 respectively. By contrast, the splenocytes from the Ad5-EBOV-NP-immunized wild-type mice
214 produced 4, 6, 4, 5, and 4 spots, respectively (Fig. 4). When HLA-A11/DR1 transgenic mice
215 were immunized with Ad5-EBOV-NP or Ad5, we found the peptide QR-9 could induce IFN- γ

216 production by the splenocytes from the Ad5-EBOV-NP immunized mice than those from the
217 immunization of Ad5. However, when compared with that in wild-type C57BL/6 mice, no
218 significant difference of IFN- γ induced in the HLA-A11/DR1 double transgenic mice, which
219 indicated that QR-9 was not specific HLA-A11-restricted epitope in the text of EBOV-NP
220 protein. Thus, these experiments with HLA-A11/DR1 mice identified five novel HLA-A11-
221 restricted CTL epitopes in the EBOV-NP protein.

222

223 4. Discussion

224 This study identified five HLA-A11-restricted CTL epitopes in the NP protein of the
225 EBOV strain that was responsible for the 2014 epidemic. Thus, these epitopes are candidate
226 EBOV vaccine targets.

227 We chose the NP of EBOV for our screening studies because although most EBOV
228 vaccine studies have investigated the immune responses to EBOV glycoprotein, which
229 induces protective responses [9, 33-38], EBOV-NP also generates protective responses and is
230 therefore also a target for vaccination [39].

231 We confirmed that EBOV-NP induces humoral responses in our study: when we
232 immunized the HLA-A11/DR1 transgenic mice and the wild-type controls three times at 3-
233 week intervals with Ad5-EBOV-NP, we found that both strains had high serum titers of anti-
234 NP IgG ten days after the final immunization (Fig. 2). However, of particular interest to us

235 were the CD8⁺ and CD4⁺ T-cell responses to EBOV-NP because several studies show they
236 play a key role in protection from EBOV infection [6-8]. Several CD8⁺ CTL epitopes in
237 EBOV-NP have been identified to date [8, 40]. These include several EBOV-NP-specific
238 CD8⁺ T-cell epitopes that are restricted by H-2 in mouse models. For example, Simmons *et al.*
239 [41] identified one H-2^d and two H-2^b-restricted epitopes in EBOV-NP. Moreover, Wilson and
240 Hart found a H-2^b class I-restricted epitope that protects wild-type C57BL/6 mice from lethal
241 EBOV infection [6]. Since specific sequences may serve as T-cell epitopes in mice but not
242 humans, several studies have also sought to identify EBOV peptides that are specific for
243 human class I alleles. Sundar *et al.* [15] found three EBOV-NP peptides (FLSFASLFL,
244 RLMRTNFLI, and KLTEAITAA) that are restricted by HLA-A2 and then showed that all
245 three induced CTL responses in HLA-A2.1 transgenic mice. Moreover, Lim and Khan
246 showed that there are multiple sequences in EBOV-NP that are predicted to bind to HLA-A2
247 and HLA-B7 and that could serve as candidate vaccine targets. They also identified one
248 EBOV-NP peptide, QTNAMVTLR, which was predicted to be restricted to HLA-A3 [18].

249 The HLA is the most polymorphic gene system in the human genome. These molecules
250 play an integral role in antigen presentation and adaptive immune responses. HLA-A11 is a
251 particularly prevalent allele in the Chinese population: more than 50% of the individuals
252 living in China carry it [20, 42]. To ensure that the Chinese population will be protected by an
253 EBOV vaccine, it is necessary to identify the HLA-A11-specific CTL epitopes in the EBOV.

254 To facilitate the design of epitope-based vaccines that will protect the population in China, we
255 generated HLA-A11/DR1 double-transgenic mice for epitope screening [23]. Such MHC
256 class I or MHC class II transgenic mice have been used previously for HLA-restricted epitope
257 screening and candidate vaccines [15, 43]. Our mice lack murine H-2 molecules and bear both
258 MHC-I and MHC-II molecules because protective CTL responses against lethal infectious
259 pathogens such as EBOV require collaboration between cytotoxic CD8⁺ T-cells and T-helper
260 cells. Our HLA double-transgenic mice have been used previously to identify HLA -restricted
261 epitopes [44, 45]. The fact that the present study showed that immunization with Ad5-EBOV-
262 NP generated high serum anti-NP IgG antibody titers in our HLA-A11/DR1 transgenic mice
263 further supports the notion that these mice can be used for screening HLA-A11-restricted CTL
264 epitopes. HLA-A11 allele is a relatively dominant MHC-I allele phenotype among Chinese.
265 CTL response had been demonstrated to play an important role in defense against EBOV
266 infection. So our study focused on the screening of candidate HLA-A11-restricted epitopes
267 against EBOV-NP protein. Furthermore, the helper T cells (Th) have been studied to play an
268 important role in preventing pathogenic infections and contribute to effective humoral and
269 cellular immunity. The HLA-A11/DR1 transgenic mice model integrated both the HLA class
270 I- and class II- alleles, has been demonstrated to have effective immune response stimulated by
271 other antigens [23].

272 The ELISPOT assay can identify antigen-specific T cells at the single-cell level without

273 long-term culture *in vitro* [46, 47]. It is an important method for identifying novel epitopes. In
274 our study, we identified putative HLA-A11-restricted CD8⁺ T-cell epitopes in the EBOV-NP
275 by using predictive algorithms and then synthesized the ten most highly ranking peptides
276 (Table 1) and used them as recall antigens in ELISPOT with splenocytes from Ad5-EBOV-
277 NP- and Ad5-immunized HLA-A11/DR1 mice. The Ad5-EBOV-NP-immunized, but not Ad5-
278 immunized transgenic mice generated significant cellular immune responses (IFN- γ secretion)
279 to six peptides, namely, GR-9, VR-9, QR-9, EK-9, PK-9, and RK-9 (Fig. 3). Furthermore,
280 when the transgenic and wild-type mice were immunized with Ad5-EBOV-NP, the transgenic
281 mice, but not the wild-type mice, responded strongly in IFN- γ ELISPOT to five of the six
282 peptides, namely, GR-9, VR-9, EK-9, PK-9, and RK-9 (Fig. 4). To our knowledge, this is the
283 first report describing EBOV-NP peptides that are both HLA-A11-restricted and induce T
284 cells to secrete IFN- γ . The identification of these promising vaccine candidate epitopes will
285 facilitate the development of epitope-based vaccines against EBOV infection.

286

287 **Conflicts of interests**

288 The authors have no conflicts of interest to declare.

289

290 **Acknowledgements**

291 This study was supported by grants from the National Project of Infectious Diseases (No.
292 2017ZX10304402-003), the National Key Research and Development Program of China (No.

293 2016YFC1202903), the National Key Plan for Scientific Research and Development of China
294 (No.2016YFD0500306), National Science and Technology Support Program
295 (2015BAI08B03).

296

297 **References**

298 [1] Wilson JA, Bosio CM, Hart MK. Ebola virus: the search for vaccines and treatments. *Cell Mol Life Sci*
299 2001;58:1826-41.

300 [2] Wauquier N, Becquart P, Padilla C, Baize S, Leroy EM. Human fatal zaire ebola virus infection is associated
301 with an aberrant innate immunity and with massive lymphocyte apoptosis. *PLoS Negl Trop Dis* 2010;4:e837.

302 [3] Baize S, Pannetier D, Oestereich L, Rieger T, Koivogui L, Magassouba N, et al. Emergence of Zaire Ebola
303 virus disease in Guinea. *N Engl J Med* 2014;371:1418-25.

304 [4] WHO Ebola Response Team, Aylward B, Barboza P, Bawo L, Bertherat E, Bilivogui P, et al. Ebola virus
305 disease in West Africa--the first 9 months of the epidemic and forward projections. *N Engl J Med*
306 2014;371:1481-95.

307 [5] WHO Ebola Response Team, Agua-Agum J, Allegranzi B, Ariyaratnam A, Aylward R, Blake IM, et al. After
308 Ebola in West Africa--unpredictable risks, preventable epidemics. *N Engl J Med* 2016;375:587-96.

309 [6] Wilson JA, Hart MK. Protection from Ebola virus mediated by cytotoxic T lymphocytes specific for the viral
310 nucleoprotein. *J Virol* 2001;75:2660-4.

311 [7] Rao M, Bray M, Alving CR, Jahrling P, Matyas GR. Induction of immune responses in mice and monkeys to
312 Ebola virus after immunization with liposome-encapsulated irradiated Ebola virus: protection in mice requires

- 313 CD4(+) T cells. *J Virol* 2002;76:9176-85.
- 314 [8] Warfield KL, Olinger G, Deal EM, Swenson DL, Bailey M, Negley DL, et al. Induction of humoral and
315 CD8+ T cell responses are required for protection against lethal Ebola virus infection. *J Immunol*
316 2005;175:1184-91.
- 317 [9] Sullivan NJ, Geisbert TW, Geisbert JB, Xu L, Yang ZY, Roederer M, et al. Accelerated vaccination for Ebola
318 virus haemorrhagic fever in non-human primates. *Nature* 2003;424:681-4.
- 319 [10] Harrison GB, Shakes TR, Robinson CM, Lawrence SB, Heath DD, Dempster RP, et al. Duration of
320 immunity, efficacy and safety in sheep of a recombinant *Taenia ovis* vaccine formulated with saponin or selected
321 adjuvants. *Vet Immunol Immunopathol* 1999;70:161-72.
- 322 [11] Price DA, Meier UC, Klenerman P, Purbhoo MA, Phillips RE, Sewell AK. The influence of antigenic
323 variation on cytotoxic T lymphocyte responses in HIV-1 infection. *J Mol Med (Berl)* 1998;76:699-708.
- 324 [12] Zivny J, DeFronzo M, Jarry W, Jameson J, Cruz J, Ennis FA, et al. Partial agonist effect influences the CTL
325 response to a heterologous dengue virus serotype. *J Immunol* 1999;163:2754-60.
- 326 [13] Hasan MA, Hossain M, Alam MJ. A computational assay to design an epitope-based Peptide vaccine
327 against saint louis encephalitis virus. *Bioinform Biol Insights* 2013;7:347-55.
- 328 [14] Oany AR, Emran AA, Jyoti TP. Design of an epitope-based peptide vaccine against spike protein of human
329 coronavirus: an in silico approach. *Drug Des Devel Ther* 2014;8:1139-49.
- 330 [15] Sundar K, Boesen A, Coico R. Computational prediction and identification of HLA-A2.1-specific Ebola
331 virus CTL epitopes. *Virology* 2007;360:257-63.

- 332 [16] Sullivan NJ, Hensley L, Asiedu C, Geisbert TW, Stanley D, Johnson J, et al. CD8⁺ cellular immunity
333 mediates rAd5 vaccine protection against Ebola virus infection of nonhuman primates. *Nat Med* 2011;17:1128-
334 31.
- 335 [17] Dikhit MR, Kumar S, Vijaymahantesh, Sahoo BR, Mansuri R, Amit A, et al. Computational elucidation of
336 potential antigenic CTL epitopes in Ebola virus. *Infect Genet Evol* 2015;36:369-75.
- 337 [18] Lim WC, Khan AM. Mapping HLA-A2, -A3 and -B7 supertype-restricted T-cell epitopes in the ebolavirus
338 proteome. *BMC Genomics* 2018;19:42.
- 339 [19] Vita R, Overton JA, Greenbaum JA, Ponomarenko J, Clark JD, Cantrell JR, et al. The immune epitope
340 database (IEDB) 3.0. *Nucleic Acids Res* 2015;43:D405-12.
- 341 [20] Lee TD, Zhao TM, Mickey R, Sun YP, Lee G, Song CX, et al. The polymorphism of HLA antigens in the
342 Chinese. *Tissue Antigens* 1988;32:188-208.
- 343 [21] Sette A, Sidney J. Nine major HLA class I supertypes account for the vast preponderance of HLA-A and -B
344 polymorphism. *Immunogenetics* 1999;50:201-12.
- 345 [22] Zhou XY, Zhu FM, Li JP, Mao W, Zhang DM, Liu ML, et al. High-Resolution Analyses of Human
346 Leukocyte Antigens Allele and Haplotype Frequencies Based on 169,995 Volunteers from the China Bone
347 Marrow Donor Registry Program. *PLoS One* 2015;10:e0139485.
- 348 [23] Zeng Y, Gao T, Zhao G, Jiang Y, Yang Y, Yu H, et al. Generation of human MHC (HLA-A11/DR1)
349 transgenic mice for vaccine evaluation. *Hum Vaccin Immunother* 2016;12:829-36.
- 350 [24] Alexander J, Oseroff C, Sidney J, Wentworth P, Keogh E, Hermanson G, et al. Derivation of HLA-A11/Kb

- 351 transgenic mice: functional CTL repertoire and recognition of human A11-restricted CTL epitopes. *J Immunol*
352 1997;159:4753-61.
- 353 [25] Pascolo S, Bervas N, Ure JM, Smith AG, Lemonnier FA, Perarnau B. HLA-A2.1-restricted education and
354 cytolytic activity of CD8(+) T lymphocytes from beta2 microglobulin (beta2m) HLA-A2.1 monochain
355 transgenic H-2Db beta2m double knockout mice. *J Exp Med* 1997;185:2043-51.
- 356 [26] Pajot A, Pancre V, Fazilleau N, Michel ML, Angyalosi G, Ojcius DM, et al. Comparison of HLA-DR1-
357 restricted T cell response induced in HLA-DR1 transgenic mice deficient for murine MHC class II and HLA-
358 DR1 transgenic mice expressing endogenous murine MHC class II molecules. *Int Immunol* 2004;16:1275-82.
- 359 [27] Jurtz V, Paul S, Andreatta M, Marcatili P, Peters B, Nielsen M. NetMHCpan-4.0: Improved Peptide-MHC
360 Class I Interaction Predictions Integrating Eluted Ligand and Peptide Binding Affinity Data. *J Immunol*
361 2017;199:3360-8.
- 362 [28] Singh H, Raghava GP. ProPred1: prediction of promiscuous MHC Class-I binding sites. *Bioinformatics*
363 2003;19:1009-14.
- 364 [29] Rammensee H, Bachmann J, Emmerich NP, Bachor OA, Stevanovic S. SYFPEITHI: database for MHC
365 ligands and peptide motifs. *Immunogenetics* 1999;50:213-9.
- 366 [30] Ledgerwood JE, Costner P, Desai N, Holman L, Enama ME, Yamshchikov G, et al. A replication defective
367 recombinant Ad5 vaccine expressing Ebola virus GP is safe and immunogenic in healthy adults. *Vaccine*
368 2010;29:304-13.
- 369 [31] Lobanova LM, Baig TT, Tikoo SK, Zakhartchouk AN. Mucosal adenovirus-vectored vaccine for measles.

- 370 Vaccine 2010;28:7613-9.
- 371 [32] Tutykhina IL, Logunov DY, Shcherbinin DN, Shmarov MM, Tukhvatulin AI, Naroditsky BS, et al.
- 372 Development of adenoviral vector-based mucosal vaccine against influenza. *J Mol Med (Berl)* 2011;89:331-41.
- 373 [33] Sullivan NJ, Sanchez A, Rollin PE, Yang ZY, Nabel GJ. Development of a preventive vaccine for Ebola
- 374 virus infection in primates. *Nature* 2000;408:605-9.
- 375 [34] Sullivan NJ, Geisbert TW, Geisbert JB, Shedlock DJ, Xu L, Lamoreaux L, et al. Immune protection of
- 376 nonhuman primates against Ebola virus with single low-dose adenovirus vectors encoding modified GPs. *PLoS*
- 377 *Med* 2006;3:e177.
- 378 [35] Henao-Restrepo AM, Longini IM, Egger M, Dean NE, Edmunds WJ, Camacho A, et al. Efficacy and
- 379 effectiveness of an rVSV-vectored vaccine expressing Ebola surface glycoprotein: interim results from the
- 380 Guinea ring vaccination cluster-randomised trial. *Lancet* 2015;386:857-66.
- 381 [36] Zhu FC, Hou LH, Li JX, Wu SP, Liu P, Zhang GR, et al. Safety and immunogenicity of a novel recombinant
- 382 adenovirus type-5 vector-based Ebola vaccine in healthy adults in China: preliminary report of a randomised,
- 383 double-blind, placebo-controlled, phase 1 trial. *Lancet* 2015;385:2272-9.
- 384 [37] Tapia MD, Sow SO, Lyke KE, Haidara FC, Diallo F, Doumbia M, et al. Use of ChAd3-EBO-Z Ebola virus
- 385 vaccine in Malian and US adults, and boosting of Malian adults with MVA-BN-Filo: a phase 1, single-blind,
- 386 randomised trial, a phase 1b, open-label and double-blind, dose-escalation trial, and a nested, randomised,
- 387 double-blind, placebo-controlled trial. *Lancet Infect Dis* 2016;16:31-42.
- 388 [38] Henao-Restrepo AM, Camacho A, Longini IM, Watson CH, Edmunds WJ, Egger M, et al. Efficacy and

- 389 effectiveness of an rVSV-vectored vaccine in preventing Ebola virus disease: final results from the Guinea ring
390 vaccination, open-label, cluster-randomised trial (Ebola Ca Suffit!). *Lancet* 2017;389:505-18.
- 391 [39] Tsuda Y, Caposio P, Parkins CJ, Botto S, Messaoudi I, Cicin-Sain L, et al. A replicating cytomegalovirus-
392 based vaccine encoding a single Ebola virus nucleoprotein CTL epitope confers protection against Ebola virus.
393 *PLoS Negl Trop Dis* 2011;5:e1275.
- 394 [40] Bounds CE, Terry FE, Moise L, Hannaman D, Martin WD, De Groot AS, et al. An immunoinformatics-
395 derived DNA vaccine encoding human class II T cell epitopes of Ebola virus, Sudan virus, and Venezuelan
396 equine encephalitis virus is immunogenic in HLA transgenic mice. *Hum Vaccin Immunother* 2017;13:2824-36.
- 397 [41] Olinger GG, Bailey MA, Dye JM, Bakken R, Kuehne A, Kondig J, et al. Protective cytotoxic T-cell
398 responses induced by venezuelan equine encephalitis virus replicons expressing Ebola virus proteins. *J Virol*
399 2005;79:14189-96.
- 400 [42] Simmons G, Lee A, Rennekamp AJ, Fan X, Bates P, Shen H. Identification of murine T-cell epitopes in
401 Ebola virus nucleoprotein. *Virology* 2004;318:224-30.
- 402 [43] Lin M, Chu CC, Chang SL, Lee HL, Loo JH, Akaza T, et al. The origin of Minnan and Hakka, the so-called
403 "Taiwanese", inferred by HLA study. *Tissue Antigens* 2001;57:192-9.
- 404 [44] Pajot A, Michel ML, Fazilleau N, Pancre V, Aurialt C, Ojcius DM, et al. A mouse model of human
405 adaptive immune functions: HLA-A2.1/HLA-DR1-transgenic H-2 class I/class II-knockout mice. *Eur J*
406 *Immunol* 2004;34:3060-9.
- 407 [45] Ru Z, Xiao W, Pajot A, Kou Z, Sun S, Maillere B, et al. Development of a humanized HLA-A2.1/DP4

408 transgenic mouse model and the use of this model to map HLA-DP4-restricted epitopes of HBV envelope
409 protein. PLoS One 2012;7:e32247.

410 [46] Anthony DD, Lehmann PV. T-cell epitope mapping using the ELISPOT approach. Methods 2003;29:260-9.

411 [47] McMurry JA, Kimball S, Lee JH, Rivera D, Martin W, Weiner DB, et al. Epitope-driven TB vaccine
412 development: a streamlined approach using immuno-informatics, ELISpot assays, and HLA transgenic mice.
413 Curr Mol Med 2007;7:351-68.

414

415

416 **Figure Legends**

417 **Figure 1. Construction and verification of Ad5-EBOV-NP.** (A) Schematic depiction of the
418 recombinant adenovirus type-5 vector-based Ebola virus (EBOV) vaccine that expresses the
419 EBOV nucleoprotein (NP). (B) Fluorescence microscope analysis of AD-293 cells that were
420 infected with recombinant Ad5-EBOV-NP. This representative image was taken 48 h after
421 infection. (C) Western blot analysis of EBOV-NP protein expression collected from the cell
422 lysis in AD-293 cells after infection with Ad5-EBOV-NP or Ad5 infection. As a control,
423 uninfected cells were also subjected to analysis.

424 **Figure 2. Specific antibodies against Ebola virus nucleoprotein (EBOV-NP) after**
425 **immunization with Ad5-EBOV-NP.** (A) HLA-A11/DR1 and C57BL/6 (wild type) mice (5
426 mice per group) were immunized three times with Ad5-EBOV-NP or Ad5 and serum was
427 obtained ten days after each immunization. ELISAs were performed to measure the EBOV-
428 NP-specific IgG antibodies in the serum at the dilution 1 : 10. (B) The serum EBOV-NP-
429 specific IgG titers of the mice in (A) were expressed as \log_{10} geometric mean titers (GMT)
430 and the transgenic mouse groups were compared by independent Student's *t*-test. *** $p < 0.001$.
431 The bars indicate standard deviations of the mean.

432 **Figure 3. Screening for T-cell epitopes in Ebola virus nucleoprotein (EBOV-NP) by using**
433 **HLA-A11/DR1 mice.** (A) The transgenic mice (5 mice per group) were immunized three

434 times with Ad5-EBOV-NP or Ad5 and their splenocytes were prepared 2 weeks after the third
435 immunization. The cells were cultured with ten predicted HLA-A11-restricted EBOV-NP
436 epitopes and the IFN- γ production by cytotoxic T lymphocytes was examined by using
437 ELISPOT. The spot numbers are expressed as mean \pm standard deviation. The mouse groups
438 were compared by independent Student's *t*-test. * p <0.05. (B) Representative spots of the IFN-
439 γ -secreting T cells.

440 **Figure 4. Assessment of the ability of the HLA-A11-restricted epitopes in Ebola virus**
441 **nucleoprotein (EBOV-NP) to serve as T-cell epitopes.** (A) The HLA-A11/DR1 transgenic
442 and C57BL/6 (wild type) mice (5 mice per group) were immunized three times with Ad5-
443 EBOV-NP and their splenocytes were prepared 2 weeks after the third immunization. The
444 cells were cultured with the six HLA-A11-restricted EBOV-NP epitopes identified in Fig. 3
445 and the IFN- γ production by cytotoxic T lymphocytes was examined by using ELISPOT. The
446 spot numbers are expressed as mean \pm standard deviation. The mouse groups were compared
447 by independent Student's *t*-test. * p <0.05. (B) Representative spots of the IFN- γ -secreting T
448 cells.

449

450 **Tables**

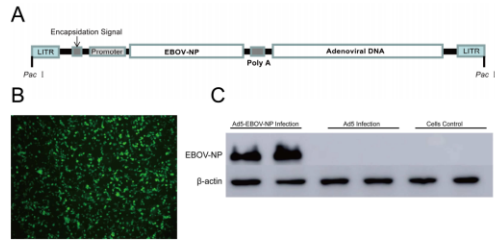
451 **Table 1. Amino-acid sequences of the predicted HLA-A11-restricted Ebola virus**
452 **nucleoprotein epitopes**

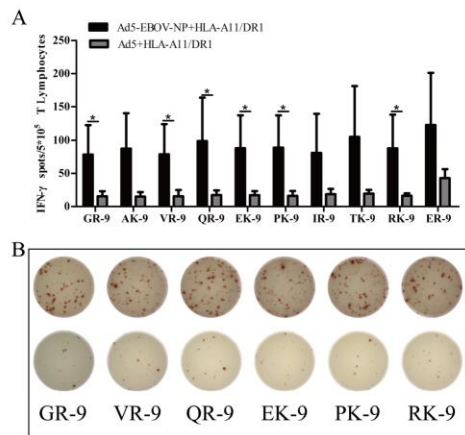
453

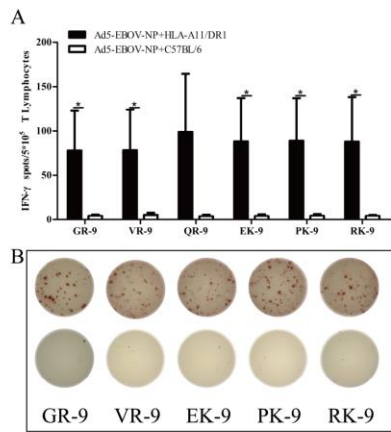
ACCEPTED MANUSCRIPT

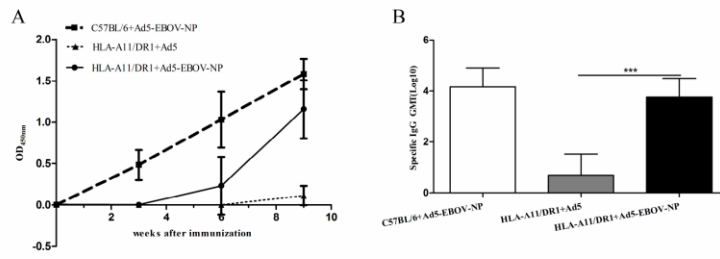
| No. | Name | Sequence | Position | Legth |
|------------|------|-----------|----------|-------|
| EBOV-N-P1 | GR-9 | GVRLHPLAR | 262 | 9 |
| EBOV-N-P2 | AK-9 | AVSSGRNIK | 123 | 9 |
| EBOV-N-P3 | VR-9 | VSSGRNIKR | 124 | 9 |
| EBOV-N-P4 | QR-9 | QTNAMVTLR | 390 | 9 |
| EBOV-N-P5 | EK-9 | EVKKCDGVK | 107 | 9 |
| EBOV-N-P6 | PK-9 | PVYRDHSEK | 609 | 9 |
| EBOV-N-P7 | IR-9 | ISNSVAQAR | 232 | 9 |
| EBOV-N-P8 | TK-9 | TLRKERLAK | 396 | 9 |
| EBOV-N-P9 | RK-9 | RSTKGGQQK | 501 | 9 |
| EBOV-N-P10 | ER-9 | ESDDEEQDR | 586 | 9 |

ACCEPTED MANUS









GENERAL DISCUSSION

CHAPTER 1

Creation of an immuno-deficient HLA-transgenic mouse (HUMAMICE) and functional validation of human immunity after transfer of HLA-matched human cells

1. The development history of immuno-deficient mouse models

1.1 The initial establishment of immuno-deficient mouse models

Animal models play a critical role in medical science researches, such as the pathogenic mechanism of tumors, immunological diseases and infectious diseases, treatment, transplantation, the invention and evaluation of drugs and vaccines. While traditional animal models need to be genetically optimized and modified to fit the demand of preclinical trials and scientific researches.

Immuno-deficient mice are capable to support a relative high level of transplantation of human cells/tissues and have been widely used in preclinical trials. During the efforts of past three decades, immuno-deficient mice such as NSG (NOD-SCID-IL-2R γ C^{null})[63], NOG, NRG (NOD-Rag 1^{null}/IL-2R γ C^{null}), BRG (BALB/c-Rag 2^{null} IL-2Rc^{null}) mice have become genetically optimized and widely popularized worldwide. Among them, NSG (NOD-SCID-IL-2R γ C^{null}) severe combined immuno-deficient mice[65] were most commonly worldwide, which resulted in the deletion of IL-2 receptor γ chain (IL-2 γ) on the background of NOD/SCID mice, lead to the lack of B cells, T cells and NK cells, the loss of adaptive immune responses, and partial depletion of innate immune responses, which could support an ideal higher level of humanized engraftment (including both human HSC and PBMC transplantation).

With the continuous advancement and rapid development of modern medical, science and intelligent technology, the research on pathogenic mechanism of diseases and human immune systems have gradually deepened. In this process, animal models had become an essential tool which are indispensable for preclinical studies on new drugs and vaccines. However, current small animal models including transgenic mouse

models still cannot fully and truly simulate and replicate human immune responses in either healthy state or pathological state, due to the species differences among human beings and other species.

Due to the lack of appropriate small animal models capable of being infected by specific virus, immuno-deficient mouse models play crucial roles in human disease researches. However, these immuno-deficient mice still have some defects and limitations which need to be overcome [68, 69]. One of the most lethal defects is that susceptible to GvHD [70, 78] after human cells/tissues transplantation. The symptoms of GvHD included the loss of weight (weight loss more than 15% of the original body weight), diarrhea, hair loss, inflammatory cell infiltration (liver, intestine, skin, etc.) and mice die 20-25 days after transplantation. Hence, it is necessary to avoid the occurrence of these GvHD complications when applied these immuno-deficient mouse models to the study of human immune system.

1.2 The optimization of immuno-deficient mouse models

Immuno-deficient animal models are animals that have inherited mutations or acquired factors that resulted in the underdevelopment or damage of a component of the adaptive immune system or/and innate immune system, lead to the development, differentiation, proliferation or metabolic abnormalities of immune cells, finally to immune dysfunction. There are various types of immuno-deficient animal models classify by whether the deficiency concerns of T cells defects, B cells defects, NK cell defects or combined immuno-deficiency. Grist discovered that nude mice without surface hairs and congenital thymic dysplasia in non-inbred strains in 1962, which lack of T lymphocytes function [129]. Rygaard and Ffiis [130] successfully transplanted human colon adenocarcinoma cells into nude mice, which set a precedent for the application of immuno-deficient animal models.

The sex-linked immuno-deficient mice (CBA/N mice), which gene symbol is *xid* located on sex chromosome, and defective of B lymphocytes [131]. CBA/N mice represent ideal models for the study of the occurrence, function and heterogeneity of B lymphocytes. NOD/SCID mice (non-obese diabetic/severe combined immuno-

deficiency) is a mutation mouse strain with congenital associated T and B lymphocytes deficiency [14]. It can be used to study the mechanism of transplantation and immunological rejection, the differentiation and function of macrophages, other natural immune cells and immune helper cells. NOD/SCID mice are also one of the most widely used immuno-deficiency mouse models in the field of tumor immunology worldwide, which is the “golden rule” to evaluate human stem cell transplantation[14]. With the absence of T and B lymphocytes in SCID mice, the function of NK cells is also lost in NOD/SCID mice[66, 67]. In both NSG mice [16] (NOD-scid IL-2R γ^{null} , which was established by Jackson Laboratory) and NOG mice [15] (NOD/SCID/ $\gamma\text{c}^{\text{null}}$, which was established by Japanese team), the gene encoding IL-2 receptor gamma chain (IL-2 γc) is knocked out. Yahata showed that T lymphocytes were reconstituted after the transplantation of human HSC into NOD/SCID/IL-2 $\gamma\text{c}^{\text{null}}$ [132]. Hiramatsu transplanted human hematopoietic stem/progenitor cells (CD34 $^{+}$) derived from umbilical cord blood (UCB) into NOD/SCID/ $\gamma\text{c}^{\text{null}}$ mice. Following by the transplantation, mature T, B and NK cells were detected in the spleen and bone marrow of the recipients, the specific IgM, IgA and IgG antibodies and CTL immune responses could be generated after the stimulation of phytohemagglutinin (PHA).

Human HSCs differentiated into all lineage blood cells, including T lymphocytes, B cells, DC cells, red blood cells (RBCs) and platelets, and produce specific mucosal immune responses. In the construction strategy of B-NSG mice, PrkDc and IL-2 γ are knocked out by CRISPR/Cas9 gene-editing technique based on NOD mice.

B-NSG mice do not have mature T and B lymphocytes, meanwhile NK cells are not functional and lose the ability of transmitting cytokine signaling. Therefore, B-NSG mice could support a much higher level of human HSC (PBMC) transplantation, which provided a more suitable environment for the growth of human cells. The occurrence of GvHD after transplantation is even weaker, and B-NSG mice is recognized as the mouse model with the highest degree of immuno-deficiency and the most suitable model for human cell/tissue transplantation at present.

1.3 The comparison between hu-SRC-SCID and hu-PBL-SCID mice

The greatest advantage of human HSC transplantation immuno-deficient mouse model (hu-SRC-SCID) is that progenitors could undergo the positive and negative selection in mouse thymus and differentiate into T and B lymphocytes after human HSC transplantation, which had applied to the study of lineage hierarchy development of human stem cells and the mechanisms of human immune system[80].

While, human PBMC transplanted immuno-deficient mice (hu-PBL-SCID) are isolated from the mononuclear cells of human peripheral blood or spleen. As the lymphocytes before transplantation are already mature, they could only support short-term (within 4 weeks) analysis of human immune responses, which applied to the short-term experiments such as immune disorders, the effects of leakage immune responses and transplant immunological rejection.

Because of the difficulties in the acquisition of neonatal umbilical cord blood (UCB) and the restriction of ethical issues[10] in the initial stage of our experiment. We regarded human peripheral blood as the sources of transplantation which was much more easily accessible. Under the condition of donors' knowledge to sign the letter of informed consent, human PBMCs were isolated for the transplantation of HUMAMICE. The occurrence of Graft-versus-Host Disease (GvHD) was the most important problem which cannot be ignored and need to be overcome during the transplantation. However, after the transplantation of HLA-A2⁺/DR1⁺ (HLA-matched) PBMCs into HUMAMICE, the body weight of HUMAMICE did not decreased significantly, and there was no appearance of GvHD characteristics, such as hair standing, trembling and inflammation. The optimized immuno-deficient mouse model - HUMAMICE effectively overcame GvHD which occurred during the transplantation of traditional NSG and NRG mice. That is why this new animal model is more suitable to the development and evaluation of immune transplantation and biological agents.

2. The construction strategy of HUMAMICE

2.1 The role of Rag2, Perforin and IL-2 γ in immune system

Recombination activating gene 2 (Rag2) is one of the most important recombinases in immune system[133]. It can specifically recognize the recombination signal sequence (RSS) on both sides of V, DH and J gene fragments of immunoglobulins and TCRs, to catalyze DNA double-strand to break, and leads to the V(D)J rearrangement, which is the main reason for the diversity of Ig and TCR repertoires. The mutation of Rag2 resulted in the partial loss of its encoded recombinase activity leading to a change in the tendency of V(D)J recombination. As a result, the development of early lymphocytes is blocked, both mature T and B lymphocytes are absent in the circulation, which causing a severe combined immune deficiency (SCID).

Perforin is a pore forming cytolytic protein which found in the granules of CTLs and NK cells. Perforin could create holes in the plasma membrane which triggers an influx of calcium and initiates membrane repair mechanisms. Perforin is the main mediator of the cytotoxic activity of NK cells[134, 135]. Targeted mutations at the perforin structural gene have major defects in the clearance of virus, delayed hypersensitivity and resistance ability to tumors, and perforin^{-/-} mice could support heightened engraftment after human HSC and PBMC transplantation.

The gene encoding IL-2 receptor gamma chain (IL-2 γ)[136] molecule is located on X-linked severe immunodeficiency complications (XSCID), XSCID is a ubiquitous genetic immune-deficiency disease characterized by the lack of T cells and NK cells, the number of B cells is relatively normal but does not have normal function simultaneously.

2.2 The establishment of HUMAMICE

Major histocompatibility complex (MHC) molecule is the most polymorphic gene group among mammals (including human beings). MHC plays a vital role in the positive and negative selection of T lymphocytes in thymus, facilitated the differentiation and maturation of T lymphocytes, activated and regulated the adaptive immune system and innate immune system. Owing to the different MHC restrictions between HLA and H-2 molecules, there exist many defects like the immunologic rejection and the low efficiency of transplantation in current traditional immuno-

deficient mouse models. Accordingly, how to construct a higher level of “humanized” transgenic mouse strain which could mimic human immune responses more accurately and reliably has become the priority in humanized animal models.

The structure and function of HLA and H-2 is quite similar, while their MHC restricted function is somehow different. HLA restriction differs markedly according to the geographical regions and ethnicity. The dominant HLA alleles in East Asia (especially China) are different from that in European, American, Middle East and other regions. HLA-A2, A11 and A24 account for 80% in China, while HLA-A2, A1 and A3 are the dominant alleles in European countries. In HLA class-II molecules, HLA-DR09, HLA-DR15 and HLA-DR01 account for 70% in China, while HLA-DR01 as well as HLA-DR03 and HLA-DR04 are the main alleles in European populations.

HUMAMICE, the human MHC transgenic immuno-deficient mouse model constructed in our study is not only characterized by the immuno-deficient state, as on top of that human cells could acquire HLA restriction after the positive and negative selection of T lymphocytes in HUMAMICE thymus after transplantation. As a “humanized immuno-deficiency mouse model”, HUMAMICE avoid the occurrence of GvHD reaction at a maximum extent and are more conducive to the development of tumors research and the relationship between HLA and transplantation.

HUMAMICE (HLA-A2^{+/+}/DR1^{+/+}/H-2-β2m^{-/-}/IAβ^{-/-}/Rag2^{-/-}/IL-2rγ^{-/-}/Perf^{-/-} mice) were generated on the background of Sure-L1 mice (HLA-A2/DR1 mice, HLA-A2^{+/+}/DR1^{+/+}/H-2-β2m^{-/-}/IAβ^{-/-}) by backcrossing with Rag2^{-/-} mice, IL-2rγ^{-/-} mice and Perf^{-/-} mice into homozygosity. The final obtained homozygotes HUMAMICE were confirmed by specific PCR and FACS in both genome and cell level. Specific PCR showed that both HLA-A2 and DR1 transgenes integrated in the mouse genome, and that there were deficient in mouse H-2-Iaβ, β2m, as well as they presented the deletion of Rag2, IL-2rγ and Perf. Flow cytometry showed that specific HLA-A2 molecules were detected on the surface of HUMAMICE lymphocytes, whereas mCD3⁺CD4⁺, mCD3⁺CD8⁺ T lymphocytes and mCD19⁺CD20⁺ B cells were absent due to the lack of Rag2, IL-2rγ and Perf genes. The absence of murine T and B cells is an important criterion for the immuno-deficient state of highly immuno-deficient mice. Then we showed that HUMAMICE had incomplete thymus and spleen, and their functional units (thymocytes and splenic corpuscles) were incomplete or even absent. These results

demonstrated that under the combined defects of Rag2, IL-2 γ and Perf, HUMAMICE were deficient of T, B and NK cells. The above results indicated that HUMAMICE is immuno-deficient with combined defect of T, B and NK cells, meanwhile under human HLA restriction in immune system.

2.3 The immuno-deficiency characteristics of HUMAMICE

The structure of spleen and thymus of HUMAMICE is not complete. To confirm the immuno-deficiency state of HUMAMICE, we subcutaneously engrafted human B-lymphoma cells (RAMOS cells) into immuno-deficient HUMAMICE and immuno-competent Sure-L1 mice (HLA-A2/DR1 mice). After 30 days of subcutaneous inoculation with human RAMOS cells into HUMAMICE, all mice developed tumors subcutaneously (tumor volume range from 500-3000 mm³). However, tumors were not able to grow in immuno-competent Sure-L1 mice. Furthermore, to verify that the inability of HUMAMICE to reject RAMOS cells is due to lack of mouse-derived immune system, we transferred the splenocytes, purified CD8⁺ T lymphocytes or other lymphocytes derived from Sure-L1 mice which had rejected RAMOS cells into HUMAMICE, which lead to subsequent tumor elimination effectively by the transfer of immune cells from RAMOS-rejected Sure-L1 mice to a certain extent. While the tumors of HUMAMICE without transfer of lymphocytes from Sure-L1 mice increased continuously. Altogether, these results confirmed that HUMAMICE were severely deficient, the immune deficiency state of HUMAMICE as an immuno-deficient mouse which could support tumorigenesis and showed no graft rejection occurs during subcutaneous inoculation.

3. The xenogeneic hPBMCs transplantation in HUMAMICE.

NSG, NOG, these immuno-deficient mouse models play decisive roles in immunology and preclinical studies. However, MHC molecules in these mice are still H-2 class I and II restriction, T lymphocytes do not undergo the “training” or “study” of human HLA class I and II molecules after transplantation, and moreover the occurrence of GvHD

cannot be completely avoided in these immuno-deficient mouse models mentioned above.

T lymphocytes of HUMAMICE could undergo the negative and positive selection in mouse thymus after human cell transplantation[62] [68]. Girardi reported the role of TCR- $\gamma\delta^+$ T lymphocytes in the clearance of viral infections and monitoring of tumor antigens[134]. The human immune response can be simulated to a higher degree on a specific HLA restriction in HUMAMICE when we used them in the preclinical trials of tumors, cancers, transplantation and immune rejection, and as pathogen infection models. As HUMAMICE could be used to study the biological effects of human HSC (or PBMC) in mice, this shows that it is also an ideal animal model for the research of tumor and malignant antigen cell therapy. HUMAMICE could also be used as specific pathogen infected animal models, as preclinical animal models for the development and evaluation of biological agents in immunotherapy and immunoprophylaxis.

PBMCs were collected from healthy volunteers, HLA-A2⁺ individuals were identified by flow cytometry and HLA-DR1⁺ individuals were confirmed by specific PCR. HUMAMICE were irradiated the day before transfer, which were given intravenous injection of hPBMCs and followed up. The body weight of mice and clinical symptoms were monitored twice per week. None of HUMAMICE showed no weight loss in 60 days after the transplantation or developed GvHD signs.

3.1 The reconstitution characteristics in HUMAMICE after hPBMC engraftment

To evaluate the engraftment in this novel model, we transferred HLA-matched (HLA-A2⁺/DR1⁺) hPBMCs into HUMAMICE. Flow cytometry analysis was done five and eight weeks after transplantation. Results of two representative mice (n=9) showed that 11.6% and 9.70% of white blood cells (WBC) were hCD45⁺ cells, with 45.2% and 49.4% of this population were hCD45⁺hCD19⁺ (B cells), 17.1% and 16.1% of hCD45⁺ being hCD3⁺ T lymphocytes: 29.0% and 30.0% of them being hCD3⁺hCD8⁺ T cells and approximately 60.9% and 59.0% being hCD3⁺hCD4⁺ T lymphocytes. Above all, after hPBMC transfer, the immune system of HUMAMICE was reconstructed.

3.2 The following HBsAg immunization of HUMAMICE

Ten days after the transplantation of human HLA-matched (HLA-A2⁺/DR1⁺) human PBMC, HUMAMICE received three intramuscular (i.m.) injections of HBsAg vaccine. HBsAg-specific IgM antibodies peak at second immunization, while HBsAg-specific IgG antibodies rise during three immunizations gradually. These results demonstrated that B lymphocytes of HUMAMICE could generate specific IgM and IgG antibodies after the transplantation of human cells (PBMCs).

The above results showed that after the transplantation of human HLA-A2⁺/DR1⁺ PBMC, human B and T lymphocytes were detected and HUMAMICE reconstituted the immune system successfully. Among them, the proportion of hCD3⁺ lymphocytes in HUMAMICE after transplantation which was consistent with the data reported previously[135].

4. The humanized optimization of immune-deficient mouse models

Immuno-deficient mice have been widely applied to many fields of immunology researches, including immune transplantation, infectious diseases and cancers. For example, immuno-deficient mouse model transplanted with human HSC provides an effective research tool for the development of preclinical trials in human immune response research[62]. It is also widely used in epidemiological infectious diseases[72], such as EB virus and HIV[137], the evaluation and development of vaccine[138], the preclinical research of cell therapy and gene therapy[73]. For example, Pablo D. Becker studied humanized IgM antibodies with BALB/c Rag2^{-/-}IL-2γc^{-/-} mice[71].

However, currently immuno-deficient mice still face some limitations and deficiencies which need to be overcome. Since the MHC restriction of immuno-deficient mice is still H-2 restriction, the engrafted-human cells cannot acquire the “train” and “education” of human HLA class I and II molecules in mouse thymus to get mature, which cannot reflect the characteristics of HLA-restricted immune responses after immunotherapy or infection with specific pathogens, in other words, T lymphocytes differentiated from human HSC after transplantation is not functional. It is also one of the aspects that need to be improved in these existing immune-deficient mouse models.

Shultz[65] constructed NSG-HLA-A2/HHD mice, both CD4⁺ and CD8⁺ T cells were developed and matured after the transplantation of human HSCs. HLA-restricted CTL responses and a variety of cytokines were detected after EBV infection, the population of CTL cells and the expression of HLA-DR molecules were up-regulated, indicated that T lymphocytes were activated after EBV infection. Simone[139] evaluated the CTL immune response and immunotherapy of anti-human HCMV virus with HLA-A2 NSG/HHD mice. Najima[140] constructed HLA-A*0201 and HLA-A*2402 in NOD/SCID/IL-2 γ KO (NSG) mice, antigen-presenting cells (APC) and memory CD8⁺ T lymphocytes were detected in the recipients after human HSC transplantation, specific HLA-restricted CTL immune responses and INF- γ were generated after the immunization of Wilms' tumor 1 (WT1) epitopes.

As preclinical animal models, NOD/scid IL-2R γ ^{null} mice were extensively used for the evaluation of dendritic cell (DC)-based human vaccines strategies[63], and the study of infection mechanisms of retroviral, such as HIV virus[72]. Traggiati[10] transplanted human CD34⁺ UCB-derived stem cells into neonatal Rag2^{-/-}IL-2 γ ^{-/-} mice via intrahepatic route to repopulate T, B and NK cells, meanwhile the effect immune response were stimulated by specific antigens. Gimeno[67] studied the mechanism of human tumor suppressor gene P53 regulated the cell cycle progression and the apoptosis of human HSC in newborn Rag2^{-/-}IL-2 γ ^{-/-} mouse model by transplanted with human CD34⁺ cells and silenced by RNA interference (RNAi) technology. Lang[64] evaluated and optimized the factors affected the efficiency of human HSC transplantation, such as the injection route in BALB/c-Rag2^{null}IL-2 γ ^{null} mouse models, the in-vitro culture environment of human HSC, the cell cryopreservation and recovery, and other multivariable terms of conditions and details which may influence human HSC transplantation. Results showed that the injection routes, subcutaneous (i.h.) and intravenous (i.v.), which have similar efficiencies after transplantation. Short-term (1-8 days) culture of human CD34⁺ HSC cells and the co-transplantation of CD34⁻ helper cells could improve and increase the efficiency of transplantation. Gonzalez[74] studied the mechanisms and immune protection of human immune based therapies by the application of NOD/SCID-IL-2 γ ^{-/-} mice, such as novel HIV vaccine. Feng Li[141] brought the in vitro fertilization (IVF) and CRISPR/Cas9 technology into the construction strategies of immuno-deficient mice, which paved the way for the optimization of humanized mouse models.

CHAPTER II

Generation of human MHC (HLA-A11/DR1) transgenic mice vaccine evaluation

1. Current situation of humanized mouse models

In the field of life sciences, the research on the function and mechanism of genes, gene networks and signaling pathway had become deepened gradually, especially after the publication of human and mouse genome sequence sketches at the beginning of this century. Since the occurrence and development process of some human diseases can be replicated by specific transgenic mouse models, the biological characteristics of the target genes could be studied at the overall level, which provided important theoretical and technical support for the pathogenesis of diseases, diagnosis and treatment technologies, as well as the development and evaluation of drugs and vaccines.

The transgenic animal models, especially the transgenic mouse models are highly praised and recommended by scientists, the researches based on transgenic mice had been increased. The humanization of experimental animals means that animals have certain human characteristics by multiple technology tools. The principle is to introduce human genes into the genome, which instead the endogenous genes of animals through genetic engineering techniques. The gene for human drug metabolism transferred into animal genomes to make animals more like humans in terms of drug metabolism, which could improve the evaluation efficiency and the safety of drugs in pre-clinical trials. The expression of human genes that affect diseases progression or therapeutic transgenic into animals can be used for the development of biological drugs and the mechanism of diseases, such as mice expressing human antibodies which are of great value in antibody drugs.

The humanization of animal models are the most important tools for the study of biopharmaceuticals and vaccines. Traditional experimental animals had been gradually replaced by new animal models with specific human diseases features (such as human

transgenic genes). In the past two decades, drugs research and development depended on genetically engineered animal models had achieved certain infusive and satisfactory results. For example, Celecoxib, a new drug for the treatment of arthritis which targeted on COX-2 was approved in 1998. Gleevec, which inhibited the oncogene BCR-ABL and treated the chronic myeloid leukemia had been approved in 2001. However, there are still many technical problems need to be overcome during the process of studying diseases with genetic engineering animal models. The main problem is that although current animal models could be applied to the study of the molecular mechanisms of diseases, wherever few models could discover or predict the imminent occurrence of human diseases in pre-clinical trials. Although drugs could cure or delay the progression of diseases in mouse models to some extent, however few drugs can exert an ideal or equal therapeutic effect to patients in clinical trials.

1.1 The defects of current mouse models

The antigen binding cleft of HLA-I molecules is closed at both ends and consists of $\alpha 1$ and $\alpha 2$ regions, most of the identified CTL epitopes are 8-11 aa peptides. CTL epitopes are the basic units of the cytotoxic response of CTL cells ($CD8^+$ T cells) and play critical killing role in response to anti-virus and anti-tumor. While, the antigen binding cleft of HLA-II molecules is comprised of $\alpha 1$ and $\beta 1$ region, which is more open than that of HLA-I molecules, which could accommodate 10-33 aa peptides (Th epitopes). Th epitopes are the basic units for Th cells ($CD4^+$ T cells) in infection, anti-tumor, immune regulation and autoimmune.

In the course of virus infection, helper T cells recognize specific Th epitopes of pathogens and exert direct anti-viral immune response[142]. At the same time, Th immunity could regulate CTL immunity and humoral immunity. Several studies have shown that the addition of Th epitopes in traditional vaccines could increase the immunogenicity of vaccines. To construct vaccines directed at specific conserved sequences of different pathogen strains, different HLA restriction and covered different population regions. Multi-epitopes vaccines could provide effective preventive measures for broad-spectrum vaccines with multiple serotypes, high mutation rate pathogenic infections and multiple pathogens.

These issues need to be considered during the construction and optimization of highly effective multi-epitopes vaccines:

- ◆ The ordering, continuity and rational combination of various epitopes.
- ◆ The selection of linker types.
- ◆ Efficient vectors.
- ◆ Safe and effective adjuvants.

Penna found that immunization of multiple CTL epitopes vaccines with chronic HBV infection patients could not eliminate HBV virus particles completely[143]. The addition of appropriate Th epitopes into multi-epitopes vaccines can improve the immunogenicity and the protective effect of vaccines effectively.

Due to the replacement of mouse endogenous H-2 class I/II molecules with HLA class I/II molecules, lymphocytes of HLA transgenic mice could develop, differentiate and mature under the regulation of HLA-I/II molecules. The immune responses of HLA transgenic mice are also mediated and regulated by HLA molecules with the characteristics of human immune responses, compared with other traditional mouse models. Therefore, the accuracy of HLA transgenic mouse models to evaluate vaccines can be improved, and the development period of drugs and vaccines can be effectively shortened.

HLA transgenic mouse models have unique advantages in the evaluation of novel vaccines and candidate vaccines, such as peptides vaccines, multi-epitopes based recombinant vaccines and therapeutic vaccines which based on different epitopes, especially T-cell epitopes and protective vaccines mainly primed cellular immune responses.

A variety of HLA single transgenic mouse models have been generated and widely used in the pathogenesis mechanism of pathogens and immunological studies during recent years. Chen identified HLA-A11 restricted CTL epitopes derived from HPV 18 virus by HLA-A11 single transgenic mouse model[123]. As we know, MHC is associated with the susceptibility of certain types of diseases. Carrington[144] found that several HLA alleles are relevant with HIV infection and the progression of AIDS. Paschetto recognized numerous poxvirus determinants from a wide variety of viral gene products with HLA-A*0201, HLA-A*1101 and HLA-B*0702 transgenic mouse models[145].

As a mouse model with good controllability, reproducibility and high degree of humanization in pre-clinical studies, HLA class-I transgenic mouse models had been widely used in the screening, development and evaluation of multiple epitopes-dependent candidate vaccines [104, 146].

However, there are still two defects that can't be ignored in these HLA single transgenic mouse models mentioned above.

- ◆ One is the presence of mouse endogenous H-2 molecules will compete with exogenous HLA transgenes, which dominated mouse immune response.
- ◆ The other one is that we could just investigate the role of only one specific HLA molecule in immune responses, while the immune system is a complex network, the interactions and effects of HLA class I and II molecules is critical, HLA is highly polymorphic and codominant.

Single HLA transgenic mice could not synergistically investigate the mechanism of interaction between HLA class I and II molecules. The HLA class I and II double transgenic mouse model constructed in our study overcame these issues which need to be resolved.

At present, the HLA class I and II double transgenic mouse models that have been reported in the world include HLA-A2/DR1 double transgenic mouse model and HLA-A2/DP1 double transgenic mouse model, which were established by our team leading by Dr. Yuchun Lone in 2004 and 2012. The first HLA class I and II double transgenic mouse model HLA-A2/DR1 transgenic mouse model was successfully generated in 2004[76], and applied to the evaluation of humoral immunity, CTL cells and Th cells mediated cellular response induced by HBV DNA vaccine, which were similar with the results obtained in human natural HBV infection, which verified the humanized mouse model at the same time. As the first HLA class-I and class II double transgenic mouse model in the world, it has been widely used in a variety of preclinical experimental studies. For example, Deng[125] carried out the research of mechanisms of chronic HBV infection and gene therapy by the utilization of HLA-A2/DR1 mice. Dr. Yuchun Lone created HLA-A2/DP4 double transgenic mouse model in 2012, identified 18 HLA-DP4-restricted Th epitopes of HBsAg and validated by clinical specimens. Further verifications confirmed that HLA-A2/DP4 transgenic mice as a basis for the

screening of epitopes and the evaluation of candidate vaccines, which was consistent with human immune responses.

1.2 The association between HLA and the occurrence of diseases

With more and more further researches, there was a consensus that closely association between HLA molecules and the occurrence of various autoimmune diseases and chronic diseases, such as AS[7], arthritis, MS and other genetic diseases, infectious diseases and epidemics. Furthermore, there are some relevance between HLA-I molecules and the occurrence and progression of AIDS, in parallel the evolution of HIV virus [147, 148].

Since MHC plays a core role in immune responses, it could present antigens to T cells, it may also important to pathogenesis.

◆ The Molecular Simulation Theory stated that the structure of HLA were similar to that of some pathogenic antigens and would be attacked by immune system of hosts. In other way, as the structure of pathogen antigens are extremely similar with that of HLA molecules, which cannot be recognized by hosts and lead to immune evasion, the hosts would be attacked by pathogens.

◆ The Receptor Theory held the idea that some HLA molecules may act as the receptors on cell surface to recognize certain pathogens. Pathogens invaded hosts and bound to HLA molecules which causing tissue damage.

◆ The Linkage Disequilibrium Theory suggested that there may be other susceptibility genes associated with the occurrence of certain diseases, and perhaps HLA molecules were only a series of genetic markers which linked to those susceptibility genes.

◆ The Immune Response Gene Theory stated that the genes encoded HLA complex were Ir genes, and specific HLA class II alleles may cause specific abnormal immune response, and the characteristics of is susceptible to a certain disease.

Therefore, we could make some imaginative but possible hypothesis of the relationships between HLA and pathogens: when pathogens invaded, will HLA

molecules affect the binding of viruses to cell surface receptors when presenting viral antigen peptides to T lymphocytes, thereby promoting or constraining the progress of pathogens infection? Perhaps that is likely to be the reason why the population carried certain HLA gens are insusceptible or sensitive to certain viruses or pathogens.

1.3 Dominant MHC alleles are different between continents

The restriction of cellular immune responses in HLA class-I/II double transgenic mouse models is completely restricted by HLA class I and II molecules, which could reflect the natural immune response of human beings. The above two HLA double transgenic mouse models represent dominate HLA alleles in worldwide, especially Europe and North America. However, they do not cover the dominant alleles in Asia, especially China.

Due to the differences in ethnic and regional distribution of HLA molecules, there are significant differences in HLA predominant alleles between Asia (especially Chinese) and European, American and Middle Eastern populations. At present, the major CTL epitopes of HLA class-I molecules are mainly concentrated on the dominant genotype HLA-A2 of European and American populations (Caucasians), while the dominant HLA-A11 and HLA-A24 restricted CTLs in Chinese populations are rarely reported and mentioned. This problem also exists in HLA class-II molecules and the corresponding transgenic mouse models. For example, the dominant alleles of HLA class-II molecules in Europe, the United States, and the Middle East are HLA-DR1, DR3 and DR4, while which dominated in Chinese population are HLA-DR09*01 and DR15*01.

Therefore, most of the existing reported CTL epitopes and Th epitopes are not applicable to Chinese population. The reasonable combination of CTL epitopes and Th epitopes of HLA dominant alleles in both European, American and Asian populations will greatly enrich current epitopes database, broaden the scope of application of the epitopes-based vaccines and improve the broad-spectrum immune efficacy of worldwide population.

In Chinese population, the haplotypes with higher frequencies of HLA class-I molecules are HLA-A*0201, A*1101 and A*2402. By comparing the sequences of three haplotypes, the homology of nucleic acids was almost 96.0%, the homology of the encoded protein was about 92.0-93.0%. Among HLA class-II molecules, the homology of nucleic acid of HLA-DRB1*0101, DRB1*0301 and DRB1*1501 β chain was about 95.0-96.0%, the homology of the encoded protein was approximately 91.0-95.0%. It illustrated that the homology of both HLA class-I and class II haplotypes is extremely high, the interaction between HLA molecules and antigen peptides is very inclusive, the members of a same family could selectively identify the antigens with peptides that have same or similar anchor residues, which could provide a brand-new idea for the identification of epitopes.

2. The development state of HLA transgenic mouse models

In recent years, HLA transgenic mouse model has played an extremely important role in the study of immunological mechanisms of diseases, the development and evaluation of vaccines and drugs. HLA transgenic mouse models had undergone a period of continuous progress and optimization. Here, we sum up the origin, development and utilization of HLA transgenic mouse models.

2.1 The strategy optimization of HLA transgenic mouse models

In the earliest stage, scientists always directly transferred the whole HLA molecules into mouse genome, such as HLA-B27 transgenic mice[149], HLA-B7 transgenic mice[150], HLA-A2 transgenic mice [151] and HLA-Cw3 transgenic mice[152]. However, the binding between the $\alpha 3$ domain of HLA molecules and mouse CD8 molecules is relatively weak [153-155]. Due to the presence of endogenous mouse H-2 molecules, which competitive inhibited HLA class I-restricted immune responses [156], H-2-I-restricted immune responses still dominated in these mouse models, which failed to reflect the authentic function and role of human HLA molecules alone in immune response. Some studies showed that the expression of HLA transgenic

molecules on the surface of mouse lymphocytes significantly decreased with the co-expression of endogenous H-2 molecules in transgenic mice[126].

In the second stage, scientists improved human MHC transgenic mouse models by two methods.

◆ The first method is to transfer the gene fragment coding for human CD4 or human CD8 molecules into mouse genome, so that mouse could express both murine and human CD4 or CD8 molecules [157], which could enhance the binding efficiency between HLA and CD4/CD8 molecules, initiate the second signal of antigen presentation efficiently simultaneously.

After the optimization by two methods above, HLA transgenic mouse models could produce certain HLA-restricted specific immune responses, nevertheless majority of cellular immune responses were still regulated by mouse-derived H-2 molecules.

2.2 The construction strategy of HLA-A11/DR1 transgenic mice

Thus, a third-stage construction strategy was adopted in the design of our HLA-A11 transgenic vector, and we constructed an HLA-A11 chimeric transgenic vector (HHD[117]) containing HLA-A11 promoter, the light chain β_2m , the heavy chain $\alpha 1$ and $\alpha 2$ regions (HLA-A11), the $\alpha 3$ region and transmembrane region of murine H-2-D^b. We knocked out the important components β_2m and IA β of mouse-derived H-2 molecules. In HLA-A11 chimeric transgene molecule, $\alpha 3$ region of mouse H-2 replaced human HLA-A11 $\alpha 3$ region, which effectively increased the binding affinity between HLA-A11 molecule and mCD8, avoided the complexity of hCD8 transduction into the mouse genome. At the same time, we knocked out the important components of H-2 class I- β_2m and II molecules-IA β (β chain of IA molecule) of murine, to replace a pseudogene fragment which longer than the original functional gene, to achieve the purpose of silencing murine H-2 molecules.

Therefore, we eliminated the competitive inhibition of endogenous H-2-I-restricted responses in HLA-A11 transgenic mice, only HLA-A11-restricted immune responses could be generated. The same strategy was implemented into the establishment of HLA

class-II transgenic mouse model. Through the above steps, HLA-A11/DR1 double transgenic mouse model (HLA-A11^{+/+}/DR1^{+/+}/H-2-β₂m⁻/IAβ⁻) was obtained, which replaced with human MHC-HLA molecules at both MHC class I and II molecules level. HLA transgenes exerted a restrictive function on antigen presentation and the regulation of immune response in mice, enabled the highest level in “humanization”, which were able to simulate human immune response at HLA level more effectively.

3. The generation of homozygous HLA-A11/DR1 transgenic mice

A chimeric HLA-A*1101 monochain fragment encompassed HLA-A11 leader sequence, α1 and α2 domains, murine H-2D^b (from the α3 domain to the COOH terminus) and human β₂m, which was covalently linked between the leader sequence and the 5' end of HLA-A11 (α1 and α2) domains via a 15 aa linker encoding Gly₄Ser₃. After the verification of HLA-A11 transgenic vector was successfully constructed, the linearized purified HLA-A11 fragment was microinjected into pronuclei from fertilized (C57BL/6×C57BL/6) F1 mouse eggs to generate transgenic embryos. Transgenic embryos were re-implanted into pseudo pregnant female mice. The foreign gene was integrated into mouse genome according to a random integration strategy, following by the acquisition of HLA-A11 transgenic founder (F1) mice. HLA-A11 founder mice showing the highest expression of HLA-A11 were crossed with HLA-A2/DR1 mice (HLA-A2^{+/+}/DR1^{+/+}H-2-β₂m⁻/IAβ⁻) which we constructed previously. After a series of backcrossing, HLA-A11/DR1 transgenic mice (HLA-A11^{+/+}/DR1^{+/+}H-2-β₂m⁻/IAβ⁻) (abbreviated as HLA-A11/DR1) were generated.

The integration of exogenous HLA-A11 and DR1 genes in mouse genome and the knockout of endogenous H-2 β₂m and IAβ were confirmed by PCR. Through the continuous self-crossing and back-crossing, HLA-A11/DR1 transgenic mouse were stably obtained, with HLA-A11^{+/+}/DR1^{+/+} double transgenic and H-2-β₂m⁻/IAβ⁻ double knockout. After confirming the exogenous HLA gene was successfully inserted into HLA-A11/DR1 transgenic mouse genome and stably genetically expressed, we further validated the HLA specific expression in splenocytes of HLA-A11/DR1 mice, which means that the exogenous genes could be translated into HLA complexes in vivo.

At the same time, through the mediated by HLA molecules in HLA-A11/DR1 mice, mCD4⁺ T cells accounted for about 92.2% of mCD3⁺ T cells, which was similar with that 64.6% in C57BL/6 mice, while mCD8⁺ T cells accounted for about 1.48% in mCD3⁺ T cells, which was significantly lower than that 11.7% of C57BL/6 mice. Nevertheless, lower number of mCD8⁺ T cells was similar with other MHC-class I transgenic mice[116, 128], such as HLA-A2/DR1 transgenic mice(2-3 %)[76] and HLA-A2/DP4 transgenic mice (2.31%)[77], which were developed by Dr. Yuchun LONE previously. Both HLA-A2/DR1 and HLA-A2/DP4 transgenic mice could produce effective humoral and cellular immune responses. These results suggested that HLA-A11 and HLA-DR1 transgenes could enable the negative and positive selection of T lymphocytes in murine thymus, following by developing and differentiating into mature and normal immune function mCD3⁺CD4⁺ and mCD3⁺CD8⁺ T lymphocytes with human HLA restriction.

HLA transgenes and H-2 knockout mice were identified by PCR genotyping, the genetic stability of offspring was confirmed. The expression of HLA transgenes in splenocytes of HLA-A11/DR1 mice was stronger than C57BL/6 and H-2-I/II knockout mice. Flow cytometric results showed that the numbers of mCD3⁺CD4⁺ and mCD3⁺CD8⁺ T cells in HLA-A11/DR1 mice were comparable with C57BL/6 mice. These results showed that HLA transgenes enabled the differentiation and maturation of T lymphocytes in HLA-A11/DR1 mice. HLA-A11/DR1 mice could mount HLA-A11 restricted responses after immunized two known HLA-A11-restricted epitopes derived from HIV-Pol₁₇₇₋₁₈₈ and HIV-GP160₃₂₋₄₅. Results showed that HLA-A11/DR1 mice could mount HLA-A11-restricted, epitope-specific, IFN- γ -producing mCD8⁺ T cellular immune response.

4. The application of HLA-A11/DR1 transgenic mice to the evaluation of vaccines

4.1 The verification of HLA-A11/DR1 mice with reported epitopes

We further explored the HLA-restricted immune response of HLA-A11/DR1 transgenic mice and its ability to stimulate specific immune responses. HLA-A11/DR1

mice were able to produce high level of HLA-A11 specific CTL immune response (IFN- γ secretion) stimulated by HLA-A11 restricted CTL epitopes HIV-Pol₁₇₇₋₁₈₈ and HIV-GP160₃₂₋₄₅, whereas no production of IFN- γ was detected in C57BL/6 mice. These results proved that our HLA-A11/DR1 mice has HLA-A11 restricted immune response function which could generate specific HLA-A11 restricted CTL responses stimulated by the immunization of HLA-A11 restricted CTL epitopes. The DR1 molecule in HLA-A11/DR1 mice was isolated from HLA-A2/DR1 mice which we constructed previously, and HLA-DR1 restriction response was verified by HLA-DR1 restriction epitope-HBsAg₁₇₉₋₁₉₄. We also successfully screened two novel HLA-DR1 restriction epitopes, named HIV-1 Gag₃₂₁₋₃₄₀ and Gag₃₃₁₋₃₅₀ by HLA-A2/DR1 mice. HLA-DR1 restriction in HLA-A11/DR1 mice was also confirmed by HLA-DR1 restricted epitope-HBsAg₁₇₉₋₁₉₄, the results were consistent with HLA-A2/DR1 mice which meet our expectation[76].

4.2 The evaluation of HLA-A11/DR1 mice in candidate vaccines and commercial vaccines

The above results confirmed that T lymphocytes could develop into mature mCD4⁺ and mCD8⁺ T lymphocytes after the negative and positive selection in murine thymus, under the regulation of exogenous HLA molecules in HLA-A11/DR1 mice. Then we verified the HLA-A11 and HLA-DR1 restricted immune responses by the utilization of HLA-A11 and HLA-DR1 restricted epitopes reported in previous studies[120] [76]. The exogenous HLA molecules could substitute for mouse H-2 molecules to initiate and regulate immune response in mice.

The greatest advantage and feature of HLA-A11/DR1 mice constructed in this study was that HLA-A11 and HLA-DR1 alleles covered a wide range of population in China, which can profit the studies of diseases and their immune prevention and control in Chinese population. According to the HLA gene frequencies reported in literatures and the database statistics, approximately one-third to one-half of Chinses population carried HLA-A11 or DR1 alleles. Construction of HLA-A11/DR1 transgenic mice and to apply it to the epitopes and application of it in epitopes-based vaccines research, the mechanism of pathogenic immunity, will provide a much more effective humanized animal model for diseases, the prevention and immunotherapy for Chinese populations.

We immunized the commercial vaccine-recombinant HBV S antigen (kindly provided by Dr. Honglin Xu) and a novel vaccine-recombinant HIV-1 protein- HIV-MEP1 (kindly provided by Dr. Zhihua Kou) with HLA-A11/DR1 mice, to evaluate the specific humoral and cellular immune responses induced by these vaccines, while to verify whether HLA-A11/DR1 mice could effectively simulate specific immune responses in humans after immunization.

HIV-1 multi-epitopes recombination protein (HIV-MEP1) was composed of twelve epitopes linked by specific linker, the epitopes contained were with Chinese dominant HLA alleles restriction and have satisfactory immunogenicity. After the immunization of HIV-MEP1 into HLA-A11/DR1 mice and HLA-A2/DR1 mice, specific anti-HIV-MEP1 IgG antibodies in serum increased to a certain level, and there was a statistically significant difference of HLA-A11/DR1 mice compared with PBS control group ($p=0.0058$). HLA-A11/DR1 mice and HLA-A2/DR1 mice produced high levels of specific IFN- γ cytokine, regardless of the immunization of recombinant protein HIV-MEP1 or specific HIV-1 peptides, whereas C57BL/6 mice could just produce low levels of IFN- γ . It verified that both HLA-A11/DR1 mice and HLA-A2/DR1 mice are ideal and efficient models which could apply to the evaluation of novel candidate vaccines.

During the evaluation of the recombinant HBV S antigen vaccine, specific humoral immunity (IgG antibodies) produced by HLA-A11/DR1 mice was similar with that of C57BL/6 mice, while the specific IFN- γ level produced by HLA-A11/DR1 mice was 3-4 times fold than WT mice. These results indicated a satisfactory cellular immune response of HLA-A11/DR1 mice and the ability to mimic human cytotoxic response, which demonstrated that this novel mouse model have the capability to estimate immune responses induced by commercial vaccines and novel vaccine candidates.

In view of the above issues about epitopes-based vaccines, we should combine the current rapid development of computer technology with high-throughput prediction to screen the epitopes, assist with more effective and safer adjuvants. Strived to construct the multivalent vaccines that with different MHC-restricted, multiple pathogens, with both conformational and linear epitopes, cover both B cell epitopes, CTL epitopes and Th epitopes to induce specific humoral and cellular immune responses and has a broad spectrum of population protection.

4.3 The identification of novel HLA-A11 restricted epitopes of EBOV and MERS-CoV

In recent years, highly pathogenic pathogens such as MERS-CoV (Middle East Respiratory Syndrome Coronavirus) and EBOV (Ebola Virus) have spread worldwide, resulting in extremely high mortality rates which up to 30% and 70%, respectively. It is the most virulent and contagious pathogen known so far. WHO has classified these two viruses as biosafety level-IV viruses. The outbreak has been defined as an “international public health emergency”. The epidemic of MERS-CoV and EBOV warn us to take preventive measures in the research and development of new vaccines and therapeutic drugs of these important pathogens, and to the capacity for disease prevention and control. However, up to now, there is still no safe and effective protective vaccine for humans that has been approved in clinical trials. The development of a novel multi-epitopes-based vaccine will hopefully make a breakthrough in the prevention and control of MERS-CoV and EBOV, and will have an important impact on the effective control of future major outbreaks.

To predict HLA-A11 restricted CTL epitopes of EBOV and MERS-CoV, we analyzed the sequence of amino acid of EBOV-GP and MERS-CoV by bio-information online software SYFPEITHI and NetMHC, next synthesized twenty-four HLA-A11 potential peptides which got the higher binding scores for further verification. The solubility of candidate epitopes was considered, whether higher (stronger binding force) and lower conventional hydrophobicity (conventional hydrophobicity <0: better dissolution; 0<conventional hydrophobicity<10: harder to dissolve; conventional hydrophobicity >10: difficult to dissolve in water and difficult to synthesize), and HLA-A11/DR1 double transgenic mouse model were applied to the screening, identification and analysis of these candidate epitopes.

Based on HLA-A11/DR1 transgenic mouse model, we evaluated and confirmed the predicted HLA-A11 restricted CTL epitopes of EBOV and MERS-CoV, benefit the study of epitopes-based vaccines. ELISPOT results showed that HLA-A11 specific CTL responses were stimulated by two epitopes of EBOV-GP (EBOV-GP₇₆₋₈₄ and EBOV-GP₄₂₃₋₄₃₁) and four of MERS-CoV-S (MERS-S₁₅₂₋₁₆₀, MERS-S₇₂₀₋₇₂₈, MERS-

S₈₈₉₋₈₉₇ and MERS-S₁₀₉₂₋₁₁₀₀). These epitopes candidates have the potential to contribute to the design of multi-epitopes-based vaccines of highly-risk pathogens.

CONCLUSIONS

In this study, we constructed an immuno-deficient MHC transgenic mouse strain (HLA-A2^{+/+}/DR1^{+/+}/H-2-β2m^{-/-}/IAβ^{-/-}/Rag2^{-/-}/IL-2rγ^{-/-}/Perf^{-/-}) and an hPBMC-transplantation mouse model, which could provide technical support to study transplantation mechanism, tumors, infectious diseases and pathogens. Meanwhile, we generated a new homozygous HLA-A11/DR1 transgenic mouse strain (HLA-A11^{+/+}/DR1^{+/+}/H-2-β2m^{-/-}/IAβ^{-/-}) which carried Chinese dominant HLA class I and II alleles, and applied to the evaluation of vaccines, the identification of HLA restricted CTL epitopes of highly pathogenic pathogens, such as MERS-CoV and EBOV. We demonstrated that:

(1) The novel immuno-deficient HLA transgenic mice "HUMAMICE" (HLA-A2^{+/+}/DR1^{+/+}/H-2-β2m^{-/-}/IAβ^{-/-}/Rag2^{-/-}/IL-2rγ^{-/-}/Perf^{-/-} mice) were established, which expressed human HLA molecules instead of murine H-2, and presented at first no lymphocytes, spleen and thymus dysplasia. This immuno-deficient state was reversed by transferring of functional HLA-matched (HLA-A2⁺/DR1⁺) hPBMCs and then producing mice with an immuno-competent state with functional human immune system. We showed that in this HLA-matched context and novel mouse model, the hPBMC-transfer led to high lymphocytes engraftment rates without GvHD symptoms over three months. Furthermore, to evaluate the ability of transferred human cells, we immunized hPBMC-HUMAMICE with HBsAg vaccine which resulted in robust and reproducible high level of humanized HBsAg-specific IgM and IgG antibodies, implying that both transferred T and B lymphocytes were functional. In conclusion, these findings indicated that the hPBMCs-HUMAMICE model represented a promising model to dissect human immune responses in various human diseases, including pathogens, infectious diseases, cancers and tumors. Hence, HUMAMICE will facilitate the development of novel vaccines, drugs and cellular therapies.

(2) The Chinese HLA alleles dominated HLA-A11/DR1 (HLA-A11^{+/+}/DR1^{+/+}/H-2-β2m^{-/-}/IAβ^{-/-}) transgenic mice strain were established. This novel mouse strain possesses human HLA-restricted characteristics and a normal specific ability to respond to antigens. The evaluation of a candidate vaccine and a commercial vaccine showed that this novel animal mouse could apply to the evaluation of vaccines. Furthermore, we identified two HLA-A11 restricted epitopes of EBOV GP protein and four of MERS-

CoV S protein. Above all, the novel HLA-A11/DR1 double transgenic mice could facilitate the identification of Chinese dominant HLA-restricted CTL and Th epitopes of important pathogens and provide a new prospective technical tool to the immunological mechanism of diseases as well as the invention and evaluation of novel vaccines.

Taken together, two novel and promising humanize mouse models carrying human HLA restriction were established, which could apply as pathogen infection models, and study tumors, transplantation mechanism, and the invention and evaluation of vaccines and drugs.

PERSPECTIVES

1. Further optimization and development of HUMAMICE

In the present study, we established immuno-deficient HUMAMICE mice, which deficiency of mouse H-2 Class I and Class II, and expressed both HLA-A2 and HLA-DR1 molecules which represented the characteristics of human HLA-restricted immune responses. HUMAMICE expressed HLA-A2 and HLA-DR1 are compatible with grafted HLA-matched hPBMCs. In this HLA-matched situation, there were no allo-like or xeno-like rejection reactions, so the non-optimal mSIRP-hCD47 interaction does not affect long-term hPBMCs engraftment. There are some optimizations needing to be developed, and some limitations of HUMAMICE model need to be overcome in the nearing future:

◆ In addition to B cells, CTL cells, Th1 and Th2 cells, the differences in features and function of T helper cell 17 (Th17) between human and mice was still conflict[158]. Th17 cells play key role in the triggering and maintaining of chronic inflammatory responses to antigens[159]. In our present study, since exogenous HLA-A2 and DR1 molecules had replaced endogenous murine H-2 molecules, CTL and Th cells (Th1, Th2 and Th17) could simultaneously undergo in-vivo thymic “training” in HUMAMICE after the transplantation of human cells or tissues. To investigate the role, cooperation and interaction of these lymphocytes in immune responses faced to the invasion of a specific pathogen or the malignant antigen, such as tumors, the optimization will benefit the research of cell therapy and immunotherapy research.

◆ Due to the ethics issues, we took advantage of human PBMCs instead of human umbilical cord blood (UCB) in this study. Although satisfactory engraftment and specific immune responses had been detected after the transplantation of hPBMCs in HUMAMICE, meanwhile the transplantation of human UCB or bone marrow (BM) derived CD34⁺ cells into HUMAMICE are under consideration, which will contribute to much higher human reconstitution and benefit to the evaluation of vaccines or drugs more accuracy in clinical trials.

◆ HUMAMICE could support high level of engraftment of human HLA-matched PBMCs. However, it must be noted that HUMAMICE is not a good model for the

engraftment of non-HLA-matched PBMC or any human stem cells, including human HSCs, due to the NOD genetic background of HUMAMICE and the lack of supporting cytokines, supporting cells such as stromal cells and human antigen presenting cells (APC) in mice. HUMAMICE carrying HLA-A2 and HLA-DR1 alleles which with the highest genetic frequency all over the world, we will create other humanized HLA transgenic immuno-deficient mice with different HLA restrictions, which could cover more population, and benefit to the establishment of humanized mouse models to evaluate pre-clinical diagnosis and therapies.

Despite some of the optimizations which need to be improved listed above, HLA-matched-hPBMC-HUMAMICE model allows the possibility of studying normal human immune responses in various human diseases, including infectious diseases and cancers in the HLA-matched population. It also represents a promising model to facilitate the development of novel vaccines and cellular therapies.

2. The improvement of HLA transgenic mouse models

In the future work, we will carry out the development of multi-HLA-restricted epitopes-based vaccines based on HLA-A11-restricted CTL epitopes identified by HLA-A11/DR1 transgenic mice, which will be reserved as the strategic defense measure and means of highly-risk pathogens. At the same time, we will predict and identify more HLA-restricted CTLs and Th epitopes of other highly-risk pathogens or conservative proteins of tumor antigens, and combined with clinical samples to validate and optimize the multi-epitopes-based vaccines with Chinese dominant HLA genotypes for a variety of important pathogens. This will be a powerful countermeasure for diseases prevention and the control of highly-risk pathogens that target on Chinese population.

The immune system is a complex and comprehensive regulatory network system. In addition to MHC molecules, there are still many key factors which could influence the course of immune responses in a directly or indirectly way. For example, the intracellular proteases, the transporter associated with antigen processing (TAP), TAP-associated protein (Tapasin)[160]. These molecules could influence and regulate the efficiency and the action mode of HLA that present HLA-restricted antigen peptides in

vivo. However, these molecules mentioned above had certain differences between different species, such as mouse and human beings. Therefore, replacing the encoded human genes of these above regulatory factors into HLA transgenic mouse models will further improve its accuracy to simulate human immune responses.

When expanding HLA transgenic mouse models into the field of pathogenesis of pathogens, the key question is whether it could be applied to the evaluation and the effectiveness of immune protection, it depends on whether it could implement the signs and symptoms of infection, to realize the proliferation of pathogens and the pathological changes effectively, as well as the effective simulation of human infection of certain pathogens.

In the next study, we could appropriately combine HLA transgenic mouse models with viral receptor transgenic mice or complement transgenic mice to study the association between HLA and the pathogenic mechanisms of pathogens, the relation between HLA and complements [161], the immune defense and immunotherapy, etc. For example, Na⁺-taurocholate co-transporting polypeptide (NTCP) is a functional receptor for human hepatitis B and D virus [162], NTCP transgenic mice combine with HLA transgenic mice will have the potential to elaborate the relation between HBV infection mechanism and specific HLA alleles populations. Yusen Zhou found that the blockade of C5a-C5aR axis lead to the decreased tissue damage induced by MERS-CoV infection, as manifested by reduced apoptosis and T cell regeneration in the spleen[163], which suggested that we could investigate the pathogenic mechanisms of pathogens with both complement transgenic mice (such as C5a transgenic mice) with HLA transgenic mice, to investigate what is the role of HLA and complement participate in the infection of MERS-CoV.

The establishment of HLA-A11/DR1 double transgenic mouse with both Chinese HLA dominant HLA class I and class II alleles, could promote the evaluation of peptides candidates, the design and development of new candidate vaccines, furthermore benefit to immunology researches, the establishment of diseases animal models, clinical immunotherapy, and the evaluation, optimization, improvement and the side-effect studies of immunotherapy, especially gene therapy.

REFERENCES

1. Netea, M.G., et al., Trained immunity: A program of innate immune memory in health and disease. *Science*, 2016. 352(6284): p. aaf1098.
2. Klein, J., Seeds of time: fifty years ago Peter A. Gorer discovered the H-2 complex. *Immunogenetics*, 1986. 24(6): p. 331-8.
3. Snell, G.D. and G.F. Higgins, Alleles at the histocompatibility-2 locus in the mouse as determined by tumor transplantation. *Genetics*, 1951. 36(3): p. 306-10.
4. Galbraith, W., et al., Imaging cytometry by multiparameter fluorescence. *Cytometry*, 1991. 12(7): p. 579-96.
5. Kelley, J., L. Walter, and J. Trowsdale, Comparative genomics of major histocompatibility complexes. *Immunogenetics*, 2005. 56(10): p. 683-95.
6. Pascolo, S., HLA class I transgenic mice: development, utilisation and improvement. *Expert Opin Biol Ther*, 2005. 5(7): p. 919-38.
7. Kuon, W., et al., Identification of novel human aggrecan T cell epitopes in HLA-B27 transgenic mice associated with spondyloarthritis. *J Immunol*, 2004. 173(8): p. 4859-66.
8. Taneja, V., et al., New humanized HLA-DR4-transgenic mice that mimic the sex bias of rheumatoid arthritis. *Arthritis Rheum*, 2007. 56(1): p. 69-78.
9. Vasilca, V., et al., HLA-A and -B phenotypes associated with tuberculosis in population from north-eastern Romania. *Roum Arch Microbiol Immunol*, 2004. 63(3-4): p. 209-21.
10. Traggiai, E., et al., Development of a human adaptive immune system in cord blood cell-transplanted mice. *Science*, 2004. 304(5667): p. 104-7.
11. Bosma, G.C., R.P. Custer, and M.J. Bosma, A severe combined immunodeficiency mutation in the mouse. *Nature*, 1983. 301(5900): p. 527-30.
12. Mombaerts, P., et al., RAG-1-deficient mice have no mature B and T lymphocytes. *Cell*, 1992. 68(5): p. 869-77.
13. Shinkai, Y., et al., RAG-2-deficient mice lack mature lymphocytes owing to inability to initiate V(D)J rearrangement. *Cell*, 1992. 68(5): p. 855-67.
14. Shultz, L.D., et al., Multiple defects in innate and adaptive immunologic

- function in NOD/LtSz-scid mice. *J Immunol*, 1995. 154(1): p. 180-91.
15. Ito, M., et al., NOD/SCID/gamma(c)(null) mouse: an excellent recipient mouse model for engraftment of human cells. *Blood*, 2002. 100(9): p. 3175-82.
 16. Shultz, L.D., et al., Human lymphoid and myeloid cell development in NOD/LtSz-scid IL2R gamma null mice engrafted with mobilized human hemopoietic stem cells. *J Immunol*, 2005. 174(10): p. 6477-89.
 17. Cosgun, K.N., et al., Kit regulates HSC engraftment across the human-mouse species barrier. *Cell Stem Cell*, 2014. 15(2): p. 227-38.
 18. Zeng, Y., et al., Creation of an immunodeficient HLA-transgenic mouse (HUMAMICE) and functional validation of human immunity after transfer of HLA-matched human cells. *PLoS One*, 2017. 12(4): p. e0173754.
 19. Doulatov, S., et al., Hematopoiesis: a human perspective. *Cell Stem Cell*, 2012. 10(2): p. 120-36.
 20. Mosier, D.E., et al., Transfer of a functional human immune system to mice with severe combined immunodeficiency. *Nature*, 1988. 335(6187): p. 256-9.
 21. McCune, J.M., et al., The SCID-hu mouse: murine model for the analysis of human hematolymphoid differentiation and function. *Science*, 1988. 241(4873): p. 1632-9.
 22. Lapidot, T., et al., Cytokine stimulation of multilineage hematopoiesis from immature human cells engrafted in SCID mice. *Science*, 1992. 255(5048): p. 1137-41.
 23. Namikawa, R., et al., Infection of the SCID-hu mouse by HIV-1. *Science*, 1988. 242(4886): p. 1684-6.
 24. Kamel-Reid, S. and J.E. Dick, Engraftment of immune-deficient mice with human hematopoietic stem cells. *Science*, 1988. 242(4886): p. 1706-9.
 25. Hesselton, R.M., et al., High levels of human peripheral blood mononuclear cell engraftment and enhanced susceptibility to human immunodeficiency virus type 1 infection in NOD/LtSz-scid/scid mice. *J Infect Dis*, 1995. 172(4): p. 974-82.
 26. Cudkowicz, G. and P.S. Hochman, Do natural killer cells engage in regulated reactions against self to ensure homeostasis? *Immunol Rev*, 1979. 44: p. 13-41.

27. Lan, P., et al., Reconstitution of a functional human immune system in immunodeficient mice through combined human fetal thymus/liver and CD34+ cell transplantation. *Blood*, 2006. 108(2): p. 487-92.
28. Denton, P.W. and J.V. Garcia, Novel humanized murine models for HIV research. *Curr HIV/AIDS Rep*, 2009. 6(1): p. 13-9.
29. Tonomura, N., et al., Antigen-specific human T-cell responses and T cell-dependent production of human antibodies in a humanized mouse model. *Blood*, 2008. 111(8): p. 4293-6.
30. Denton, P.W. and J.V. Garcia, Humanized mouse models of HIV infection. *AIDS Rev*, 2011. 13(3): p. 135-48.
31. Feuring-Buske, M., et al., Improved engraftment of human acute myeloid leukemia progenitor cells in beta 2-microglobulin-deficient NOD/SCID mice and in NOD/SCID mice transgenic for human growth factors. *Leukemia*, 2003. 17(4): p. 760-3.
32. Nicolini, F.E., et al., NOD/SCID mice engineered to express human IL-3, GM-CSF and Steel factor constitutively mobilize engrafted human progenitors and compromise human stem cell regeneration. *Leukemia*, 2004. 18(2): p. 341-7.
33. Sugamura, K., et al., The interleukin-2 receptor gamma chain: its role in the multiple cytokine receptor complexes and T cell development in XSCID. *Annu Rev Immunol*, 1996. 14: p. 179-205.
34. Cao, X., et al., Defective lymphoid development in mice lacking expression of the common cytokine receptor gamma chain. *Immunity*, 1995. 2(3): p. 223-38.
35. DiSanto, J.P., et al., Lymphoid development in mice with a targeted deletion of the interleukin 2 receptor gamma chain. *Proc Natl Acad Sci U S A*, 1995. 92(2): p. 377-81.
36. Ohbo, K., et al., Modulation of hematopoiesis in mice with a truncated mutant of the interleukin-2 receptor gamma chain. *Blood*, 1996. 87(3): p. 956-67.
37. Notta, F., S. Doulatov, and J.E. Dick, Engraftment of human hematopoietic stem cells is more efficient in female NOD/SCID/IL-2Rgc-null recipients. *Blood*, 2010. 115(18): p. 3704-7.
38. Brehm, M.A., et al., Parameters for establishing humanized mouse models

- to study human immunity: analysis of human hematopoietic stem cell engraftment in three immunodeficient strains of mice bearing the IL2rgamma(null) mutation. *Clin Immunol*, 2010. 135(1): p. 84-98.
39. Wunderlich, M., et al., AML xenograft efficiency is significantly improved in NOD/SCID-IL2RG mice constitutively expressing human SCF, GM-CSF and IL-3. *Leukemia*, 2010. 24(10): p. 1785-8.
 40. Medyouf, H., et al., Myelodysplastic cells in patients reprogram mesenchymal stromal cells to establish a transplantable stem cell niche disease unit. *Cell Stem Cell*, 2014. 14(6): p. 824-37.
 41. Rongvaux, A., et al., Development and function of human innate immune cells in a humanized mouse model. *Nat Biotechnol*, 2014. 32(4): p. 364-72.
 42. Waskow, C., et al., Hematopoietic stem cell transplantation without irradiation. *Nat Methods*, 2009. 6(4): p. 267-9.
 43. McIntosh, B.E., et al., Nonirradiated NOD,B6.SCID Il2rgamma-/-Kit(W41/W41) (NBSGW) mice support multilineage engraftment of human hematopoietic cells. *Stem Cell Reports*, 2015. 4(2): p. 171-80.
 44. Yong, K., et al., Cord blood progenitor cells have greater transendothelial migratory activity and increased responses to SDF-1 and MIP-3beta compared with mobilized adult progenitor cells. *Br J Haematol*, 1999. 107(2): p. 441-9.
 45. Voermans, C., et al., Increased migration of cord blood-derived CD34+ cells, as compared to bone marrow and mobilized peripheral blood CD34+ cells across uncoated or fibronectin-coated filters. *Exp Hematol*, 1999. 27(12): p. 1806-14.
 46. Zheng, Y., et al., Ex vivo manipulation of umbilical cord blood-derived hematopoietic stem/progenitor cells with recombinant human stem cell factor can up-regulate levels of homing-essential molecules to increase their transmigratory potential. *Exp Hematol*, 2003. 31(12): p. 1237-46.
 47. Krause, D.S., et al., CD34: structure, biology, and clinical utility. *Blood*, 1996. 87(1): p. 1-13.
 48. Dick, J.E., Stem cell concepts renew cancer research. *Blood*, 2008. 112(13): p. 4793-807.
 49. Notta, F., et al., Isolation of single human hematopoietic stem cells capable of long-term multilineage engraftment. *Science*, 2011. 333(6039): p. 218-21.

50. Goessling, W., et al., Genetic interaction of PGE2 and Wnt signaling regulates developmental specification of stem cells and regeneration. *Cell*, 2009. 136(6): p. 1136-47.
51. Hoggatt, J., et al., Prostaglandin E2 enhances hematopoietic stem cell homing, survival, and proliferation. *Blood*, 2009. 113(22): p. 5444-55.
52. Goessling, W., et al., Prostaglandin E2 enhances human cord blood stem cell xenotransplants and shows long-term safety in preclinical nonhuman primate transplant models. *Cell Stem Cell*, 2011. 8(4): p. 445-58.
53. Boitano, A.E., et al., Aryl hydrocarbon receptor antagonists promote the expansion of human hematopoietic stem cells. *Science*, 2010. 329(5997): p. 1345-8.
54. Fares, I., et al., Cord blood expansion. Pyrimidoindole derivatives are agonists of human hematopoietic stem cell self-renewal. *Science*, 2014. 345(6203): p. 1509-12.
55. Milhem, M., et al., Modification of hematopoietic stem cell fate by 5aza 2'deoxyctidine and trichostatin A. *Blood*, 2004. 103(11): p. 4102-10.
56. Bug, G., et al., Valproic acid stimulates proliferation and self-renewal of hematopoietic stem cells. *Cancer Res*, 2005. 65(7): p. 2537-41.
57. Hu, L., et al., Antioxidant N-acetyl-L-cysteine increases engraftment of human hematopoietic stem cells in immune-deficient mice. *Blood*, 2014. 124(20): p. e45-8.
58. Melief, C.J., et al., Therapeutic cancer vaccines. *J Clin Invest*, 2015. 125(9): p. 3401-12.
59. Yang, J., et al., Composite peptide-based vaccines for cancer immunotherapy (Review). *Int J Mol Med*, 2015. 35(1): p. 17-23.
60. Forsstrom, B., et al., Dissecting antibodies with regards to linear and conformational epitopes. *PLoS One*, 2015. 10(3): p. e0121673.
61. Sahin, U. and O. Tureci, Personalized vaccines for cancer immunotherapy. *Science*, 2018. 359(6382): p. 1355-1360.
62. Capitano, M.L., et al., Mild Heat Treatment Primes Human CD34(+) Cord Blood Cells for Migration Toward SDF-1alpha and Enhances Engraftment in an NSG Mouse Model. *Stem Cells*, 2015. 33(6): p. 1975-84.
63. Spranger, S., B. Frankenberger, and D.J. Schendel, NOD/scid IL-2Rg(null) mice: a preclinical model system to evaluate human dendritic cell-based

- vaccine strategies in vivo. *J Transl Med*, 2012. 10: p. 30.
64. Lang, J., et al., Generation of hematopoietic humanized mice in the newborn BALB/c-Rag2null Il2rgammanull mouse model: a multivariable optimization approach. *Clin Immunol*, 2011. 140(1): p. 102-16.
 65. Shultz, L.D., et al., Generation of functional human T-cell subsets with HLA-restricted immune responses in HLA class I expressing NOD/SCID/IL2r gamma(null) humanized mice. *Proc Natl Acad Sci U S A*, 2010. 107(29): p. 13022-7.
 66. Scheeren, F.A., et al., T cell-independent development and induction of somatic hypermutation in human IgM+ IgD+ CD27+ B cells. *J Exp Med*, 2008. 205(9): p. 2033-42.
 67. Gimeno, R., et al., Monitoring the effect of gene silencing by RNA interference in human CD34+ cells injected into newborn RAG2-/- gammac-/- mice: functional inactivation of p53 in developing T cells. *Blood*, 2004. 104(13): p. 3886-93.
 68. Manz, M.G., Human-hemato-lymphoid-system mice: opportunities and challenges. *Immunity*, 2007. 26(5): p. 537-41.
 69. Mestas, J. and C.C. Hughes, Of mice and not men: differences between mouse and human immunology. *J Immunol*, 2004. 172(5): p. 2731-8.
 70. Ali, N., et al., Xenogeneic graft-versus-host-disease in NOD-scid IL-2Rgammanull mice display a T-effector memory phenotype. *PLoS One*, 2012. 7(8): p. e44219.
 71. Becker, P.D., et al., Generation of human antigen-specific monoclonal IgM antibodies using vaccinated "human immune system" mice. *PLoS One*, 2010. 5(10).
 72. Van Duyne, R., et al., The utilization of humanized mouse models for the study of human retroviral infections. *Retrovirology*, 2009. 6: p. 76.
 73. Akkina, R., New generation humanized mice for virus research: comparative aspects and future prospects. *Virology*, 2013. 435(1): p. 14-28.
 74. Gonzalez, L., N. Strbo, and E.R. Podack, Humanized mice: novel model for studying mechanisms of human immune-based therapies. *Immunol Res*, 2013. 57(1-3): p. 326-34.
 75. Misharin, A.V., et al., Development of a new humanized mouse model to study acute inflammatory arthritis. *J Transl Med*, 2012. 10: p. 190.

76. Pajot, A., et al., A mouse model of human adaptive immune functions: HLA-A2.1-/HLA-DR1-transgenic H-2 class I-/class II-knockout mice. *Eur J Immunol*, 2004. 34(11): p. 3060-9.
77. Ru, Z., et al., Development of a humanized HLA-A2.1/DP4 transgenic mouse model and the use of this model to map HLA-DP4-restricted epitopes of HBV envelope protein. *PLoS One*, 2012. 7(3): p. e32247.
78. D'Aveni, M., et al., G-CSF mobilizes CD34+ regulatory monocytes that inhibit graft-versus-host disease. *Sci Transl Med*, 2015. 7(281): p. 281ra42.
79. Chung, Y.S., et al., Co-transplantation of human fetal thymus, bone and CD34(+) cells into young adult immunodeficient NOD/SCID IL2Rgamma(null) mice optimizes humanized mice that mount adaptive antibody responses. *Clin Immunol*, 2015. 157(2): p. 156-65.
80. Pearson, T., D.L. Greiner, and L.D. Shultz, Creation of "humanized" mice to study human immunity. *Curr Protoc Immunol*, 2008. Chapter 15: p. Unit 15.21.
81. King, M.A., et al., Human peripheral blood leucocyte non-obese diabetic-severe combined immunodeficiency interleukin-2 receptor gamma chain gene mouse model of xenogeneic graft-versus-host-like disease and the role of host major histocompatibility complex. *Clin Exp Immunol*, 2009. 157(1): p. 104-18.
82. van Rijn, R.S., et al., A new xenograft model for graft-versus-host disease by intravenous transfer of human peripheral blood mononuclear cells in RAG2-/- gammac-/- double-mutant mice. *Blood*, 2003. 102(7): p. 2522-31.
83. Hesselton, R.M., et al., Human peripheral blood xenografts in the SCID mouse: characterization of immunologic reconstitution. *J Infect Dis*, 1993. 168(3): p. 630-40.
84. Saxon, A., et al., Limited B cell repertoire in severe combined immunodeficient mice engrafted with peripheral blood mononuclear cells derived from immunodeficient or normal humans. *J Clin Invest*, 1991. 87(2): p. 658-65.
85. King, M., et al., Humanized mice for the study of type 1 diabetes and beta cell function. *Ann N Y Acad Sci*, 2008. 1150: p. 46-53.
86. Pearson, T., et al., Non-obese diabetic-recombination activating gene-1 (NOD-Rag1 null) interleukin (IL)-2 receptor common gamma chain (IL2r

- gamma null) null mice: a radioresistant model for human lymphohaematopoietic engraftment. *Clin Exp Immunol*, 2008. 154(2): p. 270-84.
87. van den Berg, T.K. and C.E. van der Schoot, Innate immune 'self' recognition: a role for CD47-SIRPalpha interactions in hematopoietic stem cell transplantation. *Trends Immunol*, 2008. 29(5): p. 203-6.
 88. Takenaka, K., et al., Polymorphism in Sirpa modulates engraftment of human hematopoietic stem cells. *Nat Immunol*, 2007. 8(12): p. 1313-23.
 89. Rozemuller, H., et al., Enhanced engraftment of human cells in RAG2/gammac double-knockout mice after treatment with CL2MDP liposomes. *Exp Hematol*, 2004. 32(11): p. 1118-25.
 90. Nervi, B., et al., Factors affecting human T cell engraftment, trafficking, and associated xenogeneic graft-vs-host disease in NOD/SCID beta2mnull mice. *Exp Hematol*, 2007. 35(12): p. 1823-38.
 91. Christianson, S.W., et al., Enhanced human CD4+ T cell engraftment in beta2-microglobulin-deficient NOD-scid mice. *J Immunol*, 1997. 158(8): p. 3578-86.
 92. Viret, C. and C.A. Janeway, Jr., MHC and T cell development. *Rev Immunogenet*, 1999. 1(1): p. 91-104.
 93. Sprent, J., E.K. Gao, and S.R. Webb, T cell reactivity to MHC molecules: immunity versus tolerance. *Science*, 1990. 248(4961): p. 1357-63.
 94. Sette, A. and J. Fikes, Epitope-based vaccines: an update on epitope identification, vaccine design and delivery. *Curr Opin Immunol*, 2003. 15(4): p. 461-70.
 95. Sette, A., et al., The development of multi-epitope vaccines: epitope identification, vaccine design and clinical evaluation. *Biologicals*, 2001. 29(3-4): p. 271-6.
 96. Comber, J.D. and R. Philip, MHC class I antigen presentation and implications for developing a new generation of therapeutic vaccines. *Ther Adv Vaccines*, 2014. 2(3): p. 77-89.
 97. Pulendran, B. and R. Ahmed, Immunological mechanisms of vaccination. *Nat Immunol*, 2011. 12(6): p. 509-17.
 98. Demento, S.L., et al., Pathogen-associated molecular patterns on biomaterials: a paradigm for engineering new vaccines. *Trends Biotechnol*,

2011. 29(6): p. 294-306.
99. Oyarzun, P., et al., A bioinformatics tool for epitope-based vaccine design that accounts for human ethnic diversity: application to emerging infectious diseases. *Vaccine*, 2015. 33(10): p. 1267-73.
 100. Himoudi, N., et al., Comparative vaccine studies in HLA-A2.1-transgenic mice reveal a clustered organization of epitopes presented in hepatitis C virus natural infection. *J Virol*, 2002. 76(24): p. 12735-46.
 101. Healey, G.D., et al., Humoral and cell-mediated adaptive immune responses are required for protection against *Burkholderia pseudomallei* challenge and bacterial clearance postinfection. *Infect Immun*, 2005. 73(9): p. 5945-51.
 102. Raffegerst, S.H., et al., Diverse hematological malignancies including hodgkin-like lymphomas develop in chimeric MHC class II transgenic mice. *PLoS One*, 2009. 4(12): p. e8539.
 103. Boesen, A., K. Sundar, and R. Coico, Lassa fever virus peptides predicted by computational analysis induce epitope-specific cytotoxic-T-lymphocyte responses in HLA-A2.1 transgenic mice. *Clin Diagn Lab Immunol*, 2005. 12(10): p. 1223-30.
 104. Ishioka, G.Y., et al., Utilization of MHC class I transgenic mice for development of minigene DNA vaccines encoding multiple HLA-restricted CTL epitopes. *J Immunol*, 1999. 162(7): p. 3915-25.
 105. Pajot, A., et al., Identification of novel HLA-DR1-restricted epitopes from the hepatitis B virus envelope protein in mice expressing HLA-DR1 and vaccinated human subjects. *Microbes Infect*, 2006. 8(12-13): p. 2783-90.
 106. BenMohamed, L., et al., Induction of CTL response by a minimal epitope vaccine in HLA A*0201/DR1 transgenic mice: dependence on HLA class II restricted T(H) response. *Hum Immunol*, 2000. 61(8): p. 764-79.
 107. Wasik, T.J., et al., Association between HIV-specific T helper responses and CTL activities in pediatric AIDS. *Eur J Immunol*, 2000. 30(1): p. 117-27.
 108. Dion, S., et al., Adeno-associated virus-mediated gene transfer leads to persistent hepatitis B virus replication in mice expressing HLA-A2 and HLA-DR1 molecules. *J Virol*, 2013. 87(10): p. 5554-63.
 109. Reiser, M., et al., The immunodominant CD8 T cell response to the human

- cytomegalovirus tegument phosphoprotein pp65(495-503) epitope critically depends on CD4 T cell help in vaccinated HLA-A*0201 transgenic mice. *J Immunol*, 2011. 187(5): p. 2172-80.
110. Smith, H.A. and D.G. McNeel, Vaccines targeting the cancer-testis antigen SSX-2 elicit HLA-A2 epitope-specific cytolytic T cells. *J Immunother*, 2011. 34(8): p. 569-80.
 111. Smith, H.A., et al., Expression and immunotherapeutic targeting of the SSX family of cancer-testis antigens in prostate cancer. *Cancer Res*, 2011. 71(21): p. 6785-95.
 112. Lee, T.D., et al., The polymorphism of HLA antigens in the Chinese. *Tissue Antigens*, 1988. 32(4): p. 188-208.
 113. Alexander, J., et al., Derivation of HLA-A11/Kb transgenic mice: functional CTL repertoire and recognition of human A11-restricted CTL epitopes. *J Immunol*, 1997. 159(10): p. 4753-61.
 114. **!!! INVALID CITATION !!!**
 115. Ureta-Vidal, A., et al., Phenotypical and functional characterization of the CD8+ T cell repertoire of HLA-A2.1 transgenic, H-2KbnullDbnull double knockout mice. *J Immunol*, 1999. 163(5): p. 2555-60.
 116. Firat, H., et al., Comparative analysis of the CD8(+) T cell repertoires of H-2 class I wild-type/HLA-A2.1 and H-2 class I knockout/HLA-A2.1 transgenic mice. *Int Immunol*, 2002. 14(8): p. 925-34.
 117. Pascolo, S., et al., HLA-A2.1-restricted education and cytolytic activity of CD8(+) T lymphocytes from beta2 microglobulin (beta2m) HLA-A2.1 monochain transgenic H-2Db beta2m double knockout mice. *J Exp Med*, 1997. 185(12): p. 2043-51.
 118. Liu, Y., et al., Three CpG oligodeoxynucleotide classes differentially enhance antigen-specific humoral and cellular immune responses in mice. *Vaccine*, 2011. 29(34): p. 5778-84.
 119. Yang, Y., et al., In silico design of a DNA-based HIV-1 multi-epitope vaccine for Chinese populations. *Hum Vaccin Immunother*, 2015. 11(3): p. 795-805.
 120. De Groot, A.S., et al., Mapping cross-clade HIV-1 vaccine epitopes using a bioinformatics approach. *Vaccine*, 2003. 21(27-30): p. 4486-504.
 121. Yang, C., et al., CpG oligodeoxynucleotides are a potent adjuvant for an

- inactivated polio vaccine produced from Sabin strains of poliovirus. *Vaccine*, 2009. 27(47): p. 6558-63.
122. Zhao, L., M. Zhang, and H. Cong, Advances in the study of HLA-restricted epitope vaccines. *Hum Vaccin Immunother*, 2013. 9(12): p. 2566-77.
 123. Chen, H.W., et al., Identification of HLA-A11-restricted CTL epitopes derived from HPV type 18 using DNA immunization. *Cancer Biol Ther*, 2009. 8(21): p. 2025-32.
 124. Gavioli, R., et al., Multiple HLA A11-restricted cytotoxic T-lymphocyte epitopes of different immunogenicities in the Epstein-Barr virus-encoded nuclear antigen 4. *J Virol*, 1993. 67(3): p. 1572-8.
 125. Deng, Q., et al., Hepatitis B virus as a gene delivery vector activating foreign antigenic T cell response that abrogates viral expression in mouse models. *Hepatology*, 2009. 50(5): p. 1380-91.
 126. Boucherma, R., et al., HLA-A*01:03, HLA-A*24:02, HLA-B*08:01, HLA-B*27:05, HLA-B*35:01, HLA-B*44:02, and HLA-C*07:01 monochain transgenic/H-2 class I null mice: novel versatile preclinical models of human T cell responses. *J Immunol*, 2013. 191(2): p. 583-93.
 127. Pajot, A., et al., The Th1 immune response against HIV-1 Gag p24-derived peptides in mice expressing HLA-A02.01 and HLA-DR1. *Eur J Immunol*, 2007. 37(9): p. 2635-44.
 128. Ramage, J.M., et al., Comparison of the immune response to a self antigen after DNA immunisation of HLA*A201/H-2Kb and HHD transgenic mice. *Vaccine*, 2004. 22(13-14): p. 1728-31.
 129. Flanagan, S.P., 'Nude', a new hairless gene with pleiotropic effects in the mouse. *Genet Res*, 1966. 8(3): p. 295-309.
 130. Rygaard, J. and C.W. Friis, The husbandry of mice with congenital absence of the thymus (nude mice). *Z Versuchstierkd*, 1974. 16(1): p. 1-10.
 131. Scher, I., et al., X-linked B-lymphocyte immune defect in CBA/N mice. II. Studies of the mechanisms underlying the immune defect. *J Exp Med*, 1975. 142(3): p. 637-50.
 132. Watanabe, Y., et al., The analysis of the functions of human B and T cells in humanized NOD/shi-scid/gammac(null) (NOG) mice (hu-HSC NOG mice). *Int Immunol*, 2009. 21(7): p. 843-58.
 133. Schatz, D.G. and Y. Ji, Recombination centres and the orchestration of

- V(D)J recombination. *Nat Rev Immunol*, 2011. 11(4): p. 251-63.
134. Girardi, M., et al., Regulation of cutaneous malignancy by gammadelta T cells. *Science*, 2001. 294(5542): p. 605-9.
 135. King, M., et al., A new Hu-PBL model for the study of human islet alloreactivity based on NOD-scid mice bearing a targeted mutation in the IL-2 receptor gamma chain gene. *Clin Immunol*, 2008. 126(3): p. 303-14.
 136. Liao, W., J.X. Lin, and W.J. Leonard, IL-2 family cytokines: new insights into the complex roles of IL-2 as a broad regulator of T helper cell differentiation. *Curr Opin Immunol*, 2011. 23(5): p. 598-604.
 137. Zhang, L. and L. Su, HIV-1 immunopathogenesis in humanized mouse models. *Cell Mol Immunol*, 2012. 9(3): p. 237-44.
 138. Koo, G.C., A. Hasan, and R.J. O'Reilly, Use of humanized severe combined immunodeficient mice for human vaccine development. *Expert Rev Vaccines*, 2009. 8(1): p. 113-20.
 139. Thomas, S., et al., Evaluating Human T-Cell Therapy of Cytomegalovirus Organ Disease in HLA-Transgenic Mice. *PLoS Pathog*, 2015. 11(7): p. e1005049.
 140. Najima, Y., et al., Induction of WT1-specific human CD8+ T cells from human HSCs in HLA class I Tg NOD/SCID/IL2rgKO mice. 2016. 127(6): p. 722-34.
 141. Li, F., et al., Efficient genetic manipulation of the NOD-Rag1-/- IL2RgammaC-null mouse by combining in vitro fertilization and CRISPR/Cas9 technology. *Sci Rep*, 2014. 4: p. 5290.
 142. Swain, S.L., et al., CD4+ T-cell memory: generation and multi-faceted roles for CD4+ T cells in protective immunity to influenza. *Immunol Rev*, 2006. 211: p. 8-22.
 143. Penna, A., et al., Cytotoxic T lymphocytes recognize an HLA-A2-restricted epitope within the hepatitis B virus nucleocapsid antigen. *J Exp Med*, 1991. 174(6): p. 1565-70.
 144. Carrington, M. and S.J. O'Brien, The influence of HLA genotype on AIDS. *Annu Rev Med*, 2003. 54: p. 535-51.
 145. Pasquetto, V., et al., HLA-A*0201, HLA-A*1101, and HLA-B*0702 transgenic mice recognize numerous poxvirus determinants from a wide variety of viral gene products. *J Immunol*, 2005. 175(8): p. 5504-15.

146. Tourdot, S., et al., A general strategy to enhance immunogenicity of low-affinity HLA-A2. 1-associated peptides: implication in the identification of cryptic tumor epitopes. *Eur J Immunol*, 2000. 30(12): p. 3411-21.
147. Goulder, P.J. and B.D. Walker, HIV and HLA class I: an evolving relationship. *Immunity*, 2012. 37(3): p. 426-40.
148. Goulder, P.J. and D.I. Watkins, HIV and SIV CTL escape: implications for vaccine design. *Nat Rev Immunol*, 2004. 4(8): p. 630-40.
149. Kievits, F., et al., HLA-restricted recognition of viral antigens in HLA transgenic mice. *Nature*, 1987. 329(6138): p. 447-9.
150. Chamberlain, J.W., et al., Cell surface expression and alloantigenic function of a human class I MHC heavy chain gene (HLA-B7) in transgenic mice. *J Immunol*, 1988. 140(4): p. 1285-92.
151. Bernhard, E.J., et al., Cytotoxic T lymphocytes from HLA-A2 transgenic mice specific for HLA-A2 expressed on human cells. *J Exp Med*, 1988. 168(3): p. 1157-62.
152. Dill, O., et al., Immunological function of HLA-C antigens in HLA-Cw3 transgenic mice. *Proc Natl Acad Sci U S A*, 1988. 85(15): p. 5664-8.
153. Connolly, J.M., et al., The Lyt-2 molecule recognizes residues in the class I alpha 3 domain in allogeneic cytotoxic T cell responses. *J Exp Med*, 1988. 168(1): p. 325-41.
154. Engelhard, V.H., E. Lacy, and J.P. Ridge, Influenza A-specific, HLA-A2.1-restricted cytotoxic T lymphocytes from HLA-A2.1 transgenic mice recognize fragments of the M1 protein. *J Immunol*, 1991. 146(4): p. 1226-32.
155. Irwin, M.J., W.R. Heath, and L.A. Sherman, Species-restricted interactions between CD8 and the alpha 3 domain of class I influence the magnitude of the xenogeneic response. *J Exp Med*, 1989. 170(4): p. 1091-101.
156. Barra, C., et al., Abrogation of H-2-restricted CTL responses and efficient recognition of HLA-A3 molecules in DBA/2 HLA/A24 responder mice. *J Immunol*, 1993. 150(9): p. 3681-9.
157. LaFace, D.M., et al., Human CD8 transgene regulation of HLA recognition by murine T cells. *J Exp Med*, 1995. 182(5): p. 1315-25.
158. Korn, T., et al., IL-17 and Th17 Cells. *Annu Rev Immunol*, 2009. 27: p. 485-

517.

159. Miossec, P., T. Korn, and V.K. Kuchroo, Interleukin-17 and type 17 helper T cells. *N Engl J Med*, 2009. 361(9): p. 888-98.
160. Momburg, F. and P. Tan, Tapasin-the keystone of the loading complex optimizing peptide binding by MHC class I molecules in the endoplasmic reticulum. *Mol Immunol*, 2002. 39(3-4): p. 217-33.
161. Walport, M.J., Complement. First of two parts. *N Engl J Med*, 2001. 344(14): p. 1058-66.
162. Yan, H., et al., Sodium taurocholate cotransporting polypeptide is a functional receptor for human hepatitis B and D virus. *Elife*, 2012. 3.
163. Jiang, Y., et al., Blockade of the C5a-C5aR axis alleviates lung damage in hDPP4-transgenic mice infected with MERS-CoV. *Emerg Microbes Infect*, 2018. 7(1): p. 77.

Synthèse en Français

ÉCOLE DOCTORALE N°568
Signalisations et Réseaux intégratifs en Biologie (Biosigne)

Présentée par
M^{me} Yang ZENG

Titre: La création du modèle "HUMAMICE": le développement de souris humanisée pour évaluation des innovations en biothérapies; immunothérapies et les thérapies cellulaire

Mots clés: HUMAMICE, Souris immunodéficientes, reconstitution immunitaire, CMH, HLA-A11/DR1 souris transgénique

Résumé: Les modèles animaux jouent un rôle crucial dans les recherches précliniques, mais il existe plusieurs limites. Les états physiologiques et immunologiques chez les murins et les primates non humains sont radicalement différents de ceux de l'homme, en particulier la restriction au CMH, qui ne peut éliminer l'influence de la spécificité de l'espèce dans les expériences précliniques. Le but du travail était de générer un niveau plus élevé de souris transgéniques «HLA humanisées» qui pourraient imiter les réponses immunitaires humaines avec plus de précision et de fiabilité; à viser d'appliquer pour l'évaluation préclinique de la transplantation humaine, à l'identification de nouveaux épitopes et à l'évaluation des vaccins et des médicaments candidats.

Dans la première partie, nous rapportons d'une nouvelles souris transgéniques HLA immunodéficiente «HUMAMICE». Des souris HLA-A2^{+/+}/DR1^{+/+}/H-2-β₂m^{-/-}/IAβ^{-/-}/Rag2^{-/-}/IL-2γ^{-/-}/Perf^{-/-} ont été établies, lesquelles exprimaient des molécules HLA humaines au lieu de H-2 murines et ne présent pas de lymphocytes murins. Ce statut immunodéficient a été inversé en transférant les cellules hPBMC HLA appariées fonctionnelles pour produisant des souris ayant un statut immuno-compétent avec un système immunitaire humain fonctionnel. L'immunisation du vaccin HBsAg a permis d'obtenir une production robuste et reproductible d'anticorps spécifiques.

En conclusion, ces résultats indiquent que le modèle hPBMC-HUMAMICE représente un modèle prometteur pour disséquer les réponses immunitaires humaines aux maladies humaines.

Dans la seconde partie de cette étude, les souris HLA-A11^{+/+}/DR1^{+/+}/H-2-β₂m^{-/-}/IAβ^{-/-}

ont été établies. Cette nouvelle souche de souris possède une caractéristique restreinte par HLA-A11 et une capacité normale à répondre aux antigènes. L'immunisation de souris avec un vaccin recombinant HBsAg contre le VHB ou une protéine recombinante du VIH-1 a entraîné la génération de lymphocytes T cytotoxiques producteurs d'IFN- γ et d'anticorps spécifiques. En outre, nous avons identifié deux épitopes restreints par HLA-A11 de la protéine GP EBOV et quatre de la protéine MERS-CoV S. En fin, ce modèle de souris HLA-A11/DR1 pourra faciliter l'identification des épitopes de lymphocytes cytotoxiques et auxiliaires restreints par le HLA-A11 dominant en Chine. Le modèle constitue un nouvel outil technique prometteur pour comprendre les mécanismes immunologiques et les nouveaux vaccins pour les populations d'Asie de l'Est.

Durant cette thèse, nous avons créé deux modèles de souris humanisées novateurs et prometteurs portant une restriction HLA humaine qui pourraient servir de modèles d'infection pathogène et étudier les tumeurs, les mécanismes de transplantation et l'évaluation des vaccins et des médicaments.

Annexe

Résumé:

Contexte, rationnel de l'étude et les résultats:

A l'heure actuelle, aucun modèle d'expérimentation pré clinique ne permet d'explorer fidèlement les réponses immunitaires humaines. En effet, le fonctionnement du système immunitaire entre l'homme et l'animal est différent: les réponses humaines sont spécifiquement restreintes aux complexes HLAs alors que les souris expriment les complexes H2 et non HLAs. Les contraintes éthiques des essais cliniques soulèvent une nécessité urgente d'améliorer les modèles animaux pouvant mimer fidèlement les réponses humaines, en particulier les réponses du système immunitaire humain (HIS).

Les souris dites « humanisées » ou « HIS » ont été récemment générées en greffant des cellules souches hématopoïétiques humaines (hHSCs) ou des cellules mononucléées du sang périphérique humain (hPBMCs) dans des souris profondément immunodéficientes, telles que les souris NSG ou souris NOG et les souris NRG, qui sont des modèles bien validés. Cependant, un inconvénient majeur pour les études expérimentales utilisant le modèle de souris hHSC-NSG (Cellules souches humaine: hHSC) est que les réponses sont H2-restreintes et non-HLA-restreintes. Alors que dans le modèle de souris hPBMC-NSG, est l'apparition rapide, d'une maladie du greffon contre l'hôte (xénoGVHD).

Dans la première partie de cette thèse, nous voulons surmonter cette limitation (compatibilité HLA entre donneur/receveur) en générant une nouvelle souris "HUMAMICE" immunodéprimée et qui exprime des molécules HLA humaines (HLA-A2 et HLA-DR1) à la place des molécules du CMH de souris (H-2). HUMAMICE correspond à une version améliorée des modèles de référence actuels de souris immunodéprimées NSG ou NOG. En effet, le modèle HUMAMICE permet au système immunitaire humain transféré dans la souris de fonctionner correctement et physiologiquement, en respectant la compatibilité HLA entre donneur et receveur. Nous avons montré que le transfert de hPBMC-HLA-compatibles dans cette souris HUMAMICE permet de reverser son statut immuno-déficient en statut immuno-compétent avec un système immunitaire humain fonctionnel. L'immunisation du vaccin HBsAg contre infection du virus de l'Hépatite B a permis d'obtenir une production

robuste et reproductible d'anticorps spécifiques. En conclusion, ce modèle représente l'unique modèle expérimental pré-clinique, dans lequel les cellules immunitaires humaines transférées dans la souris conservent leurs propriétés et sont capables de générer des réponses immunitaires identiques à celles observées chez l'homme.

Dans la deuxième partie de cette thèse, une lignée de souris HLA-A11/DR1 (HLA-A11^{+/+}/ DR1^{+/+}/ H-2-β2m^{-/-}/ IAβ^{-/-}) a été établie. La réponse immunitaire induite chez cette lignée de souris est complètement sous la dépendance des molécules HLA de l'homme (y compris la collaboration entre les cellules CD4 et les cellules CD8). Il n'y a ni concurrence ni ingérence de la réponse immunitaire des gènes murins CMH et humains HLA. Ainsi, la prédiction et la transposition des données de la souris à l'homme seront plus fiables. Nous avons vérifié que cette nouvelle souris possède une caractéristique fonctionnelle de restriction par HLA-A11 et une capacité normale à répondre aux antigènes. L'immunisation de souris avec un vaccin recombinant HBsAg contre infection du virus de l'Hépatite B (VHB) ou une protéine recombinante du VIH-1 a entraîné la génération de lymphocytes T cytotoxiques producteurs d'IFN- et d'anticorps spécifiques.

Ce modèle de souris humanisée HLA-A11/DR1 facilite l'identification des épitopes HLA-A11 restreints des lymphocytes cytotoxiques dominants en Chine et HLA-DR1 restreints des lymphocytes auxiliaires. Ce modèle représente un outil puissant à la fois pour l'évaluation et la comparaison des protocoles de vaccination et de formulation des vaccins. Ils seront ainsi indéniablement importants pour faciliter la sélection des candidats vaccins, ou des thérapies innovantes pouvant être directement appliqués dans les essais cliniques humains.

Durant cette thèse, deux épitopes restreints par HLA-A11 de la protéine GP EBOV et quatre de la protéine MERS-CoV S ont été identifiés.

En conclusion, les deux modèles de souris HLA humanisées sont créés. Ils sont novateurs et prometteurs portant une restriction HLA humaine pourraient servir de modèles préclinique d'étude d'infection pathogène; de cancérologie, les mécanismes de transplantation; la thérapie ou les immunothérapies cellulaires ainsi que l'évaluation des candidats vaccins et des médicaments.

Titre: La création du modèle "HUMAMICE": le développement de souris humanisée pour évaluation des innovations en biothérapies; immunothérapies et les thérapies cellulaire

Mots clés: HUMAMICE, Souris immunodéficientes, reconstitution immunitaire, CMH, HLA-A11/DR1 souris transgénique

Résumé: Les modèles animaux jouent un rôle crucial dans les recherches précliniques, mais il existe plusieurs limites. Les états physiologiques et immunologiques chez les murins et les primates non humains sont radicalement différents de ceux de l'homme, en particulier la restriction au CMH, qui ne peut éliminer l'influence de la spécificité de l'espèce dans les expériences précliniques. Le but du travail était de générer un niveau plus élevé de souris transgéniques «HLA humanisées» qui pourraient imiter les réponses immunitaires humaines avec plus de précision et de fiabilité; à viser d'appliquer pour l'évaluation préclinique de la transplantation humaine, à l'identification de nouveaux épitopes et à l'évaluation des vaccins et des médicaments candidats.

Dans la première partie, nous rapportons d'une nouvelles souris transgéniques HLA immunodéficiente «HUMAMICE». Des souris HLA-A2^{+/+}/DR1^{+/+}/H-2-β₂m^{-/-}/IAβ^{-/-}/Rag2^{-/-}/IL-2rγ^{-/-}/Perf^{-/-} ont été établies, lesquelles exprimaient des molécules HLA humaines au lieu de H-2 murines et ne présentent pas de lymphocytes murins. Ce statut immunodéficient a été inversé en transférant les cellules hPBMHC HLA appariées fonctionnelles pour produisant des souris ayant un statut immuno-compétent avec un système immunitaire humain fonctionnel. L'immunisation du vaccin HBsAg a permis d'obtenir une production robuste et

reproductible d'anticorps spécifiques.

En conclusion, ces résultats indiquent que le modèle hPBMHC-HUMAMICE représente un modèle prometteur pour disséquer les réponses immunitaires humaines aux maladies humaines.

Dans la seconde partie de cette étude, les souris HLA-A11^{+/+}/DR1^{+/+}/H-2-β₂m^{-/-}/IAβ^{-/-} ont été établies. Cette nouvelle souche de souris possède une caractéristique restreinte par HLA-A11 et une capacité normale à répondre aux antigènes. L'immunisation de souris avec un vaccin recombinant HBsAg contre le VHB ou une protéine recombinante du VIH-1 a entraîné la génération de lymphocytes T cytotoxiques producteurs d'IFN-γ et d'anticorps spécifiques. En outre, nous avons identifié deux épitopes restreints par HLA-A11 de la protéine GP EBOV et quatre de la protéine MERS-CoV S. En fin, ce modèle de souris HLA-A11/DR1 pourra faciliter l'identification des épitopes de lymphocytes cytotoxiques et auxiliaires restreints par le HLA-A11 dominant en Chine. Le modèle constitue un nouvel outil technique prometteur pour comprendre les mécanismes immunologiques et les nouveaux vaccins pour les populations d'Asie de l'Est.

Durant cette thèse, nous avons créé deux modèles de souris humanisées novateurs et prometteurs portant une restriction HLA humaine qui pourraient servir de modèles d'infection pathogène et étudier les tumeurs, les mécanismes de transplantation et l'évaluation des vaccins et des médicaments.

Title: The creation of novel humanized mouse models for the assessment of innovative immunotherapies and vaccine evaluation

Keywords: HUMAMICE, immuno-deficient mice, immune reconstitution, MHC, HLA-A11/DR1 transgenic mice

Abstract: Animal models play critical roles in pre-clinical researches, while there are several limitations. The physiological and immunological states in murine and non-human primates are still distinct from those of human to a certain extent, especially the MHC restriction, which cannot eliminate the influence of species specificity in pre-clinical experiments. The aim of our work was to generate a higher level of "HLA humanized" transgenic mice which could mimic human immune responses with more accuracy and reliability; furthermore, to apply the novel models to the evaluation of human transplantation, the identification of new epitopes, and the evaluation of candidate vaccines and drugs.

In the first part, a novel immuno-deficient HLA transgenic mouse strain HLA-A2^{+/+}/DR1^{+/+}/H2-β₂m^{-/-}/IAβ^{-/-}/Rag2^{-/-}/IL-2rγ^{-/-}/Perf^{-/-} HUMAMICE were established, which expressed human HLA molecules instead of murine H-2 and present no murine lymphocytes. This immuno-deficient status was reversed by transferring the functional HLA-matched hPBMCs and thus producing mice with an immuno-competent status. Then, led to high lymphocyte engraftment without GvHD. Immunization of HBsAg vaccine resulted robust and reproducible production of

specific antibodies. In conclusion, these results indicated that the hPBMCs-HUMAMICE model represents a promising model to dissect human immune responses towards human diseases.

In the second part, the Chinese/East Asian HLA dominant HLA-A11/DR1 (HLA-A11^{+/+}/DR1^{+/+}/H-2-β₂m^{-/-}/IAβ^{-/-}) transgenic mouse strain was established. This novel mouse strain possesses HLA-A11-restricted characteristics and capacity to respond to antigens. Immunization of mice with a recombinant HBV vaccine or a recombinant HIV-1 protein resulted in the generation of IFN-γ-producing cytotoxic T lymphocytes and specific antibodies. Furthermore, we identified two HLA-A11 restricted epitopes of EBOV GP protein and four of MERS-CoV S protein. Above all, HLA-A11/DR1 mice could facilitate the identification of Chinese dominant HLA-restricted CTL and Th epitopes and provide a new promising technical tool to understand immunological mechanisms and new vaccines.

Taken together, we created two novel and promising humanized mouse models carrying human HLA restriction which could be applied as pathogen infection models, in tumor studies, transplantation mechanism, and the evaluation of vaccines and drugs.

